ROLES OF MALIC ENZYMES OF *RHIZOBIUM*

THE ROLES OF MALIC ENZYMES IN *RHIZOBIUM* CARBON METABOLISM

By

YE ZHANG, M.Sc.

A Thesis Submitted to the School of Graduate Studies in Partial Fulfillment of the Requirements for the Degree Doctor of Philosophy

McMaster University

Doctor of Philosophy (2013) McMaster University

(Biology) Hamilton, Ontario

TITLE: The Roles of Malic Enzymes in Central Carbon Metabolism of *Sinorhizobium*

AUTHOR: Ye Zhang, M.Sc (Saint Mary's University)

SUPERVISOR: Professor T.M. Finan

NUMBER OF PAGES: xvi, 282

ABSTRACT

C_4-dicarboxylic acids appear to be metabolized via the TCA cycle in N_2-fixing bacteria (bacteroids) within legume nodules. In *Sinorhizobium meliloti* bacteroids from alfalfa, NAD^+-malic enzyme (DME) is required for symbiotic N_2-fixation and this activity is thought to be required for the anaplerotic synthesis of pyruvate. In contrast, in the pea symbiont *Rhizobium leguminosarum* pyruvate synthesis can occur via either the DME pathway or a pathway catalyzed by phosphoenolpyruvate carboxykinase (PCK), pyruvate kinase (PYK), and pyruvate dehydrogenase. Here we report that *dme* mutants of *Sinorhizobium sp*. NGR234 formed root nodules on a broad range of plants and that the level of N_2-fixation varied from 90% to 20% of wild type depending on the host plants inoculated. NGR234 bacteroids had significant PCK activity and while single *pckA* and single *dme* mutants fixed N_2 on *Macroptilium atropurpureum* and *Leucaena leucocephala* (albeit at a reduced rate), a *pckA dme* double mutant had no N_2-fixing activity (Fix^-). Thus, NGR234 bacteroids appear to synthesize pyruvate from TCA cycle intermediates via DME or PCK pathways. These NGR234 data, together with other reports, suggested that the completely Fix^- phenotype of *S. meliloti dme* mutants may be specific to the alfalfa-*S. meliloti* symbiosis. We therefore examined the ME-like genes *azc3656* and *azc0119* from *Azorhizobium caulinodans*, as *azc3656* mutants were previously shown to form Fix^- nodules on the tropical legume *Sesbania rostrata*. We found that purified AZC3656 protein is an NAD (P) $^+$-malic enzyme whose activity is inhibited by acetyl-coenzyme A (acetyl-CoA) and stimulated by succinate and fumarate. Thus, whereas

DME is required for symbiotic N_2 fixation in *A. caulinodans* and *S. meliloti*, in other rhizobia this activity can be bypassed via another pathway(s).

In *S. meliloti* both malic enzymes DME and TME share similar apparent K_ms for substrate and cofactors, but differ in their responses to TCA cycle intermediates, with DME activity inhibited by acetyl-CoA and induced by succinate and fumarate. Previous results in our laboratory indicated that DME is essential for symbiotic N_2 fixation, while TME fails to functionally replace DME. One possible reason for it is that a high ratio of NADPH/$NADP^+$ in *S. meliloti* bacteroids prevents TME from functioning in nodules. We sought to lower the NADPH/$NADP^+$ ratio by overexpressing a soluble pyridine nucleotide transhydrogenase (STH). However, metabolite measurements indicated that overproducing STH failed to lower the ratio of NADPH/$NADP^+$ in *S. meliloti*.

Previous studies assumed that DME and TME might play different roles in central carbon metabolism. To gain insight of their physiological functions, genome-wide microarray analysis was conducted in *S. meliloti* single *dme and tme* mutants grown on glucose or succinate. The most striking changes of gene expression were observed in *S. meliloti dme* mutants grown on succinate. The functions of upregulated genes suggested that DME might play an important role in regulating TCA cycle intermediates, important for the maintenance of metabolic flux through TCA cycle during C_4-dicarboxylate oxidation. However, changes of gene expression found in *tme* mutants were not significant enough to predict the physiological functions of TME protein in central carbon metabolism.

ACKNOWLEDGMENTS

I would like to express my gratitude to Dr. Turlough M. Finan for the opportunity to complete this work in his laboratory, for the rigorous training, and for his continued guidance and support throughout the course of this study. I sincerely thank him for his efforts on my behalf.

I would like to thank the members of my supervisory committee, Dr. Robin K. Cameron and Dr. Jianping Xu, for their patience, comments, and willingness to engage on this work. I would like to thank Dr. Richard A. Morton for his critical scientific discussions and encouragement. Furthermore, I would also like to thank the past and present members of the Finan lab for all their help, support, and friendship over the years.

I would like to thank Dr. Herb E. Schellhorn for the use of his HPCL, Dr. Toshihiro Aono for providing *Azorhizobium caulinodans* ORS571 strains and seeds of *Sesbania rostrata*, and Dr. W. R. Streit for sharing the NGR234 genome sequence data with us prior its public release.

Finally, I want to express my heartfelt thanks to my wife Xiaotian and my daughters, Siobhan and Aisling, who supported me in all I have done to realize the completion of this thesis. This work will never be finished without your love, understanding and encouragement.

TABLE OF CONTENTS

LIST OF TABLES

TITLE PAGE

LIST OF FIGURES

TITLE PAGE

ABBREVIATIONS

ADP	adenosine 5′-diphosphate
Amp	ampicillin
ARA	acetylene reduction assay
APS	ammonium per sulfate, $(NH_4)_2S_2O_8$
ATP	adenosine-5'-triphosphate
BSA	bovine serum albumin
bp	base pair
BLAST	Basic Local Alignment Search Tool
cAMP	cyclic adenosine monophosphate
Cm	chloramphenicol
CoA	coenzyme A
ddH_2O	distilled and deionized water
DME	diphosphopyridine dependent malic enzyme
DNA	deoxyribonucleic acid
dNTP	deoxyribonucleotide triphosphate
DTT	dithiothreitol
EDTA	ethylenediaminetetraacetic acid
EPS	exopolysaccharides
FAME	fatty-acid methyl ester
Fix	nitrogen fixation phenotype
FRT	FLP recognition target
GABA	gamma-aminobutyrate shunt
Gm	gentamicin
HPLC	high-performance liquid chromatography
Km	kanamycin
kDa	kilo dalton
LB	Luria-Bertani medium
LBmc	Luria-Bertani medium with 2.5 mM $MgSO_4$, and 2.5 mM $CaCl_2$
LCO	lipo-chitooligosaccharide
Mb	Megabyte
ME	malic enzyme

MOPS	3-(N-morpholino)propanesulfonic acid
NAD^+	nicotinamide adenine dinucleotide
$NADP^+$	nicotinamide adenine dinucleotide phosphate
NF	nodulation factor
Nm	neomycin
OAA	oxaloacetate
OD	optical density
ONPG	2-Nitrophenyl-β-galactoside
PAGE	polyacrylamide gel electrophoresis
PBM	peribacteroid membrane
PCK	phosphoenolpyruvate carboxykinase
PCR	Polymerase Chain Reaction
PEP	phosphoenolpyruvate
PNPG	4-Nitrophenyl β-D-glucuronide
PQQ	pyrroloquinoline quinone
PTA	phosphotransacetylase enzyme
PYC	pyruvate carboxylase
rDNA	ribosomal DNA
RNA	ribonucleic acid
RPM	revolutions per minute
rRNA	ribosomal ribonucleic acid
SDS	sodium dodecyl sulfate
Sm	streptomycin
Sp	spectinomycin
STH	soluble pyridine nucleotide transhydrogenase
TAE	tris-acetate-EDTA buffer
Tc	tetracycline
TCA	tricarboxylic acid cycle
TEMED	*N*,*N*,*N*′,*N*′-Tetramethylethylenediamine**,** $(CH_3)_2NCH_2CH_2N(CH_3)_2$
TME	triphosphopyridine dependent malic enzyme
thio-NAD^+	thionicotinamide adenine dinucleotide
Tm	melting temperature
TY	tryptone-yeast medium

Chapter 1 Literature Review

1.1 Introduction

Nitrogen is one of the most important elements for the growth of all organisms and is a key nutrient in agriculture. It is found predominately in the form of nitrogen gas (N_2) in the Earth's atmosphere. N_2 is unavailable for use by organisms unless it is first reduced to ammonia (NH_3) in the nitrogen fixation process. Ammonia is an excellent source of reduced nitrogen, and can be assimilated directly by plants for growth. Only prokaryotic organisms carry out biological N_2 fixation, this process contributes more than half of the biosphere's available nitrogen (Lodwig *et al*. 2003) (Figure 1).

Organisms capable of fixing N_2 are diazotrophs, and these are found among all the microbial taxonomic groups including Proteobacteria, Actinobacteria, Cyanobacteria, and Endospora (Dyer, 2003). Diazotrophs can be divided into three groups. Free-living diazotrophs (e.g. *Azotobacter, Beijerinckia, Clostridium, Bacillus, Klebsiella, Chromatium,* and *Rhodospirillum*) live and fix N_2 independently of other organisms. Associative diazotrophs (*Azospirillum, Klebsiella, Enterobacter,* and *Alcaligenes*) contribute fixed nitrogen passively to plants while living in the rhizosphere environment. They do not induce any differentiated structures on the plants. Symbiotic diazotrophs infect host plants and induce nodule-like organs where they can convert N_2 to ammonia.

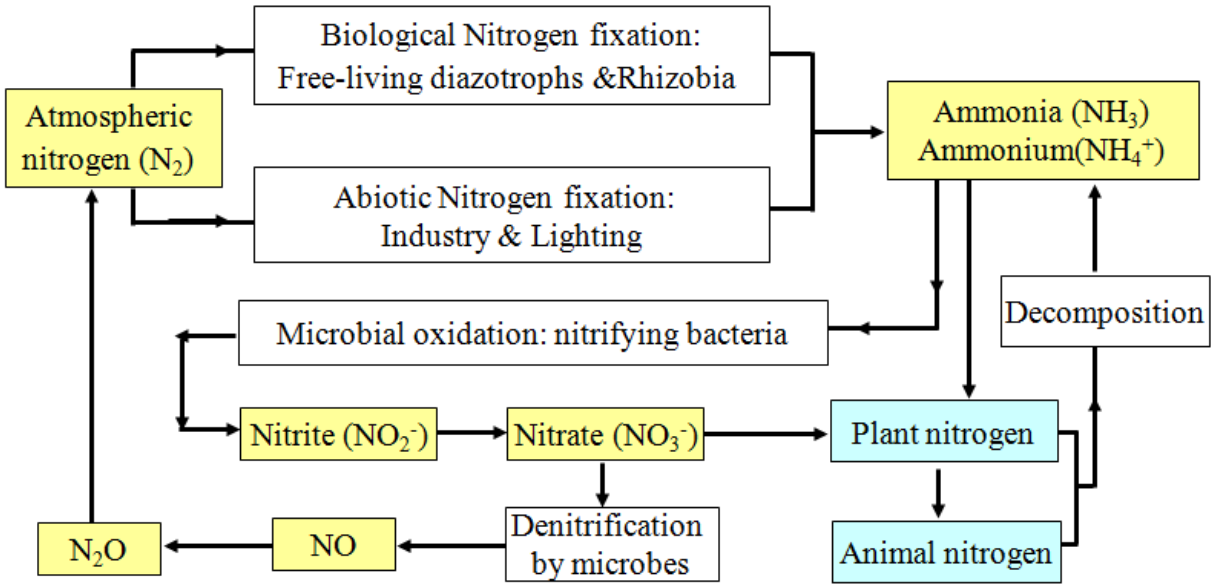

Figure 1 the Global Nitrogen Cycle

Biological nitrogen fixation is the major contributor of available nitrogen in the biosphere. This is performed predominately by rhizobia in symbiosis with legumes (e.g. *Rhizobium, Bradyrhizobium, Sinorhizobium, Azorhizobium,* and *Mesorhizobium*) and less so by free-living diazotrophs (e.g. *Azotobacter, Beijerinckia, Clostridium, Bacillus, Klebsiella, Chromatium, Rhodospirillum*).

Frankia species, the gram-positive filamentous actinomycetes, engage in a symbiosis with a broad-spectrum of non-leguminous actinorhizal plants from eight families: Betulaceae, Casuarinaceae, Coriariaceae, Datiscaceae, Elaeagnaceae, Myricaceae, Rhamnaceae and Rosaceae (Benson 1988; Benson and Silvester 1993; Clawson and Benson 1999; Guan *et al*. 1998). Rhizobia is a collective term that designates bacteria capable of forming N_2-fixing nodules with plant species belonging to the leguminous family, commonly known as legumes (e.g. beans, pea, soybean, clover and peanut) (MacLean *et al*. 2007; Spaink 2000). Cultivating legume crops in rotation with non-symbiotic crops reduces the detrimental environmental impacts of over-using artificial nitrogenous fertilizers and pesticides (Drinkwater *et al*. 1998; Vitousek *et al*. 1997).

1.2 Diversity of Legumes

Rhizobia form nodules on plants that are almost exclusively from the Leguminosae family, but a single non-legume taxon, *Parasponia* (Ulmaceae) was found to be nodulated by rhizobia (Lafay *et al*. 2006; Trinick and Hadobas 1989). The Leguminosae family contains more than 650 genera and 1800 species and is very diverse in morphology, habitat, and ecology. Their ability to establish nodules with rhizobia is mainly due to some genetic specialization of the legumes (Doyle, 2001). Legumes are divided into three subfamilies, Caesalpinioideae, Mimosoideae, and Papilionoideae. The Papilionoidea contains the largest total number of genera and contains most of the important agricultural crops (Doyle, 2001). Over 90% of the advanced subfamilies Mimosoideae and Papilionoideae are nodulated, while less than 30% species from the less specialized subfamily Caesalpinioideae are able to form nodules (De-Faria *et al.* 1989).

1.3 Diversity and Taxonomy of Rhizobia

Rhizobia are gram-negative bacteria that form N_2-fixing nodules on legumes. They are taxonomically and physiologically diverse. In the soil, they survive in the rhizosphere for years as non-symbiotic free-living rhizobia. The first species of rhizobia, *Rhizobium leguminosarum*, was identified in 1889, and all further species were placed in the *Rhizobium* genus (Sebbane *et al*. 2006).

The early taxonomic classification of rhizobia was according to the principle of cross-inoculation groupings, based on the ability of *Rhizobium* isolates to form nodules on a limited number of species of legumes related to one another (Fred *et al*. 1932). This taxonomical system would be perfect if the host-ranges of rhizobia reflected legume groups. However, this host-dependent classification was abandoned due to increased aberrant cross-infection and interchange of rhizobia among cross-inoculation groups (Graham *et al.* 1991). Later, rhizobia were classified by using the polyphasic approach which takes into account all available phenotypic and genotypic data, such as morphological and biochemical characteristics, genetic fingerprinting (Sebbane *et al.* 2006), fatty-acid methyl ester (FAME) analysis (Tighe *et al*. 2000), and 16S rRNA (rrs) gene-sequence analysis (Dupuy *et al*. 1994; Laguerre *et al*. 1994; Willems and Collins 1993; Yanagi and Yamasato 1993; Zahran *et al*. 2003; Zakhia and de 2006). The polyphasic taxonomy has resulted in continuous increase and distinction of new rhizobial genera and species (Vandamme *et al.* 1996). The currently recognized rhizobia consist of 98 species in 13 genera, and new additions occur almost every week (http://www.rhizobia.co.nz/taxonomy/rhizobia).

The majority of rhizobial species, belonging to the Rhizobiaceae family in the α-*Proteobacteria* subdivision, are divided into five different genera: the fast-or moderately-growing *Rhizobium, Sinorhizobium* and *Mesorhizobium,* and the slow-growing *Bradyrhizobium* and stem-nodulating *Azorhizobium* (Table 1). Interestingly, recently some isolates recovered from nodules on new legumes were identified in non-rhizobia genera, belonging to subdivisions of α- *Proteobacteria* (e.g. *Methylobacterium, Ochrobactrum, Devosia, Phyllobacterium,* and *Shinella*) (Jourand *et al*. 2004; Lin *et al*. 2008; Ngom *et al*. 2004; Rivas *et al*. 2002; Sy *et al*. 2001; Trujillo *et al*. 2005; Valverde *et al*. 2005) and β- *Proteobacteria* (e.g. *Burkholderia* and *Cupriavidus*) (Table 1 & Figure 2) (Chen *et al*. 2001; Moulin *et al*. 2001; Vandamme and Coenye 2004). It is apparent that these species obtained plasmids or islands containing essential genes required for symbiotic nitrogen fixation from typical rhizobia via multiple horizontal gene transfer events (Finan 2002; Giraud and Fleischman 2004; Suominen *et al*. 2001). This discovery indicated that rhizobial species are distributed within distantly related lineages of α- and β-*Proteobacteria* subdivisions instead of belonging to a homogenous clade (Moulin *et al*. 2001). Moreover, the same genus or even species in current classification often contains a mixture of rhizobia and non-rhizobial species such as photosynthetic bacteria and plant and animal pathogens. Also based on phylogenetic analysis we can observed that many non-symbiotic bacteria are closely related to rhizobia.

Table 1 Examples of rhizobial species and their host plant genera

α- Proteobacteria			
Family/*Genus*	*Species*	Host plant genera	Reference or source
Bradyrhizobiaceae			
Bradyrhizobium	*B. japonicum*	*Glycine, Vigna, and Macroptilium*	(Keyser *et al*. 1982)
	B. yuanmingense	*Lespedeza*	(Yao *et al*. 2002)
Brucellaceae			
Ochrobactrum	*O. lupini*	*Lupinus*	(Trujillo *et al*. 2005)
Hyphomicrobiaceae			
Azorhizobium	*A. caulinodans*	*Sesbania*	(Goormachtig *et al*. 1998)
	A. doebereinerae	*Sesbania*	(Maria de Souza *et al*. 2006)
Devosia	*D. neptuniae*	*Neptunia*	(Rivas *et al*. 2003)
Methylobacteriaceae			
Methylobacterium	*M. nodulans*	*Crotalaria*	(Jourand *et al*. 2005; Sy *et al*. 2001)
Rhizobiaceae			
Rhizobium	*R. leguminosarum bv trifolii*	*Trifolium*	(Leung *et al*. 1994; Reeve *et al*. 2010b)
	R. tropici	*Phaseolus, Leucaena*	*(Martinez-Romero et al. 1991)*
Sinorhizobium	*S. meliloti*	*Medicago, Melilotus, Trigonella*	*(Guo et al. 2005)*
	S. medicae	*Medicago*	*(Rome et al. 1996)*
Shinella	*S. kummerowiae*	*Kummerowia*	(Lin *et al*. 2008)
Phyllobacteriaceae			
Mesorhizobium	*M. loti*	*Lotus*	(Kumar *et al*. 2005)
	M. plurifarium	*Acacia, Prosopis, Leucaena*	(de *et al*. 1998)
Phyllobacterium	*P. trifolii*	*Trifolium, Lupinus*	(Valverde *et al*. 2005)
β- Proteobacteria			
Family/*Genus*	*Species*	Host plant genera	Reference or source
Burkholderiaceae			
Burkholderia	*B. phymatum*	*Machaerium, Mimosa*	(Elliott *et al*. 2007; Vandamme *et al*. 2002)
	B. tuberum	*Aspalathus,*	(Vandamme *et al*. 2002)
Cupriavidus	*C. taiwanensis*	*Mimosa*	(Chen *et al*. 2001)

Figure 2 Unrooted phylogenetic tree of 16S rDNA sequences from selected α-, β-, and γ-*proteobacteria*.

Genera in bold font contain rhizobia. Rhizobial species or strains whose genomes have been fully sequenced are indicated in parentheses. Genome sequences have been published for *Cupriavidus taiwanensis* (Amadou *et al*. 2008), *Mesorhizobium loti* (Kaneko *et al*. 2000), *Sinorhizobium meliloti* (Galibert *et al*. 2001), *Sinorhizobium medicae (Reeve et al. 2010a)* , *Rhizobium leguminosarum* (Young *et al*. 2006), *Rhizobium etli* (Gonzalez *et al*. 2006), *Azorhizobium caulinodans* (Lee *et al*. 2008), *Sinorhizobium sp*. strain NGR234 (Schmeisser *et al*. 2009), *Bradyrhizobium japonicum* (Kaneko *et al*. 2002) and *Bradyrhizobium sp.* BTAi1 and ORS278 (Giraud *et al*. 2007). Accession numbers for unpublished genomes: CP001043-46 (*Burkholderia. phymatum*) and CP001349-56 (*Methylobacterium, nodulans*). (Masson-Boivin *et al*. 2009)

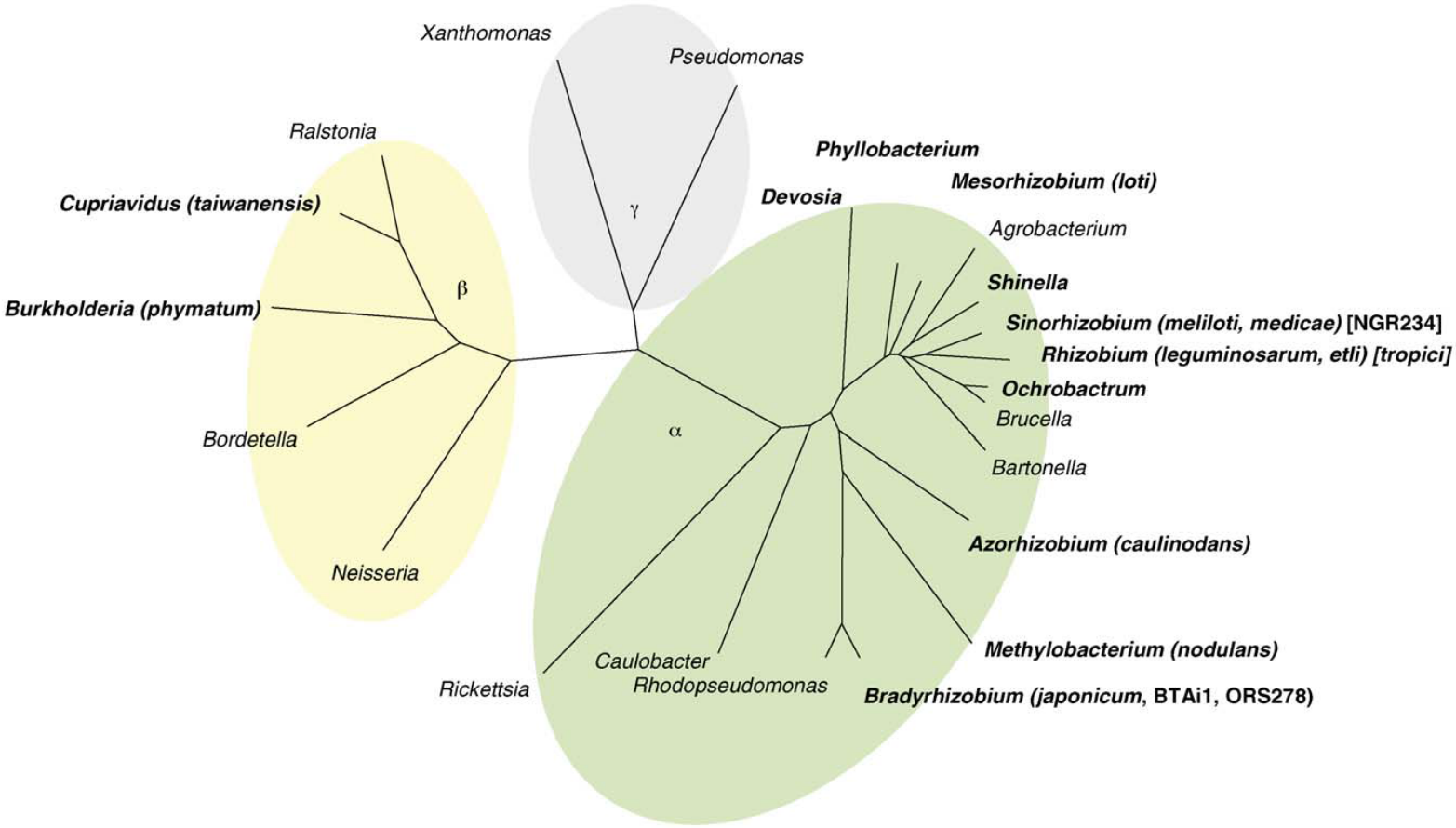
Xanthomonas
Pseudomonas
γ
Ralstonia
Cupriavidus (taiwanensis)
β
Burkholderia (phymatum)
Bordetella
Neisseria
Phyllobacterium
Mesorhizobium (loti)
Devosia
Agrobacterium
Shinella
Sinorhizobium (meliloti, medicae) [NGR234]
Rhizobium (leguminosarum, etli) [tropici]
Ochrobactrum
Brucella
α
Bartonella
Azorhizobium (caulinodans)
Methylobacterium (nodulans)
Caulobacter
Rhodopseudomonas
Rickettsia
Bradyrhizobium (japonicum, BTAi1, ORS278)

For example, *M. nodulans* was the only rhizobial species identified in the *Methylobacterium* genus which contains saprophytic bacteria (Table 1 & Figure 2) (Jourand *et al*. 2004; Kaparullina *et al*. 2011; Renier *et al*. 2008), whereas the *Cupriavidus taiwanensis* species includes strains isolated from both nodules and clinical samples (Table 1 & Figure 2) (Amadou *et al*. 2008).

Rhizobial species vary tremendously in the degree of host specificity. Some strains have highly specific narrow host range, for example, *Sinorhizobium meliloti* which only forms symbiotic relationship with legumes from the genera *Medicago, Melilotus* and *Trigonella* (Guo *et al*. 2005), while others have a very broad host range, such as *Sinorhizobium sp*. NGR234, able to establish symbiosis with legumes from over 112 genera as well as the non-legume *Parasponia* (Pueppke and Broughton 1999). Isolates recovered and characterized from legumes belonging to a wider range of genera will certainly reveal even greater diversity of rhizobia.

1.4 The Structure of the Rhizobial Genomes

Since the first complete genomic sequence of *Haemophilus influenzae* (Fleischmann *et al*. 1995), many bacterial genomes have been sequenced and analyzed. The complete sequence of the symbiotic plasmid of *Sinorhizobium sp*. NGR234 was the first genomic project among the genera of rhizobia (Freiberg *et al*. 1996), and the completion of the genomes of *M. loti* (Kaneko *et al*. 2000), *S. meliloti* (Galibert *et al*. 2001) and *B. japonicum* (Kaneko *et al.* 2002) are important landmarks in symbiotic N_2-fixation research. Since then, the number of complete rhizobial genome sequences has

been increased to 26, including 23 species in 5 genera from the α-*Proteobacteria* and 2 species in 2 genera from the β-*Proteobacteria*.

Rhizobial species tend to have larger genomes and their genomic architecture varies considerably (Table 2). The *B. japonicum,* chromosome is 9.2Mb in size (Bentley and Parkhill 2004) and many rhizobial genomes (5-9Mb) are multipartite with main circular chromosomes and additional plasmid(s) which are smaller in size (Table 2). Most rhizobial species from the α - subdivision contain one chromosome, while two rhizobial species belonging to β- subdivision carry two chromosomes (Table 2). *Rhizobium leguminosarum* and *Rhizobium etli* have six plasmids*; Sinorhizobium meliloti and Mesorhizobium loti* have two plasmids. *Cupriavidus. taiwanensis* has one plasmid, while the genomes of two *Bradyrhizobium* and one *Azorhizobium* species do not contain plasmids. In species of *Rhizobium leguminosarum*, one isolate, *R. leguminosarum bv viciae 3841,* has six plasmids, whereas another isolate, *R. leguminosarum bv trifolii WSM1325,* contains five plasmids (Table 2).

A large inventory of genes are presumably required by the rhizobial species to maximize the survival of free-living cells in the complex and heterogeneous soils, establish symbiosis with a host plant, and carry out nitrogen fixation in plant nodules. It was proposed that the rhizobial genomes were gradually expanded, primarily through lateral gene transfer and gene duplication, to adapt to stresses caused by the multiphasic lifestyle (Batut *et al*. 2004). The majority of symbiotically related genes (*nod*, *nif* and *fix*) in rhizobial species are normally clustered on the large plasmids (e.g. *S. meliloti, R. etli, R. leguminosarum,* and *Sinorhizobium* sp. NGR234) or within genomic islands, called

symbiosis islands (e.g. *M. loti* and *B. japonicum*) (Barnett *et al*. 2001; Freiberg *et al*. 1997; Galibert *et al*. 2001; Gonzalez *et al*. 2003; Gonzalez *et al*. 2006; Kundig *et al*. 1993; Sullivan and Ronson 1998; Young *et al*. 2006). It was presumed that non-rhizobial species acquired capabilities of symbiotic nitrogen fixation via one step. A nonsymbiotic strain of *M. loti* was reported to show symbiotic capabilities after its genome accepted a symbiosis island from *M. loti* strain ICM3153 (Sullivan and Ronson 1998).

Generally, rhizobial genomes are considered to be highly dynamic structures due to the distribution of insertion sequence (IS) elements and transformation of large plasmids. IS elements are mobile genetic elements commonly present in bacterial genomes. In rhizobial genomes, they often appear within the symbiotic clusters. In the genomes of *M. loti* and *B. japonicum*, most of transposase genes and IS-related sequences were found within the symbiotic islands (Gottfert *et al*. 2001; Kaneko *et al*. 2000; Kaneko *et al*. 2002; Sullivan *et al*. 2002). Also, IS elements were reported to be abundant in the large plasmid involved in symbiotic functions, such as pSymA of *S. meliloti* (Galibert *et al*. 2001), pNGR234a of *Sinorhizobium* sp. NGR234 (Viprey *et al*. 2000), and p42d of *R. etl*i (Gonzalez *et al*. 2006). The presence of sequences potentially related to conjugal transfer, such as *oriTs* (original of transfer) and *tra* (transfer) gene, in large plasmids of *S. meliloti, R. etli*, and *R. leguminosarum* indicates the potential ability to be transferred among bacteria via conjugation. Two types of rhizobial plasmid transfer systems have been documented: a quorum sensing (QS) regulated conjugal transfer system and a RctA-repressed conjugal transfer system (Danino *et al*. 2003; He *et al*. 2003; Perez-Mendoza *et al*. 2004; Sepulveda *et al*. 2008; Tun-Garrido *et al*. 2003; Wilkinson *et al*. 2002).

Table 2 Architecture of selected rhizobial genomes

α- Proteobacteria				
Genus/Species	Gnomic Architecture(Mb)	Total size (Mb)	No. of ORFs	Reference or source
Azorhizobium				
A. caulinodans ORS571	Chr(5.37)	5.37	4782	(Tsukada *et al*. 2009)
Bradyrhizobium				
B. japonicum USDA110	Chr(9.11)	9.11	8373	(Kaneko *et al*. 2002)
Bradyrhizobium sp. ORS 278	Chr(7.46)	7.46	6818	(Giraud *et al*. 2007)
Bradyrhizobium sp. BTAi1	Chr(8.26), pBBTA01(0.23)	8.49	7807	(Giraud *et al*. 2007)
Mesorhizobium				
M. loti MAFF303099	Chr(7.04), pMLa(0.35), pMLb(0.21)	7.6	7333	(Kaneko *et al*. 2000)
Rhizobium				
R. etli CFN 42	Chr(4.38), p42a(0.19), p42b(0.18), p42c(0.25), p42d(0.37), p42e(0.51), p42f(0.64)	6.53	6093	(Gonzalez *et al*. 2006)
R. leguminosarum bv. trifolii WSM1325	Chr(4.77), pR132501(0.83), pR132502(0.66), pR132503(0.52), pR132504(0.35), pR132505(0.3),	7.42	7294	(Reeve *et al*. 2010b)
R. leguminosarum bv viciae 3841	Chr(5.1), pRL7(0.15), pRL8(0.15), pRL9(0.35),pRL10(0.49), pRL1(0.68), pRL12(0.87),	7.75	7348	(Young *et al*. 2006)
Sinorhizobium				
S. meliloti 1021	Chr(3.65), pSymA(1.35), pSymB(1.68)	6.69	6292	(Galibert *et al*. 2001)
S. medicae WSM419	Chr(3.78), pSMED01(1.57), pSMED02(1.25), SMED03(0.22),	6.82	6585	(Reeve *et al*. 2010a)
Sinorhizobium sp. NGR234	Chr(3.93), pNGR234a(0.54), pNGR234b(2.43)	6.89	6473	(Schmeisser *et al*. 2009)
β- Proteobacteria				
Genus/Species	Gnomic Architecture(Mb)	Total size (Mb)	No. of ORFs	Reference or source
Burkholderia				
B. phymatum STM815	Chr1(3.48), Chr2(2.7) pBPHY01(1.91), pBPHY02(0.6)	8.68	7899	(DOE Joint Genome Institute, 2008)
Cupriavidus				
C. taiwanensis LMG 19424	Chr1(3.42), Chr2(2.5), pRALTA(0.56)	6.48	6064	(Amadou *et al*. 2008)

Comparative genomic analysis indicates that rhizobial genomes are abundant in transport, regulatory and stress-related systems, which are required for survival in complex soil environments as free-living cells (Boussau *et al*. 2004). For instance, the genomes of both *Bradyrhizobium* Sp. strains, BTAi1 and ORS278, are very complex and amazingly abundant in genes involved in various metabolic pathways, which enable these strains to grow as heterotrophs, autotrophs, and phototrophs in the external environments and also enter into symbiosis with a number of legumes from the genus *Aeschynomene* (MacLean *et al*. 2007). Rhizobial genomes may also contain one or more nonsymbiotic accessory plasmids, such as the 144 kb pSmeSM11a which was isolated from *S. meliloti*. Most genes in this accessory plasmid are involved in DNA replication, recombination, and repair, and also include genes encoding various metabolic enzymes and transport system (Stiens *et al*. 2006). Therefore, the accessory plasmids may have a function to improve the overall fitness of rhizobia during growth as free-living cells in the complex soil environment.

1.5 Rhizobium-Legume Symbiosis

1.5.1 The Infection Process and Nodule Organogenesis

The Rhizobium-legume symbiosis is a complex process regulated by the concerted signal exchange between the two interacting species. In the rhizosphere plant root exudates include high levels of nutrients, such as sugars, amino acids and various dicarboxylic acids and these are utilized by rhizobia for growth. Rhizobia move toward and locate on the surface of young growing root hairs (Figure 3A) (Caetano-Anolles *et al*. 1992; Dowling and Broughton 1986; Gulash *et al*. 1984). Initially, the loose attachment

of compatible rhizobia to the root hair surface may be caused by the specific binding between host plant lectins and particular bacterial exopolysaccharides (EPS), mediating certain specificity in the rhizobium-legume symbiosis (Fraysse *et al*. 2003; Williams *et al*. 2008). Later, aggregation of additional rhizobial cells at the adhesion site leads to formation of the rhizobial biofilms on the root surface (Danhorn and Fuqua 2007; Fujishige *et al*. 2006).

Flavonoid signal molecules released by the host plant cause a transcriptional response in compatible rhizobia in the rhizosphere. The nodulation (nod) genes are induced and the resulting Nod proteins are responsible for the synthesis and secretion of lipo-chitooligosaccharide signal molecules (Nodulation Factors, NF) that are perceived by the host plant (Capela *et al*. 2005; Perret *et al*. 2000). The NFs induce expression of plant genes involved in early nodulation, which make the young root hair curl and deform sufficiently to trap the attached rhizobial cells in a pocket of the host cell well (Figure 3B&C) (Limpens and Bisseling 2003; Van Brussel *et al*. 1986). After entrapment, a local degradation of the root hair cell wall and invagination of the plasma membrane initiate an infection thread, which grows inwardly by continuously depositing new cell well materials at the growing tip and reorganizing the plant cytoskeleton (Newcomb *et al.* 1979; Turgeon and Bauer, 1982 &1985). The infection thread is filled with rhizobia which proliferate in the growing tip, using nutrients provided by the host plant (Figure 3D). Concomitant with root hair infection, NFs activate mitosis of cortical cells below the sites of infection to form a nodule primordium (Figure 3D) (Newcomb, 1981; Vasse and Truchet, 1984; Wood and Newcomb, 1989).

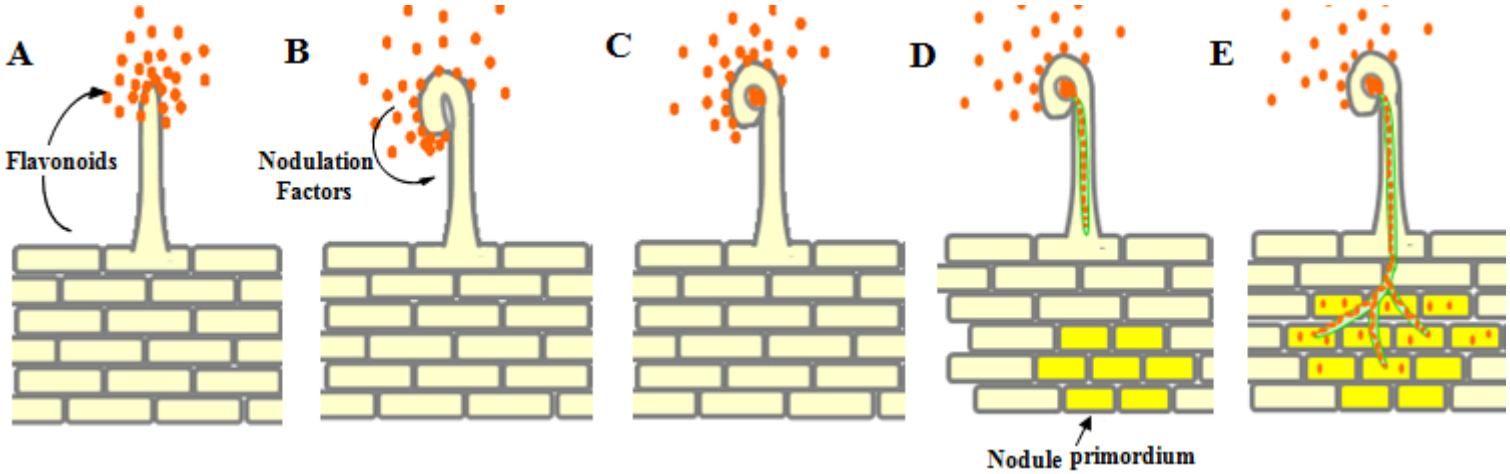

Figure 3 Schematic model of Nodulation Factor (NF)-induced infection by rhizobia.

(A) Rhizobia (indicated as red dots) move toward and attach to the surface of young growing root hairs. Specific flavonoid signals released from host legume plant were perceived by rhizospheric rhizobia. (B) The perception of rhizobia-derived NFs make root hairs curl and deform. (C) The root hairs are curling enough to trap a few attached rhizobia within the pocket of the curl. (D) An infection thread is formed and filled with proliferating rhizobia. Particular cortical cells below the sites of infection divide to form a nodule primordium. (E) The infection thread grows toward the developing nodule primordium and rhizobial cells are released into the cytoplasm. Picture adapted from: (Batut *et al*. 2004)

Then, the infection threads penetrate several layers of underlying root cortex toward the developing nodule primordia where rhizobial cells are released into the cytoplasm via an endocytotic–type mechanism that engulfs the rhizobial cells in a plant-derived membrane (Figure 3E). It results in the formation of organelle-like structures, referred to as symbiosomes, within which one or several differentiated rhizobial cells (bacteroids) fix N_2 (Ferguson *et al*. 2010; Gibson *et al*. 2008; Oldroyd and Downie 2008; Perret *et al*. 2000; van and Vanderleyden 1995).

Most of the temperate legumes studied so far are invaded by rhizobia via NF-induced formation of infection threads through root hairs (Gage 2004; Gibson *et al*. 2008). However, many tropical or subtropical legumes were reported to be invaded by rhizobia via cracks in the epidermis, a process called “crack entry” (Boogerd and van Rossum, 1997; Sprent 1989). It seemed that the mechanism for “crack entry” invasion varies according to the legume species (Bonaldi *et al*. 2011; van and Vanderleyden 1995). In *Sesbania rostrata* (Capoen *et al*. 2010) and *Neptunia natans* (Subba-Rao *et al*, 1995), the invasion is initiated by direct intercellular infection with rhizobial cells that proliferate highly to fill wide intercellular spaces. The spaces then extend inward to form infection threads growing toward the meristematic zone (nodule primordium) induced in cortex. While in legumes such as *Stylosanthes spp*. and *Arachis hypogeal*, rhizobium invasion does not lead to the formation of infection thread and the distant induction of a nodule primordium. Instead, rhizobial cells infect host plants directly via epidermal fissures caused by the growth of lateral roots and spread intercellularly through the middle lamella. Some cortical cells are then directly invaded by the intercellular rhizobia via endocytosis.

The newly infected cortical cells divide repeatedly to form a nodule (Chandler, 1978 & 1982).

It was a long-held belief that flavonoid-induced lipo-chitooligosaccharides (LCO) released by rhizospheric rhizobia are essential for the nodulation of legumes. Two recently identified rhizobial species, *Methylobacterium nodulans* and *Cupriavidus taiwanensis,* which are phylogenetically distant, utilize the same NF-dependent strategy to infect host plants and provoke nodule morphogenesis (Amadou *et al*. 2008; Masson-Boivin *et al*. 2009). However, some studies recently indicated that a group of photosynthetic *Bradyrhizobium* strains are able to use a NF-independent strategy to establish symbiosis with some *Aeschynomene* species (Bonaldi *et al*. 2011; Masson-Boivin *et al*. 2009). Two *Bradyrhizobium sp*. strains, BTAi1 and ORS278, are able to induce stem- and root- nodules on a group of *Aeschynomene* plants. However, both of them are unable to produce lipochitooligosaccaridic NFs and their genomes lack *nodABC* genes (Giraud *et al*. 2007). In *Bradyrhizobium* species, strains able to produce NFs have a broader host range, involving all stem-nodulated *Aeschynomene* species, compared with *nod*-lacking strains which only nodulate a small group of *Aeschynomene* species, including *A. sensitiva* and *A. indica* (Giraud and Fleischman 2004). Deletion of *nod* genes prevents *Bradyrhizobium sp* ORS285 from nodulating *Aeschynomene* species except for *A. sensitiva* and *A. indica* (Giraud *et al*. 2007). Therefore, Nodulation Factors are not absolutely required by rhizobia to initiate symbiosis with host plants. However, it is still quiet common for rhizobia to infect and nodulate legumes via NF-dependent pathway.

1.5.2 Flavonoid: the Early Signal from Legumes to Rhizobia

Flavonoids are produced from the phenylpropanoid pathway of plants. The common structure of the compounds consists of two aromatic rings and a heterocyclic pyran or pyrone ring (Figure 4C). The specific modifications of the basic structure group flavonoids into several classes, including flavones, flavonols, flavanones, isoflavones, flavanols, and anthocyanidines (Harborne and Williams 2000; Harborne and Williams 2001). So far, more than 4000 different flavonoids have been found in vascular plants. However, only a portion of them are involved in legume-rhizobium symbiosis (Perret *et al*. 2000). The roots of a legume plant appeared to exude a diverse cocktail of flavonoids into the soil. However, only compatible flavonoids can be sensed by rhizobia within rhizosphere. Flavonoids are involved in setting up certain aspects of host specificity ahead of the physical interaction between rhizobia and roots of host legumes (Hirsch *et al*. 2001; Parniske and Downie 2003; Perret *et al*. 2000). Flavonoids induce expression of genes required for Nodulation Factor synthesis via activating the regulatory protein NodD (Figure 4A). In addition to the flavonoids, some other non-flavonoid molecules (e.g. betains, jasmonate, vanillin, chlorogenic acid, tetronic acid, etc.) have been identified as inducers of *nod* gene expression, but they function at much higher concentrations than flavonoids (Figure 4A) (Cooper 2007; Kape *et al*. 1991; Spaink 2000).

1.5.3 Nodulation Factor: the Early Signal from Rhizobia to Legumes

Nodulation Factors (NF) trigger multiple responses in host legumes, including altered root hair growth, initiation of cell division, and expression of nodule-specific genes in host legumes. The structure of NF from *S. meliloti* was reported in 1990

(Lerouge *et al*. 1990) and since then NFs from more than 30 rhizobial stains have been studied in detail. Broad host range rhizobial species likely produce a mixture of NF compounds, from 2 to 60 distinct molecules (Perret *et al*. 2000).

NFs comprise an oligosaccharide backbone of three or five β-1-4-linked N-acetyl glucosamine residues with fatty acyl chain (typically 16-18 carbons) attached to the terminal glucosamine (Figure 4B) (van and Vanderleyden 1995). The NF backbone is generated by enzymes encoded by three *nod* genes, *nodA* (acyl-transferase), *nodB*(deacetylase), and *nodC* (N-acetylglucosamine transferase), which are conserved in most rhizobial strains (Figure 4A) (Hartwig *et al*. 1990; Roche *et al*. 1996; van and Vanderleyden 1995). Rhizobial strains with *nodABC* mutations are unable to initiate any symbiotic reaction in host legumes, including root hair curling, infection thread formation, cortical cell divisions, and nodule formation (Long 1989). In addition to the common *nod* genes, many host specific *nod (hsn*) genes, including *nod* genes and some other so-called *nol* and *noe* genes, are responsible for the diversity of NFs from different rhizobia species via introducing various host-specific modifications to this conserved backbone (Figure 4A&B), including the presence or absence of strain-specific substituents (e.g. sulphate, methyl, carbamoyl, acetyl, fucosyl, arabinosyl, etc.), variation of the structure of fatty acyl moiety attached, and the presence and the absence of special α, β -unsaturated fatty acyl moieties (Long 1996; Spaink 2000; van and Vanderleyden 1995). Host-specific *nod* (*hsn*) genes are not conserved among rhizobia.

Figure 4 Schematic model of Legume-Rhizobium symbiosis

A). Signal exchanges in nodulation (Masson-Boivin *et al*. 2009). Flavonoids released by host legume activate NodD positive regulators that induce the expression of nodulation genes to synthesize the Nodulation Factors (NFs) which in turn initiate the infection of legume roots by rhizobia and the formation of root nodules. (a) Several non-flavonoid compounds (e.g. betains, jasmonate, vanillin, etc) identified in root exudates only have the capacity to induce the expression of *nod* genes at the concentrations which are much higher than flavonoids. (b) The *nodABC* genes are conserved in all rhizobia and responsible for the synthesis of the NF backbone. Host-specific *nod* (*hsn*) genes, including *nod, nol*, and *noe* genes, are involve in the addition of various modifications to the backbone of NFs. (c) In addition to NodD proteins, several other regulators (e.g. SyrM, NodV/NodW, NolA, NolR) are involved in modulating NF synthesis in various rhizobial species.

B). General structure of nodulation Factors (NF) synthesized by rhizobia (Spaink 2000). The occurrence of substituents (R1-R9) is based on stain specificity.

C). Structures of the major classes of flavonoids

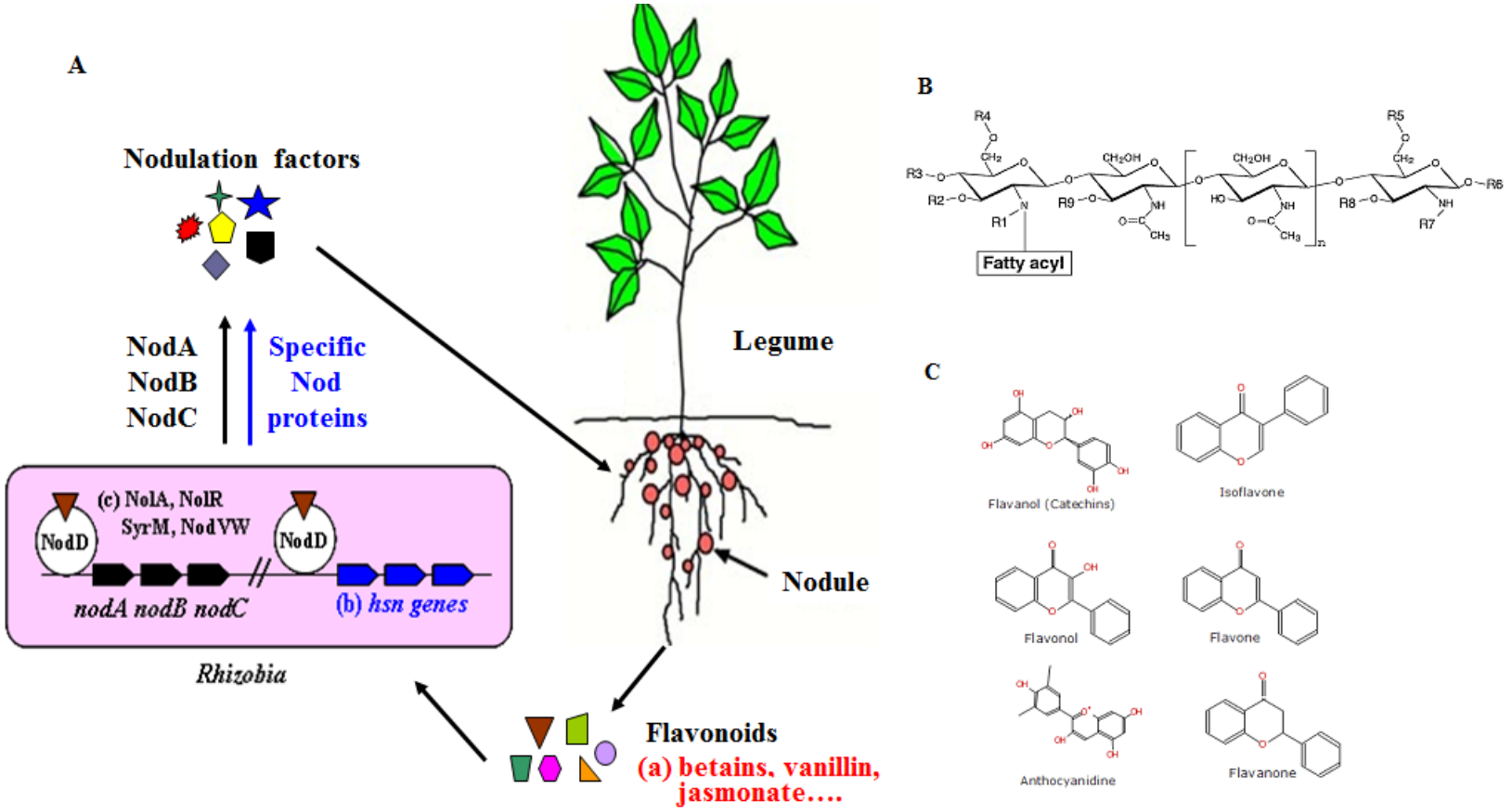
A
Nodulation factors
NodA
NodB
NodC
Specific
Nod
proteins
(c) NolA, NolR
SyrM, NodVW
NodD
NodD
nodA nodB nodC
(b) hsn genes
Rhizobia
Legume
Nodule
Flavonoids
(a) betains, vanillin,
jasmonate....
B
Fatty acyl
C
Flavanol (Catechins)
Isoflavone
Flavonol
Flavone
Anthocyanidine
Flavanone

Recently studies of several legume plants including *M. truncatula and L. japonicum* indicated that host plants perceive the NFs released from rhizobia via serial intracellular signaling cascades. NFs are first sensed by LysM receptor-like kinases (LsyM-RLKs) in the plasma membrane of root epidermal cells (Madsen *et al*. 2003; Radutoiu *et al*. 2003). The activation of LsyM-RLKs then results in changes in the growth of root hairs and calcium spiking in the nucleus through the putative cation channels in the nuclear membrane (Endre *et al*. 2002; Stracke *et al*. 2002). In the nucleus, the calcium-spiking signal is perceived by a calcium- and calmodulin-dependent protein kinase (CCaMK) (Levy *et al*. 2004; Mitra *et al*. 2004). The activated CCaMK, together with various transcriptional regulators such as nodulation signaling pathway1 (NSP1), NSP2, Ets2 repressor factor (ERF) and so on, regulates the expression of early nodulin genes (*ENOD*s) (Smit *et al*. 2005). The perception and transduction of NF signals also initiate cell division within the nodule meristem via accumulating the plant hormones cytokinin and auxin in underlying cortical cells (Tirichine *et al*. 2007; Wasson *et al*. 2006). Finally, all responses to the NF signals trigger nodule organogenesis.

1.5.4 Root Nodule Structure

During nodule organogenesis, temporal and spatial variations in gene expression elicit vast developmental changes in the legume host plant, most of which result in the micro aerobic environment that is a good fit for symbiotic nitrogen fixation (Lohar *et al*. 2006). Also, it is common for the cortical cells within the nodules to replicate their genome without mitosis and cytokinesis. The cortical cells with multi-copy genomes in

nodules typically have larger size, extra organelle and higher metabolic activity, which is suitable for bacteroid accommodation (Vinardell *et al*. 2003).

Nodules induced by rhizobia on legumes are divided into indeterminate and determinate morphological groups according to their meristem growth pattern. The nodule type is determined by the host legume. Indeterminate nodules (Figure 5A) are typically cylindrical in shape and maintain an active apical meristem derived from the cells in the inner cortex (Ferguson *et al*. 2010). They are formed on most temperate legumes such as *Pisum* (pea), *Medicago* (alfalfa), *Trifolium* (clover), and *Vicia* (vetch) (van and Vanderleyden 1995). The persistent activity of the meristem keeps nodules growing continuously by adding new cells to the distal end. The newly added cells are infected by rhizobia released from infection threads. The different stages of development/symbiosis can be seen in longitudinal sections from a single mature indeterminate nodule (Figure 5A) (Nap and Bisseling 1990; van and Vanderleyden 1995). From the distal end of nodule to the root, these sections have been named: 1) the active meristem (Zone I) where new nodule tissue is formed and will later differentiate into the other zones of the nodule; 2) the invasion zone (Zone II) where rhizobia are released from infection threads and plant cells increase in size and stop mitotic divisions; 3) the interzone (Zone II/III) where released rhizobia invade plant cells and begin differentiating into nitrogen-fixing bacteroids; 4) the nitrogen fixation zone (Zone III) where newly differentiated bacteroids fix nitrogen actively; 5) the senescent zone (Zone IV) where the plant cells and bacteroids are being degraded (Gibson *et al*. 2008; Patriarca *et al*. 2002;

Vasse *et al*. 1990). Thus, symbiotic nitrogen fixation is almost simultaneous with the growth of indeterminate nodules.

Determinate nodules (Figure 5B) are typically spherical in shape and found in most tropical legumes including *Glycine* (soybean), *Phaseolus* (common bean), *Lotus*, and *Vigna* (van and Vanderleyden 1995). The basal meristem of determinate nodules is induced in the root outer cortex where rhizobia released from infection threads invade actively dividing meristematic cells. Infected cells lose meristematic activity after rounds of cell division in a short period. Synchronous differentiation of infected cells results in the formation of a nitrogen-fixing central tissue in nodules (Newcomb, 1981). The further growth of nodules depends on increase in cell size rather than in cell number. Thus, only a relatively homogenous population of nitrogen fixing symbiosomes can be observed in a mature determinate nodule at any particular moment (Figure 5B) (Cermola *et al*. 2000; Gibson *et al*. 2008; Patriarca *et al*. 2002).

1.5.5 Bacteroid Differentiation

Rhizobia released into plant cortical cells within nodules, differentiate into distinct N_2-fixing forms, referred as bacteroids. Bacteroids release the fixed nitrogen to the host plants and in return, the host plants provide bacteroids with dicarboxylates as a source of energy to drive symbiotic nitrogen fixation.

The first report about bacteroid differentiation was presented by Beijernick in 1888. He found that rod-shaped rhizobia were transformed to Y-shaped cells surrounded by a plant-derived membrane (Oke and Long 1999b).

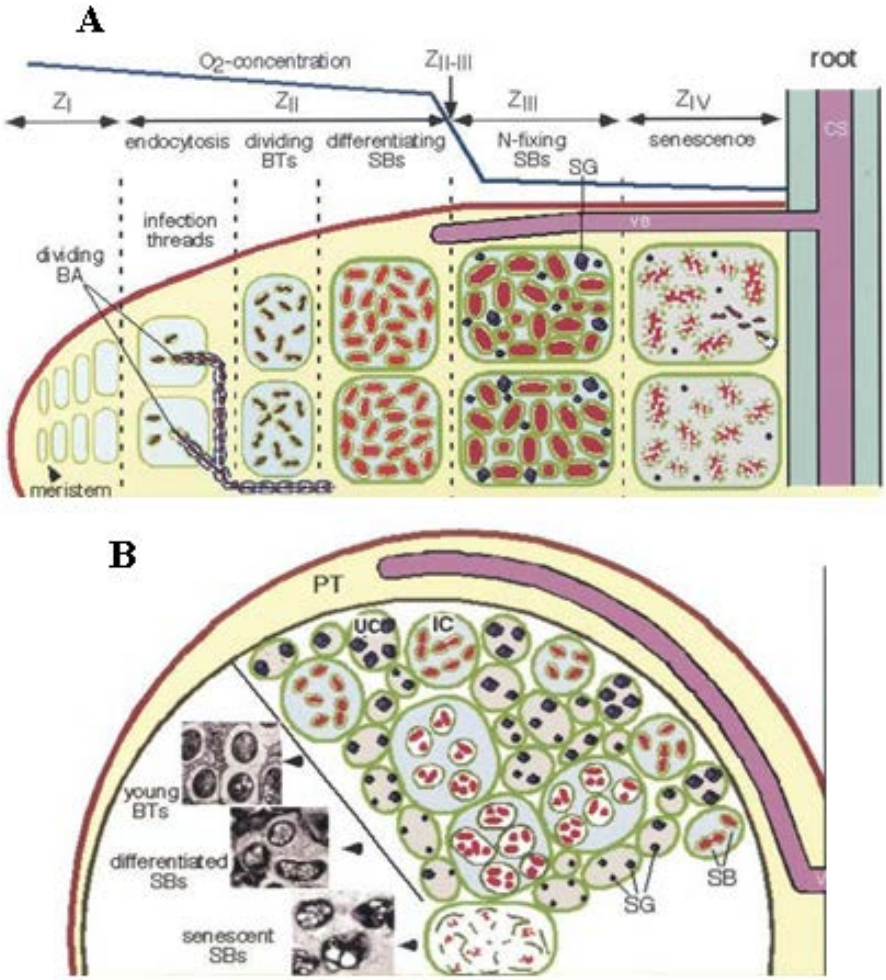

Figure 5 Diagram of nodule structure

A) The indeterminate elongated nodule. BA, bacteria; BTs, bacteroids; SBs, symbiosomes; SG, starch grain; CS, central stele; VB, vascular bundle. The nodule zones (Z_I -Z_{IV}) represent different stage of development/symbiosis. B) The determinate globose nodule. CS, central stele; VB, vascular bundle; PT, peripheral tissue; BTs, bacteroids; SBs, symbiosomes; SG, starch grain; IC, invaded cell; UC, uninvaded cell. (Patriarca *et al*. 2002)

The pattern of bacteroid differentiation is mainly under the control of the host plants. In indeterminate nodules, rhizobial cells divide one or a few times in plant cells whose mitotic division is inactivated. The rhizobia then undergo morphological changes; for example, *S. meliloti* alfalfa bacteroids are four to seven times longer than vegetative cells, while *R. leguminosarum bv. trifolii* bacteroids are distorted to Y shapes in clover nodules (Oke and Long 1999b). In determinate nodules, the released rhizobial cells divide many times within self-dividing plant cells and may remain the same size or enlarge after differentiation (Oke and Long 1999b). Several genes that may be involved in bacteroid differentiation have been reported in different rhizobial strains. Some of the genes are related to nutritional uptake, such as *dctA* gene which codes a transporter for dicarboxylic acids. Mutants in this gene result in a fix deficiency (Finan *et al*. 1983; Ronson *et al*. 1981). Also, nodules induced by mutants with deletion of *glmS* gene which encodes glucosamine synthase tend to senesce at earlier stage (Marie *et al*. 1992). Another important gene required by bacteroid formation is *bacA*, disruption of which hinders bacteroid differentiation (Glazebrook *et al*. 1993; Ichige and Walker 1997).

In nodules, bacteroids are surrounded by a plant derived membrane, called the peribacteroid membrane (PBM), which separates bacteroids from the plant cytosol, with the intervening peribacteroid space (PBS) (Robertson *et al*. 1978). This newly formed structure is referred to as a symbiosome (Whitehead & Day, 1997). In indeterminate nodules, bacteroids and symbiosomes divide synchronously, which mostly results in single bacteroid within individual symbiosomes (Figure 5A). However, in determinate nodules, individual symbiosomes typically carry many bacteroids because bacteroids

undergo rounds of cell-division within the PBM (Figure 5B) (Prell and Poole 2006). Bacteroid differentiation elicits global changes in gene expression and genes needed for micro aerobic respiration and nitrogen fixation are up-regulated whereas genes related to cell division and growth are down-regulated (Becker *et al*. 2004; Capela *et al*. 2006; Karunakaran *et al*. 2009; Oke and Long 1999a; Prell and Poole 2006).

1.6 Symbiotic Nitrogen Fixation

Nitrogen fixation is catalyzed by the enzyme nitrogenase in a high energy requiring reaction. 16-18 ATP molecules and eight electrons are consumed in the reduction of N_2 to ammonia and the associated reduction of $2H^+$ to H_2 (Roberts and Brill 1981). It is estimated that about 5-10 grams of reduced carbon are consumed for each gram of N_2 fixed (Phillips 1980). The majority of the ammonia produced is transferred to the legume hosts, where it is assimilated into amino acids, nucleotides and other plant components. However, some ammonia seems to be assimilated by bacteroids themselves (Lodwig and Poole 2003). Activities of two potential ammonia-assimilating enzymes, alanine dehydrogenase (EC 1.4.1.1) and glutamate dehydrogenase (EC 1.4.1.2), are detected at high levels in mature bacteroids of *S. meliloti* (Miller *et al*, 1991).

1.6.1 Nitrogenase Structure and Mechanism in Rhizobia

Molybdenum (Mo)-dependent nitrogenase, found in most rhizobia, is a structurally and mechanistically conserved enzyme system composed of two separable component proteins: dinitrogenase (Mo-Fe protein) and dinitrogenase reductase (Fe protein) (Halbleib and Ludden 2000). Dinitrogenase is a Mo-Fe protein of about 220kDa, containing two α-subunits and two β-subunits. Each αβ pair has one P-cluster and a MoFe

cofactor, which act as the catalytic site for N_2 reduction (Chan *et al*. 1993; Kim and Rees 1992). Dinitrogenase reductase is a homodimeric Fe protein (60kDa) that contains a single 4Fe-4S cluster and two MgATP binding sites (Georgiadis *et al*. 1992). N_2- fixation is initiated when the Fe protein first receives an electron from a low redox potential reductant (ferredoxin or a flavodoxin), and this switches the Fe-protein [4Fe-4S] cluster from the 2^+ reduction state to the 1^+ state (Chan *et al*. 2000; Georgiadis *et al*. 1992). Two Fe proteins with reduced $[4Fe\text{-}4S]^{1+}$ clusters and two bound MgATP associate with one Mo-Fe protein at αβ interface to form a complex, which turns on the activity of nitrogenase (Chan *et al*. 2000; Rees and Howard 2000). A single electron is then transferred from the Fe protein $[4Fe\text{-}4S]^{1+}$ cluster to the MoFe protein P-cluster via hydrolysis of MgATP to MgADP. In the MoFe protein, the electron is finally passed from the P-cluster to the FeMo-cofactor, where bound substrates are reduced. After electron transfer and MgATP hydrolysis, MoFe protein and Fe protein with an oxidized $[4Fe\text{-}4S]^{2+}$ cluster and two bound MgADP draw apart from each other, which turns off nitrogenase activity (Einsle *et al*. 2002; Hageman and Burris 1978; Seefeldt *et al*. 2004).

Nitrogenase is irreversiblely inactivated by oxygen due to the sensitivity of a surface-exposed [4Fe-4S] cluster crossing over the two subunits of Fe protein dimer. The legume-rhizobium symbiosis has evolved several strategies to provide a micro aerobic environment to reach the balance between the aerobic requirements of bacteroid metabolism and the oxygen sensitivity of nitrogenase (Dixon and Kahn 2004; Hill 1988). The nodule cortex, acting as an oxygen diffusion barrier, maintains low levels of free-oxygen in the infected nodule cells by blocking oxygen diffusion (Batut and Boistard

1994; Dixon and Kahn 2004). In pink mature nodules, the infected cells contain high concentrations of plant-derived leghemoglobin (Lb), which have an extremely high affinity for free-oxygen. Reversible binding of free-oxygen enable Lbs to diffuse oxygen at low oxygen concentrations, which supports actively aerobic respiration of bacteroids within infection zone of nodules (Kuzma *et al*. 1993;Ott *et al*. 2005). In addition, a symbiosis-specific cbb3-type cytochrome C oxidase is induced in bacteroids. Its ultra-high affinity for oxygen makes it possible for bacteroids to perform aerobic respiration in a micro aerobic environment (Preisig *et al*. 1996; Schluter *et al*. 1997).

1.6.2 Functions of Nitrogen Fixation Genes in Rhizobia

Genes for symbiotic nitrogen fixation are encoded by the *nif* and *fix* genes. Conserved *nif* genes found in rhizobia are structurally homologous to those of free-living diazotrophs such as *K. pneumoniae* (Fischer 1994). The α and β subunits of the MoFe protein are encoded by *nifD* and *nifK* respectively, and *nifH* encodes the Fe protein. The *nifDKH* genes are in one operon in *S. meliloti*, while *nifDK* and *nifH* belong to two separate transcriptional units in *B. japonicum* (Corbin *et al*. 1982; Singh *et al*. 1988). Other *nif* genes are required for assembly of the nitrogenase system (Fischer 1994); *nifB, nifE* and *nifN* are involved in the biosynthesis of the FeMo-cofactor (Brigle *et al*. 1987). *nifA*, encodes a *nif* gene transcriptional activator (Szeto *et al*. 1984). The *nifX* gene in *B. japonicum* may be a negative regulator for nitrogenase expression (Gosink *et al*. 1990;Hennecke 1990) and *nifW* in *A. caulinodans* may be involved in protecting the FeMo protein against free-oxygen (Kim and Burgess 1996).

The *fix* genes are important for nitrogen fixation but no orthologs are found in free-living diazotrophs. This implies that they may play an important role in facilitating bacteroids to fix nitrogen in a micro aerobic environment. Mutants in *fix* genes tend to fail to fix nitrogen in symbiotic nodules (Fischer 1994). For example, *fixABCX* and *fixNOQP* genes, belonging to two separate operons, were first identified in *S. meliloti* and then found in *B. japonicum, R. leguminosarum,* and *A. caulinodans* (Fischer 1994;Renalier *et al*. 1987;Ruvkun *et al*. 1982). According to the predicted amino acid sequences, the FixABCX proteins are likely to assist in electron transport from donors to nitrogenase, and the *fixNOQP* operon may play a role in supporting bacteroid respiration at low oxygen concentrations in root nodules (Earl *et al*. 1987; Fischer 1994; Mandon *et al*. 1994; Preisig *et al*. 1993).

1.6.3 Regulation of Nitrogen Fixation Genes

In free-living diazotrophs such as *K. pneumoniae,* both environmental nitrogen and free-oxygen conditions are involved in regulating transcription of nitrogen fixation genes. By contrast, the transcriptional regulation of nitrogen fixation genes in rhizobia is tightly controlled by oxygen, not nitrogen. An exception is *A. caulinodans*, which can fix N_2 in both free-living cells and differentiated bacteroids. The general nitrogen regulatory system (*ntr*) in *A. caulinodans* was reported to be partly involved in symbiotic nitrogen fixation (D'hooghe *et al*. 1995; Dixon and Kahn 2004; Fischer 1994; Kaminski and Elmerich 1991; Virts *et al*. 1988).

Previous studies indicated that symbiotic nitrogen fixation is tightly controlled by a two-level hierarchy in response to the oxygen/redox conditions within nodules. The

first level of the regulatory hierarchy is based on the two-component systems, which predominantly regulate transcription of *nifA* and *fix* genes. The second level of the regulatory hierarchy is provided by NifA, which controls transcription of *nif* genes by its oxygen sensitivity (David *et al*. 1988; Dixon and Kahn 2004; Fischer 1994; Nellen-Anthamatten *et al*. 1998). In *S. meliloti*, transcription of both *nifA* and *fix* genes is controlled by the oxygen-responsive FixL-FixJ two-component system, together with FixK, a member of the Crp-Fnr superfamily. FixL protein is a histidine kinase with a PAS domain containing a heme moiety, which reversibly binds to oxygen, thereby regulating kinase activity. Low oxygen conditions specifically induce kinase activity which leads to FixL autophosphorylation. The phosphoryl group is then transferred from phosphorylated FixL to FixJ, which results in FixJ activation. Accumulation of phosphorylated FixJ finally stimulates transcription of *fixK* and *nifA* (Lois *et al*. 1993; Monson *et al*. 1992; Virts *et al*. 1988; Weinstein *et al*. 1993). By contrast, the oxygen-responsive FixL-FixJ in *B. japonicum* is only involved in regulating transcription of *fixK*, while transcription of *nifA* is tightly regulated by another two-component system, referred as to RegS-RegR, in response to the redox conditions (Anthamatten *et al*. 1992; Bauer *et al*. 1998; Emmerich *et al*. 2000; Mesa *et al*. 2008). Thus, transcription of *nif* and *fix* gene is regulated by oxygen conditions in *S. meliloti*, and oxygen and redox conditions respectively in *B. japonicum.*

1.7 Carbon Metabolism in Bacteroids

In the rhizosphere and soil environment, free-living rhizobia can use a wide range of carbon compounds for growth. However, in nodules, bacteroids can only

consume reduced carbon compounds provided by host plants. It is generally believed that the principle source of reduced carbon utilized by mature bacteroids are C_4-dicarboxylates such as malate, succinate, and fumarate, which are ultimately derived from photosynthate transported from the shoot to the nodules in the form of sucrose via the phloem (Lodwig and Poole 2003). In bacteroids these C_4-dicarboxyliates are predominantly metabolized through the tricarboxylic acid cycle (TCA) and electron transport chain (ETC) to generate enough ATP and reductant to fuel the highly energetic N_2-fixation process.

1.7.1 Carbon Sources Supplied to Bacteroids for Nitrogen Fixation

In nodules, the sucrose transported from the shoot is first hydrolyzed by sucrose synthase to produce UDP-glucose, which is then metabolized via the glycolytic pathway to generate phosphoenolpyruvate (PEP). It was reported that activities of sucrose synthase and glycolytic enzymes are required for symbiotic nitrogen fixation and higher in nodule cells compared to uninfected roots, while generally low or undetectable in bacteroids (Copeland *et al*. 1989a; Copeland *et al*. 1989b; Day and Copeland 1991; Gordon *et al*. 1999; Kouchi *et al*. 1988; Lodwig and Poole 2003; Rosendahl *et al*. 1990). Furthermore, activities of enzymes responsible for the further metabolism of PEP, including phosphoenolpyruvate carboxylase (PEPC) and malate dehydrogenase (MDH) are enhanced in nodules, which results in the accumulation of C_4-dicarboxylates (e.g. malate and succinate) in nodules at high concentrations (malate: ~3.4mM) (Day and Copeland 1991; Kouchi *et al*. 1988; Lodwig and Poole 2003; Rosendahl *et al*. 1990). Feeding legumes with $^{13}CO_2$ or $^{14}CO_2$ lead to quick accumulation of radioactive labeled organic

acids in root nodules, especially malate (Copeland *et al*. 1989b; Kouchi and Nakaji 1985; Rosendahl *et al*. 1990; Salminen and Streeter 1992). This suggests that sucrose is mainly metabolized by nodule cells, not bacteroids to form dicarboxylates for symbiotic N_2-fixation in bacteroids (Gordon *et al*. 1999).

A number of sugars, including mono and disaccharides, can be used as carbon source by free-living rhizobia. However, bacteroids (e.g. *B. japonicum, R. leguminosarum,* and *Sinorhizobium sp.* NGR234) isolated from nodules can neither transport nor metabolize sugars due to the absence of transporters for most sugars and an incomplete glycolytic pathway. Mutants of rhizobia blocked in sugar transport and metabolism still maintain the ability to symbiotically fix nitrogen (Dilworth and Glenn 1984; Glenn and Dilworth 1981; Glenn *et al*. 1984; Hudman and Glenn 1980; and Saroso *et al*. 1986). Thus, it is believed that sugars in nodules are not the carbon sources metabolized in bacteroids to fuel the symbiotic nitrogen fixation (Copeland *et al*. 1989b).

1.7.2 Transport of Dicarboxylates from the Plant Cytosol into Bacteroids

A plant derived membrane, the peribacteroid membrane (PBM), surrounds bacteroids to form organelle-like structures, referred to as symbiosomes (Robertson *et al*. 1978). Studies on transport across the PBM indicate that the PBM is generally impermeable to sugars and amino acids and the rate of sugar and amino acid crossing the PBM from the plant cytosol to the bacteroids is too slow to satisfy the high energetic requirement of N_2-fixation (Herrada *et al*.1989; Reibach and Streeter 1984; Udvardi and Day 1997). By contrast, C_4-dicarboxylates are rapidly transported with a high affinity and

accumulate in symbiosomes from various legumes (Ou Yang *et al*. 1990; Udvardi and Day 1997).

A transporter on the PBM acts as a uniport for the monovalent dicarboxylate anion through which the electron potential ($\Delta\Psi$) across the PBM powers the movement of dicarboxylates, such as malate and succinate, from the plant cytosol to the symbiosomes (Udvardi and Day 1989; Udvardi and Day 1997). In addition to this uniport, phosphorylated Nodulin 26 protein on the PBM shows channel activity which is able to transport malate together with other anions (Weaver *et al*. 1994). In isolated soybean symbiosomes, the uptake of malate is stimulated as PBM proteins are phosphorylated, while dephosphorylation of PBM proteins inhibits the uptake of malate. Nodulin 26 protein was found to be the major protein phosphorylated on the PBM in soybean, suggesting the possibility that Nodulin 26 protein is a PBM transporter for dicarboxylates (Ouyang *et al*. 1991; Weaver *et al*. 1991). However, activity of the ion channel reconstituted by purified Nodulin 26 protein is rather nonspecific (Weaver *et al*. 1994).

Rhizobia and bacteroids take up C_4-dicarboxylates rapidly from surrounding medium by using an energy-dependent C_4-dicarboxylate transport (Dct) system which is similar among various rhizobial species (Yurgel and Kahn 2004). The Dct system is encoded by three genes: *dctA*, encoding the C_4-dicarboxylate transporter (DctA), *dctB* and *dctD*, which encode a two component regulatory system (DctB & DctD) (Ronson *et al*. 1981; Watson 1990; Yarosh *et al*. 1989). Normally, this *dctABD* is the only dicarboxylate transport system present in most rhizobia. Mutations in any of the three *dct* genes generally make rhizobia fail to transport and grow on C_4-dicarboxylates in free-living

cultures (Ronson *et al*. 1987; Watson *et al*. 1988; Yarosh *et al*. 1989; Yurgel and Kahn 2004). However, *Sinorhizobium Sp*. NGR234 was found to have two C_4-dicarboxylate transport systems. The one similar to *dctA* is located on the symbiotic plasmid and the other one on the chromosome is uncharacterized. NGR234 can use both systems to transport C_4-dicarboxylate in free-living cultures, but only the *dctA*-like system was essential to symbiotic nitrogen fixation (van Slooten *et al*. 1992). In addition to the *dctABD* system, another succinate transport system, which is unrelated to symbiotic nitrogen fixation, was also identified in *R. tropici* (Batista *et al*. 2001).

The C_4- dicarboxylate transporter (DctA) has been extensively characterized in *S. meliloti*, *R. leguminosarum*, and *B. japonicum*. It is a cytoplasmic membrane protein, containing 12-membrane spanning domains, with the N- and C-terminuses located in the cytoplasm (Jording and Puhler 1993). DctA is a dicarboxylate proton symport system able to transport a wide range of C_4- dicarboxylates but the relative rate of transport and *Km* may be variable among substrates (Bhandari and Nicholas 1985; Finan *et al*. 1981; McAllister and Lepo 1983; Udvardi and Day 1997). The minimum requirement for potential substrates to be recognized by DctA mentioned by previous reports are two carbonyl groups separated by two carbon atoms (Yurgel *et al*. 2000). In general, DctA transports malate, succinate, fumarate, and oxaloacetate (OAA) with a high affinity (*Km*: 2-15μM; V_{max}: 10-80nmol/min/mg protein) in various rhizobial species (Finan *et al*. 1981; Finan *et al*. 1983; Udvardi and Day 1997; Yurgel and Kahn 2004). On the other hand, in *S. meliloti*, aspartate and orotate are transported via DctA with a much lower affinity (Km: ~10mM for aspartate, 1.7mM for orotate) (McRae *et al*. 1989; Watson *et al*. 1993; Yurgel

et al. 2000; Yurgel and Kahn 2004). Normally, *dctA* mutants are able to nodulate host plants but the induced nodules are unable to fix nitrogen. The bacteroids isolated from these ineffective nodules cannot transport C_4- dicarboxylates (el-Din 1992; Finan *et al*. 1983; Lodwig and Poole 2003; Ronson *et al*. 1981; Watson *et al*. 1988). This further supports the conclusion that C_4-dicarboxylates are the primary carbon source supplied by the host plants to fuel the symbiotic nitrogen fixation in bacteroids.

DctB and DctC are members of the two component sensor-regulator family and regulate transcription of the σ^{54}-dependent *dctA* promoter in response to the presence of dicarboxylates. DctB is considered to be a membrane-bound sensor protein, which phosphorylates and activates DctD and DctD~Pi, in association with σ^{54}, stimulates transcription of *dctA* (Udvardi and Day 1997; Yurgel and Kahn 2004). According to this model, transcription of *dctA* should be turned off in the absence of C_4-dicarboxylates. However, it was found that the *dctA* promoter directed a constitutive transcription in a *dctA* mutant background (Yarosh *et al*. 1989). One possible explanation is that, in the absence of C_4-dicarboxylates, DctB is deactivated after associating with DctA. Perceiving the presence of C_4- dicarboxylates results in the dissociation of DctA-B complex, which converts DctB into activated mode, thereby DctD is activated (Yurgel and Kahn 2004). In many rhizobia, strains mutated in *dctB* or *dctD* are defective in nitrogen fixation, but nodules induced by *S. meliloti* strains with *dctBD* mutations are still able to fix nitrogen at the rate nearly close to wild type and isolated bacteroids transport C_4- dicarboxylates. This suggests that *S. meliloti* strains with *dctBD* mutations might utilize an alternative

symbiotic activator to stimulate *dctA* expression during symbiotic nitrogen fixation (Lodwig and Poole 2003; Udvardi and Day 1997; Watson 1990; Yarosh *et al*. 1989).

1.7.3 C_4-dicarboxylate Metabolism in Bacteroid

To provide enough energy and reducing power for the N_2-fixation, C_4-dicarboxylates must be efficiently metabolized through the tricarboxylic acid cycle (TCA) which is known to be present in the bacteroids (Figure 6) (Mckay *et al*. 1988). A full TCA cycle was first reported in *B. japonicum* bacteroids (Stovall and Cole 1978). Since then the activities of all TCA cycle enzymes have been detected in nitrogen-fixing bacteroids of various rhizobia (Figure 6) (e.g. *B. japonicum, R. leguminosarum, S. meliloti, and R. tropici*), and normally at high levels (Karr *et al*. 1984; Kim and Copeland 1996; Lodwig and Poole 2003; Mckay *et al*. 1989; Romanov *et al*. 1994). Mutants deficient in these enzymes always fail to fix nitrogen (Finan *et al*. 1983; Finan *et al*. 1988; Finan *et al*. 1991; Lodwig and Poole 2003; Mckay *et al*. 1989). However, *B. japonicum* mutants lacking key TCA cycle enzymes such as 2-oxoglutarate dehydrogenase (ODGH) are still able to fix nitrogen in soybean nodules, which suggests that *B. japonicum* do not need an intact TCA cycle for metabolizing C_4-dicarboxylates in bacteroids (Green and Emerich 1997). The potential alternate pathways, such as the glyoxylate cycle or the gamma-aminobutyrate (GABA) shunt, may be utilized to bypass the ODGH step in TCA cycle (Figure 6). Acetyl coenzyme A (acetyl-CoA) is required in order to synthesize citrate from oxaloacetic acid during the metabolism of C_4-dicarboxylates through the TCA cycle in nitrogen-fixing bacteroids (Figure 6).

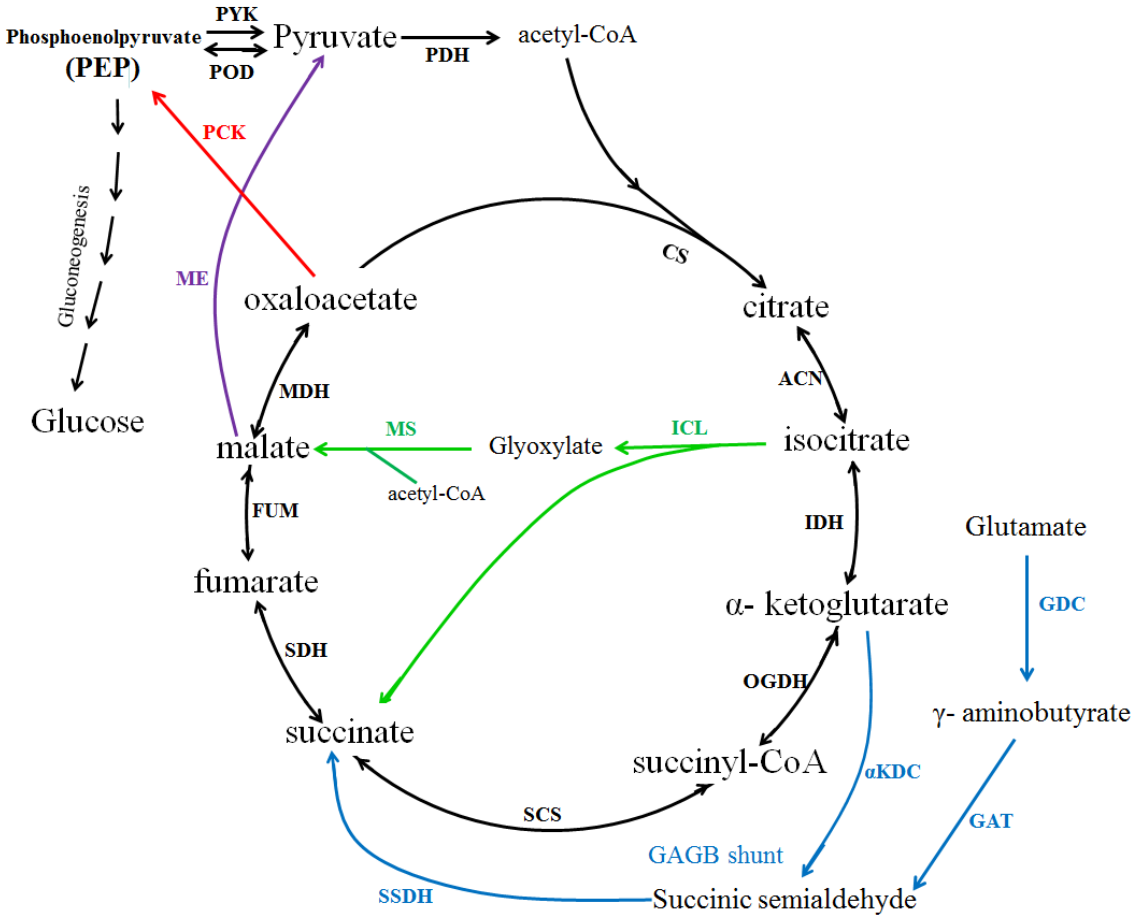

Figure 6 The Tricarboxylic acid (TCA) cycle and two possible pathways used to bypass the ODGH step in the bacteroids.

ACN: aconitase, αKDC: α- ketoglutarate decarboxylase, CS: citrate synthase, FUM: fumarase, GAT: γ- aminobutyrate aminotransferase, GDC: glutamate decarboxylase, IDH: isocitrate dehydrogenase, MDH: malate dehydrogenase, ME: malic enzyme, OGDH: α-ketoglutarate dehydrogenase, PCK: phosphoenolpyruvate carboxykinase, PDH: pyruvate dehydrogenase, POD: pyruvate orthophosphate diskinase, PYK: pyruvate kinase, SCS: succinyl-CoA synthetase, SDH: succinate dehydrogenase, SSDH: succinic semialdehyde dehydrogenase

In the N_2-fixing bacteroids of the alfalfa symbiont *S. meliloti*, acetyl-CoA generation from malate appears to occur via the combined activities of malic enzyme (ME) and pyruvate dehydrogenase (PDH) (Figure 6) (Driscoll and Finan 1993; Driscoll and Finan 1996). Malic enzymes catalyze the oxidative decarboxylation of malate to pyruvate and CO_2 with the simultaneous reduction of NAD^+/ $NADP^+$ to NADH/NADPH (Wedding 1989). *S. meliloti* contains two distinct malic enzymes: DME, which is $NAD(P)^+$-dependent, and TME, which is strictly $NADP^+$-dependent (Voegele *et al*. 1999). DME is considered an important enzyme for regulating C_4-dicarboxylate metabolism in N_2-fixing bacteroids because its activity is strongly inhibited by acetyl-CoA and stimulated by fumarate and succinate. DME activity is present in free-living cells and bacteroids of *R. leguminosarum*, *B. japonicum* and *S. meliloti* (Copeland *et al*. 1989a; Copeland *et al*. 1989b; Driscoll and Finan 1996; Driscoll and Finan 1997; Mckay *et al*. 1988). In *S. meliloti* bacteroids, TME activity is markedly lower than that in free-living cells and the amount of DME protein is about 10 times greater than that of TME (Mitsch *et al*. 2007). *S. meliloti dme*$^-$ mutants form alfalfa root nodules which fail to fix nitrogen (Fix^-), while *tme*$^-$ mutants induce wild-type nitrogen-fixing root nodules (Fix^+) (Driscoll and Finan 1996; Driscoll and Finan 1997). The levels of N_2 fixation were reduced in *S. meliloti* bacteroids containing reduced DME activity whereas increased TME activity failed to rescue the nitrogen fixation deficiency of *dme* mutants (Driscoll and Finan 1993; Mitsch *et al*. 2007). It was recently reported that the Fix efficiency of *R. leguminosarum dme & tme* double mutant on pea as measured by total nitrogenase activity per plant were about 150% of the wild-type (Mulley *et al*. 2010). This indicated that an alternative

pathway exists in *R. leguminosarum* for conversion of dicarboxylic acids to acetyl-CoA that is not present or expressed in *S. meliloti* bacteroids.

Another possible route for the formation of acetyl-CoA from C_4-dicarboxylic acids is via the combined activities of phosphoenolpyruvate carboxykinase (PCK), pyruvate kinase (PYK), and pyruvate dehydrogenase (PDH) (Figure 6). The enzyme PCK catalyzes the decarboxylation of oxaloacetate (OAA) to phosphoenolpyruvate (PEP). It is the first step in the gluconeogenic pathway in which TCA cycle intermediates are converted to hexose sugars (Figure 6). Biochemical and genetic analyses in previous studies have shown that PCK is essential to the metabolism of C_4-dicarboxylic acids and other TCA cycle intermediates in free-living cells of *S. meliloti, R. leguminosarum*, and *Sinorhizobium* sp. NGR234 (Arwas *et al*. 1985; Finan *et al*. 1988; Mckay *et al*. 1985).

However, the importance of PCK to symbiotic nitrogen fixation is plant host-dependent as the Fix phenotype of *pck*$^-$ mutants varies depending on the symbiotic plant host. *R. leguminosarum pck*$^-$ mutants showed no reduction in their symbiotic nitrogen fixation phenotype whereas *pckA* mutants of *S. meliloti* showed a reduction in symbiotic nitrogen fixation efficiency (Finan *et al*. 1988; Mckay *et al*. 1985). Interestingly PCK activity was present at low levels in wild-type bacteroids of *R. leguminosarum*, and it was not detected in wild-type bacteroids of *S. meliloti* (Finan *et al*. 1991; Mckay *et al*. 1985). Expression of the *pckA* gene from *R. leguminosarum* in *S. meliloti dme* mutants restored about 30% of wild-type efficiency of symbiotic nitrogen fixation (acetylene reduction) in alfalfa bacteroids (Mulley *et al*. 2010). Thus, *S. meliloti* alfalfa bacteroids are able to employ the PckA pathway to generate acetyl-CoA at a very low level. In NGR234, *pck*$^-$

mutants exhibited a host-dependent symbiotic phenotype. *pck*$^-$ mutants lost about 40% and 80% of nitrogen fixation efficiency in *Leucaena leucocephala* and *Macroptilium atropurpureum*, respectively, and showed a nitrogen fixation deficiency in *Vigna unguiculata* (Osteras *et al.* 1991).

1.8 Malic Enzymes (ME)

Malic enzymes (ME) are responsible for the oxidative decarboxylation of malate to pyruvate and CO_2 with the simultaneous reduction of NAD^+ or $NADP^+$ to NADH or NADPH (Wedding 1989). Since the first identification of malic enzyme in pigeon liver, malic enzymes from a wide variety of sources have been studied (Cushman 1992; Mitsch *et al*. 1998; Ochoa *et al*. 1948; Walter *et al.* 1994). The prokaryotic malic enzymes reported so far are fewer in number and more varied in structure than their eukaryotic counterparts (Mitsch *et al*. 1998). On the basis of cofactor requirement and their ability to metabolize oxaloacetic acid (OAA), the International Union of Biochemistry classified malic enzymes into 3 groups. The first group (EC1.1.1.38), reported in bacteria and plants, but rarely in animals, uses NAD^+ as preferential cofactor but shows some activity when supplied with $NADP^+$. This group has the ability to decarboxylate OAA to pyruvate. The second group (EC.1.1.1.39), only detected in plant mitochondria, shows the same cofactor requirement as the first group, but these enzymes cannot decarboxylate OAA. The third group (EC1.1.1.40), common in plants, animal and bacteria, is strictly $NADP^+$-dependent and can decarboxylate OAA (Wedding 1989).

Early studies with *E.coli* identified two malic enzymes, NAD^+ and $NADP^+$ dependent MEs (Murai *et al*. 1971a). Activity of the NAD^+-dependent enzyme is

regulated by inhibitors, such as CoA, oxaloacetate, and ATP, and inducers such as aspartate, which suggests that the NAD^+-dependent malic enzyme is involved in catabolizing malate and controlling C_4-dicarboxylate concentrations in cells (Murai *et al*. 1971a; Sanwal 1970; Yamaguchi *et al*. 1973). By contrast, the $NADP^+$-dependent enzyme is inhibited by acetyl-CoA and cAMP, which suggests that $NADP^+$-dependent malic enzyme plays a role in anabolic processes such as lipid biosynthesis via providing cells with acetyl-CoA and NADPH (Murai *et al*. 1971b; Sanwal *et al*. 1968; Sanwal and Smando 1969a; Sanwal and Smando 1969b).

In *S. meliloti*, two distinct malic enzymes were identified: DME (diphosphopyridine nucleotide-dependent malic enzyme), which is $NAD(P)^+$-dependent and belongs to the EC1.1.1.39 class, and TME (triphosphopyridine nucleotide dependent malic enzyme), which is strictly $NADP^+$-dependent and belongs to the EC1.1.1.40 class (Voegele *et al*. 1999). However, only DME is essential for symbiotic nitrogen fixation. The DME and TME proteins of *S. meliloti* consist of an approximately 400-amino-acid long N-terminal region similar to characterized malic enzymes and an approximately 300-amino-acid domain at the C- terminus similar in sequence to previously characterized phosphotransacetylases (PTA, EC2.3.1.8). The PTA domain is not present in malic enzymes of some prokaryotes, such as *Bacillus stearothermophilus* and *Streptococcus bovis* (Mitsch *et al*. 1998; Mitsch *et al*. 2007; Voegele *et al*. 1999). The phosphotransacetylase (PTA)-like domain at the C-termini of DME is not essential for enzyme activity and symbiotic nitrogen fixation of *S. meliloti* bacteroids, but deletion of this domain abolishes the oligomerization and the allosteric nature of DME. This means

that allosteric regulation is not essential for DME to function in bacteroids (Mitsch *et al*. 2007).

The only function of both DME and TME should be the synthesis of pyruvate from malate based on their biochemical characterization and all of the previous reported physiological evidence (Driscoll and Finan 1997; Mitsch *et al*. 2007; Voegele *et al*. 1999). DME has *Km* for L-malate of 9.4 mM with a V_{max} of 60μmol/min/mg protein, and is allosterically regulated by inducers, such as succinate and fumarate, and the inhibitor, acetyl-CoA (Voegele *et al*. 1999). TME has a similar *Km* and V_{max} for L-malate (12.5mM and 53μmol/min/mg protein), but there is no evidence of allosteric regulation found for TME (Voegele *et al*. 1999). Acetyl-CoA strongly inhibited DME activity without having any negative effect on TME (Voegele *et al*. 1999). Activity of DME can be regulated by acetyl-CoA at concentrations as low as 100μM which is well within the concentration range measured in bacterial cells (60-300μM) (Voegele *et al*. 1999). Besides its substrate (malate), two other TCA cycle intermediates, fumarate and succinate, have the ability to stimulate the activity of DME, while they have no effect on TME (Voegele *et al*. 1999). It suggests that DME, not TME, is an important enzyme regulating the levels of TCA cycle intermediates.

Previous metabolome studies in the Finan laboratory (Smallbone, L.A., 2006, M.Sc thesis) indicated that DME and TME may play different roles in the metabolism of *S. meliloti* in free-living cultures. *S. meliloti dme* mutants grown in M9-succinate accumulated intracellular 6-phosphate sugars (fructose-6-phosphate, mannose-6-phosphate, and sucrose-6-phosphate) and excreted at least 10- fold more malate and

fumarate compared to those of the *tme* mutant. One possible explanation is that the *dme* mutation may lead to disturbance of the central carbon metabolism in *S. meliloti* due to a shortage of acetyl-CoA required for the TCA cycle. The excess malate or fumarate is then either excreted or passed though the gluconeogenic pathway (malate to OAA to PEP) to generate 6-phosphate sugars. This suggests that DME is principally involved in providing the TCA cycle with acetyl-CoA by converting malate to pyruvate in *S. meliloti,* whereas the TME may have a secondary function within free-living cells, such as providing NADPH for biosynthesis.

1.9 This Work

The main aim of this work is to extend our understanding of the different roles of DME and TME in the central carbon metabolism of *Sinorhizobium*. The major findings of this thesis are discribed in four sections as following:

1.9.1 Symbiotic Phenotypes of *Sinorhizobium Sp.* NGR234 *dme* Mutants on Different Host Plants (Chapter 3)

S. meliloti dme$^-$ mutants form alfalfa root nodules which fail to fix nitrogen (Fix$^-$), while a *dme* mutant of *R. leguminosarum* was recently reported to be Fix$^+$ on pea (Mulley *et al*. 2010). It seemed that DME is necessary for symbiotic nitrogen fixation in *S. meliloti* bacteroids, but not essential for symbiotic nitrogen fixation in *R. leguminosarum* bacteroids. Thus, it was hypothesized that the symbiotic phenotype of *dme* mutants is dependent on the host plants. Here we report the cloning of the *dme* gene from the broad-host range *Sinorhizobium sp* NGR234, and the symbiotic phenotypes of NGR234 *dme* mutants and *dme pck* double mutant on five different hosts. The NGR234 *dme* mutants

showed N_2-fixation activity (27 to 83% of wild-type) on different host plants, and the *dme pck* double mutant formed only Fix deficient nodules on all test host plants. These data, together with previous reports, indicated that DME activity is not absolutely required for symbiotic N_2-fixation. NGR234 appears to employ both PCK and DME pathways to generate pyruvate and acetyl-CoA required by the TCA cycle in bacteroids, and the carbon sources made available to rhizobia in different plant hosts may differ in both their nature and quantity.

1.9.2 Characterization of Putative Malic Enzymes of *A. caulinodans* (Chapter 4)

The proteins encoded by *azc_0119* and *azc_3656* from *Azorhizobium caulinodans* ORS571 were considered as putative malic enzymes based on BlastP analyses. The nodules formed by *azc_3656*::Tn5 mutants lacked nitrogen-fixing ability, which suggested that this putative malic enzyme is essential for symbiotic nitrogen fixation (Suzuki *et al*. 2007). The *azc_3656* encoding protein was 69% and 47% identical to the *S. meliloti* DME and TME proteins respectively, based on the amino acid sequence deduced from its DNA sequence (Tsukada *et al*. 2009). However, its nucleotide cofactor specificity and physiological role has not been formally established. Here we described the purification of His-tagged proteins encoded by *azc_0119* and *azc_3656*. The *A. caulinodans* AZC3656 protein is an $NAD(P)^+$-malic enzyme who's kinetic and allosteric properties are remarkably similar to those of the DME protein from *S. meliloti*. Both proteins share similar apparent K_{ms} for L-malate, NAD^+, and $NADP^+$, and both activities are stimulated by succinate and fumarate and inhibited by acetyl-CoA. Thus, the Fix^-

phenotype of *A. caulinodans azc_3656* insertion mutants on *Sesbania rostrata* appears to be identical to the Fix^- phenotype of *S. meliloti dme* mutants.

1.9.3 Why TME is not Essential to Symbiotic Nitrogen Fixation? (Chapter5)

In *S. meliloti*, the only function of both DME and TME should be the synthesis of pyruvate from malate based on their biochemical characterization and all of the previous reported physiological evidence (Driscoll and Finan 1997; Voegele *et al*. 1999). However, DME and TME function differently in N_2-fixing bacteroids, and the reason why DME, but not TME is essential for symbiotic nitrogen fixation is largely unknown. Based on the similar kinetic parameters of DME and TME, neither differences in the catalytic rate nor the affinity for L-malate were considered as the reason causing the failure of TME to restore symbiotic nitrogen fixation in *dme* mutants. A hypothesis mentioned in previous studies pointed out that the high ratio of NADPH to $NADP^+$ in bacteroids may be the reason why TME was prevented from functioning in nodules. To lower the ratio of NADPH to $NADP^+$, here we report the expression of a soluble pyridine nucleotide transhydrogenase (*sth*) from *Pseudomonas aeruginosa* in different *S. meliloti* backgrounds. However, *sth* expression did not restore any symbiotic nitrogen fixation to *S. meliloti dme* mutants. HPLC data showed that STH activity raised NADH / NAD^+, but did not lower the NADPH/$NADP^+$ ratio in *S. meliloti* bacteroids.

1.9.4 Microarray Analysis of *S. meliloti* Single *dme* and Single *tme* Mutants Grown in Minimal Medium with Glucose or Succinate (Chapter 6)

More generally, it was hypothesized that DME and TME play different roles in central carbon metabolism of *S. meliloti*. A previous metabolome study (Smallbone, L.A.,

2006, M.Sc thesis) indicated that the primary role of the DME enzyme is to convert malate to pyruvate whereas the physiological role of TME is still not clear. To gain insight into the function of malic enzymes in central carbon metabolism in *S. meliloti*, we conducted genome-wide microarray analyses, comparing the transcriptome profiles of *dme* and *tme* mutants to wild type, grown in MOPS-buffered minimal medium containing 2mM inorganic phosphate (MOPS-P2) with glucose or succinate as a carbon source. The most striking changes of gene expression were observed in succinate-grown cells of the *S. meliloti dme* mutant. The functions of those highly upregulated genes hinted a disturbance in the central carbon metabolism, which suggested that DME might play an important role in regulating the levels of TCA cycle intermediates that are important for the maintenance of metabolic flux through TCA cycle during C_4-dicarboxylate oxidation. However, changes of gene expression found in *tme* mutants were not significant enough to predict the physiological functions of TME protein in central carbon metabolism.

Chapter 2 Materials and Methods

2.1 Bacterial Strains and Growth Conditions

Bacterial strains and plasmids utilized in this study are list in Table 3. Buffers, antibiotics, and microbiological media were obtained from Fisher Scientific (Nepean, ON) and Sigma Chemical Co. (Oakville, ON). *E. coli* cultures were grown at either 30°C or 37°C in Luria-Bertani medium (LB): 10 g of Bacto Typtone per liter, 5 g of yeast extract per liter, and 5 g of NaCl per liter (Miller, 1972). *S. meliloti* cultures were grown at 30 °C in LB supplemented with 2.5 mM $MgSO_4$ and 2.5 mM $CaCl_2$, and this medium is referred to as LBmc. *A. caulinodans* and *Sinorhizobium sp* NGR234 cultures were cultivated at 30°C in tryptone-yeast medium (TY): 5 g of Bacto Typtone per liter, 3 g of yeast extract per liter, and 1.2 g of $CaCl_2 \cdot 2H_2O$ per liter (Osteras *et al*. 1991). MOPS (3-(N-morpholino) propanesulfonic acid)-buffered minimal medium supplemented with 2 mM inorganic phosphate (MOPS-P2) was used to grow *S. meliloti* wild-type, single *dme* and single *tme* mutants for microarray assay (Chapter 6). MOPS-P2 minimal medium consists of 40 mM MOPS, 20 mM KOH, 20 mM NH_4Cl, 1.2 mM $CaCl_2$, 100 mM NaCl, 2 mM $MgSO_4$, 2 mM KH_2PO_4, 0.5μg/ml biotin, and 1x trace minimal (1 mg/l H_3BO_3, 1 mg/l $ZnSO_4 \cdot 7H_2O$, 0.5 mg/l $CuSO_4 \cdot 5H_2O$, 0.5 mg/l $MnCl_2 \cdot 4H_2O$, 1 mg/l $Na_2MoO_4 \cdot 2H_2O$, 10 mg/l $Na_2EDTA \cdot 2H_2O$, 2 mg/l NaFeEDTA) (Bardin *et al*. 1998), and one of 15 mM succinate or 15 mM glucose were used as carbon sources. Solid media were prepared by adding 15 g of agar per liter.

Table 3 Bacterial strains and plasmids used for this study

Strain or plasmid	Relevant characteristics	Source or reference
Strains		
Sinorhizobium strains.		
Rm1021	*S. meliloti* SU47, str-21	(Meade *et al* 1982)
RmP110	Rm1021 with changed wild-type *pstC*	(Yuan *et al*. 2006)
SmFL581	RmP110, *Smc03269,03754,03272:: gusA rfp*	(Cowie *et al*. 2006)
SmFL673	RmP110, *pqqABCDE :: gusA rfp*	(Cowie *et al*. 2006)
SmFL686	RmP110, *Sma0034,0031:: gfp lacZ*	(Cowie *et al*. 2006)
SmFL925	RmP110, *pdhABC, Smc01033,01034, IpdA1:: gusA rfp*	(Cowie *et al*. 2006)
SmFL1212	RmP110, *thiCO:: gusA rfp*	(Cowie *et al*. 2006)
SmFL1318	RmP110, *Smc03787,bfr :: gfp lacZ*	(Cowie *et al*. 2006)
SmFL1445	RmP110, *Smb20283,20282,20281:: gusA rfp*	(Cowie *et al*. 2006)
SmFL1728	RmP110, *Smc2349,2351,2353::gusA rfp*	(Cowie *et al*. 2006)
SmFL1896	RmP110, *Smb21441::gusA rfp*	(Cowie *et al*. 2006)
SmFL1913	RmP110, *asnO, Smb20482:: gfp lacZ*	(Cowie *et al*. 2006)
SmFL2489	RmP110, *Smc03269,03754,03272:: gfp lacZ*	(Cowie *et al*. 2006)
SmFL2754	RmP110, *Smb21691,20571 :: gfp lacZ*	(Cowie *et al*. 2006)
SmFL3033	RmP110, *Smc03766,03765::gfp LacZ*	(Cowie *et al*. 2006)
SmFL3195	RmP110, *Smb20342,20343:: gusA rfp*	(Cowie *et al*. 2006)
SmFL3339	RmP110, *sucDC,mdh :: gfp lacZ*	(Cowie *et al*. 2006)
SmFL3347	RmP110, *Smb20724, 20725 :: gfp lacZ*	(Cowie *et al*. 2006)

SmFL3438	RmP110, *dppB1C1D1F1:: gusA rfp*	(Cowie *et al*. 2006)
SmFL3780	RmP110, *Smc00778,00779::gusA rfp*	(Cowie *et al*. 2006)
SmFL4227	RmP110, *Smc01418,01420,01421,rpoE1::gusA rfp*	(Cowie *et al*. 2006)
SmFL4290	RmP110, *fdh,Smb20171,20172:: gfp lacZ*	(Cowie *et al*. 2006)
SmFL4546	RmP110, *hslV, Smc02576, hslU :: gfp lacZ*	(Cowie *et al*. 2006)
SmFL5233	RmP110, *gcvTHP::gfp lacZ*	(Cowie *et al*. 2006)
SmFL5343	RmP110, *ffhm,pheAe :: gusA rfp*	(Cowie *et al*. 2006)
SmFL5711	RmP110, *GroES5L5::gusA rfp*	(Cowie *et al*. 2006)
SmFL6081	RmP110, *Smb20174,20175,20176 :: gusA rfp*	(Cowie *et al*. 2006)
SmFL6073	RmP110, *Smb21133, 21132,21131,21130::gusA rfp*	(Cowie *et al*. 2006)
RmG455	Rm1021,*dme-3*::Tn5	(Driscoll and Finan 1993)
RmG694	NGR234R, *rif-1*, Nod $^{+}$, Fix $^{+}$	(Stanley *et al*. 1988)
RmG694*pckA*	NGR234R, *pckA* :: Ω Sp^{r}	(Osteras *et al*. 1991)
RmG994	Rm1021, *dme-3*::Tn*5 tme-4*:: Ω Sp^{r}	(Driscoll and Finan 1996)
RmH897	RmG994::p*dme-tme*$^{+}$	(Mitsch *et al*. 2007)
RmP1809	NGR234R, *dme-9*::Ω Sp^{r}	This study
RmP1814	NGR234R, *dmeΔ14*::Ω Sp^{r}	This study
RmP2179	RmP110, *tme* :: Ω Sp^{r}	This study
RmP2189	RmP110, *dme* :: Ω Sp^{r}	This study
RmP2190	RmP1809 (pTH1582)	This study
RmP2191	RmP1809 (pTH2584)	This study
RmP2192	RmP1814 (pTH1582)	This study
RmP2193	RmP1814 (pTH2584)	This study

RmP2312	RmG455 (pTH1582)	This study
RmP2313	RmG455 (pTH2638)	This study
RmP2314	RmH897 (pTH1582)	This study
RmP2315	RmH897 (pTH2638)	This study
RmP2333	Rm1021 (pTH1582)	This study
RmP2334	Rm1021 (pTH2638)	This study
RmP2386	RmP110, *tme* :: Ω Sp^r, *Smc03269,03754,03272:: gusA rfp*	This study
RmP2387	RmP110, *dme* :: Ω Sp^r, *Smc03269,03754,03272:: gusA rfp*	This study
RmP2388	RmP110, *tme* :: Ω Sp^r, *Sma0034,0031:: gfp lacZ*	This study
RmP2389	RmP110, *dme* :: Ω Sp^r, *Sma0034,0031:: gfp lacZ*	This study
RmP2390	RmP110, *tme* :: Ω Sp^r, *pqqABCDE :: gusA rfp*	This study
RmP2391	RmP110, *dme* :: Ω Sp^r, *pqqABCDE :: gusA rfp*	This study
RmP2392	RmP110, *tme* :: Ω Sp^r, *pdhABC, Smc01033,01034, IpdA1:: gusA rfp*	This study
RmP2393	RmP110, *dme* :: Ω Sp^r, *pdhABC, Smc01033,01034, IpdA1:: gusA rfp*	This study
RmP2394	RmP110, *tme* :: Ω Sp^r, *thiCO:: gusA rfp*	This study
RmP2395	RmP110, *dme* :: Ω Sp^r, *thiCO:: gusA rfp*	This study
RmP2396	RmP110, *tme* :: Ω Sp^r, *Smc03787,bfr :: gfp lacZ*	This study
RmP2397	RmP110, *dme* :: Ω Sp^r, *Smc03787,bfr :: gfp lacZ*	This study
RmP2398	RmP110, *tme* :: Ω Sp^r, *Smb20283,20282,20281:: gusA rfp*	This study
RmP2399	RmP110, *dme* :: Ω Sp^r, *Smb20283,20282,20281:: gusA rfp*	This study
RmP2400	RmP110, *tme* :: Ω Sp^r, *Smc2349,2351,2353::gusA rfp*	This study
RmP2401	RmP110, *dme* :: Ω Sp^r, *Smc2349,2351,2353::gusA rfp*	This study
RmP2402	RmP110, *tme* :: Ω Sp^r, *Smb21441::gusA rfp*	This study

RmP2403	RmP110, *dme* :: Ω Sp^r, *Smb21441::gusA rfp*	This study
RmP2404	RmP110, *tme* :: Ω Sp^r, *asnO, Smb20482:: gfp lacZ*	This study
RmP2405	RmP110, *dme* :: Ω Sp^r, *asnO, Smb20482:: gfp lacZ*	This study
RmP2406	RmP110, *tme* :: Ω Sp^r, *Smc03269,03754,03272:: gfp lacZ*	This study
RmP2407	RmP110, *dme* :: Ω Sp^r, *Smc03269,03754,03272:: gfp lacZ*	This study
RmP2408	RmP110, *tme* :: Ω Sp^r, *Smb21691,20571 :: gfp lacZ*	This study
RmP2409	RmP110, *dme* :: Ω Sp^r, *Smb21691,20571 :: gfp lacZ*	This study
RmP2410	RmP110, *tme* :: Ω Sp^r, *Smc03766,03765::gfp LacZ*	This study
RmP2411	RmP110, *dme* :: Ω Sp^r, *Smc03766,03765::gfp LacZ*	This study
RmP2412	RmP110, *tme* :: Ω Sp^r, *Smb20342,20343:: gusA rfp*	This study
RmP2413	RmP110, *dme* :: Ω Sp^r, *Smb20342,20343:: gusA rfp*	This study
RmP2414	RmP110, *tme* :: Ω Sp^r, *sucDC,mdh :: gfp lacZ*	This study
RmP2415	RmP110, *dme* :: Ω Sp^r, *sucDC,mdh :: gfp lacZ*	This study
RmP2416	RmP110, *tme* :: Ω Sp^r, *Smb20724, 20725 :: gfp lacZ*	This study
RmP2417	RmP110, *dme* :: Ω Sp^r, *Smb20724, 20725 :: gfp lacZ*	This study
RmP2418	RmP110, *tme* :: Ω Sp^r, *dppB1C1D1F1:: gusA rfp*	This study
RmP2419	RmP110, *dme* :: Ω Sp^r, *dppB1C1D1F1:: gusA rfp*	This study
RmP2420	RmP110, *tme* :: Ω Sp^r, *Smc00778,00779::gusA rfp*	This study
RmP2421	RmP110, *dme* :: Ω Sp^r, *Smc00778,00779::gusA rfp*	This study
RmP2422	RmP110, *tme* :: Ω Sp^r, *Smc01418,01420,01421,rpoE1::gusA rfp*	This study
RmP2423	RmP110, *dme* :: Ω Sp^r, *Smc01418,01420,01421,rpoE1::gusA rfp*	This study
RmP2424	RmP110, *tme* :: Ω Sp^r, *fdh,Smb20171,20172:: gfp lacZ*	This study
RmP2425	RmP110, *dme* :: Ω Sp^r, *fdh,Smb20171,20172:: gfp lacZ*	This study

RmP2426	RmP110, *tme* :: Ω Sp^r, *hslV, Smc02576, hslU :: gfp lacZ*	This study
RmP2427	RmP110, *dme* :: Ω Sp^r, *hslV, Smc02576, hslU :: gfp lacZ*	This study
RmP2428	RmP110, *tme* :: Ω Sp^r, *gcvTHP::gfp lacZ*	This study
RmP2429	RmP110, *dme* :: Ω Sp^r, *gcvTHP::gfp lacZ*	This study
RmP2430	RmP110, *tme* :: Ω Sp^r, *ffhm,pheAe :: gusA rfp*	This study
RmP2431	RmP110, *dme* :: Ω Sp^r, *ffhm,pheAe :: gusA rfp*	This study
RmP2432	RmP110, *tme* :: Ω Sp^r, *GroES5L5::gusA rfp*	This study
RmP2433	RmP110, *dme* :: Ω Sp^r, *GroES5L5::gusA rfp*	This study
RmP2434	RmP110, *tme* :: Ω Sp^r, *Smb20174,20175,20176 :: gusA rfp*	This study
RmP2435	RmP110, *dme* :: Ω Sp^r, *Smb20174,20175,20176 :: gusA rfp*	This study
RmP2436	RmP110, *tme* :: Ω Sp^r, *Smb21133, 21132,21131,21130::gusA rfp*	This study
RmP2437	RmP110, *dme* :: Ω Sp^r, *Smb21133, 21132,21131,21130::gusA rfp*	This study
RmP2455	RmP110 (pTH2657, single cross-over); P_{phbBA} *:: gusA rfp*	This study
RmP2456	RmP2179 (pTH2657, single cross-over); P_{phbBA} *:: gusA rfp*	This study
RmP2457	RmP2189 (pTH2657, single cross-over); P_{phbBA} *:: gusA rfp*	This study
RmP2458	RmP110 (pTH2658, single cross-over); $P_{Smc02199,\ 02203}$ *:: gusA rfp*	This study
RmP2459	RmP2179 (pTH2658, single cross-over); $P_{Smc02199,\ 02203}$ *:: gusA rfp*	This study
RmP2460	RmP2189 (pTH2658, single cross-over); $P_{Smc02199,\ 02203}$ *:: gusA rfp*	This study
RmP2461	RmP110 (pTH2659, single cross-over); $P_{Smc00822,\ 00823}$ *:: gusA rfp*	This study
RmP2462	RmP2179 (pTH2659, single cross-over); $P_{Smc00822,\ 00823}$ *:: gusA rfp*	This study
RmP2463	RmP2189 (pTH2659, single cross-over); $P_{Smc00822,\ 00823}$ *:: gusA rfp*	This study
RmP2464	RmP110 (pTH2660, single cross-over); $P_{Sma2239,\ 2241}$ *:: gusA rfp*	This study
RmP2465	RmP2179 (pTH2660, single cross-over); $P_{Sma2239,\ 2241}$ *:: gusA rfp*	This study

RmP2466	RmP2189 (pTH2660, single cross-over); $P_{Sma2239,\ 2241}$ *:: gusA rfp*	This study
RmP2467	RmP110 (pTH2661, single cross-over); P_{cbtJKL} *:: gusA rfp*	This study
RmP2468	RmP2179 (pTH2661, single cross-over); P_{cbtJKL} *:: gusA rfp*	This study
RmP2469	RmP2189 (pTH2661, single cross-over); P_{cbtJKL} *:: gusA rfp*	This study
RmP2473	RmP110 (pTH2663, single cross-over); $P_{Smb20173}$ *:: gusA rfp*	This study
RmP2474	RmP2179 (pTH2663, single cross-over); $P_{Smb20173}$ *:: gusA rfp*	This study
RmP2475	RmP2189 (pTH2663, single cross-over); $P_{Smb20173}$ *:: gusA rfp*	This study
RmP2476	RmP110 (pTH2664, single cross-over); $P_{cysD,N}$ *:: gusA rfp*	This study
RmP2477	RmP2179 (pTH2664, single cross-over); $P_{cysD,N}$ *:: gusA rfp*	This study
RmP2478	RmP2189 (pTH2664, single cross-over); $P_{cysD,N}$ *:: gusA rfp*	This study
RmP2479	RmP110 (pTH2665, single cross-over); $P_{SMb20280\text{-}20278}$ *:: gusA rfp*	This study
RmP2480	RmP2179 (pTH2665, single cross-over); $P_{SMb20280\text{-}20278}$ *:: gusA rfp*	This study
RmP2481	RmP2189 (pTH2665, single cross-over); $P_{SMb20280\text{-}20278}$ *:: gusA rfp*	This study
RmP2648	NGR234R, *pckA*:: Ω Sp^r & Δ*dme::kan*	This study
RmP2651	NGR234R, *pckA*:: Ω Sp^r & Δ*dme*	This study
Azorhizobium strains		
RmP2649	*A. caulinodans* ORS571 wild type; Cb^r	(Tsukada *et al*. 2009)
RmP2662	RmP2649, *azc_3656* :: Tn5 (Ao30-B02)	(Tsukada *et al*. 2009)
RmP2663	RmP2649, *azc_3656* :: Tn5 (Ao58-F11)	(Tsukada *et al*. 2009)
Pseudomonas stains		
M14	*P. aeruginosa* PA01, prototrophic, Alg^-	(Timm and Steinbuchel 1992)
E. coli strains		
BW25113	$lacI^q$ $rrnB_{T14}$ Δ$lacZ_{WJ16}$ *hsdR514* Δ$araBAD_{AH33}$ Δ$rhaBAD_{LD78}$	(Datsenko and Wanner, 2000)

MT616	MT607(MM294A recA56):pRK600	(Finan *et al.*, 1986)
Top10	F^- mcrA Δ(mrr-hsdRMS-mcrBC) φ80lacZΔM15 ΔlacX74 nupG recA1 araD139 Δ(ara-leu)7697 galE15 galK16 rpsL(Str^R)endA1 λ^-	Invitrogen
J287	DH5α (pJQ200mp18)	(Quandt and Hynes 1993)
J298	DH5α (pHP45Ω Sp^r Sm^r)	(Prentki and Krisch 1984)
J637	Top10 (pBAD/HisA)	Invitrogen
M462	DH5α (pTH1582)	(Yuan *et al*. 2005)
M589	DH5α (pTH1703)	(Cowie *et al*. 2006)
M1349	DH5α (pTH2415)	This study
M1365	DH5α (pTH2429)	This study
M1392	DH5α (pTH2457)	This study
M1397	DH5α (pTH2462)	This study
M1404	DH5α (pTH2467)	This study
M1418	BW25113 (pKD13)	(Datsenko and Wanner 2000)
M1420	BW25113 (pKD46)	(Datsenko and Wanner 2000)
M1449	DH5α (pTH2505)	unpublished
M1477	DH5α (pTH2530)	This study
M1479	BW25113(pKD46, pTH2530)	This study
M1481	BW25113 (pTH2532)	This study
M1611	DH5α (pTH2576)	This study
M1613	DH5α (pTH2578)	This study
M1619	DH5α (pTH2584)	This study
M1735	DH5α (pTH2632)	This study

M1747	DH5α (pTH2638)	This study
M1748	DH5α (pTH2639)	This study
M1789	DH5α (pTH2657)	This study
M1790	DH5α (pTH2658)	This study
M1791	DH5α (pTH2659)	This study
M1792	DH5α (pTH2660)	This study
M1793	DH5α (pTH2661)	This study
M1795	DH5α (pTH2663)	This study
M1796	DH5α (pTH2664)	This study
M1797	DH5α (pTH2665)	This study
M1906	Top10 (pTH2754)	This study
M1907	Top10 (pTH2755)	This study
Plasmids		
pBAD/HisA	Expression vector; Ap^r	Invitrogen
pHP45 Ω	pBR322 derivative carrying Ω interposon spectinomycin resistance cassette, pHP45 replicon, Sp^r, Sm^r, Ap^r	(Prentki and Krisch 1984)
PJQ200-mp18	Mobilisable suicide vector, *oriV*(p15A), Gm^r, $5\%Sucrose^s$	(Quandt and Hynes 1993)
pKD13	*bla* FRT *ahp* FRT PS1 PS4 *oriV*(R6K), Km^r	(Datsenko and Wanner 2000)
pKD46	*bla* PBAD *gam bet exo* pSC101 *oriT*S, Amp^r	(Datsenko and Wanner 2000)
pRK7813	Broad-host-range cosmid vector; Mob, IncP, Tc^r	(Jones and Gutterson 1987)
pTH1522	Reporter vector containing FRT site; Gm^r	(Cowie *et al*. 2006)
pTH1582	pJP2 with *gusA* from pFUS1; Tc^r	(Yuan *et al*. 2005)

pTH1703	pTH1522 derivative with unique *Xho*I, *Swa*I, *Kpn*I, *Not*I, *Sph*I, *Nsi*I, *Apa*I, *Pac*I, and *Bgl*II sites in the multiple cloning site	(Cowie *et al*. 2006)
pTH2415	PJQ200-mp18, 1,729 bp from NGR234 *dme*	This study
pTH2429	pTH2415 *dme*::ΩSp^r Sm^r at 418bp	This study
pTH2457	PJQ200-mp18; bp -471 to 87 of NGR234 *dme*	This study
pTH2462	PJQ200-mp18; bp -471 to 87 and 587 to 1186 of NGR234 *dme*	This study
pTH2467	pTH2462::ΩSp^r Sm^r (between 87and 587)	This study
pTH2505	FLP gene in pRK7813	unpublished
pTH2530	PJQ200-mp18; bp -471 to 87 and 1832 to +920 of NGR234 *dme*	This study
pTH2532	pTH2530 Δ*dme*::FRT-Km^r/Nm^r-FRT from pKD13	This study
pTH2576	PJQ200-mp18; bp -534 to 1019 of *S. meliloti dme*	This study
pTH2578	pTH2576 *dme*::ΩSp^r Sm^r at 161 bp	This study
pTH2584	pTH1582; sequence from bp -284 and complete NGR234 *dme* gene	This study
pTH2632	a 250 bp fragment carrying promoter region of neomycin resistant gene into pTH1582 via *HindIII/NsiI*, which led to Pneo::*gusA*	This study
pTH2638	*sth* gene from *P. aeruginosa* PA01 into pTH2632 via *NsiI/SacI*, leading to Pneo :: *sth* :: *gusA*	This study
pTH2639	*sth* gene from *S. meliloti* into pTH2632 via *NsiI/SacI*, leading to Pneo :: *sth* :: *gusA*	This study
pTH2657	Promoter region of operon *phbBA* into pTH1703 via *NsiI/BglII*, leading to P_{phbBA} *:: gusA rfp*	This study
pTH2658	Promoter region of operon *Smc02199-02203* into pTH1703 via *BglII/NsiI*, leading to transcriptional fusion with *gusA* and *rfp*	This study
pTH2659	Promoter region of operon *Smc00822-00823* into pTH1703 via *BglII/NsiI*, leading to transcriptional fusion with *gusA* and *rfp*	This study

pTH2660	Promoter region of operon *SMa2239-2241* into pTH1703 via *BglII/NsiI*, leading to transcriptional fusion with *gusA* and *rfp*	This study
pTH2661	Promoter region of operon *cbtJKL* into pTH1703 via *BglII/NsiI*, leading to transcriptional fusion with *gusA* and *rfp*	This study
pTH2663	Promoter region of *Smb20173* into pTH1703 via *BglII/NsiI*, leading to transcriptional fusion with *gusA* and *rfp*	This study
pTH2664	Promoter region of operon *cysDN* into pTH1703 via *NsiI/BglII*, leading to transcriptional fusion with *gusA* and *rfp*	This study
pTH2665	Promoter region of operon *Smb20280-20278* into pTH1703 via *NsiI/BglII*, leading to transcriptional fusion with *gusA* and *rfp*	This study
pTH2754	*A. caulinodans* ORS571 *azc_3656* gene into pBAD/HisA via 5' NheI site and 3' *HindIII* site	This study
pTH2755	*A. caulinodans* ORS571 *azc_0119* gene into pBAD/HisA via 5' NheI site and 3' *HindIII* site	This study

Antibiotics were added when required and the final concentrations (μg/ml) of antibiotics in media are given as follows, **(a)** for NGR234 strains: gentamicin (Gm), 20; rifampin (Rif), 20; spectinomycin (Sp), 50; and streptomycin (Sm), 50; **(b)** for *S. meliloti* strains: Gm, 60; neomycin (Nm), 200; rifampin (Rif), 50; Sp, 200; Sm, 200; and tetracycline (Tc), 10; **(c)** for *E. coli* strains: ampicillin (Amp), 100; chloramphenicol (Cm), 10; Gm, kanamycin (Km), 50; 10; Sp, 100; Sm, 30; Tc, 10.

2.2 Transduction

The bacteriophage ΦM12 (Finan *et al*. 1984) was used for all transductions in this study. The work solution of phage lysate was prepared by 20-fold dilution in LBmc just prior to use.

2.3 Conjugal Transfer of Plasmids

Bacterial conjugation is the transfer of genetic material between bacterial cells by direct cell-to-cell contact or by a bridge-like connection between two cells. Plasmids used in this study, such as PJQ200-mp18 (Quandt and Hynes 1993), pTH1703 (Cowie *et al*. 2006), and pTH1582, (Yuan *et al*. 2005), carries the RK2 *oriT* which enables them to be transferred between bacterial strains. All conjugations in this study were carried by using a helper *E .coli* strain MT616, which carries the plasmid pRK600 (Finan *et al.* 1986). The *E. coli* donor strain carrying the plasmid to be transferred; rhizobial recipient strain, and the MT616 *E. coli* helper strain were inoculated in 5 ml of rich broth (LB or TY) and grown overnight to good density. 1ml of each culture was transferred micro centrifuge tube individually and centrifuged at 13,000 rpm for 1minute in Eppendorf

5424 centrifuges with FA-45-24-11 rotor. Cell pellets were washed with 1 ml of sterile saline three times and then resuspended in 0.5 ml of sterile saline. 50 μl of each strain was mixed together in a micro centrifuge tube, and then the resulting 150 μl of mixture was spotted onto LB or TY plates followed by incubation at 30°C overnight for growth of all three cultures and plasmid transfer. The overnight mating spots were collected with a sterile wooden stick and resuspended in 0.5 ml sterile saline followed by preparation of serial dilutions ranging from 10^{-1} to 10^{-6}. 150 μl of each dilution was spread on appropriate plates for selection. In general, 10^{-3} or 10^{-4} dilutions were good enough to select rhizobial strains with conjugally transferred broad-host-range plasmids, while 10^{-1} or 10^{-2} dilutions were required to obtain rhizobial strains with suicide plasmid integrated in genome. The resulting colonies were purified three times prior to us in further experiments.

2.4 Preparation of Genomic DNA

Rhizobia strains were inoculated in 5 ml of rich broth (LB or TY) and grown overnight. All 5 ml of cells were centrifuged at 3000 rpm for 1 minute in 2-ml tubes (Eppendorf 5424 centrifuge with FA-45-24-11 rotor). Cells pellets were washed with 1ml saline once and then suspended in 600 μl of $T_{10}E_{25}$ (10 mM Tris, 25 mM EDTA, pH 8.0) followed by the addition of SDS to 1%, Proteinase K (Sigma) to 0.5 mg/ml, and NaCl to 1 M. Samples were mixed gently and incubated at 65 °C over 2 hours. DNA was extracted once with equal volume Tris buffer-saturated phenol (pH 8.0), twice with equal volume phenol-chloroform (1:1), and once with 1 ml chloroform. The clean supernatant was transferred to a micro centrifuge tube followed by the addition of sodium acetate to

0.5 M and equal volume of isopropanol. The precipitated nucleic acids appeared as white strands, which were spooled out with yellow tip and washed with 1ml of 70% ice-cold ethanol followed by centrifugation at 3000 rpm for 2 minute in an Eppendorf 5424 centrifuge. Pellets were dried by air after pouring out ethanol. The dried pellets were dissolved in 400 µl of $T_{10}E_1$ (10 mM Tris, 1 mM EDTA, pH 8.0) with 20 µg/ml RNaseA followed by incubation at 37°C for 30 minutes. DNA was extracted once with equal volume phenol-chloroform (1:1) and twice with equal volume chloroform. Genomic DNA was precipitated, washed and dried as above. The dried DNA pellets were dissolved in proper volume of ddH_2O. The quality and concentration of genomic DNA samples were determined via measuring the optical density at 260nm (OD_{260}) and 280nm (OD_{280}) or running 2-5 µl samples through 0.7 % agarose gels in TAE buffer. Qualified DNA samples were aliquoted and stored in -20°C prior to use.

2.5 DNA Manipulations

Plasmid DNA was purified from *E. coli* strains by using QIAprep plasmid kits (Qiagen). Restriction endonucleases and DNA modifying enzymes (Invitrogen, New England Biolabs, and Fermentas) were used according to the manufacturer's instructions. When required, reactions were purified using the QIAquick PCR purification kit (Qiagen) or alternatively run on an agarose gel followed by purification of specific DNA fragments using the QIAquick gel extraction kit (Qiagen), DNA sequencing was performed by using a model 3730 DNA analyzer (Mobix lab) at McMaster University. Agarose gel electrophoresis, preparation of transformation competent *E. coli* cells, and other recombinant DNA techniques were done as previously described (Sambrook *et al*. 1989).

2.6 Polymerase Chain Reaction (PCR)

Primers were designed by using the Primer Premier 5.0 program (PREMIER Biosoft, USA). Primers used this study were list in Table 4 and ordered from Sigma-Aldrich or Integrated DNA Technologies. Primers were dissolved in ddH_2O to a final concentration of 100 μM and stored at -20°C. Platinum® *Taq* DNA polymerase High Fidelity and Platinum® *Pfx* DNA polymerase (Invitrogen) were used for all PCR reactions in this study. Generally, each 50 μl of PCR reaction mixture consisted of 1x PCR buffer, 0.2-0.4 mM dNTP, 1-4 mM $MgSO_4$, 0.2-0.4 μM forward and reverse primers, 1 unit polymerase, and 10-100ng template DNA. All PCR reactions were carried out in a Eppendorf mastercycler® ep thermocycler with four-step cycling programmed as following: one cycle of 94°C for 4 minutes; five cycles of 94°C for 30 seconds, T_1 (5 °C below T_2) for 30 seconds, and 68 °C for 1 minute per kb extension; 25-30 cycles of 94°C for 30 seconds, T_2 (2-5°C below the highest Tm of the two primers) for 30 seconds, and 68 °C for 1 minute per kb extension; a final extension at 68 °C for 10 minutes; storage of the reactions at 4 °C for short-term. PCR reactions were run on an agarose gel to verify fragment production. Targeted PCR products were recovered from gel and purified by using QIAquick Gel Extraction Kit (QIAGEN). Purified PCR fragments were digested by appropriate restriction endonucleases and used for further cloning.

Table 4 Primers used in this study

Primer names	Primer sequences	RE site	Target
DME-NGR-FP1	5'-GTBCTCGGVCTCGGCAATATCGG-3'	n.a.	bp 264 at NGR234 *dme*
DME-NGR-FP2	5'-GACCTTCGGCGGCATCAA-3'	n.a.	bp 422 at NGR234 *dme*
DME-NGR-RP1	5'-GGATCGGGCCGACATGCAG-3'	n.a.	bp 2205 at NGR234 *dme*
DME-NGR-RP2	5'-CKWRCGCTTGCCGATGATCTG-3'	n.a.	bp 1764 at NGR234 *dme*
DME-NGR-RP6	5'-CCGCTCGACTTCAAAGCACTCC-3'	n.a.	bp 483 at NGR234 *dme*
DME-NGR-FP8	5-GACATTCTTCACCGACACCTAT-3	n.a.	bp 1814 at NGR234 *dme*
DME-NGR-RP9	5-GTCGATTGAGGTTTCGCTTTGTC-3	n.a.	bp 35 at NGR234 *dme*
DME-NGR-FP11	5'-ATAAGATCTCGTCGGAAATGAACAGCGTC-3'	*BglII*	bp 246 **up** NGR234 *dme*
DME-NGR-RP13	5'-TATATGCATGGGTTTCGATGATCTGTGGA-3'	NsiI	bp 1483 at NGR234 *dme*
DME-NGR-FP15v	5' TCGTGGTTACCGGGAATG-3'	n.a.	bp 460 **up** NGR234 *dme*
DME-NGR-RP16v	5'-ACCGACCAGGGCGAAGTA-3'	n.a.	bp 1596 at NGR234 *dme*
DME-NGR-FP18	5'-ATAAGATCTGCATGAACTCGTCGTGGTT-3'	*BglII*	bp 471 **up** NGR234 *dme*
DME-NGR-RP18	5'-GATCTAGAAGGGTAGCGGTGGAAGAAA-3'	*XbalI*	bp 87 at NGR234 *dme*
DME-NGR-FP20	5'-GGTCTAGAGGACATCACCAAGGCAAAG-3'	*XbalI*	bp 587 at NGR234 *dme*
DME-NGR-RP20	5'-TATATGCATAGGCGAGGGGATGAGGTAG-3'	*NsiI*	bp 1185 at NGR234 *dme*
DME-NGR-FP21v	5'-GCCGTGCAGGACAAGGTA-3'	n.a.	bp 566 **up** NGR234 *dme*
DME-NGR-FP30	5'-TCTGTCTAGATCACCGACACCTATGTGAGC-3’	*XbalI*	bp 1832 at NGR234 *dme*
DME-NGR-RP31	5’-AACTGCAGTGGGAAATCCACCCGTTA-3’	*PstI*	bp 920 **down** NGR234 *dme*
DME-NGR-FP32	5'-GAAATCATGCCAAAAGGCCCCGATATAGAAAGAG GGATGTACAGGCGATTGTGTAGGCTGGAGCTGCTTC-3'	n.a.	bp 27 at plasmid pKD13

DME-NGR-RP32	5'-GTGGGTGGCCGGGGAATCGCCTAAAGGGCGATCG TTCCGCAAGCCATCCCTAATTCCGGGGATCCGTCGA-3'	n.a.	bp 1337 at plasmid pKD13
DME-Sm-F1	5'-AGGAGCTCGAGGAACTCGTCGTGATTG-3'	*SacI*	bp 534 **up** *S. meliloti dme*
DME-Sm-R2	5'-CAAAACTGCAGAAGATATGCGGGAAACAGA-3'	*PstI*	bp 1019 at *S. meliloti dme*
DME-NGR-F37	5'-CGTAAGCTTGCAGGTAGTCCGTCTTGGC-3'	*HindIII*	bp 284 **up** NGR234 *dme*
DME-NGR-R37	5'-GGAAGATCTTCAAGCGGGATGGCTTG-3'	*BglII*	bp 2313 at NGR234 *dme*
Tme-Sm-F2v	5'-GGCAATCTAGGCGCACTCGC-3'	n.a.	bp 267 at *S. meliloti tme*
Tme-Sm-R2v	5'-TTGTTGACCTGGTTCGGATAGTCC-3'	n.a.	bp 967 at *S. meliloti tme*
DME-Sm-F6v	5'-GCTTCCTCGGTCACGACTTTC-3'	n.a	bp 842 **up** *S. meliloti dme*
DME-Sm-R6v	5'-CTTCATTTCTTCGTTGATGGTGC-3'	n.a	bp 1069 at *S. meliloti dme*
FP001	5'-ATACTATTGAATAAGCTTCC GCTCGAGTATCTGGACAAG-3'	*HindIII*	bp 981 at plasmid pTH1937
RP001	5'-ATAATACAATGCATGCG AAACGATCCTCATCCTGT-3'	*NsiI*	bp 1231 at plasmid pTH1937
FP002	5'-AATACAATGCATGAGGAGTCGT TCATGAACCAGTACGATCTCA-3'	*NsiI*	at the begin of *S. meliloti sth*
RP002	5'-AGTACAGATCAGGAGCTCT CACTCCGCCTTGATCTCTCC-3'	*SacI*	at the end of *S. meliloti sth*
FP003	5'-AATACAATGCATGAGGAGTCGTT CATGGCTGTCTACAACTACGACGT-3'	*NsiI*	at the begin of *P. aeruginosa* PA01 *sth*
RP003	5'-AGTACAGATCAGGAGCTCTC AAAAAAGCCGGTTGAGGC-3'	*SacI*	at the end of *P. aeruginosa* PA01 *sth*
F006	5'-TTAAATAATGCATCAGCACCTGACCGAGGAT-3'	*NsiI*	bp 159 at *S. meliloti phbA*
R007	5'-TCTCAACAGATCTCTGGCGGAGAAAGGAAAT-3'	*BglII*	bp 465 **up** *S. meliloti phbA*
F008	5'-TCTCAACAGATCTAAGCCGAAAGGCAGTAAG-3'	*BglII*	bp 300 **up** *S. meliloti Smc02199*
R009	5'-TTAAATAATGCATTGGGTCGAAATGATGAGG-3'	*NsiI*	bp 263 at *S. meliloti Smc02199*

F010	5'-TCTCAACAGATCTTCGTCAGTTGCTGGACAT-3'	*BglII*	bp 423 **up** *S. meliloti Smc00822*
R011	5'-TTAAACTATGCATCACCGAACATCGACTTCA-3'	*NsiI*	bp 139 at *S. meliloti Smc00822*
F012	5'-TCTCAACAGATCTTTCGGAAGGATAGCATTG-3'	*BglII*	bp 440 **up** *S. meliloti Sma2239*
R013	5'-AAAACTGCAGGTTCTGGCTCCACTCGTA-3'	*PstI*	bp 170 at *S. meliloti Sma2239*
F014	5'-TCTCAACAGATCTCTGCTGTTGACGAACGTA-3'	*BglII*	bp 537 **up** *S. meliloti cbtJ*
R015	5'-TACCGTATGCATTAGAGGATCTCGGTGCTG-3'	*NsiI*	bp 197 at *S. meliloti cbtJ*
F018	5'-TCTCAATAGATCTCTTCCGCAAGTGTCAGGC-3'	*BglII*	bp 466 **up** *S. meliloti Smb20173*
R019	5'-TTAAATAATGCATTGGAGTAGCGCAGGTTGG-3'	*NsiI*	bp 148 at *S. meliloti Smb20173*
F020	5'-TTAAATAATGCATATTGTGCAGTTCCGTTTC-3'	*NsiI*	bp 36 at *S. meliloti cysD*
R021	5'-TATCAATAGATCTAAGCCACTCCAGCGAATA-3'	*BglII*	bp 350 **up** *S. meliloti cysH*
F022	5'-TAAATAATGCATGCCCAGCAGGTTCTTCG-3'	*NsiI*	bp 300 at *S. meliloti Smb20280*
R023	5'-TTATGAATAGATCTCGCGTCTTCAAGGGTGC-3'	*BglII*	bp 932 at *S. meliloti Smb20281*
F040	5-CCGTGCAGGACAAGGTAGT-3	n.a	bp 564 **up** NGR234 *dme*
R041	5-CATCTTTCGCTCCATCGTTT-3	n.a	bp 1065 **down** NGR234 *dme*
F042	5'-TTTTTTAAGCTTTCAGGCTTCGCTCTGGGCT-3'	*HindIII*	at the end of *A. caulinodans* ORS571 *azc_3656*
R043	5'-CTACTAGCTAGCATGTCGAACATTTCCGAGGATCT-3'	*NheI*	at the begin of *A. caulinodans* ORS571 *azc_3656*
F044	5'-CTACTAGCTAGCATGGCGGACACGAAAATG-3'	*NheI*	at the begin of *A. caulinodans* ORS571 *azc_0119*
R045	5'-TTTTTTAAGCTTTCAATAGTGGGGCTTGTAGAG-3'	*HindIII*	at the end of *A. caulinodans* ORS571 *azc_0119*

2.7 RNA Isolation

S. meliloti strains were inoculated in 5 ml of LBmc and grown overnight. The culture was washed with sterile saline three times and then subcultured in 50 ml of MOPS-P2 minimal medium supplemented with 15 mM of succinate or glucose as the sole carbon source and grown to an OD_{600} of approximately 0.7. 45 ml of the culture was transferred directly from the incubator to a 50 ml conical Falcon tube and mixed together with 5 ml of cell-stop solution (5% phenol in 100% absolute ethanol) by inverting rapidly and vigorously. The resulting 50 ml of mixture was spun at 4500 rpm for 10 minutes in Beckman Allegra X-22R bench top centrifuge with SX4250 rotor. Cell pellets were flash frozen in liquid N_2 and then store at -80°C.

Cell pellets were thawed on ice prior to use, and then resuspended in 1ml RNase-free water by vortexing. Each 0.5 ml of sample was mixed together with equal volume of hot phenol solution (16.7 mM Tris, 333.3 mM NaCl, 33.3 mM EDTA, 0.83% SDS, 16.7% phenol, pH 7.5) at room temperature in a micro centrifuge tube followed by incubation at 95°C (water bath) for 1 minute. The cell lysate was spun at 1, 3000 rpm for 10 minutes in Eppendorf 5424 centrifuges with FA-45-24-11 rotor to yield clean supernatant and discrete white pellet. The supernatant was transferred to a micro centrifuge tube and RNA was extracted once with 600µl of phenol-chloroform (1:1) and once with 1 ml chloroform. The clean supernatant was transferred to a micro centrifuge tube followed by the addition of sodium acetate to 0.3 M and 2 volume of isopropanol. The resulting mixture was stored on ice for 20-30 minutes and then centrifuged at 3000 rpm for 10 minutes in Eppendorf 5424 centrifuge (FA-45-24-11 rotor) to pellet

precipitated nucleic acids. White pellets were washed with 1ml of 70% ethanol (-20°C) and dried by air. The dried pellets were dissolved in 85 µl of RNase-free water followed by the addition of 10 µl of DNaseI buffer and 5 µl of DNaseI. After incubation at room temperature for 30 minutes, two 100 µl of reactions were pooled and mixed with 300 µl of RNase-free water, leading to a final volume at 500 µl. Total RNA was precipitated, washed, and dried as above. RNA pellets were dissolved in 100 µl of RNase-free water. The concentration of the RNA was determined by measuring a 200-fold dilution in a Varian Cary 1E UV-visible spectrophotometer at 260 nm (Absorbance of 1.0 = 40 µg/ml). The quality of purified RNA sample was estimated by measuring a fraction of OD_{260} to OD_{280}, which should be approach 2.0. Also, an aliquot of sample was run on 1% agarose gel to verify RNA isolation and absence of DNA. The purified total RNA samples were stored at -80°C prior to use.

2.8 Protein Determination

Protein concentrations of the various cell-free extracts and purified target protein samples were measured with Coomassie® Brilliant Blue G-250 dye using a modified Bradford assay (Bradford 1976). 5-10 µl volumes of the sample or a10-fold dilution were mixed together with ddH_2O to a final volume of 800µl in a micro centrifuge tube followed by the addition of 200 µl of protein assay dye reagent concentrate (Bio-Rad). The resulting mixture was vortexed and incubated at room temperature for 15 minutes. The absorbance at 595 nm was measured by using a Varian Cary 1E UV-Visible spectrophotometer. A standard curve (X: µg of BSA vs. Y: OD_{595}) generated by using BSA protein standard (1 to 10µg; Bio-Rad) was fitted as a linear function, $Y = a * X$ (a:

around 0.0572 in this work). The concentration of protein was calculated as μg /μl via the following formula: Conc. of protein = (OD_{595} * fold of dilution) / (a * μl of sample).

2.9 Preparation of His-tagged Fusion Proteins

In this study, His-tagged fusion proteins were purified from *E. coli* strain Top10 carrying pBAD/HisA derived plasmids (Table 3). The pBAD/His plasmids are pBR322-derived expression vectors designed for regulated, dose-dependent His-tagged fusion protein expression and purification in *E. coli*. The important elements carried by pBAD/His plasmids are described as following, 1) araBAD promoter (P_{BAD}), providing tight, dose-dependent regulation of fusion protein; 2) Optimized ribosome binding site, increasing efficiency of fusion protein expression; 3) Initiation codon (ATG), providing a translation site for the fusion protein; 4) N-terminal polyhistidines (His tag), providing a metal-binding site (Co^{2+}, Ni^{2+}) for affinity purification of the fusion protein on a metal-chelating resin; 5) Anti-Xpress™ epitope (Asp-Leu-Tyr-Asp-Asp-Asp-Asp-Lys), allowing the fusion protein to be detected by proper antibodies; 6) Enterokinase cleavage site (Asp-Asp-Asp-Asp-Lys), permitting enterokinase to remove the N-terminal His tag for yielding native protein; 7) multiple cloning site (MCS): allowing insertion of target gene for expression; 8) *rrnB* transcription termination region, providing a strong signal to stop mRNA synthesis; 9) Ampicillin resistance gene coding β-lactamase, providing an antibiotic mark for selection of *E. coli* strains carrying this plasmid; 10) pBR322 origin, controlling low copy replication of the plasmid in *E. coli*; 11) *araC gene*, encoding a regulatory protein for tight regulation of the P_{BAD} promoter.

The *E. coli* strain Top10 carrying pBAD/HisA derived plasmid was inoculated in 20 ml of LB broth containing 50µg/ml ampicillin and grown overnight. The culture was then subcultured in 500 ml of LB broth containing 50µg/ml ampicillin and grown to an OD_{600} of ~ 0.5. 5ml of sample (S1) was taken as the non-induced control immediately before the induction. L-arabinose was added to a final concentration of 1.3 to13 mM (0.02 to 0.2%) to induce expression of His-tagged fusion protein and the culture was incubated at 37°C for an additional 3-6 hours. Another 2 ml of sample (S2) was taken as the induced control. Cells from both non-induced and induced controls (S1 & S2) were pelleted at 13,000 rpm for 1 minute in an Eppendorf 5424 centrifuge (FA-45-24-11 rotor) and stored at -20°C until SDS-PAGE analysis. Induced cells were harvested from 500 ml culture by centrifugation at 7,000 rpm for 15 minutes at 4°C in a Sorvall RC-5B super speed centrifuge with GSA rotor. Cell pellets were flash frozen in liquid N_2 and then store at -80°C until purification of His-tagged fusion protein.

The cell pellet from the 500 ml culture was thawed on ice 15 minutes prior to use, and then resuspended in 10 ml of native lysis buffer (50 mM NaH_2PO_4, 300 mM NaCl, 10 mM imidazole, and pH 8.0) followed by the addition of 100 µl of protease inhibitor cocktail (Sigma). Cells were lysed by passage 2 to 4 times through a French Pressure Cell Disrupter (Thermo Electron Co.) at 20,000 psi. Cell lysate was centrifuged at 40,000 rpm for 1 hour at 4°C in a Beckman L8-M ultracentrifuge with SW50.1 rotor to pellet the cellular debris. 20 µl aliquot of supernatant (S3) was sampled and stored at -20°C until SDS-PAGE analysis. The Ni-NTA resin (QIAGEN) was regenerated and equilibrated according to the manufacturer's instructions. 2 ml of Ni-NTA resin was added to the

clean supernatant (~10 ml) in a 15ml conical Falcon tube followed by gentle mixing at 4 °C for 30 minutes. The resulting mixture was carefully loaded into an Econo-Column Chromatography Column (1.5 cm x 10cm, Bio-Rad) and the lysate was then flowed through the columns slowly at 4°C. 20 µl aliquot of flow-through lysate (S4) was sampled and stored at -20°C until SDS-PAGE analysis. The Ni-NTA resin was washed three times with 10 ml of washing buffer (50 mM NaH_2PO_4, 300 mM NaCl, 20 mM imidazole, and pH 8.0). 20 µl aliquot of flow-through washing buffer (S5) was sampled and stored at -20°C until SDS-PAGE analysis. The His-tagged fusion protein was eluted at 4°C with 3-6 ml elution buffer (50 mM NaH_2PO_4, 300 mM NaCl, and pH 8.0) supplemented with imidazole from 100 to 250 mM. The elute was collected in 1 ml fractions and 20 µl aliquots of each fraction (S_E) was stored at -20°C for analysis. Samples of each elute fraction were run on 10% SDS-PAGE to detect which fraction(s) contained the majority of target protein and estimate the quantity and purity of target protein in each elute fraction. Fractions containing the majority of the target protein were pooled together in a Spectro/pro 4 multi-purpose dialysis tubing (MWCO: 12-14 kD, Fish Scientific) and dialyzed against 100-fold volume of storage buffer (50 mM Tris, 100 mM KCl, 2 mM $MgCl_2$, 2 mM DTT, 10% glycerol, and pH 8.0) at 4°C with two or three buffer changes over the period of 12 - 24 hours. After dialysis, concentration of protein was measured by using a Bradford protein assay. Dialyzed samples were flash frozen in liquid nitrogen and stored at -80°C in 100-µl aliquot prior to further experiments.

2.10 Preparation of Bacteroid and Free-Living Cell Extracts

Bacteroids were prepared by grinding (with ice-cold mortar and pestle) ~3 g of fresh nodules with 10ml of sterile ice-cold MMS buffer (40mM MOPS, 20mM KOH, 20mM $MgSO_4$, 0.3M Sucrose, and pH 7.0). After filtration through four layers of cheesecloth with ice-cold MMS buffer, the homogenates were centrifuged at 1000 rpm for 10 minutes at 4 ºC in Beckman Allegra X-22R bench top centrifuge with SX4250 rotor to remove nodule debris. The resulting supernatant was transferred into a fresh tube and centrifuged at 4500 rpm for 10 minutes at 4 ºC in Beckman Allegra X-22R bench top centrifuge with SX4250. The pellet was washed twice with ice-cold, MMS buffer, flash freeze in liquid nitrogen, and store at -80 ºC prior to use.

20 ml LBmc-grown free-living cell cultures grown to an OD_{600} of ~ 1 were centrifuged at 4500 rpm for 10 minutes in Beckman Allegra X-22R bench top centrifuge (SX4250 rotor). The resulting pellet was washed twice with 1ml of ice-cold saline and then resuspended with 500 µl of ice-cold sonication buffer (25 mM Tris, 100 mM KCl, 1 mM $MgCl_2$, 10% glycerol, 10 mM 2-mercaptoethanol, and pH 8) in a micro centrifuge tube.

To prepare extracts, the bacteroid or free-living cell pellet were thawed on ice and resuspended in 1ml of ice-cold MMS. Cells were disrupted by using a Cell Disrupter 350 (Branson Ultrasonics, USA) at an output level of 4 for 10 to 15 cycles per sample at 10 seconds per cycle. Samples were placed in an ice bath for 3 min after each cycle. The cell lysates were centrifuged at 4 ºC and 13,000 rpm for 30 minutes in Eppendorf 5424

centrifuge (FA-45-24-11 rotor) to pellet unlysed cells and the cellular debris. The resulting supernatant was aliquoted, flash frozen in liquid nitrogen, and stored at -80 ºC.

2.11 SDS-PAGE and Western Blot Analysis

Proteins were separated by SDS-PAGE in gels cast and run in the Mini-PROTEAN® 3 Cell (Bio-Rid) system. Separating gels were made up of 375 mM Tris (pH 8.8), 0.1% SDS, 8-10% Acrylamide/Bis (37.5/1, Bio-Rad), 0.05% APS, and 0.05% TEMED. The stacking gel consisted of 125 mM Tris (pH 6.8), 0.1% SDS, 4% Acrylamide/Bis (37.5/1, Bio-Rad), 0.05% APS, and 0.1% TEMED. Generally, 30 µl of protein sample was mixed together with 10µl of 4x protein loading dye (250 mM Tris, 8% SDS, 0.04% bromophenol blue, 40% glycerol, 0.4M DTT, and pH 6.8) in a micro centrifuge tube. The resulting mixture was boiled for 5 minutes and centrifugation at 13,000 rpm for 2 minutes in an Eppendorf 5424 centrifuge (with FA-45-24-11 rotor). 5-10 µl of clean supernatants were loaded onto a SDS-PAGE gel and run at 150 volts for approximately 1 hour or until the bromophenol blue dye reached the bottom of the gel. Gels were stained for several hours with stain solution (0.25% Coomassie brilliant blue R250 in destain solution) and destained via repeated changes of destain solution (40% methanol, 10% acetic acid, and 50% ddH_2O) until protein bands were visible.

For Western blot analysis the proteins were transferred from SDS-PAGE gels to membrane using the Trans-Blot® SD Semi-Dry Transfer Cell system (Bio-Rad). Thick blotting paper and Hybond-P PVDF membrane (Amersham Pharmacia biotech) were cut to the same size as the gel. The PVDF membrane was pretreated in 100% methanol for 1 minute and equilibrated in transfer buffer (48mM Tris, 39mM glycine, and 20% methanol)

for 30 minutes. The thick blotting paper was soaked in transfer buffer and then stacked on the anode plate of electroblotter followed by the membrane, gel, and another layer of blotting paper. The cathode was place over the top of the stack and transfer was run at 10 volts for 60-75 minutes. The membrane was carefully removed from the stack and incubated with Blocking Buffer (5% skim milk in Tris-Buffered Saline with Tween (TBST): 20 mM Tris pH 7.5, 500mM NaCl, and 0.05% Tween20) for 1-2 hours with shaking at room temperature. The membrane was then washed three times with 20 ml of TBST for 10 min with shaking at room temperature. The membrane was treated with primary antibody for 1-2 hours in 20ml of TBST containing 5% skim milk and anti-DME or anti-TME serum (Voegele *et al*. 1999) made in rabbit (1000-fold dilution, adjust according to the titer of antibodies) with shaking at room temperature. After washed three times with 20ml of TBST for 10 min, the membrane was exposed to secondary antibody for 1-2 hours in 20ml of TBST containing 5% skim milk and goat anti-rabbit IgG-AP conjugate (3000-fold dilution, or as directed by supplier: Bio-Rad) with shaking at room temperature. The membrane was then washed three times with 20 ml of TBST for 10 min with shaking at room temperature. In a clean dish, the membrane was equilibrated for 5 min in AP buffer (100 mM Tris, 0.5mM $MgCl_2$, and pH9.5) followed by removing excess buffer. 10ml of AP buffer containing 0.3mg/ml NBT and 0.15mg/ml BCIP (Promega) was then added to the membrane followed by incubation in the dark at room temperature until the development of dark purple color (5-10min). The membrane was immersed in ddH_2O for 10 min to stop color development.

2.12 Plant Assays

Cajanus cajan cv. Pigeon pea, *Lablab purpureus* cv. Dolichos Rongai, *Leucaena leucocephala* (Lain.) de Wit, *Macroptilium atropurpureum* cv. Aztec Atro, and *Vigna unguiculata* cv. Red Caloona cowpea seeds were obtained from Queensland Agricultural Seeds Pty Ltd (Toowoomba, Queensland, Australia). Prior to germination, these hardcoated seeds were scarified by treatment with concentrated H_2SO_4 (5 minutes for *C. cajan*, 15-20 minutes for *L. purpureus*, 5-10 minutes for *M. atropurpureum*, and 10 minutes for *V. unguiculata*). They were then thoroughly rinsed with sterile ddH_2O, and soaked in sterile H_2O until swollen. Seeds were then surface sterilized in 3% sodium hypochlorite for 10 min and repeatedly rinsed with sterile ddH_2O over 1 hour. Seeds were then evenly placed on 1.5% water agar and allowed to germinate in the dark for 2 to 4 days, depending on the species. Alfalfa seeds (*Medicago sativa*, OSC Seeds) were treated differently as above. They were surface sterilized using 95% ethanol (5 min) and 2.5% sodium hypochloride (20 min) followed by rinsed with sterile water for 1 hour before being transferred to 1.5% water agar plates for germination.

Leonard assemblies were made up of two plastic pots that are connected by a cotton wick which extends from top into the bottom chamber. The top pot was filled with nitrogen free sand and vermiculite mixture with a ratio of 1 to 1 in volume followed by the addition of 250 ml Jensen's medium (pH 7.0) composed of (per litre): 1 g $CaHPO_4$, 0.2 g K_2HPO_4, 0.2 g $MgSO_4 \cdot 7\ H_2O$, 0.2 g NaCl, 0.1 g $FeCl_3$, 1 ml of 1000x trace solution (1 g/l H_3BO_3, 1 g/l $ZnSO_4 \cdot 7H_2O$, 0.5 g/l $CuSO_4 \cdot 5H_2O$, 0.5 g/l $MnCl_2 \cdot 4H2O$, 1 g/l $Na_2MoO_4 \cdot 2H_2O$, 10 g/l $Na_2EDTA \cdot 2H_2O$, and 2 g/l NaFeEDTA). Leonard

assemblies were covered and autoclaved for 30 minutes on liquid cycle. According to the size of plants, 4-8 seedlings, 1-2 cm in length were planted approximately 2 cm deep in each pot and these were placed in a Conviron growth chamber for 2 to 5 days prior to inoculation. For each pot, seedlings were inoculated with approximately 1x 10^8 log-phase cells. Growth chamber conditions were 16 hours of light at 28°C (tropical legumes) or 21°C (temperate legumes) and 8 hours dark at 20°C (tropical legumes) or 17°C (temperate legumes). Plants were watered with sterile distilled H_2O as required and grown until the non-inoculation controls displayed clear symptoms of nitrogen deficiency (yellowing of leaves and stunted growth). For *M. sativa, C. cajan, M. atropurpureum,* and *V. unguiculata,* this occurred after 4 to 6 weeks of growth, while *L. purpureus* and *L. leucocephala* were grown for 10 weeks All plant assays were carried out in triplicate and were repeated at least twice.

2.13 Nodulation Kinetic Assays

Nodulation kinetic assays were performed in sterile glass tubes containing 1% agar slants of Jansen's medium (2.12 plant assay). The pH of the Jansen's medium was adjusted to 7.0 before it was added. The tops of the tubes were closed with aluminum foil. A single seedling with 1-2 cm in length (around 2-day germination in dark at room temperature) was transferred to each slant using sterile technique followed by incubation in a Conviron growth chamber for 3 days. Each seedling was inoculated with 1x 10^6 log-phase rhizobial cells. Plants were grown for up to 20 days with growth chamber parameters set as above (2.12 plant assay). For each strain, 15 plants were examined every two days and the number of nodules was recorded.

2.14 Shoot Dry Weight Determination and Acetylene Reduction Assay (ARA)

Plants were harvested and cut at the root-shoot junction. All plants from each pot were put together in a paper bag and dried in an oven at 70°C over a period of two weeks. Dry weights were measured on a Mettler PE600 balance. After acetylene reduction assay, all functional nodules (pink) from each pot were counted and weighed.

Nitrogenase activity was measured by monitoring the reduction of acetylene to ethylene by total root systems from each pot. The root systems were cut from the plants, and immediately placed in a bottle, and sealed with a serum stopper. 10% total volume of air in the bottle was replaced with acetylene (Liquid Air Ltd, Burlington, ON). After incubation at room temperature for 15 minutes, 50 µl gas samples were removed from the bottle and injected using Hamilton ® 1719N syringe (100µl, gastight; Fisher Scientific) into an Agilent HP6890 GC gas chromatograph equipped with an Agilent J&W GS-Gas pro column (L × I.D.: 30m × 0.32 mm) with N_2 carrier gas. GC settings were inlet, 250°C at 100 ml min^{-1} split flow; column constant flow at 1.4 ml min^{-1}; oven, 90°C; and flame ionization detector, 260°C, with H_2 flow at 40 ml min^{-1} and airflow at 450 ml min^{-1}. Retention times for the ethylene and acetylene peak were108 and 138 seconds respectively.

A standard curve (X: nmol of ethylene vs.Y: area of ethylene peak) was generated by using the 507ppm (22.6µM) ethylene standard (0 to 5 nmol; Liquid Air Ltd, Burlington, ON) and fitted as a linear function, $Y = 7.574 * X$ (R^2=0.9952). Therefore the

specific activity of nitrogenase was calculated as nmol ethylene produced/hour/plant (or gram of fresh nodules) via using the following formula: S.A = (area of the ethylene peak * µl of bottle * 60) / (7.574 * µl of gas sample * minutes of incubation * number of plants or g of fresh nodules).

2.15 Malic Enzyme Assay

Malic enzyme (ME) catalyses the reaction: malate + $NAD(P)^+$ $\rightleftharpoons$ pyruvate + CO_2 + NAD(P)H. Malic enzyme activity in crude extracts was measured via a colorimetric assay based on the L-malate-dependent formation of pyruvate as detected with 2,4-dinitrophenylhydrazine (Friedmen and Haugen, 1943). 5 µl of cell extract (~20 µg total protein) was mixed together with 500 µl of reaction buffer (100 mM Tris pH 7.8, 30 mM Sodium-L-Malate, 3 mM $MnCl_2$, 5 mM NH_4Cl, and 0.3 mM NAD^+ for DME assay or 0.3 mM $NADP^+$ for TME assay) in a micro centrifuge tube followed by incubation at 30 °C for 30 minutes. The reaction was stopped by adding 165 µl of 0.1% 2, 4-dinitrophenylhydrazine (in 2 M HCl). After 10 minutes incubation at room temperature, 835 µl of 2.5 M NaOH was added and the resulting mixtures were centrifuged at 3000 rpm for 5 minutes in Eppendorf 5424 centrifuged to pellet the precipitate. The absorbance at 445 nm of the supernatant of each reaction was measured in a Varian Cary 1E UV-Visible spectrophotometer. A standard curve (X: nmol of pyruvate vs. Y: OD_{445}) made with pyruvate standard (0 to 110 nmol; Sigma) was fitted as a linear function, Y = 0.0092 * X (R^2=0.9957). The specific activity was calculated as nmol of pyruvate produced/minute/mg protein via using the following formula: S.A. = (OD_{445} * 1000) / (0.0092 * minutes of incubation * µg of total protein).

The activity of purified malic enzyme was determined by monitoring the formation of NAD(P)H based on the change in the absorbance at 340 nm (Scrutton, 1971). The molar extinction coefficient of NAD(P)H at 340 nm was taken as 6.22×10^{-3} ml $nmol^{-1}$ cm^{-1}. The reaction was initiated by mixing 5 µl of sample together with 1ml assay buffer (100 mM Tris pH 7.8, 30 mM Sodium-L-Malate, 3 mM $MnCl_2$, 5 mM NH_4Cl, and 1.5 mM NAD^+ for DME assay or 1.5 mM $NADP^+$ for TME assay) in a 1.5 ml cuvette. The absorbance at 340 nm was recorded every 10 seconds over 2 minutes in a Varian Cary 1E UV-Visible spectrophotometer. The specific activity of malic enzyme was calculated as nmol of NAD(P)H produced/minute/mg protein via using the following formula: $S.A = (\Delta OD_{340} * 10^3) / (\Delta minutes * 6.22 * mg\ of\ total\ protein)$. For both assays, all samples were done in triplicate and the background activity was measured for the complete reaction mixture without adding protein.

2.16 Malate Dehydrogenase Assay

Malate dehydrogenase (MDH) catalyses the reaction: malate + NAD^+ $\rightleftharpoons$ oxaloacetate (OAA) + NADH. Malate dehydrogenase activity in crude extracts was measured via observing the change in absorbance at 340 nm due to the reduction of NAD^+ to NADH (Englard and Siegal, 1969). The reaction was initiated by mixing 5 µl of cell extract or 10-fold dilution together with 1ml assay buffer (100 mM Glycine-NaOH pH10.0, 90 mM sodium-L-Malate, and 2.5 mM NAD^+) in a 1.5 ml cuvette. The absorbance of sample at 340 nm was recorded by a Varian Cary 1E UV-Visible spectrophotometer at every 10 seconds over 2 minutes. MDH specific activity was calculated as nmol of NADH produced/minute /mg protein via using the following

formula: S.A = (ΔOD_{340} * 10^3) / (Δminutes * 6.22 * mg of total protein). All samples were done in triplicate and the background activity was measured for the complete reaction mixture without adding protein.

2.17 Phosphoenolpyruvate Carboxykinase Assay

Phosphoenolpyruvate carboxykinase (PCK) catalyzes the reaction: oxaloacetate (OAA) + ATP $\rightleftharpoons$ Phosphoenolpyruvate (PEP) + CO_2 + ADP. The PCK specific activity was assayed by monitoring the change in absorbance at 340 nm due to phosphoenolpyruvate-dependent oxidation of NADH to NAD^+ in an assay system coupled with MDH (Englard and Siegal, 1969; Blasing *et al*. 2000). The reaction was initiated by mixing 5 µl of cell extract together with 1ml assay buffer (50 mM $NaHCO_3$, 100 mM imidazole pH6.6, 2 mM reduced glutathione, 1.25 mM ADP, 2 mM $MnCl_2$, 0.1 mM NADH, 2.5 mM PEP, and 5 U/ml MDH) in a 1.5 ml cuvette. The absorbance at 340 nm was measured as described above every 30 seconds over 3 to5 minutes. The resulting slope (S1: ΔOD_{340} /Δminutes) was contributed by the total oxidation of NADH to NAD^+ in a reaction mixture. The second slope (S2: ΔOD_{340} /Δminutes) associated with background NADH oxidase activity was then measured by mixing another 5 µl of cell extract together with 1ml assay buffer without PEP and monitoring the change in absorbance at 340 nm at every 30 seconds over 3 to5 minutes. PCK specific activity was calculated as nmol of NADH oxidized/minute /mg protein via using the following formula: S.A = [(S1-S2) * 10^3] / (6.22 * mg of total protein). All samples were done in triplicate.

2.18 Soluble Pyridine Nucleotide Transhydrogenase Assay

The soluble pyridine nucleotide transhydrogenase (STH) catalyses the reaction: $NAD^+ + NADPH \rightleftharpoons NADH + NADP^+$. Transhydrogenase activity in crude extracts was measured via observing the change in absorbance at 400 nm due to the reduction of thionicotinamide adenine dinucleotide (thio-NAD^+) to thio-NADH (French *et al*. 1997). The molar extinction coefficient of thio-NADH at 400 nm was taken as 11.3×10^{-3} ml $nmol^{-1}$ cm^{-1} (Cohen and Kaplan 1970b). The reaction was initiated by mixing 5 µl of cell extract together with 1ml assay buffer (50 mM Tris pH 7.0, 200 µM NADPH, 200 µM thio-NAD^+) in a 1.5 ml cuvette. The absorbance at 400 nm was measured as described above every 30 seconds over 2 to 5 minutes. STH specific activity was calculated as nmol of thio-NADH produced/minute/mg protein via using the following formula: $S.A = (\Delta OD_{400} * 10^3) / (\Delta minutes * 11.3 * mg\ of\ total\ protein)$. All samples were done in triplicate and the background activity was measured for the complete reaction mixture without adding protein.

2.19 Reporter Enzyme Assays

Report gene fusion strains (*S. meliloti*) were grown overnight in 2 ml of LBmc, washed with sterile saline three times, and subcultured into 5 ml of MOPS-P2 minimal medium supplemented with 15 mM of succinate or glucose as the sole carbon source and grown to an OD_{600} of approximately 1. One hundred microliters of each culture was transferred to a fresh 96-well plate and culture turbidity (OD_{600}) was measured.

The green fluorescent protein (GFP) is a protein composed of 238 amino acid residues (26.9kDa) that exhibits bright green fluorescence when exposed to light in the blue to ultraviolet range (Tsien 1998). The GFP used in this study has major excitation peak at 485 nm and emission peak at 510 nm (Cowie *et al*. 2006). The OD_{600} and fluorescence emission at 510 nm (480 nm excitation wavelength) of 100 µl of cultures in 96-well plates were measured using a Tecan Safire microplate spectrophotometer. Relative fluorescence (R.F.) was calculated using the following formula, R.F. = fluorescence at 510 nm (culture – MOPS minimal medium)/OD_{600}.

β-Galactosidase (LacZ) cleaves the synthetic analogue 2-Nitrophenyl-β-galactoside (ONPG) to produce 2-nitrophenol which has an absorbance maximum of 420 nm (Miller, 1972). β-Galactosidase assays were initiated by mixing 10 µl of culture together with 90 µl of assay buffer (60 mM Na_2HPO_4, 40 mM NaH_2PO_4, 10 mM KCl, 1 mM $MgSO_4$, and 0.8 mg/ml ONPG) in a fresh 96-well plate followed by incubation at room temperature for 30 to 60 minutes. The reactions were stopped by adding 100 µl of 1 M Na_2CO_3 and the absorbance at 420 nm was measured in a Tecan Safire microplate spectrophotometer. Specific activity was = (1000 * OD_{420}) / (minutes * OD_{600} *µl of culture).

β-glucuronidase (GusA) cleaves 4-Nitrophenyl β-D-glucuronide (PNPG) releasing 4-nitrophenol (Jefferson *et al*. 1986). Assays were initiated by mixing 10 µl of culture together with 90 µl of assay buffer (50 mM Sodium Phosphate buffer pH7, 50 mM DTT, 1 mM EDTA, 0.0125% SDS, and 0.5 mg/ml PNPG) in a 96-well plate and incubating at room temperature for 30 to 60 minutes. The reactions were stopped by

adding 100 µl of 1 M Na_2CO_3 and the absorbance measured at 405 nm with a Tecan Safire microplate spectrophotometer. Specific activity was = (1000 * OD_{405}) / (minutes * OD_{600} *µl of culture).

All assays were carried out in triplicate for statistical analysis and verification of reproducibility.

2.20 Determination of Intracellular Pyridine Nucleotides

Extraction of intracellular pyridine nucleotides, such as NAD^+, $NADP^+$, NADH, and NADPH, was performed using alkaline extraction (Sanchez *et al*. 2006; Stocchi *et al*. 1985). *S. meliloti* strains grown overnight in 5 ml of LBmc were subcultured in 20 ml of LBmc and grown to an OD_{600} of approximately 1.5. Cells were harvested by centrifugation at 4500 rpm and 4°C for 10 minutes in Beckman Allegra X-22R bench top centrifuge with SX4250 rotor. Cell pellets were washed with 1 ml of sterile ice-cold saline twice. Free-living cell pellets prepared as above and bacteroid cell pellets from 1-2 g of nodules were completely resuspended in 1ml ice-cold 0.5 M KOH by vigorous shaking and left to stand on ice for 10 minutes. 1 ml of ice-cold ddH_2O was added and the mixture was left on ice for 10 minutes. The resulting solutions were immediately sonicated (five 10-s bursts) to ensure maximal extraction of the nucleotides and centrifuged at 4 ºC and 13,000 rpm for 5 minutes in Eppendorf 5424 to remove unlysed cells and cellular debris. After passage through a 0.2 µm filter (Millipore) to remove residual cell debris, the supernatants were loaded in Amicon Ultra-centrifugal filters (MWCO: 10kD, Millipore) and centrifuged at 4 ºC and 13,000 rpm for 10 to 15 minutes in an Eppendorf 5424 centrifuge. The resulting solution was neutralized with 0.1 volume

of 1 M KH_2PO_4, pH 6, and filtered through a 0.2 µm syringe filter (Millipore) before injection into the HPLC. A 100-µl aliquot of each sample were immediately used for measuring intracellular pyridine nucleotides by HPLC, and the rest were flash frozen in liquid nitrogen and stored at -80°C in 200-µl aliquot for short term.

NAD^+, $NADP^+$, NADH, and NADPH were determined using an Agilent 1200 HPLC equipped with a Sigma SUPELCOSIL^{TM} LC-18-T (5 µm particle size, L × I.D.: 25 cm × 4.6 mm), as described by Stocchi *et al* (1985). Data were acquired and analyzed by using a program; Agilent EZChrom Elite. The mobile phase consisted of two eluants: buffer A (0.1M potassium phosphate, pH 6.0) and buffer B (buffer A with 10% methanol). 5 µl of each sample was injected for assay. The chromatographic conditions used to obtain the chromatograms were set as following: the column was run at room temperature, the flow rate was 1.3 ml per minute, and the detection was performed at 254 nm; 9 minutes at 100% buffer A, 6 minutes at up to 25% of buffer B, 2.5 minutes at up to 90% of buffer B, 2 minutes at up to 100% of buffer B, and hold for 3 minutes. The gradient was then returned to 100% of buffer A in 2.5 minutes. Identities of peaks were further confirmed by co-elution with relative standards. Figure 7 showed the separation of a standard mixture where ATP, NAD^+, $NADP^+$, NADH, and NADPH were completely separated in 22 minutes

Quantitative measurements were carried by injection of standard solutions with concentrations ranged from 10 µM to 10mM. Nucleotide standards (NAD^+, $NADP^+$, NADH, and NADPH) of the highest grad available were obtained from Sigma. For each standard, the stock solution was prepared before use in buffer A (0.1M potassium

phosphate, pH6.0) and the work solutions were prepared by serial 10-fold dilutions from the stock solution in 10x buffer A. All standard solutions were left to stand on ice during HPLC analysis. For each compound a standard curve generated (X: nmol of standard vs. Y: area of peak/10000) and fitted to a linear equation as: NAD^+, Y = 36 * X (R^2=1); $NADP^+$, Y = 40 * X (R^2=1); NADH, Y = 63 * X (R^2=0.9999); NADPH, Y = 55 * X (R^2=1). The concentrations of intracellular pyridine nucleotides from each sample were calculated as µmol/L via using the following formula: NAD^+ = (area of peak) / (360 * µl of injection); $NADP^+$ = (area of peak) / (400 * µl of injection); NADH = (area of peak) / (630 * µl of injection); NADPH = (area of peak) / (500 * µl of injection). All samples including standards were assayed in triplicate for statistical analysis and verification of reproducibility.

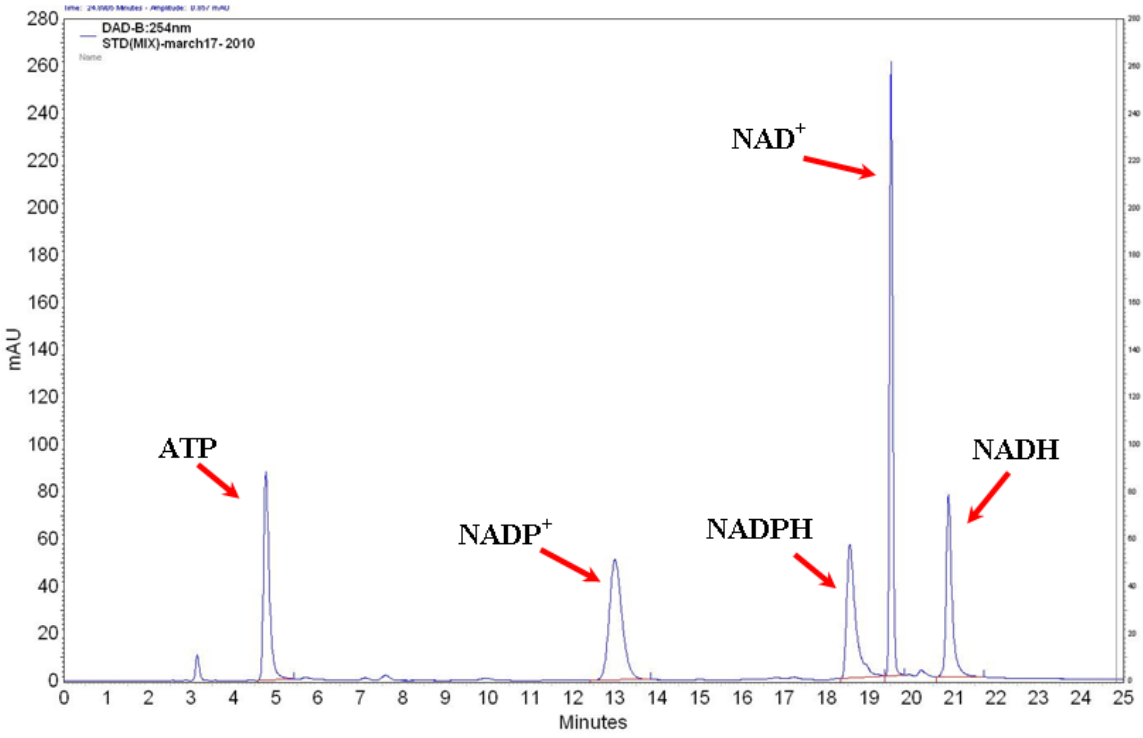

Figure 7 Separation of a standard mixture of five selected nucleotides by HPLC

Supelcosil LC-18-T column: 5µm particles, 25cm x 4.6mm ID. The compounds were monitored at 254nm (UV). Flow-rate: 1.3ml/min. Mobile phase: (buffer A) 0.1 M potassium phosphate pH=6.0, (buffer B) 0.1M potassium phosphate with 10% methanol. Gradient program: 0 to 9min (buffer A: 100%), 9 to 15min (buffer A: 100 to 75%), 15 to 17.5min (Buffer A: 75 to 10%), 17.5 to 19.5min (Buffer A: 10 to 0%), 19.5 to 22.5min (Buffer A: 0%), 22.5 to 25min (Buffer A: 0 to 100%)

Chapter 3 Symbiotic N_2-fixation by NAD^+-Malic Enzyme Mutants of *Sinorhizobium* Sp. Strain NGR234

3.1 Abstract

N_2 fixation requires a high energy input, and the primary carbon and energy sources supplied to bacteroids appear to be C_4-dicarboxylic acids, such as malate and succinate. To provide energy and reductant for nitrogen fixation, these C_4-dicarboxylic acids appear to be metabolized via the tricarboxylic acid (TCA) cycle in N_2-fixing bacteria (bacteroids) within legume nodules. The maintenance of metabolic flux through the TCA cycle during C_4-dicarboxylate oxidation requires acetyl-coenzyme A (acetyl-CoA), generated from malate via malic enzyme, and from oxaloacetate via the enzyme phosphoenolpyruvate carboxykinase (PCK). In *Sinorhizobium meliloti* bacteroids from alfalfa, NAD^+-malic enzyme (DME) is required for N_2 fixation, and this activity is thought to be required for the anaplerotic synthesis of pyruvate. In contrast, in the pea symbiont *Rhizobium leguminosarum*, pyruvate synthesis occurs via either DME or a pathway catalyzed by phosphoenolpyruvate carboxykinase (PCK) and pyruvate kinase (PYK). Thus, it raised the possibility that the symbiotic phenotype of *dme* mutants is dependent on the host plants. To gain further insight into the role of malic enzymes in nodules, we sequenced the NGR234 *dme* gene and isolated *dme* and *dme pckA* mutants of

the broad-host range *Sinorhizobium* strain NGR234. The NGR234 *dme* mutants were found to form Fix^+ nodules whose level of N_2 fixation varied from 27 to 83% (plant dry weight) of the wild-type level, depending on the host plant inoculated. NGR234 bacteroids had significant PCK activity, and while single *pckA* and single *dme* mutants fixed N_2 at reduced rates, a *pckA dme* double mutant had no N_2-fixing activity (Fix^-). Thus, NGR234 bacteroids appear to synthesize pyruvate from TCA cycle intermediates via DME or PCK pathways. Moreover, in other studies, *dme* mutants of *B. japonicum* and *Mesorhizobium loti* were reported to form Fix^+ nodules on soybean and *Lotus*, respectively. Together, these findings demonstrated that the N_2 fixation phenotype of *dme* mutants is host plant dependent and also suggest that the completely Fix^- phenotype of *S. meliloti dme* mutants is unusual and perhaps unique to the *S. meliloti*-alfalfa symbiosis.

3.2 Materials and Methods

Bacterial strains and plasmids utilized are listed in Table 3. Primers used are listed in Table 4 and ordered from Sigma-Aldrich or Integrated DNA Technologies. Methods are summarized in Chapter 2 of this thesis.

3.2.1 Cloning of the *dme* Gene, DNA Sequencing, and Computer Analysis

The NGR234 *dme* gene was cloned and sequenced prior to the release of the NGR234 genome sequence (Schmeisser *et al*. 2009) and the procedure employed to sequence and clone this gene is shown here. Degenerate primers were designed on the basis of highly conserved regions identified through alignment of the *dme* genes from 5 related strains belonging to alphaproteobacteria, *R. leguminosarum* bv. viciae 3841, *Rhizobium etli* CFN 42, *S. medicae* WSM419 ctg39, *Agrobacterium tumefaciens* str. C58,

and *S. meliloti* 1021 (Figure 8). The locations of the primers listed below are indicated relative to their 5' position in the NGR234 *dme* gene. Two pairs of degenerate primers, DME-NGR-FP1 (bp 264) plus DME-NGR-RP1 (bp 2205) and DME-NGR-FP2 (bp 422) plus DME-NGR-RP2 (bp 1764), were first used to PCR amplify the *dme* gene region, using genomic DNA of NGR234 (Figure 9). After purification, two target PCR fragments, FP1/RP1 (~2kb) and FP2/RP2 (~1.3kb), were sequenced in both directions. The DNA sequences extending to either side of *dme* were obtained directly from genomic DNA by using primers, DME-NGR-FP8 (bp 1814), DME-NGR-RP6 (bp 483), and DME-NGR-RP9 (bp 35) (Figure 9). All sequencing was performed using a model 3730 DNA analyzer (Mobix) at McMaster University. DNA sequences were assembled and analyzed with DNAMAN 6.0 (Lynnon Co.). The nucleotide sequence of the NGR234 *dme* region was assigned GenBank/NCBI accession number FJ215683.

3.2.2 Construction and Complementation of *Sinorhizobium* sp. NGR234 *dme* Mutants

In order to construct *dme* mutants of NGR234, we introduced the $\Omega Sp^r/Sm^r$ cassette (Blondelet-Rouault *et al*. 1997) into the coding sequence of *dme* gene as follows. Plasmid pTH2415 was constructed by inserting the NGR234 *dme* gene region from positions 246 to 1483 (amplified using the primers DME-NGR-FP11 and DME-NGR-RP13) into the Gm^r plasmid pJQ200-mp18 (Figure 10) via *Bgl*II/*Bam*HI and *Pst*I/*Nsi*I. Plasmid pTH2457 was constructed by inserting the NGR234 *dme* gene region from positions from positions bp -471 (upstream) to 87 (amplified using the primers DME-NGR-FP18 and DME-NGR-RP18) into the Gm^r plasmid pJQ200-mp18 via *Bgl*II/*Bam*HI

and *XbalI*. The NGR234 *dme* gene region from positions 587 to 1186 (amplified using the primers DME-NGR-FP20 and DME-NGR-RP20) was inserted into pTH2457 via *XbalI* and *PstI/NsiI*, generating pTH2462. Plasmid pTH2429, carrying a 2-kb ΩSp^r Sm^r cassette inserted at the *SalI* site at position 418 relative to the ATG *dme* start codon (the *dme-9*::ΩSp^r Sm^r allele) (Figure 9), and pTH2467, in which the *dme* gene region from bp 88 to 586 was deleted and replaced with the 2-kb ΩSp^r Sm^r cassette (the *dme*Δ*14*::ΩSp^r Sm^r allele) (Figure 9), were transferred from *E. coli* to the wild type NGR234 strain RmG694 (Stanley *et al*. 1988). The transconjugants, RmP1809 (NGR234R, *dme-9*::Ω Sp^r) and RmP1814 (NGR234R, *dme*Δ*14*::Ω Sp^r) were identified as Rif^r Sp^r Gm^s colonies growing with 5% sucrose. The structure of the *dme* mutations in genomic DNAs from RmP1809 (*dme-9*) and RmP1814 (*dme*Δ*14*) was verified by restriction analysis following PCR amplification of the *dme* region by use of primers from outside the region employed for mutant construction, DME-NGR-FP15v (bp -460 upstream), DME-NGR-RP16v (bp 1596), and DME-NGR-FP21v (bp -566), and the absence of the DME protein was verified by Western Blot analysis.

To construct the NGR234 *pckA dme* double mutant (RmP2648), we deleted the whole *dme* gene from the *pck* mutant (RmG694*pckA*) (Figure 14). A PCR fragment containing the NGR234 *dme* gene region from positions bp 1832 to +920 (downstream) (amplified using the primers DME-NGR-FP30 and DME-NGR-RP31) was inserted into pTH2457 via *XbalI* and *PstI*, generating pTH2530, which contained the NGR234 *dme* gene region together with its flanking DNA at both sides. Plasmid pTH2530 was transferred into an *E. coli* strain BW25113 (M1420), carrying a lambda Red recombinase

expression plasmid pKD46 (Figure 11) (Datsenko and Wanner 2000), generating a new strain M1479. M1479 was grown in 100ml of SOB medium (2% Bacto tryptone, 0.5% Bacto yeast extract, 10 mM NaCl, and 2.5 mM KCl) with ampicillin and 1 mM L-arabinose at 30 °C to an OD600 of ~0.5, and electroporation-competent cells were prepared by washing these cells three times with ice-cold 10% glycerol and concentrating the cells 100-fold. A PCR fragment containing a Km^r/Nm^r cassette flanked by FLP recombinase recognition target (FRT) sites and 50-bp homologies to the upstream and downstream sequences adjacent to NGR234 *dme* gene was amplified from pKD13 (Figure 12) (Datsenko and Wanner 2000) (using the primers DME-NGR-FP32 and DME-NGR-RP32) and transferred into competent cells (M1479). Electroporation was done by using a Gene Pulser ® II Electroporation System (Bio-Rad) according to the manufacturer's instruction by using 75µl of cells and 50-500 ng of PCR product. Shocked cells were added to 1 ml of SOC medium (SOB plus 10 mM $MgCl_2$, 10 mM $MgSO_4$, and 20 mM glucose) with 1 mM L-arabinose, incubated at 37°C for 1-2 hours, and spread onto agar plates to select Km^r transformants at 37°C. The resulting plasmid (pTH2532), in which the *dme* gene region was completely deleted and replaced with the FRT-flanked Km^r/Nm^r cassette, was transferred from *E. coli* into the NGR234 *pckA*::Ω Sp^r, and the transconjugants, RmP2648 (NGR234, *pckA*:: Ω Sp^r & Δ*dme*:: FRT- Km^r/Nm^r-FRT), were identified as Rif^r Sp^r Nm^r Gm^s colonies growing with 5% sucrose. Subsequently, the Km^r/Nm^r cassette was eliminated upon transfer of the plasmid pTH2505 that expresses Flp recombinase.

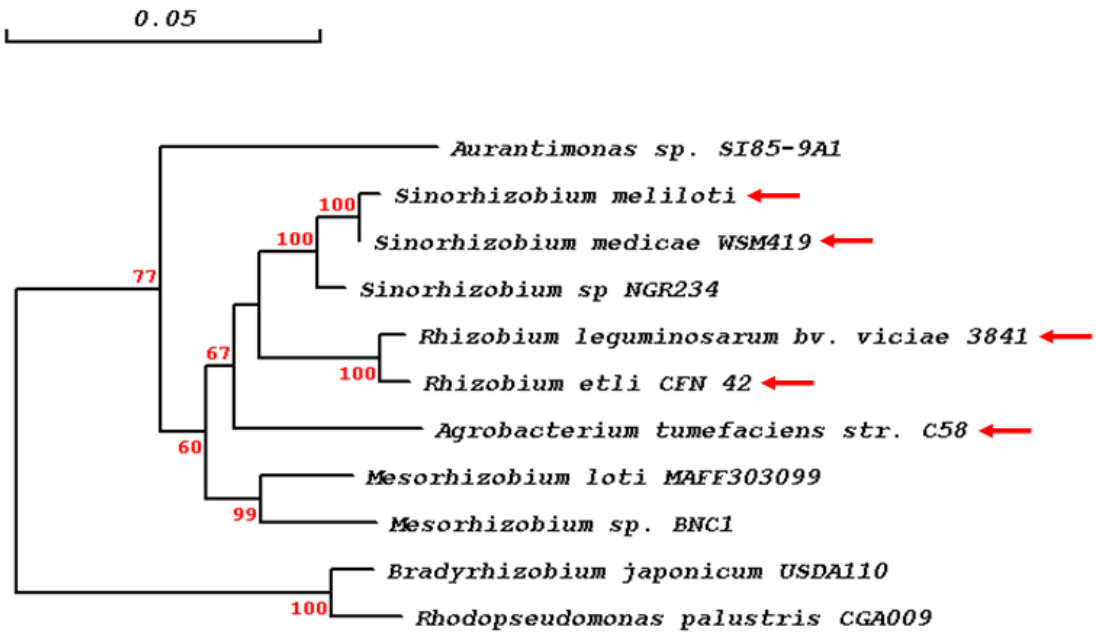

Figure 8 Phylogenetic tree of selected α-proteobacteria strains based on 16S rDNA sequence analysis.

Sequences were aligned using DNAMAN 6.0 and the tree was constructed by using maximum-likelihood method. Numbers adjacent to the branches are support values from 1,000 maximum parsimony bootstrap replicates if larger than 50%. The strains whose *dme* sequences were involved in designing degenerate primers for sequencing NGR234 *dme* gene were marked with a red arrow**.** Genebank accession numbers of sequences used for analysis are as follows: (1) *Agrobacterium tumefaciens* str. C58 (AE007870.2); (2) *Aurantimonas* sp. SI85-9A1 (AJ786360.1); (3) *Bradyrhizobium japonicum* USDA110 (BA000040.2); (4) *Mesorhizobium loti* MAFF303099 (BA000012.4); (5) *Mesorhizobium* sp. BNC1 (CP000390.1); (6) *Sinorhizobium* sp NGR234 (AY260147.1); (7) *Rhizobium leguminosarum* bv. viciae 3841 **(**AM236080.1**)**; (8) *Rhizobium etli* CFN 42 **(**CP000133.1**)**; (9) *Rhodopseudomonas palustris* CGA009 (BX572608.1); (10) *Sinorhizobium medicae* WSM419 (CP000738.1**)**; (11) *Sinorhizobium meliloti* (JX524428.1)

Figure 9 *Sinorhizobium* sp. NGR234 *dme* gene region

The *dme* gene is shown together with relevant restriction sites and the locations of the *dmeΔ14::ΩSp*^{r} and *dme-9::ΩSp*^{r} insertion mutation. NGR_c16870 encodes a putative metallophosphoesterase protein, and NGR_c16890 encodes a transcriptional regulator (NgrR). The thick line indicates the 3,328-bp region sequenced in this work, and the lower line indicates the *dme* region cloned into the complementing plasmid pTH2584. Sequencing primers are indicated as arrows. Forward primers (red): (A) DME-NGR-FP1 (bp 264); (B) DME-NGR-FP2 (bp 422); (C) DME-NGR-FP8 (bp 1814). Reverse primers (green); (D) DME-NGR-RP1 (bp 2205); (E) DME-NGR-RP2 (bp 1764); (F) DME-NGR-RP6 (bp 483); (G) DME-NGR-RP9 (bp 35)

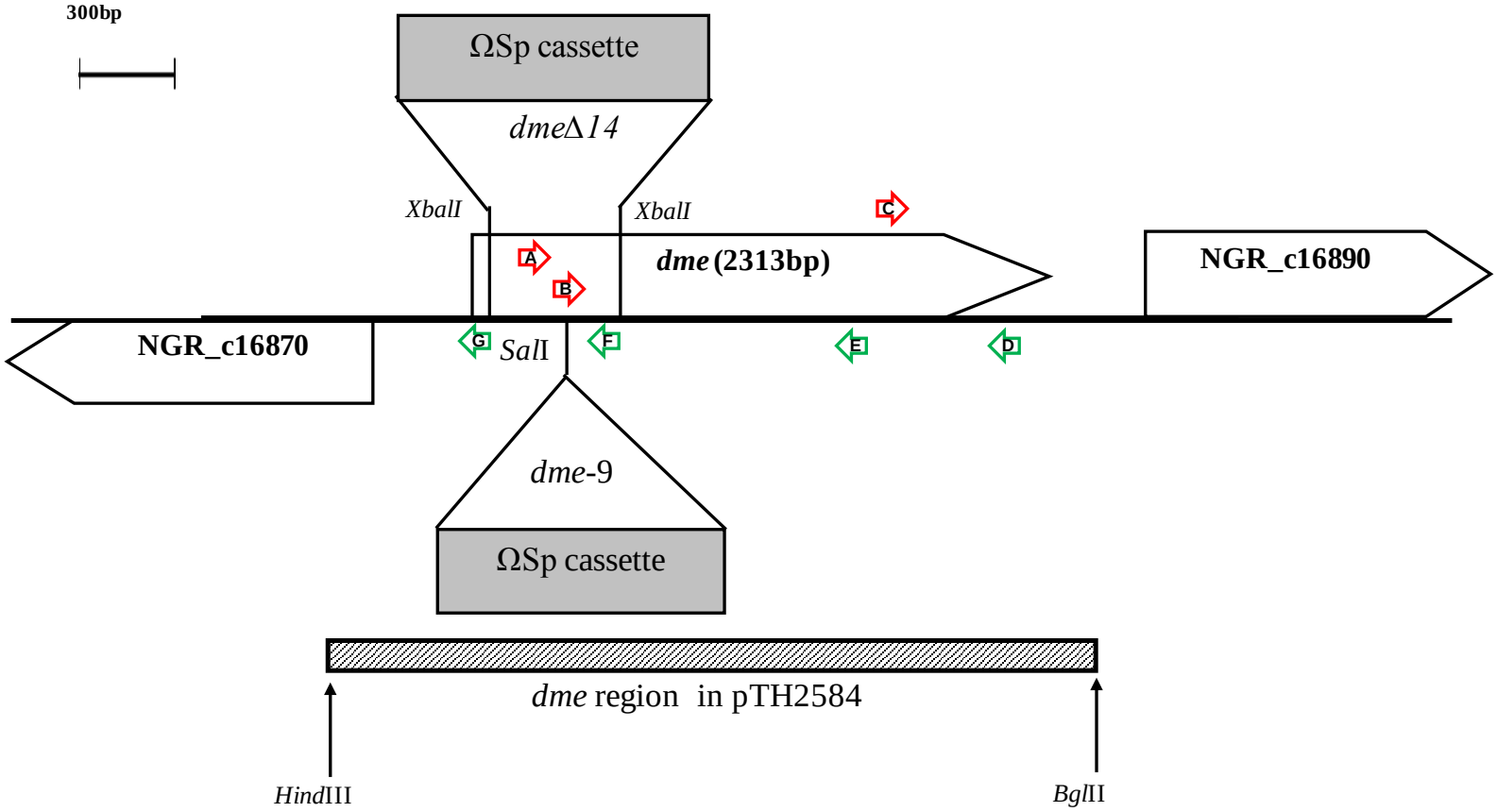
300bp
ΩSp cassette
dmeΔ14
XbaI
XbaI
C
A
B
dme (2313bp)
NGR_c16890
NGR_c16870
G
SalI
F
E
D
dme-9
ΩSp cassette
dme region in pTH2584
HindIII
BglII

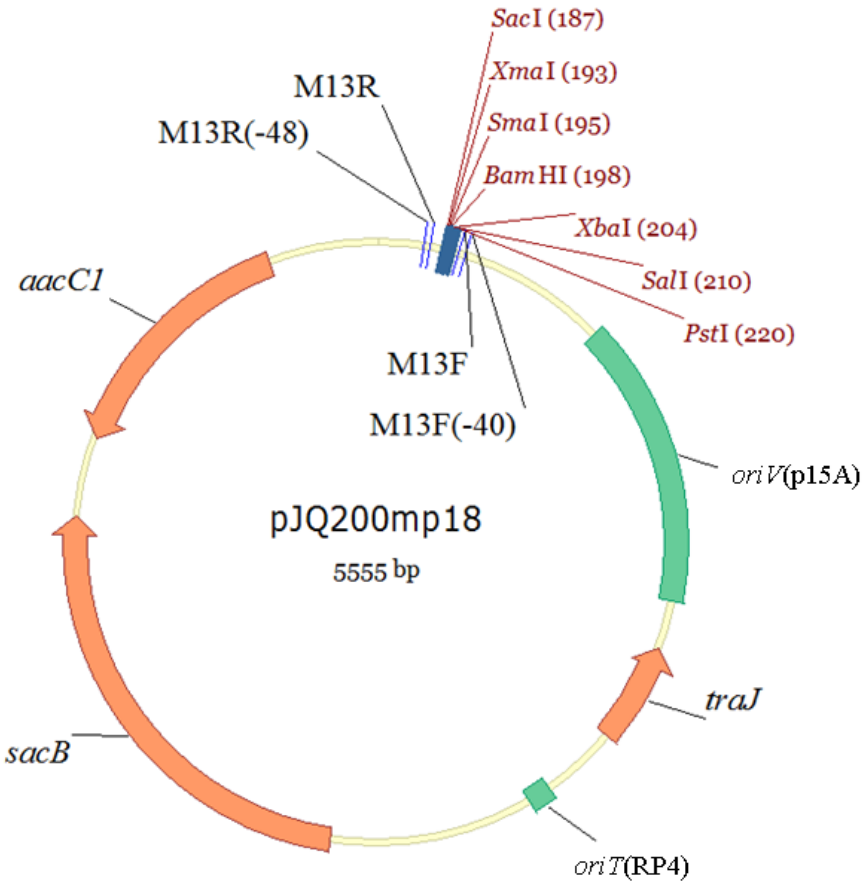

Figure 10 Schematic vector map of pJQ200-mp18

pJQ200-mp18 is a derivative of plasmid pACYC184 (Quandt and Hynes 1993). The important elements of this vector were summarized as following: (1) *oriV*(p15A): p15A origin of replication (low copy: ~10/cell), which restricts plasmid replication only in enterobacteria (Chang and Cohen 1978); (2) *oriT* (RP4): RP4 origin of transfer, which allows the plasmid to mobilize into a wide range of Gram negative bacteria; (3) *traJ*: the product of this gene sets off a cascade of other transfer genes, *which* are necessary for conjugation to occur; (4) *aacC*: gentamicin (Gm) resistance gene from pPHlJ1 plasmid; (5) *sacB*: a gene from *Bacillus subtilis* cause lethal in Gram negative bacteria grown in media with 5% sucrose, which allows the selection for loss of the plasmid (Steinmetz *et al*. 1985); (6) M13R, M13R (-48), M13F, and M13F (-40) are priming sites for sequencing cloned fragment.

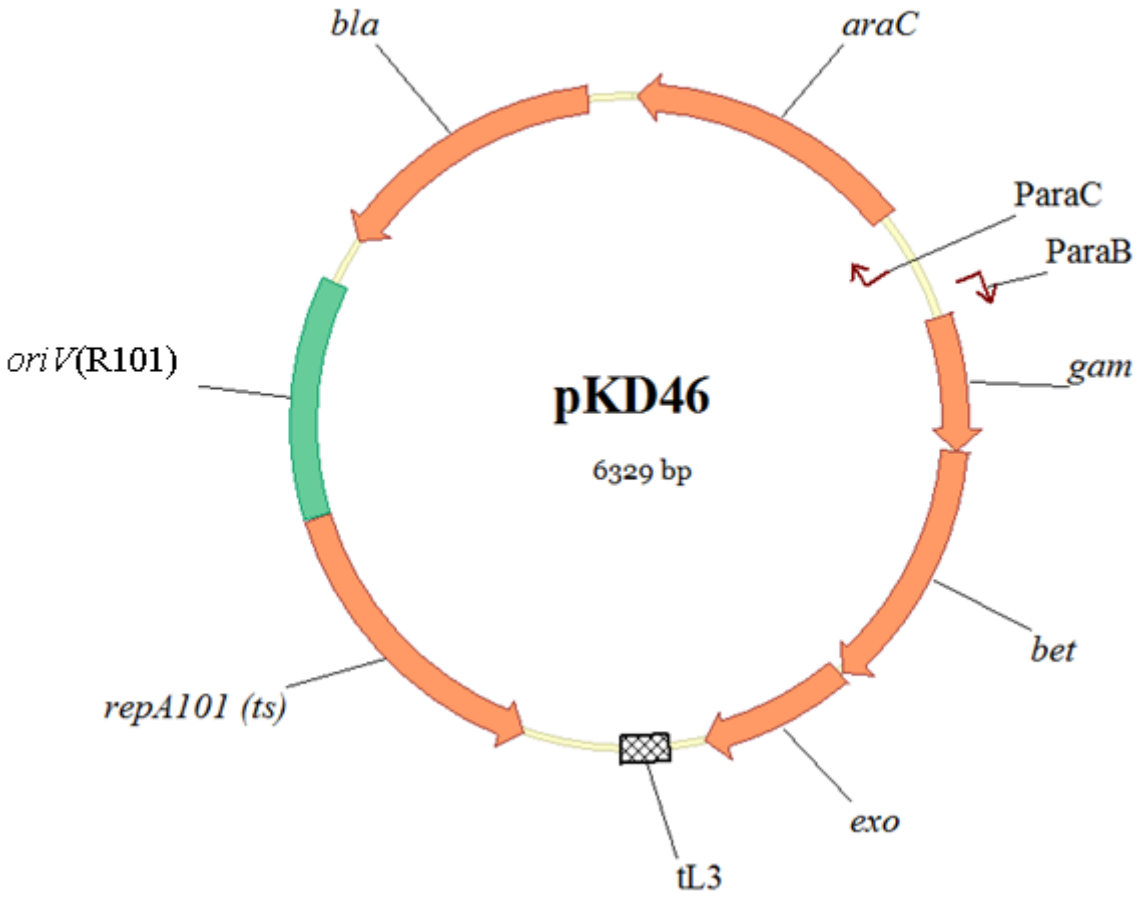

Figure 11 Schematic vector map of pKD46

The Lambda Red recombinase expression plasmid pKD46 is a derivative of pINT-ts plasmid. This plasmid can be maintained in a strain grown at 30°C, whereas cured from a strain grown at 37-42°C without Amp^r selection. The important elements of this vector were summarized as following: (1) *repA10* (ts): *oriV*(R101) replication initiation gene and its product, the heat-labile protein, loses activity significantly at 37°C, and near-completely at 42°C; (2) *oriV*(R101): R101origin of replication (*oriV*) derived from the pSC101 replication origin; (3) P*araC*: constitutive promoter of *araC* gene. (4) P*araB*: an L-arabinose inducible promoter highly repressed by AraC protein; (5) *araC*: regulatory gene whose product (AraC protein) tightly represses *araBAD* promoter (P*araB*); (6) *gam, bet, and exo*: λ Red recombinase genes under the control of P*araB*; (7) tL3: native terminator downstream of *exo* gene, which maintains plasmid stability during L-arabinose induction; (8) *bla*: ampicillin (Amp) resistance gene.

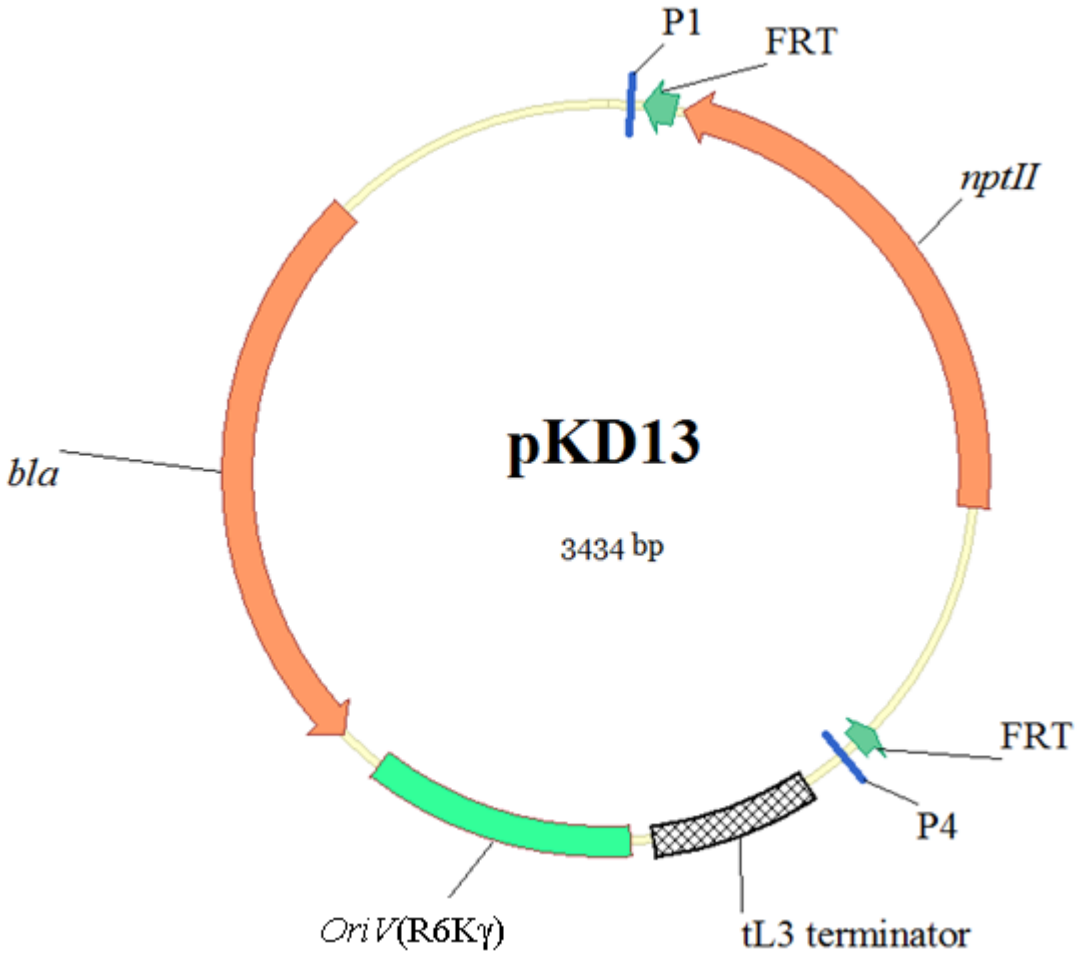

Figure 12 Schematic vector map of pKD13

Plasmid pKD13, a derivative of pANTSγ plasmid with FRT-flanked kanamycin-cassette was used as a template plasmid for gene disruption. The important elements of this vector were summarized as following: (1) FRT: recognition target for FLP recombinase of yeast; (2) *oriV* (R6Kγ): R6Kγ origin of replication, which requires the *pir* gene product for activity; (3) *bla*: ampicillin (Amp) resistance gene; (4) *nptII*: kanamycin (Km)/neomycin (Nm) resistance gene; (5) P1 &P4: priming sites for PCR amplifying the FRT-flanked kanamycin-cassette.

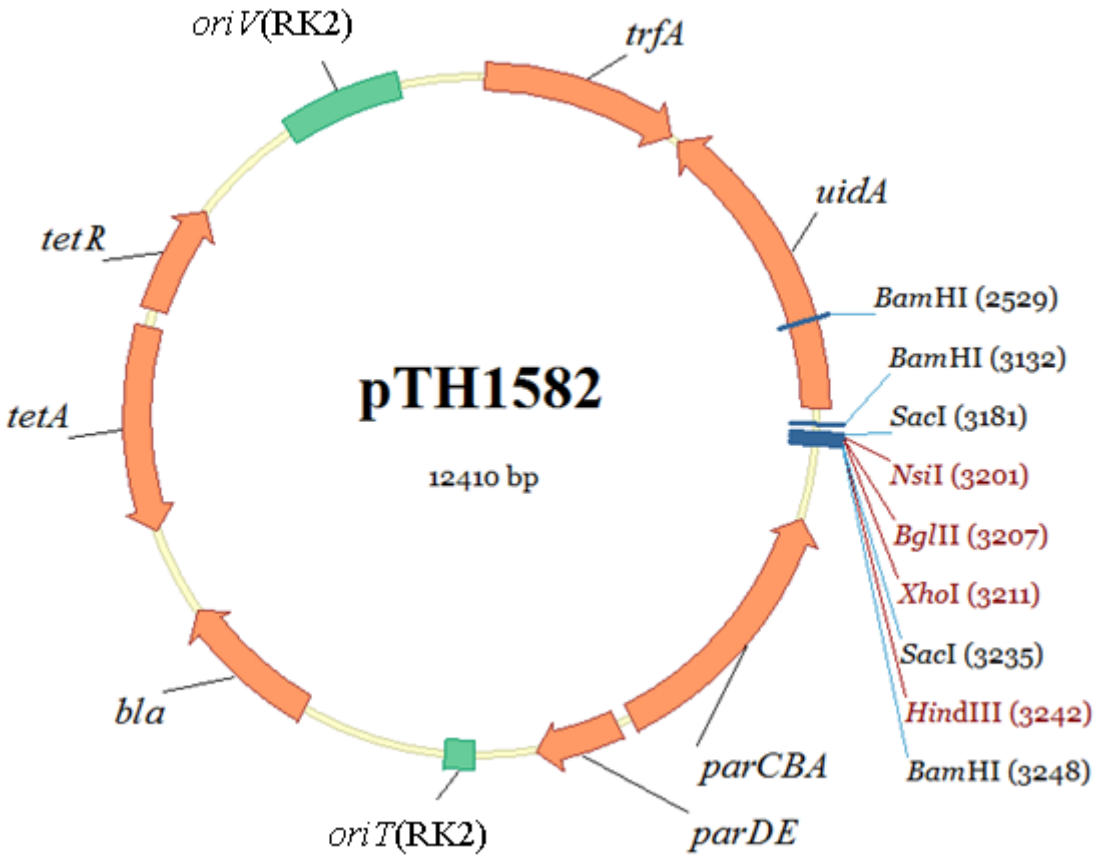

Figure 13 Schematic vector map of pTH1582

pTH1582 is a derivative of the broad-host-range plasmid pJP2 (Prell *et al*. 2002) and was constructed by Yuan *et al* (2005). The functional elements of this vector were summarized as following: (1) *oriV*(RK2): RK2 origin of replication (very low copies: ~3/cell); (2) *trfA*: *oriV*(RK2) replication initiation gene; (3) *oriT*(RK2): RK2 origin of transfer; (4) *parCBA* and *parDE*: two operons carry genes ensuring plasmid stability without selection of antibiotics; (5) *uidA*: gene encoding β-glucuronidase (GusA); (6*) tetA* & *tetR*: tetracycline (Tc) resistance gene; (7) *bla*: ampicillin (Amp) resistance gene.

Figure 14 Schematic diagram illustrating the strategy to delete *dme* gene from NGR234 *pck* mutant

Step 1) the FRT-flanked Km^r/Nm^r cassette was PCR amplified from pKD13 using primers including 50-bp homology extensions (H1& H2) and 20-bp priming sequences (P1&P4) for pKD13; **Step2)** the *dme* region on plasmid pTH2530 was completely deleted and replaced with the FRT-flanked Km^r/Nm^r cassette in homology extensions (H1& H2) by using the Lambda Red recombinase expressed from pKD46; **Step3)** the *dme* gene of the NGR234 *pck* mutant (RmG694*pck)* was deleted and replaced with the FRT-flanked Km^r/Nm^r cassette via homologous recombination between plasmid pTH2532 and genomic DNA; **Step4)** the Km^r/Nm^r cassette was excised from RmP2648 (NGR234 *pck*::Ω Sp^r & Δ*dme*:: FRT- Km^r/Nm^r-FRT) genome by using the Flp recombinase expression plasmid (pTH2505) to generate RmP2651 (NGR234 *pck*::Ω Sp^r & Δ*dme*:: FRT)

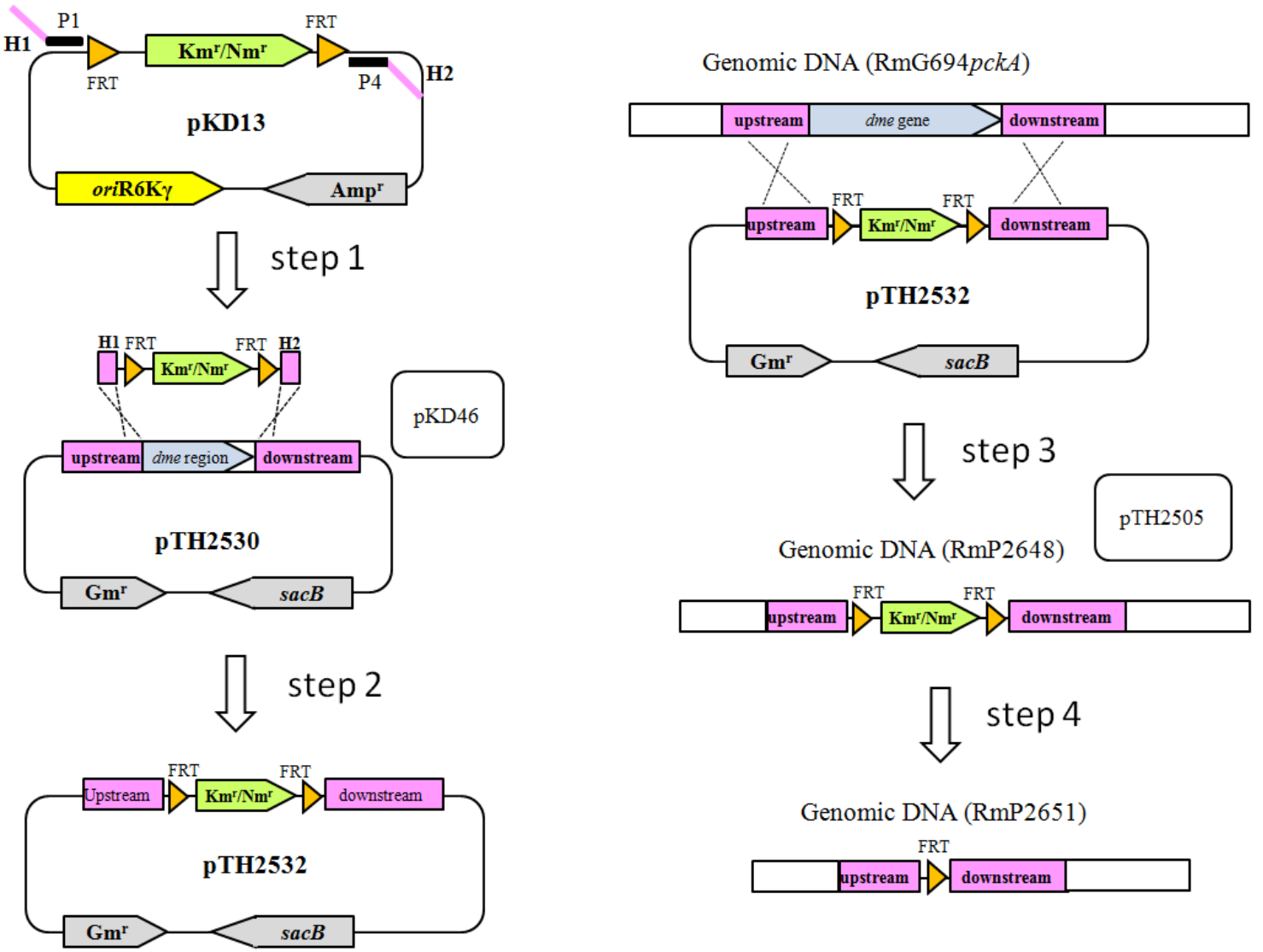
P1
H1
FRT
Km^r/Nm^r
FRT
P4
H2
pKD13
oriR6Kγ
Amp^r
step 1
H1
FRT
Km^r/Nm^r
FRT
H2
upstream
dme region
downstream
pKD46
pTH2530
Gm^r
sacB
step 2
FRT
Upstream
Km^r/Nm^r
FRT
downstream
pTH2532
Gm^r
sacB
Genomic DNA (RmG694pckA)
upstream
dme gene
downstream
FRT
upstream
Km^r/Nm^r
FRT
downstream
pTH2532
Gm^r
sacB
step 3
pTH2505
Genomic DNA (RmP2648)
FRT
upstream
Km^r/Nm^r
FRT
downstream
step 4
Genomic DNA (RmP2651)
FRT
upstream
downstream

The deletion of *dme* and the Km^r/Nm^r cassette in strain RmP2651 (*pckA*:: Ω Sp^r & Δ*dme*:: FRT) was verified by the PCR amplification using primers from outside the region employed in the deletion construction, F040 (bp -564 upstream) and R041 (bp +1065 downstream), and the absence of the DME protein was verified by Western Blot analysis.

A 2.6-kb PCR fragment carrying the NGR234 wild-type *dme* gene and its promoter region (284-bp upstream sequence) (Figure 9) was amplified (using the primers DME-NGR-F37 and DME-NGR-R37) and inserted into a broad-host-range plasmid pTH1582 (Figure 13), via *Bgl*II and *HindIII*. The resulting plasmid (pTH2584) was then transferred into the NGR234 *dme* mutants, RmP1809 (*dme-9*::Ω Sp^r) and RmP1814 (*dme*Δ*14*::Ω Sp^r), and used for *dme* complementation.

3.3 Results

3.3.1 Nucleotide Sequence of the NGR234 *dme* Gene

The NGR234 *dme* gene was PCR amplified, cloned, and sequenced as outlined in Materials and Methods (Figure 9). The 3328-bp DNA sequence contained one major and complete open reading frame (ORF) of 2313 nucleotides, which was the NGR234 *dme* gene coding region. The NGR234 *dme* gene showed a clear G + C bias of 81% at the third nucleotide position of the codons compared to the total G + C content of 64%. A potential ribosome-binding site (5'-AGGGA-3') was 10 base pairs upstream of ATG start codon and promoter-like sequences, -35 element (CTGT) and -10 element (AAAT), were located at positions similar to those in the *S. meliloti dme* gene (Mitsch *et al*. 1998). In consensus phylogenetic trees (Figure 15), the NGR234 *dme* gene and its predicted protein were grouped together with *dme* genes / DME proteins, rather than *S meliloti tme* gene /

TME protein. The NGR234 and *S. meliloti dme* genes were 87% identical, and their predicted proteins were 95% identical. Predicted protein of the NGR234 *dme* gene contained three conserved domains: the malic enzyme N-terminal domain (fam00390), the malic enzyme NAD binding domain (pfam03949), and a phosphate acetyl/butaryl transferase-like domain (cl00390) (Marchler-Bauer *et al*. 2011). In addition, the gene region flanking the NGR234 *dme* gene (Schmeisser *et al*. 2009) was highly syntenic with the *S. meliloti dme* gene region.

3.3.2 *Sinorhizobium* sp. NGR234 *dme* Mutants and Enzymology

NGR234 *dme* mutants were constructed (Materials and Methods) and extracts along with appropriate controls were assayed for NAD^+ and $NADP^+$ -dependent malic enzyme, malate dehydrogenase (MDH), and phosphoenolpyruvate carboxykinase (PCK) activities. The results are shown in Table 5. The malic enzyme activities were assayed as the NAD^+- and $NADP^+$-dependent formation of pyruvate from L-malate. Since the 2,4-dinitrophenylhydrazine used to detect pyruvate also reacts with other keto acids, such as oxaloacetate, this assay is complicated by the presence of substantial cross-reactivity that is likely to arise from the NAD^+-dependent formation of oxaloacetate from L-malate by the enzyme malate dehydrogenase. In previous reports, a background apparent NAD^+-malic enzyme activity was detected in the extracts of *S. meliloti dme* mutants (Driscoll and Finan 1993). The NAD^+-dependent malic enzyme activity detected in the extracts of NGR234 strains carrying the *dme-9*, *dme*Δ*14*, and Δ*dme* & *pckA* mutants (RmP1809, RmPP1814, and RmP2651, respectively) was approximately 50% of that present in the extract of the wild-type NGR234 (RmG694).

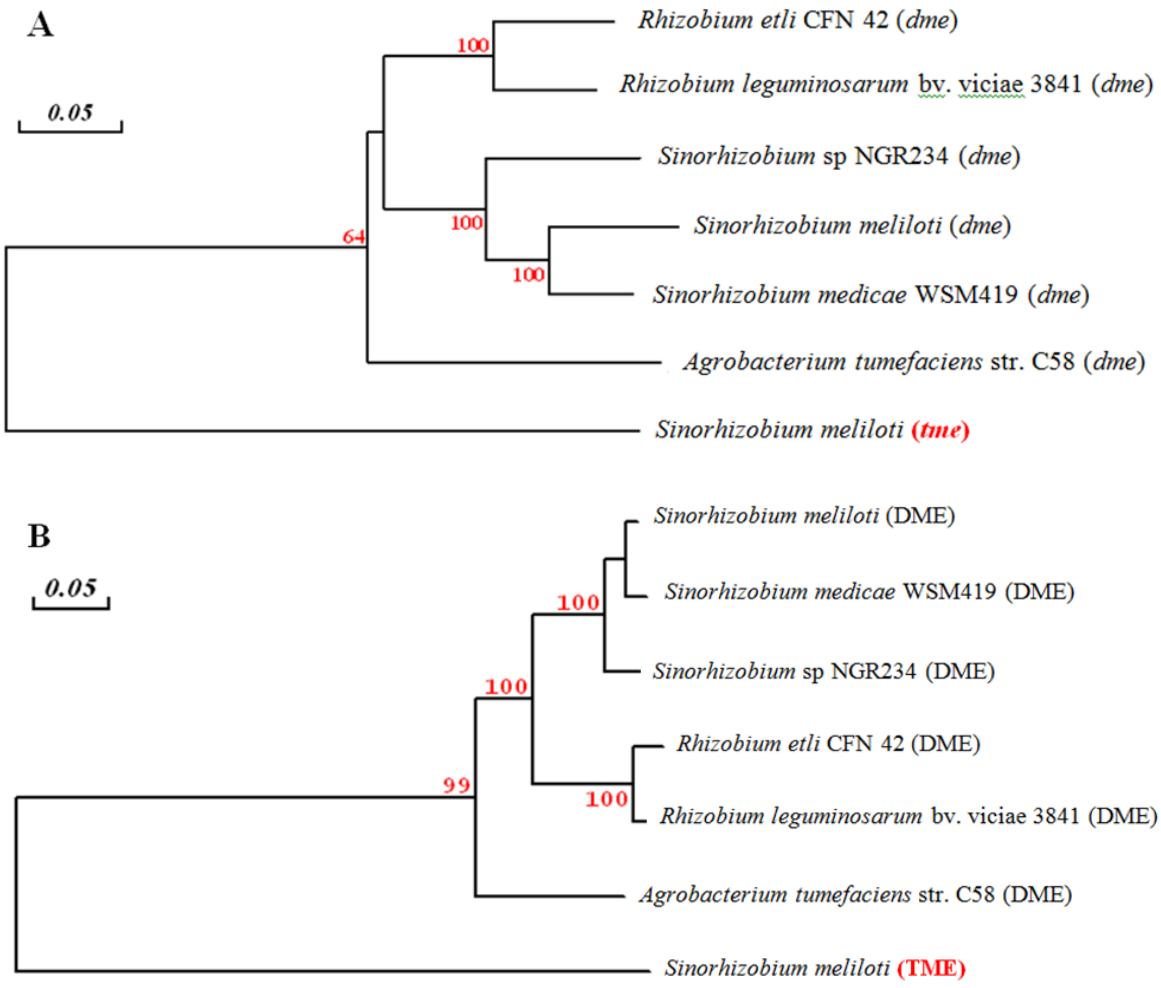

Figure 15 phylogenetic trees of *dme* genes and their predicted proteins from selected rhizobial strains

(A) Phylogenetic tree based on *dme* genes and (B) Phylogenetic tree based on predicted DME proteins. Sequences were aligned using DNAMAN 6.0 and the tree was constructed by using maximum-likelihood method. Numbers adjacent to the branches are support values from 1,000 maximum parsimony bootstrap replicates if larger than 50%. Genebank accession numbers of *dme* gene/DME protein sequences from following strains: (1) *Rhizobium etli* CFN 42 (CP000133.1/ABC91135.1); (2) *Rhizobium leguminosarum* bv. viciae 3841 (AM236080.1/AM236080.1), (3) *Sinorhizobium meliloti* (AL591688.1/CAC46416.1), (4) *Sinorhizobium medicae* WSM419 (CP000738.1/ABR60400.1), (5) *Sinorhizobium* sp NGR234 (FJ215683/ACI39939.1), (6) *Agrobacterium tumefaciens* str. C58 (AE007869.2/AAK87427.2).

Table 5 Enzyme assays on free-living cell extracts obtained from various *Sinorhizobium* sp. NGR234 strains

Strains	Genotypes	Enzyme specific activity			
		DME	TME	MDH	PCK
RmG694	NGR234 wild type	103 ± 13	80 ± 4	995 ± 50	52 ± 4
RmG694*pckA*	NGR234 *pckA*::ΩSp^r	91 ± 10	74 ± 8	896 ± 33	10 ± 2
RmG994	*S. meliloti dme-3*::Tn5 & *tme-4*:: ΩSp^r	54 ± 4	0	1,219 ± 87	N.D.
RmP1809	NGR234 *dme-9*::ΩSp^r	51 ± 3	67 ± 6	1,395 ± 153	N.D.
RmP1814	NGR234 *dme*Δ*14*::ΩSp^r	44 ± 7	61 ± 8	1,191 ± 49	N.D.
RmP2190	NGR234 *dme-9*::ΩSp^r/pTH1582	46 ± 2	55 ± 6	1,288 ± 43	N.D
RmP2191	NGR234 *dme-9*::ΩSp^r/*dme*$^+$	225 ± 10	101 ± 7	826 ± 38	N.D
RmP2192	NGR234 *dme*Δ*14*::ΩSp^r/pTH1582	41 ± 6	43 ± 4	1,215 ± 42	N.D
RmP2193	NGR234 *dme*Δ*14*::ΩSp^r/*dme*$^+$	213 ± 9	92 ± 8	847 ± 46	N.D
RmP2651	NGR234 *pckA*::ΩSp^r& Δ*dme*::FRT	39 ± 3	44 ± 2	1,153 ± 37	7 ± 3

Values are means ± standard error for triplicate samples. For DME (NAD^+-dependent malic enzyme) and TME ($NADP^+$-dependent malic enzyme), specific activity is shown as nanomoles of pyruvate formed/minute/mg protein; for MDH (malate dehydrogenase) specific activity is shown as nanomoles of NADH formed/minute/mg protein; and for PCK (phosphoenolpyruvate carboxykinase), specific activity is shown as nanomoles of NADH oxidized/minute/mg protein. N.D.: not determined. NGR234 strains were grown in TY, *S. meliloti* strains were grown in LBmc, and cell extracts were prepared as described (Chapter 2 Material and Method). *dme*$^+$: the wild-type *dme* gene and its promoter (Figure 9) cloned into a broad-host-range plasmid pTH1582.

This activity is at a similar level to the "background" activity to that detected in the *S. meliloti dme tme* double mutant RmG994 (Table 5). Thus, the results suggested that the *dme* gene was disrupted in the NGR234 strains RmP1809, RmPP1814, and RmP2651. The $NADP^+$-dependent malic enzyme activities in extracts of three NGR234 *dme* mutants were at wild-type levels, but generally reduced relative to the values of wild-type strain RmG694 (Table 5). This was expected, as the $NADP^+$-dependent malic enzyme activity of wild-type extracts was catalyzed by both the NAD^+- and $NADP^+$-dependent malic enzymes. $NADP^+$-dependent malic enzyme activity was undetectable in the extract of *S. meliloti dme tme* double mutant RmG994. Malate dehydrogenase activity in the extracts of three NGR234 *dme* mutants (RmP1809, RmP1814, and RmP2651) and *S. meliloti dme tme* double mutant RmG994 was slightly higher than that in the wild-type strain RmG694 (Table 5). These results are similar to those reported previously for *dme* mutants of *S. meliloti* and *R. leguminosarum* (Driscoll and Finan 1993; Mulley *et al*. 2010).

NAD^+- and $NADP^+$-dependent malic enzyme proteins in cell extracts were also detected by Western blot analyses with antibody prepared against purified DME and TME proteins from *S. meliloti* (Voegele *et al*. 1999). The DME and TME proteins (~82 kDa) in cell extracts were detected as a purple band located between protein standards of 72 kDa and 95 kDa as shown in Figure 16. DME and TME proteins were not detected in the cell extract of *S. meliloti dme tme* double mutant RmG994 (lane 2), but each was detected in the cell extracts of wild-type *S. meliloti* and NGR234 strains (lane 1 and lane 3). Thus, antibodies present in the anti-serum prepared against *S. meliloti* DME or TME proteins were able to bind with NGR234 DME or TME protein.

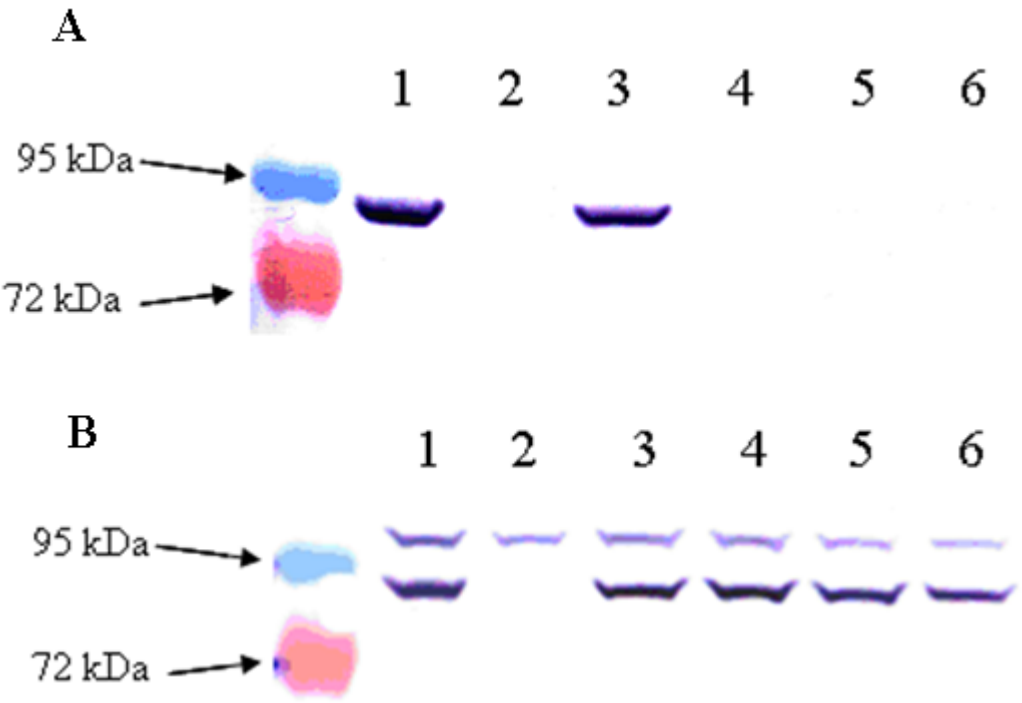

Figure 16 DME and TME proteins in free-living cell extracts from NGR234 strains

Western blots were probed with anti-DME antibody (A) and anti-TME antibody (B). DME (A) and TME (B) proteins are indicated by the purple band appearing at the position between protein standards of 95 kDa and 72 kDa. In addition to the TME protein, anti-TME antiserum detects an additional protein band that migrates at 95 kDa and is present in extracts from *S. meliloti* and NGR234. Each lane was loaded with 25 µg of total protein/sample. Lane 1, *S. meliloti* wild type RmP110; lane 2, *S. meliloti* strain carrying *dme-3*::Tn*5* *tme-4*:: Ω Sp^r insertion (RmG994). Lanes 3-6 show cell extracts from NGR234 strains, as follows: lane 3, NGR234 wild type (RmG694); lane 4, NGR234 *dme-9*::ΩSp^r (RmP1809); lane 5, NGR234 *dme*Δ*14*::ΩSp^r (RmP1814); and lane 6, NGR234 *pckA*::ΩSp^r& Δ*dme*::FRT (RmP2651). Prestained protein standards of 95 kDa and 72 kDa are shown in the outer left lane. NGR234 strains were grown in TY, *S. meliloti* strains were grown in LBmc, and cell extracts were prepared as described (Chapter 2 Material and Method).

Secondly, none of the NGR234 *dme* mutants showed detectable DME protein (Figure 16A, lanes 4-6), but the TME protein was present at wild-type levels in all these NGR234 *dme* mutants (Figure 16B, lanes 4-6). This confirmed that NAD^+- dependent malic enzyme was absent in the NGR234 *dme* mutants.

3.3.3 Complex Symbiotic Phenotypes of *dme* Mutants on Divergent Legume Genera

The symbiotic nodulation and N_2-fixation phenotype of the NGR234 mutants on the host plants *C.cajan*, *L. purpureus*, *L. leucocephala*, *M. atropurpureum*, and *V.unguiculata* growing in Leonard assemblies were determined. Following 6 to 10 weeks growth, the plants were collected and assayed for N_2-fixing activity by measuring the shoot dry weight and nitrogenase activity in nodules via the acetylene reduction assay. Shoot dry weight reflects the cumulative amount of N_2 fixed by the plants over the course of the experiment, whereas acetylene reduction measures the ability to fix N_2 at the actual time the assay is performed. In addition, root nodules of plants in each pot were counted and weighed and bacteroid extracts were assayed for enzyme activity.

In Figure 17, all host plants inoculated with the NGR234 strains carrying *dme-9*::ΩSp^r and *dme*Δ*14*::ΩSp^r insertions (RmP1089 and RmP1084, respectively) were green and obvious growth compared to uninoculated controls, which indicated that both *dme* mutants formed nitrogen-fixing nodules on all host plants. While the symbiotic nitrogen fixation efficiency of each of the *dme* mutants was the same on a given host plant, the symbiotic phenotype varied depending on the host plant. This observation was confirmed upon measuring shoot dry weight and acetylene reduction activities.

Results obtained from five independent experiments indicated that the effect of both NGR234 *dme* mutations on symbiotic nitrogen fixation was host-dependent. The average weight of dry shoot per plant formed by the NGR234 *dme* mutants varied from 27 to 83% of the wild-type levels, depending on the host plant inoculated (Table 6). On *C. cajan*, *L. purpureus*, and *M. atropurpureum*, the nitrogen-fixing efficiencies of the *dme* mutants indicated by shoot dry weight per plant were similar to those calculated by acetylene reduction activity per plant. However, comparison of acetylene reduction activity calculated by per plant with per gram nodules revealed that reduction of nitrogen fixation by *dme* mutants on different host plants might be due to different reasons. On *L. purpureus* and *M. atropurpureum*, nitrogen-fixing efficiencies indicated by acetylene reduction activity per gram nodules (46-61% of the wild-type levels) were not significantly different from those calculated by acetylene reduction activity per plant (46-56% of the wild-type levels) (Table 6). It suggested that the reduction of nitrogen fixation by *dme* mutants on *L. purpureus* and *M. atropurpureum* was mainly due to the loss of nitrogenase activity in bacteroids. However, on *C. cajan*, nitrogen-fixing efficiencies of the *dme* mutants indicated by acetylene reduction activity per gram nodule (92-96% of the wild-type levels) were significantly higher than those calculated by acetylene reduction activity per plant (60-76% of the wild-type levels) (Table 6).

Figure 17 Photographs of four host plants inoculated with NGR234 *dme* mutants

(A) *Cajanus cajan* cv. Pigeon pea (6 weeks). (B) *Vigna unguiculata* cv. Red Caloona cowpea (6 weeks). (C) *Macroptilium atropurpureum* cv. Aztec Atro (6 weeks). (D) *Lablab purpureus* cv. Dolichos Rongai (10 weeks). Seedlings were planted in Leonard assemblies with N-free Jensen's medium and watered with sterile ddH_2O as required. Plants were incubated in a growth chamber with 16 hours light at 28°C and 8 hours dark at 20°C. Photographs were taken until the uninoculated controls displayed clear symptoms of nitrogen deficiency (yellowing of leaves and stunted growth). Strains: RmG694 (NGR234 wild type), RmP1809 (NGR234 *dme-9*), and RmP1814 (NGR234 *dmeΔ14*). Uni.: uninoculated control. wt: wild type.


A
Uni
dme-9
dmeΔ14
wt


B
Uni
dme-9
dmeΔ14
wt

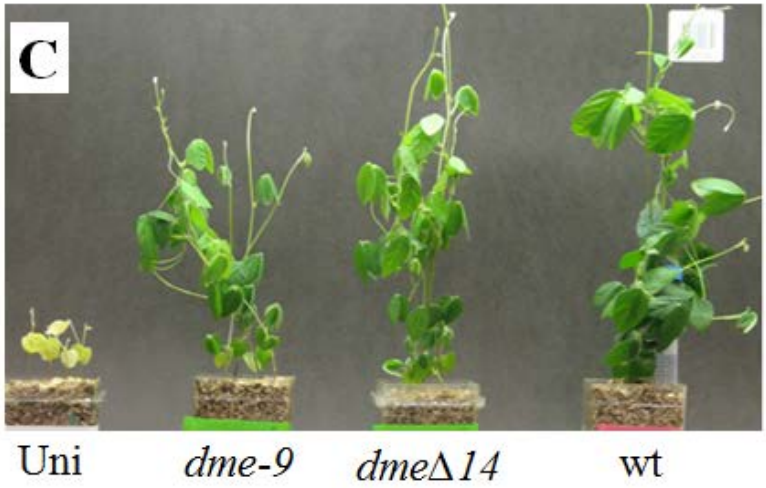
C
Uni
dme-9
dmeΔ14
wt

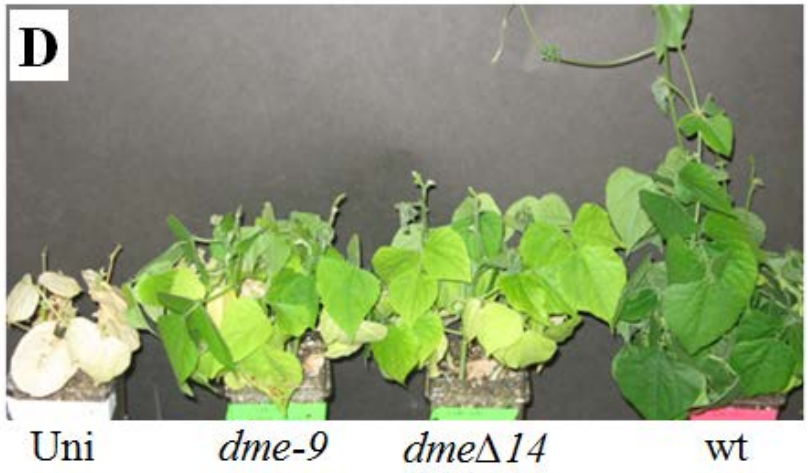
D
Uni
dme-9
dmeΔ14
wt

Table 6 Acetylene reduction assays and shoot dry weights of different host plants inoculated with wild-type *Sinorhizobium* sp. NGR234 and *dme* mutants

[a-d] Five independent experiments (12 plants per strain per experiment) were made for each host. Date are means ± standard deviation. Values followed by the same letter do not differ at the 0.05 level of probability based on one-way ANOVA test. ND, not determined. [e]Calculated by shoot dry weight per plant: (test-uninoculated)/(wild type-uninoculated). alculated as the amount of acetylene reduced per plant: test/wild type. [g] Calculated as the amount of acetylene reduced per gram of fresh nodules: test/wild type. [h] Nitrogenase activity assayed by acetylene reduction assay (μmol C_2H_4 produced/hour).

Host (growth period)	Strain (genotype)	Shoot dry weights per plant (mg)	Fix% [e]	AR activity[h] (per plant)	Fix% [f]	AR activity[h] (per g of nodules)	Fix% [g]
Cajanus cajan (six weeks)	Uninoculated control	97 ± 9[a]	0%	0[a]	0%	0[a]	0%
	RmG694(NGR234 wild type)	542 ± 48[b]	100%	2.5 ± 0.3[b]	100%	7.5 ± 0.9[b]	100%
	RmP1809 (NGR234 *dme-9*::ΩSp^r)	467 ± 32[c]	83%	1.9 ± 0.2[c]	76%	7.2 ± 0.9[b]	96%
	RmP1814 (NGR234 *dme*Δ*14*::ΩSp^r)	358 ± 24[d]	58%	1.5 ± 0.2[d]	60%	6.9 ± 0.2[b]	92%
Lablab purpureus (ten weeks)	Uninoculated control	173 ± 10[a]	0%	0a	0%	0[a]	0%
	RmG694(NGR234 wild type)	1,560 ± 124[b]	100%	7.1 ± 1.7[b]	100%	8.4 ± 1.2[b]	100%
	RmP1809 (NGR234 *dme-9*::ΩSp^r)	1,002 ± 116[c]	60%	4 ± 0.6[c]	56%	4.7 ± 0.8[c]	56%
	RmP1814 (NGR234 *dme*Δ*14*::ΩSp^r)	1,024 ± 108[c]	61%	3.5 ± 0.4[c]	49%	3.9 ± 0.3[c]	46%
Leucaena leucocephala (ten weeks)	Uninoculated control	77 ± 7[a]	0%	0[a]	0%	ND	ND
	RmG694(NGR234 wild type)	285 ± 16[b]	100%	1.4 ± 0.2[b]	100%	ND	ND
	RmP1809 (NGR234 *dme-9*::ΩSp^r)	226 ± 20[c]	72%	0.96 ± 0.16[b]	70%	ND	ND
	RmP1814 (NGR234 *dme*Δ*14*::ΩSp^r)	240 ± 23[c]	78%	1 ± 0.17[b]	75%	ND	ND
Macroptilium atropurpureum (six weeks)	Uninoculated control	19 ± 1[a]	0%	0[a]	0%	0[a]	0%
	RmG694(NGR234 wild type)	362 ± 38[b]	100%	2.6 ± 0.4[b]	100%	9.9 ± 1[b]	100%
	RmP1809 (NGR234 *dme-9*::ΩSp^r)	222 ± 37[c]	59%	1.3 ± 0.1[c]	50%	6 ± 0.3[c]	61%
	RmP1814 (NGR234 *dme*Δ*14*::ΩSp^r)	218 ± 29[c]	58%	1.2 ± 0.1[c]	46%	5.6 ± 0.2[c]	57%
Vigna unguiculata (six weeks)	Uninoculated control	204 ± 39[a]	0%	0a	0%	0[a]	0%
	RmG694(NGR234 wild type)	2,245± 166[b]	100%	2.9 ± 0.4[b]	100%	3.6 ± 0.1[b]	100%
	RmP1809 (NGR234 *dme-9*::ΩSp^r)	790 ± 106[c]	29%	3.3 ± 0.3[b]	114%	5.1 ± 0.3[c]	142%
	RmP1814 (NGR234 *dme*Δ*14*::ΩSp^r)	758 ± 87[c]	27%	3.4 ± 0.7[b]	117%	5.4 ± 0.4[c]	150%

It suggested that the reduction of nitrogen fixation by *dme* mutants on *C. cajan* mainly because the *dme* mutants formed fewer nodules compared with the wild-type NGR234.

In the case of *V. unguiculata* plants inoculated with the *dme* mutants, we observed that greening of the leaves and vigorous growth occurred about 2 weeks later than those for plants inoculated with wild-type bacteria. These observations were reflected in the dry weight values of the plant shoots, which were about 30% of the wild-type level in the case of the *dme* mutants (Table 6). However, measurements of nitrogenase activity by *V. unguiculata* nodules revealed acetylene reduction activities for the *dme* mutants that were not significantly different from those for wild-type NGR234 (Table 6). The lack of congruence between the plant dry weight and nitrogenase activity measurements suggested a Fix-delay phenotype of NGR234 *dme* mutants on *V. unguiculata*. A Fix-delay phenotype can be caused by a delay in the process of nodulation or in nitrogen fixation. To investigate this, the kinetics of nodule formation of the *dme* mutants and wild-type NGR234 were determined on *V. unguiculata.* Two day old seedlings were transferred to test tubes containing slants of Jensen's medium solidified with 1% agar, inoculated with RmP1809 or RmP1814 (the *dme* mutants), RmP2191 or RmP2193 (the *dme/dme*$^+$ merodiploid strains), or RmG694 (NGR234 wild type). Root systems of these plants were examined and scored for nodules every second day. Results were recorded every second day and are presented as a percent of plants nodulated as well as number of nodules formed per plant (Figure 18). For all strains, nodules were first visible on the roots of seedlings 8 days after inoculation, and the percentage of plants with visible nodules approached 100% by 16 days postinoculation.These experiments revealed

that while *dme* mutants formed fewer nodules per plant, a short delay in nodule initiation was apparent. Thus, the *dme* mutations resulted in a delay in the onset of N_2 fixation in *V. unguiculata* nodules.

Results shown in Table 7 indicated that disruption of NGR234 *dme* gene resulted in complex symbiotic phenotypes. In the case of *C. cajan* and *V. unguiculata*, the number of nodules formed by the *dme* mutants was 20 to 30% lower than the wild-type NGR234, while the average weight per *dme* mutant nodule was not significantly different from the wild-type NGR234 (Table 7). It suggested that disruption of *dme* gene may be disadvantageous to nodule initiation on *C. cajan* and *V. unguiculata*, leading to fewer nodules formed by the *dme* mutants. On *M. atropurpureum*, the average weight per *dme* mutant nodule was significantly lower than that of wild-type NGR234, while all strains formed a similar numbers of nodules (Table 7). In this case, it suggested that disruption of *dme* gene may be disadvantageous to the development of root nodule on *M. atropurpureum*, resulting in the smaller nodules formed by the *dme* mutants.

About 100 colonies per strain per host were isolated from fresh nodules and patched on TY plate with rifampin and YT plates with Streptomycin. All results showed that colonies isolated from nodules induced by the *dme* mutants showed 100% of Sm^r and Rif^r, while those isolated from nodules induced by the wild-type NGR234 were 100% of Rif^r and Sm^s. Western blot assays of bacteroid extracts from four host plants, using rabbit antiserum raised against the DME and TME proteins from *S. meliloti*, showed that the *dme* mutants (RmP1809 & RmP1814) lacked the DME protein, but TME protein was present at wild-type levels in both *dme* mutants (Figure 19).

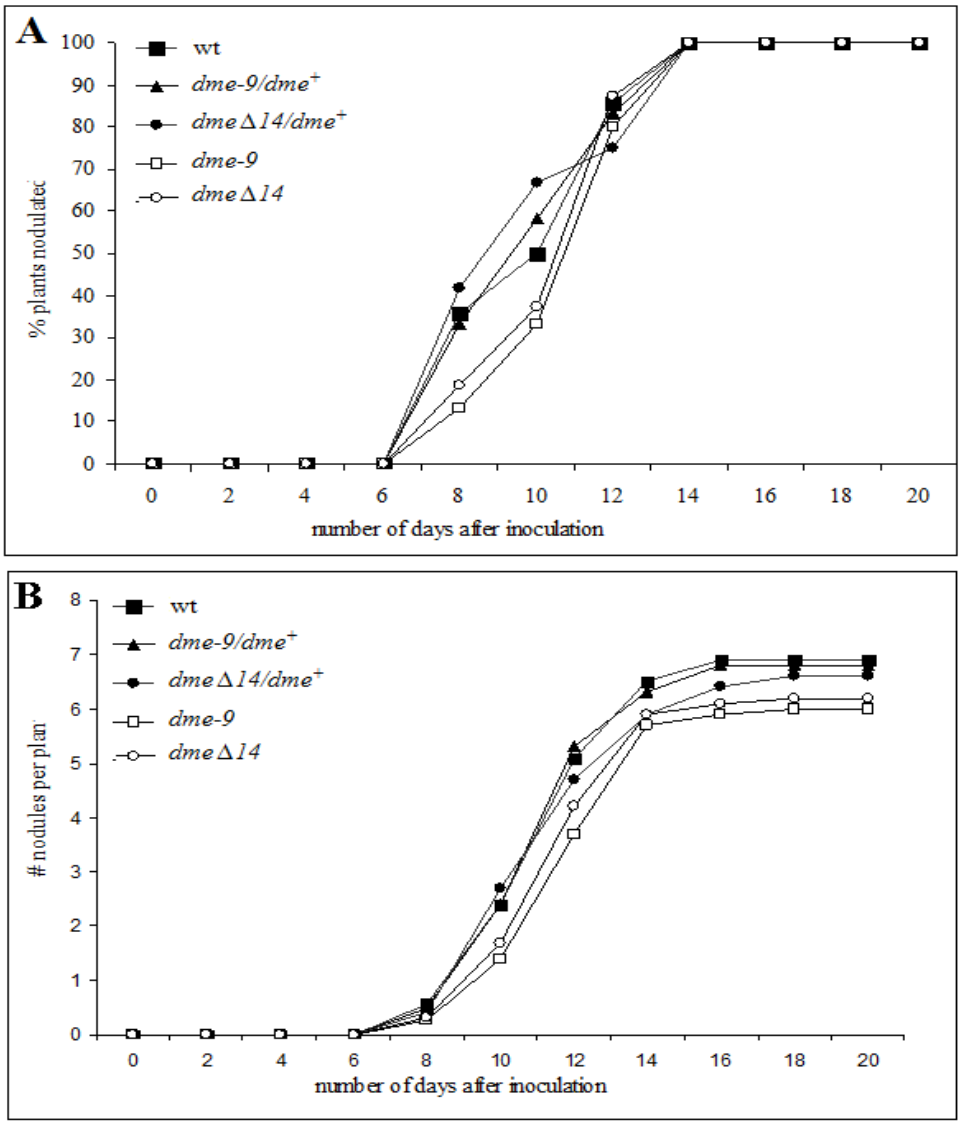

Figure 18 Nodulation kinetics of wild-type *Sinorhizobium* sp. NGR234 and *dme* mutants on *V. unguiculata* cv. Red Caloona

(A) percentage of plants nodulated over 20 days. (B) number of nodules per plant over 20 days Standard errors were < 10% of the mean values. Stains: RmG694 (NGR234 wild type), RmP1809 (NGR234 *dme-9*), RmP1814 (NGR234 *dmeΔ14*), RmP2191 (NGR234 *dme-9/dme*$^+$), and RmP2193 (NGR234 *dme Δ14/dme*$^+$). wt: wild type. *dme*$^+$: the wild-type *dme* gene and its promoter (Figure 9) cloned into a broad-host-range plasmid pTH1582. For each strain, 15 plants were examined every two days.

Table 7 Nodulation by wild-type *Sinorhizobium* sp NGR234 and *dme* mutants on different host plants

Host (growth period)	Strain (genotype)	No. of nodules per plant	Fresh nodule weight (mg)	Fresh nodule weight per plant (mg)
Cajanus cajan (six weeks)	Uninoculated control	0^{a}	0^{a}	0^{a}
	RmG694(NGR234 wild type)	26 ± 3^{b}	14 ± 2^{b}	334 ± 39^{b}
	RmP1809 (NGR234 *dme-9*::ΩSp^{r})	19 ± 2^{c}	13 ± 1^{b}	228 ± 17^{c}
	RmP1814 (NGR234 *dme*Δ*14*::ΩSp^{r})	18 ± 3^{c}	12 ± 1^{b}	213 ± 32^{c}
Lablab purpureus (ten weeks)	Uninoculated control	0^{a}	0^{a}	0^{a}
	RmG694(NGR234 wild type)	19 ± 2^{b}	43 ± 6^{b}	831 ± 85^{b}
	RmP1809 (NGR234 *dme-9*::ΩSp^{r})	20 ± 3^{b}	42 ± 4^{b}	829 ± 60^{b}
	RmP1814 (NGR234 *dme*Δ*14*::ΩSp^{r})	21 ± 4^{b}	44 ± 6^{b}	890 ± 49^{b}
Macroptilium atropurpureum (six weeks)	Uninoculated control	0^{a}	0^{a}	0^{a}
	RmG694(NGR234 wild type)	21 ± 4^{b}	13 ± 2^{b}	268 ± 27^{b}
	RmP1809 (NGR234 *dme-9*::ΩSp^{r})	23 ± 2^{b}	9 ± 1^{c}	204 ± 16^{c}
	RmP1814 (NGR234 *dme*Δ*14*::ΩSp^{r})	23 ± 3^{b}	9 ± 1^{c}	205 ± 15^{c}
Vigna unguiculata (six weeks)	Uninoculated control	0^{a}	0^{a}	0^{a}
	RmG694(NGR234 wild type)	83 ± 6^{b}	10 ± 1^{b}	825 ± 96^{b}
	RmP1809 (NGR234 *dme-9*::ΩSp^{r})	68 ± 5^{c}	9.5 ± 0.4^{b}	641 ± 38^{c}
	RmP1814 (NGR234 *dme*Δ*14*::ΩSp^{r})	71 ± 7^{c}	8.4 ± 0.5^{c}	595 ± 61^{c}

$^{a\text{-}c}$ Four independent experiments (12 plants per strain per experiment) were made for each host. Date are means ± standard deviation. Values followed by the same letter do not differ at the 0.05 level of probability based on one-way ANOVA test.

Figure 19 DME and TME protein in bacteroid extracts from different host plants

Western blots were probed with anti-DME antibody (A) and anti-TME antibody (B). DME and TME proteins are indicated by the purple band appearing at the position between protein standards of 95 kDa and 72 kDa. In addition to the TME protein, anti-TME antiserum detects an additional protein band that migrates at 95 kDa and is present in extracts from *S. meliloti* and NGR234. Each lane was loaded with 25 μg of total protein/sample. Lane 1, free-living *S. meliloti* wild type RmP110; lane 2, free-living *S. meliloti* strain carrying *dme-3*::Tn*5 & tme-4*:: Ω Sp^r insertions (RmG994). Lanes 3 to 14 show bacteroid extracts from nodules, as follows: lane 3, *C. cajan* plus NGR234; lane 4, *C. cajan* plus NGR234 *dme-9*::ΩSp^r; lane 5, *C. cajan* plus NGR234 *dme*Δ*14*::ΩSp^r; lane 6, *L. purpureus* plus NGR234; lane 7, *L. purpureus* plus NGR234 *dme-9*::ΩSp^r; lane 8, *L. purpureus* plus NGR234 *dme*Δ*14*::ΩSp^r; lane 9, *M. atropurpureum* plus NGR234; lane 10, *M. atropurpureum* plus NGR234 *dme-9*::ΩSp^r; lane 11, *M. atropurpureum* plus NGR234 *dme*Δ*14*::ΩSp^r; lane 12, *V. unguiculata* plus NGR234; lane 13, *V. unguiculata* plus NGR234 *dme-9*::ΩSp^r; and lane 14, *V. unguiculata* plus NGR234 *dme*Δ*14*::ΩSp^r. Data for *L. leucocephala* are not shown. Prestained protein standards of 95 kDa and 72 kDa are shown in the outer left lane. wt, NGR234 (RmG694); mt1, NGR234 *dme-9*::ΩSp^r(RmP1809); mt2, NGR234 *dme*Δ*14*::ΩSp^r (RmP1814). *S. meliloti* strains were grown in LBmc. Cell-freeing extracts were prepared as described (Chapter 2 Material and Method).

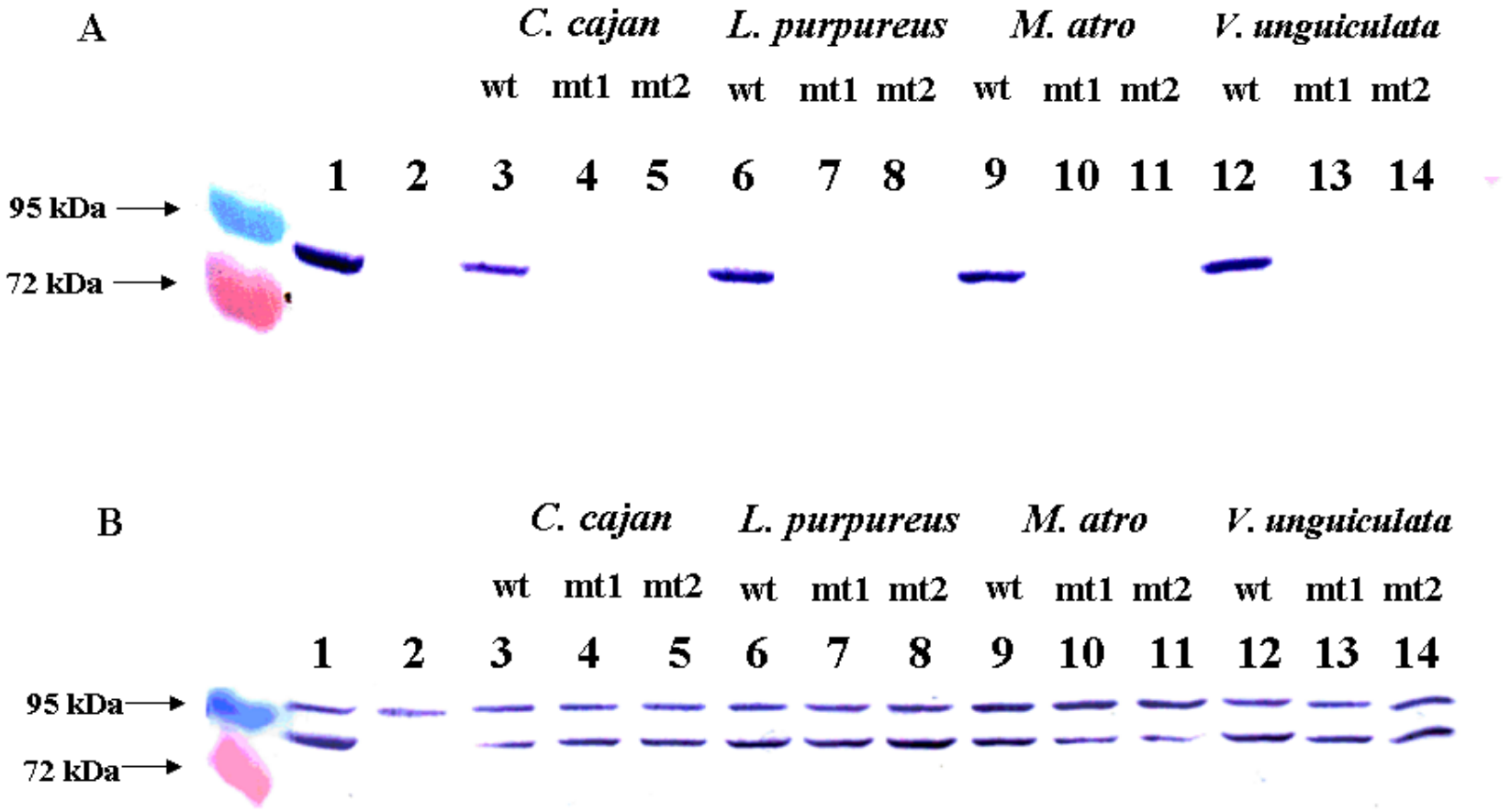
A
C. cajan
L. purpureus
M. atro
V. unguiculata
wt mt1 mt2 wt mt1 mt2 wt mt1 mt2 wt mt1 mt2
1 2 3 4 5 6 7 8 9 10 11 12 13 14
95 kDa
72 kDa
B
C. cajan
L. purpureus
M. atro
V. unguiculata
wt mt1 mt2 wt mt1 mt2 wt mt1 mt2 wt mt1 mt2
1 2 3 4 5 6 7 8 9 10 11 12 13 14
95 kDa
72 kDa

3.3.4 Complementation of *dme* Mutants

To confirm that the Fix phenotype of NGR234 *dme* mutants resulted from a lack of DME enzyme, the wild-type *dme* gene and its promoter were cloned into a broad-host-range plasmid (pTH2584) and transferred into the *dme* mutant strains. The symbiotic phenotype of the resulting strains was determined with *M. atropurpureum* and *V. unguiculata* as host plants. As shown in Table 8, there was no significant difference found in the shoot dry weights of plants inoculated with the wild-type strain RmG694 versus the *dme*/*dme*$^+$ merodiploid strains RmP2191 &RmP2193 , whereas plants inoculated with the *dme* mutants RmP1809 &RmP1814 showed the same reduced N_2 fixation phenotype as that noted in Table 6. These results showed that the wild-type *dme* gene complemented the *dme* mutants and we therefore conclude that the symbiotic phenotype of the NGR234 mutants resulted from a loss of the *dme* gene rather than possible polar or other effects that may result from the *dme* mutations.

3.3.5 Enzyme Activities in NGR234 Bacteroids

DME, TME, MDH and PCK activities were measured in bacteroid extracts of root-nodules from *C. cajan, L. purpureus, L. leucocephala, M. atropurpureum, and V. unguiculata* (Table 9). Apparent DME activities detected in the *dme* mutant bacteroids (RmP1809 & RmP1814) were less than half the wild-type NGR234 (RmG694) whereas both TME and MDH activities from the *dme*$^-$ bacteroids were similar to those in wild-type bacteroids (Table 9).

Table 8 Complementation of Fix phenotype of NGR234 *dme* mutants by pTH2584 carrying the NGR234 *dme* gene

Strains	Genotypes	*Macroptilium atropurpureum* (six weeks)				*Vigna unguiculata* (five weeks)	
		Shoot dry weight per plant (mg)	Fix%[d]	AR activity[f] (per plant)	Fix%[e]	Shoot dry weight per plant (mg)	Fix%[d]
Uninoculated control		27 ± 4[a]	0%	0[a]	0%	369 ± 12[a]	0%
RmG694	NGR234 wild type	245 ± 23[b]	100%	2.08 ± 0.27[b]	100%	944 ± 71[b]	100%
RmP1809	NGR234 *dme-9*::ΩSp^r	130 ± 16[c]	47.2%	0.73 ± 0.13[c]	35%	ND	ND
RmP1814	NGR234 *dme*Δ*14*::ΩSp^r	114 ± 13[c]	40%	0.74 ± 0.12[c]	36%	483 ± 63[c]	19.8%
RmP2190	NGR234 *dme-9*::ΩSp^r/pTH1582	125 ± 18[c]	45%	0.75 ± 0.16[c]	36%	ND	ND
RmP2191	NGR234 *dme-9*::ΩSp^r/ *dme*$^+$	223 ± 20[b]	90%	1.7 ± 0.21[b]	82%	ND	ND
RmP2192	NGR234 *dme*Δ*14*::ΩSp^r /pTH1582	127 ± 27[c]	45.9%	0.77 ± 0.12[c]	37%	478 ± 42[c]	19%
RmP2193	NGR234 *dme*Δ*14*::ΩSp^r / *dme*$^+$	215 ± 22[b]	86.3%	1.6 ± 0.22[b]	77%	948 ± 55[b]	101%

a-c Two independent experiments (12 plants per strain per experiment) were made for each host. Date are means ± standard deviation. Values followed by the same letter do not differ at the 0.05 level of probability based on one-way ANOVA test. ND, not determined. *d* Calculated by shoot dry weight per plant: (test-uninoculated)/(wild type-uninoculated). *e* Calculated as the amount of acetylene reduced per plant: test/wild type. *f* Nitrogenase activity assayed by acetylene reduction assay (μmol C_2H_4 produced/hour). *dme*$^+$: the wild-type *dme* gene and its promoter (Figure 9) cloned into a broad-host-range plasmid pTH1582.

Table 9 Enzyme activities of *Sinorhizobium* sp. NGR234 wild-type and *dme* mutant bacteroid extracts from different host plants

Bacteroids were isolated from nodules of 6-week-old *Cajanus cajan*, 10-week-old *Lablab purpureus*, 6-week-old *Macroptilium atropurpureum*, and 6-week-old *Vigna unguiculata* plants. Bacteroid extracts were prepared as described (Chapter 2 Material and Method). Values are means ± standard error for triplicate samples. For DME (NAD-dependent malic enzyme), specific activity is shown as nanomoles of pyruvate formed/minute/mg protein; for TME (NADP-dependent malic enzyme), specific activity is shown as nanomoles of pyruvate formed/minute/mg protein; for PCK (phosphoenolpyruvate carboxykinase), specific activity is shown as nanomoles of NADH oxidized/minute/mg protein; and for MDH (malate dehydrogenase), specific activity is shown as nanomoles of NADH formed/minute/mg protein. Enzyme activities in *S. meliloti* bacteroids were measured as 184 ± 7 nmol/min/mg protein for DME, 5,078 ± 109 nmol/min/mg protein for MDH, and 12 ± 3 nmol/min/mg protein for PCK. Enzyme activities in *S. meliloti dme tme* double mutant (RmG994) free-living cells (LBmc) were measured as 54 ± 4 nmol/min/mg protein for DME and 0 nmol/min/mg protein for TME

Host plant	Enzyme	Specific activity		
		RmG694 (NGR234 wild type)	RmP1809 (NGR234 *dme-9*::ΩSp^r)	RmP1814 (NGR234 *dme*Δ*14*::ΩSp^r)
Cajanus cajan	DME	42 ± 1	10 ± 1	10 ± 2
	TME	26 ± 3	27 ± 3	20 ± 4
	PCK	99 ± 9	95 ± 4	86 ± 2
	MDH	2,919 ± 157	3,394 ± 183	3,466 ± 463
Lablab purpureus	DME	46 ± 3	7 ± 3	7 ± 1
	TME	53 ± 4	38 ± 3	42 ± 5
	PCK	75 ± 6	52 ± 1	54 ± 2
	MDH	2,675 ± 89	3,137 ± 94	3,223 ± 61
Leucaena leucocephala	DME	49 ± 2	24 ± 2	22 ± 2
	TME	15 ± 2	11 ± 3	9 ± 2
	PCK	47 ± 2	41 ± 3	38 ± 4
	MDH	1,648 ± 129	1,818 ± 109	1,577 ± 117
Macroptilium atropurpureum	DME	67 ± 4	21 ± 4	21 ± 1
	TME	45 ± 5	39 ± 4	33 ± 4
	PCK	182 ± 10	160 ± 1	156 ± 3
	MDH	2,592 ± 74	3,344 ± 204	3,912 ± 91
Vigna unguiculata	DME	74 ± 2	23 ± 2	21 ± 1
	TME	50 ± 5	35 ± 4	35 ± 1
	PCK	113 ± 4	100 ± 1	96 ± 3
	MDH	1,736 ± 211	1,613 ± 74	2,301 ± 193

For comparative purposes, we also assayed *S. meliloti* bacteroid extracts from alfalfa nodules and detected DME (184 ± 7 nmol/minute/mg), MDH (5,078 ± 109 nmol/minute/mg), and PCK (12 ± 3 nmol/minute/mg) activities at levels similar to previously reported for alfalfa nodules (Mitsch *et al*., 2007). The NGR234 bacteroid enzyme activities (Table 9) revealed several differences from enzyme activity levels reported for *S. meliloti* bacteroids. DME activities were lower in wild-type NGR234 bacteroids (40-70 nmole/minute/mg) than *S. meliloti* bacteroids (~180 nmole/minute/mg). MDH activities detected in *S. meliloti* bacteroids were about double those measured in wild-type NGR234 bacteroids. Most significantly, PCK activities were high in the NGR234 bacteroids isolated from the different host plants (50-180 nmole/minute/mg), while PCK activity was not detected in *S. meliloti* bacteroids from alfalfa.

3.3.6 Symbiotic Phenotype of *dme pckA* Double Mutant

In view of the high PCK activity in NGR234 bacteroids and the recent finding that PCK can function in pyruvate synthesis in pea bacteroids (Mulley *et al*., 2010), we constructed an NGR234 *pckA dme* double mutant RmP2651 (*pckA*:: ΩSp & *Δdme*) and determined its symbiotic phenotype. The acetylene reduction data (Table 10) showed that the NGR234 *pckA* mutant formed N_2-fixing nodules on both *L. leucocephala* (0.24 ± 0.05 μmol C_2H_4/plant /hour) and *M. atropurpureum* (0.37 ± 0.04 μmol C_2H_4 /plant /hour). While the level of N_2-fixation on *L. leucocephala* was less than that previously reported (Osteras *et al*., 1991), nodules formed by the *pckA::ΩSp* Δ*dme* double mutant failed to fix N_2 (0.0 μmol C_2H_4 /hour).

Table 10 Symbiotic phenotypes of *Sinorhizobium* sp. NGR234 *pckA* mutant and *dme pckA* double mutant

Host (growth period)	Strains (genotypes)	Shoot dry weights per plant (mg)	Fix%[d]	AR activity[f] (per plant)	Fix%[e]
Leucaena leucocephala (ten weeks)	Uninoculated control	77 ± 7^{a}	0%	0^{a}	0%
	RmG694 (NGR234 wild type)	285 ± 16^{b}	100%	1.4 ± 0.2^{b}	100%
	RmG694*pckA* (NGR234 *pckA*::ΩSp^{r})	123 ± 12^{c}	22%	0.24 ± 0.05^{c}	17%
	RmP2651 (NGR234 *pckA*::ΩSp & *Δ dme*)	83 ± 9^{a}	2%	0^{a}	0%
Macroptilium atropurpureum (five weeks)	Uninoculated control	20 ± 4^{a}	0%	0^{a}	0%
	RmG694 (NGR234 wild type)	297 ± 25^{b}	100%	2.3 ± 0.3^{b}	100%
	RmG694*pckA* (NGR234 *pckA*::ΩSp^{r})	53 ± 7^{c}	12%	0.37 ± 0.04^{c}	16%
	RmP2651 (NGR234 *pckA*::ΩSp^{r} & *Δ dme*)	21 ± 4^{a}	0%	0^{a}	0%

a-c Two independent experiments (12 plants per strain per experiment) were made for each host. Date are means ± standard deviation. Values followed by the same letter do not differ at the 0.05 level of probability based on one-way ANOVA test. ND, not determined. *d* Calculated by shoot dry weight per plant: (test-uninoculated)/(wild type-uninoculated). *e* Calculated as the amount of acetylene reduced per plant: test/wild type. *f* Nitrogenase activity assayed by acetylene reduction assay (μmol C_2H_4 produced/hour).

This result was similar to that of *R. leguminosarum* where individual *dme* or *pckA* mutants fix N_2, but *dme pckA* double mutants are completely devoid of symbiotic N_2-fixing activity (Mulley *et al*., 2010). Thus NGR234 bacteroids appear to employ either malic enzyme or phosphoenolpyruvate carboxykinase pathways in the synthesis of pyruvate and acetyl-CoA. We note that wild-type *S. meliloti* bacteroids isolated from alfalfa nodules have very low PCK activity (Osteras *et al*. 1997; Finan *et al*. 1991), whereas NGR234 bacteroids isolated from nodules on *C. cajan, L. purpureus, L. leucocephala, M. atropurpureum,* and *V. unguiculata* have high PCK activity (50-180 nmoles/min/mg protein,Table 9). Thus the PCK activity in NGR234 bacteroids presumably accounts for the symbiotic N_2-fixation by NGR234 *dme* mutants.

3.4 Discussion

In this chapter, the symbiotic phenotypes of *Sinorhizobium* sp. NGR234 *dme* mutants were examined on five host plants: *C. cajan, L. purpureus, L. leucocephala, M. atropurpureum,* and *V. unguiculata.* Data showing that *dme* mutants of *Sinorhizobium* sp. NGR234 form N_2-fixing root nodules on diverse host plants (Table 6) clearly suggests that NAD^+-dependent malic enzyme activity is not absolutely required for symbiotic N_2-fixation by NGR234. This conclusion is mitigated by the possibility that, in addition to DME, another NAD^+-dependent malic enzyme may function in NGR234. However, we failed to detect such an enzyme in our search of the NGR234 genome where only the DME (ACP25453) and TME (ACP23834) proteins were detected. The enzyme assay used to detect ME activity in crude extracts relies upon the detection of keto acids (Friedemann & Haugen 1943). Thus using this assay, the NGR234 *dme* mutants retained

about 50% of the NAD^+-dependent ME activity of the wild type. This activity is almost certainly a background activity that results in part from activity mediated by malate dehydrogenase, and this residual activity was also present at similar levels in *dme* mutants of *S. meliloti* and *R. leguminosarum.*

The symbiotic phenotypes of *dme* (Fix^+), *pck* (Fix^+), and *dme pck* double (Fix^-) mutants of NGR234 suggested that pyruvate and acetyl-CoA can be generated via malic enzyme or phosphoenolpyruvate carboxykinase pathways. This result was similar to those obtained for *R. leguminosarum,* where *dme* and *pckA* mutants were Fix^+ while *dme pckA* double mutants were Fix^-. We note that in the case of *R. leguminosarum*, the effect of combining the *pckA* and *dme* mutations was more clear-cut as the individual *dme* and *pckA* mutations had little effect on the pea nodule nitrogen fixation phenotype (Mulley *et al*., 2010). However, in the case of NGR234, the *dme* and *pckA* mutations did affect symbiotic N_2-fixation and the extent of the symbiotic defects was found to be dependent on the host plant (Table 6) (Osteras *et al*., 1991).

The PCK activity in NGR234 bacteroids was presumably associated with the Fix^+ symbiotic phenotype of the *dme* mutants. As the level of N_2-fixation of the NGR234 *dme* mutants varied depending on the host legume plant (Table 6), we were interested in determining whether the extent of the symbiotic nitrogen fixation of the *dme* mutants was reflected in the PCK activity measured in the NGR234 bacteroids from the different hosts plants (Table 9). However, no clear correlation between PCK activity and N_2-fixation was evident (Table 6 & Table 9). This may reflect the complexity of the host-dependent phenotypes of the *dme* mutants, which include N_2 fixation, growth of nodules as reflected

by nodule size, and perhaps the initiation of nodule formation. *C. cajan* and *V. unguiculata* plants inoculated with *dme* mutants formed significantly fewer nodules than plants inoculated with the wild type (Table 7). Since DME plays a role in central carbon metabolism, its absence could influence the levels of various metabolic intermediates (Figure 6). Thus, depending on the carbon sources made available to the bacteria by different host plants, the absence of DME could influence Nod factor synthesis, with possible effects on nodule number.

Chapter 4 Purification and Biochemical Characterization of Putative Malic Enzymes in *Azorhizobium caulinodans*

4.1 Abstract

Azorhizobium caulinodans is a Gram-negative α-proteobacterium belonging to the family *Xanthobacteraceae*. It forms nitrogen fixing nodules on the stems and roots of the semi-aquatic tropical legume *Sesbania rostrata. A. caulinodans* contains a single chromosome of 5.37 Mb, which is the smallest genome among the known rhizobia. *azc0119* and *azc3656* are two malic enzyme-like genes found in the genome of *A. caulinodans*. The *azc0119* encoded protein is similar to plant or animal $NADP^+$-dependent malic enzymes, while the *azc3656* encoded protein is 69% and 47% identical to the *S. meliloti* DME and TME proteins respectively. In a large-scale symbiotic mutant screen of *A. caulinodans ORS571*, two *azc3656* insertion mutants formed nodules lacking nitrogen-fixing ability (Fix^-). In another study, transcription of the malic-enzyme like gene (*azc0119*) was also found to be induced in *A. caulinodans* bacteroids. To investigate the nucleotide cofactor specificity and gain insight into the physiological role of each malic enzyme-like protein of *A. caulinodans*, we purified the two putative malic enzymes as N-terminal His-tagged protein and investigated their malic enzyme-related activities. The AZC3656 protein was found to be an $NAD(P)^+$-dependent malic enzyme (DME) whose activity is inhibited by acetyl-coenzyme A (acetyl-CoA) and simulated by succinate and fumarate while the AZC3656 protein lacked ME activity.

4.2 Materials and Methods

Bacterial strains, plasmids and primers used in this work are listed in Table 3 and Table 4. Primers were from Sigma-Aldrich or Integrated DNA Technologies. Methods other than those outlined below are summarized in Chapter 2 of this thesis.

4.2.1 Overexpression and Purification of AZC0119 and AZC3656 Proteins

The vectors used for overexpressing His-tagged AZC0119 and AZC3656 proteins were constructed as follows. *azc0119* and *azc3656* were PCR amplified from *A. caulinodans* ORS571 genomic DNA using two pairs of primers (F044/R045 and F042/R043, respectively), and cloned into the expression vector pBAD/HisA between the His tag and the transcriptional terminator via *HindIII* and *NheI* restriction sites. DNA sequencing of the cloned regions confirmed the absence of mutation within the 1,677-bp *azc0119* and 2,280-bp *azc3656* gene fragments. The resulting plasmids pTH2754 and pTH2755 (carrying *azc3656* and *azc0119*, respectively, Figure 20) were transferred into *E.coli* Top10 strain (Invitrogen), generating *E.coli* Top10 strains M1906 (pTH2754) and M1907 (pTH2755). Overnight cultures of *E.coli* Top10 strains M1906 (pTH2754) and M1907 (pTH2755) were subcultured into 500 ml of LB liquid medium (with 50μg/ml ampicillin) and grown to an optical density at 600nm (OD_{600}) of approximately 0.6. Expression of *azc3656* and *azc0119* were induced with 0.02% (1.3 mM) L-arabinose for 4 hours at 37 °C. Cells were pelleted and stored at -80 °C prior to lysis. His-tagged AZC0119 and AZC3656 proteins were purified as described in Chapter 2. The deduced molecular masss of the AZC0119 and AZC3656 proteins (including the His-tags) are 62 kDa and 82 kDa, respectively.

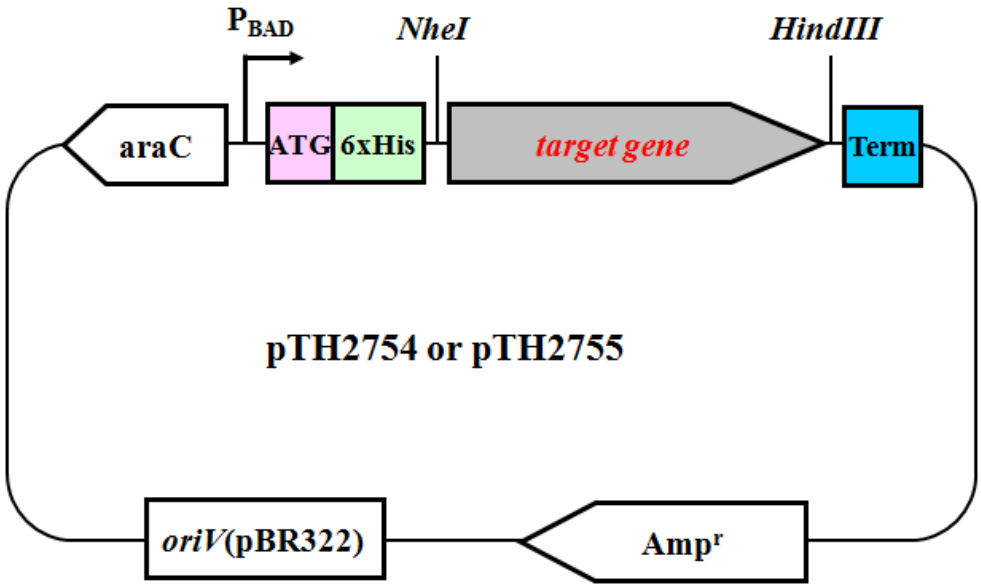

Figure 20 Schematic map of plasmids overexpressing *A. caulinodans* ORS571 AZC0119 and AZC3656 proteins carrying an N-terminal His-tag.

The target gene was cloned into the expression vector pBAD/HisA via *HindIII* and *NheI* restriction sites: pTH2754 (carrying *azc3656*) and pTH2755 (carrying *azc0119*). P_{BAD}, *araBAD* promoter; ATG, initiation ATG codon; 6XHis: N-terminal polyhistidine tag; Term: *rrn*B transcription termination region; *araC*: gene encoding the regulatory protein for tight regulation of the PBAD promoter; and AMP^r, ampicillin (Amp) resistance gene.

4.3 Results

4.3.1 Overexpression and Purification of AZC0119 and AZC3656 Proteins

In a symbiotic mutant screen of *A. caulinodans* ORS571, two insertion mutants with mutations in a malic enzyme-like gene (*azc3656*) were found to form Fix^- nodules (Suzuki *et al*. 2007). In a subsequent study, transcription of a second malic enzyme-like gene (*azc0119*) was found to be much higher in *A. caulinodans* bacteroids than in free-living cells (Suzuki *et al*. 2007). The interpretation of these results was hindered by an absence of functional data on either the *azc3656* or *azc0119* gene product. To examine the malic enzyme-related activities of the proteins encoded by *azc3656* and *azc0119*, these genes were cloned and their encoded proteins were overexpressed and purified as N-terminally His-tagged fusion proteins. Accordingly, *azc0119* and *azc3656* were overexpressed in *E.coli* and the fusion proteins were eluted from a Nickel chromatography column with imidazole. The quantity and purity of target protein in each eluted fraction were examined by running eluted fractions on 10% SDS-PAGE gels (Figure 21). The fractions with highly purified AZC0119 (Figure 21A, lane9 & lane10) or AZC3656 (Figure 21B, lane8 & lane9) were pooled together followed by dialysis. 100-µl aliquots of His-tagged AZC0119 (7 mg/ml) and AZC3656 (2 mg/ml) were flash frozen in liquid nitrogen and stored at -80°C prior to use.

Figure 21 Overexpression and purification of *A. caulinodans* ORS571 AZC0119 and AZC3656 proteins carrying an N-terminal His-tag.

(A) His tagged AZC0119 protein (~62 kDa). (B) His tagged AZC3656 protein (82 kDa). Target gene was cloned on vector pBAD/HisA (Invitrogen) and expressed in *E.coli* Top10 strain (Invitrogen) grown in LB with 0.02% (1.3mM) L-arabinose at 37℃ for 4 hrs. Protein samples were visualized by 10% SDS-PAGE gel followed by straining with Coomasie brilliant blue. Each lane was loaded with 5 µl of sample. Line 1, crude cell lysate obtained from uninduced cells; lane 2, crude cell lysate obtained from L-arabinose-induced cells; lane 3, supernatant of crude cell lysate obtained from L-arabinose-induced cells; lane 4, flow though of lysate supernatant (induced cells) collected from Ni-NTA column; lane 5, elute collected from 20 mM imidazole wash; lane 6, elute collected from 50 mM imidazole wash; lane 7, elute collected from 100 mM imidazole wash; lane 8, elute collected from 150 mM imidazole wash; lane 9, elute collected from 200 mM imidazole wash; lane 10, elute collected from 250 mM imidazole wash; PageRuler Unstained Protein Ladder (Thermo) are shown in the outer left lane.

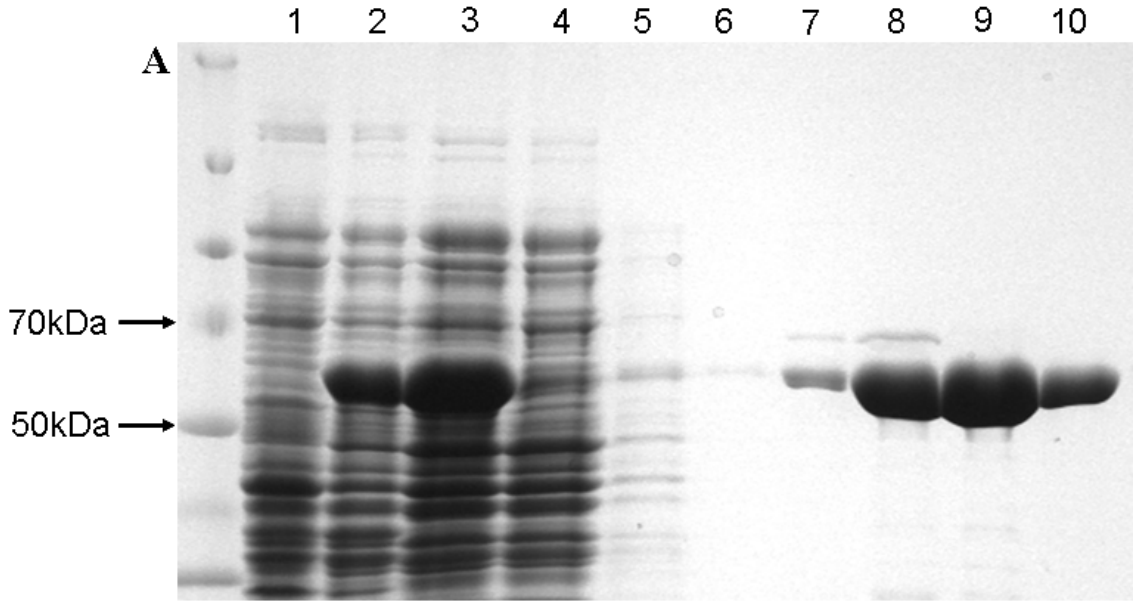
1 2 3 4 5 6 7 8 9 10
A
70kDa
50kDa

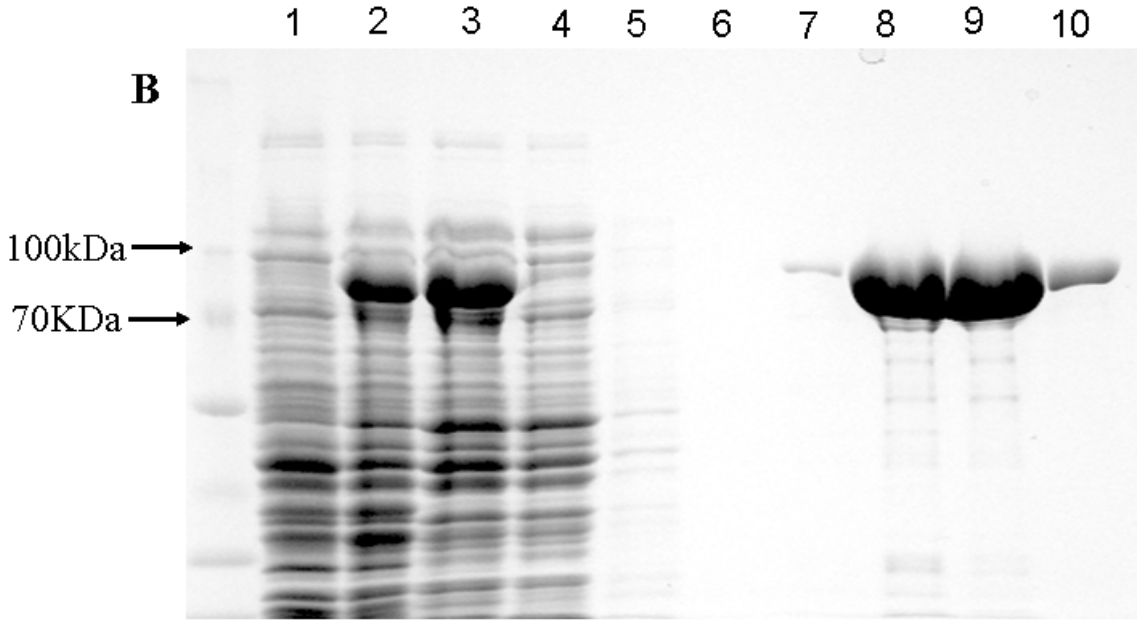
1 2 3 4 5 6 7 8 9 10
B
100kDa
70KDa

4.3.2 pH Optima for Malic Enzyme Activities of AZC3656 and AZC0119 Proteins

The malic enzyme activities of the His-tagged AZC3656 and AZC0119 proteins over a pH range from 5 to 10 are presented in Figure 22. Activities were measured by following the formation of NADH or NADPH at 340nm. AZC3656 malic enzyme activity peaked at pH 7.8 (NAD^+) and 7.0 ($NADP^+$) and this protein showed high NAD^+ - dependent activity (37μmol/min/mg at pH 7.8), while its $NADP^+$ - dependent activity was relatively low (approximately 3 μmol/min/mg at pH 7.0) (Figure 22A). The AZC3656 NAD $(P)^+$-dependent malic enzyme activity was very similar to that of the *S. meliloti* DME protein. In contrast, the AZC0119 protein had less than 2% of the AZC3656 protein $NAD(P)^+$-dependent malic enzyme activity over a range of pHs (Figure 22B). These data suggest that the AZC0119 protein is not a malic enzyme.

4.3.3 The kinetic properties of AZC3656 protein

We reasoned that the determination of the basic kinetic properties of the malic enzyme-like protein encoded by *azc3656*, such as affinity for L-malate and $NAD(P)^+$, would aid in the elucidation of the physiological function of the AZC3656 protein in *A. caulinodans* carbon metabolism. The apparent K_m and V_{max} values for L-malate and $NAD(P)^+$ reported here were calculated from linear regressions derived from the data plotted as Hanes–Woolf plots, X: [S] vs. Y: [S]/*v* ([S] = L-malate or $NAD(P)^+$ concentration, mM; V = enzyme specific activity, μmol NAD(P)H/min/mg). The calculated K_m and V_{max} values were not significantly different from those obtained via analyses using Lineweaver-Burke plots and the Michaelis-Menten equation (Table 11).

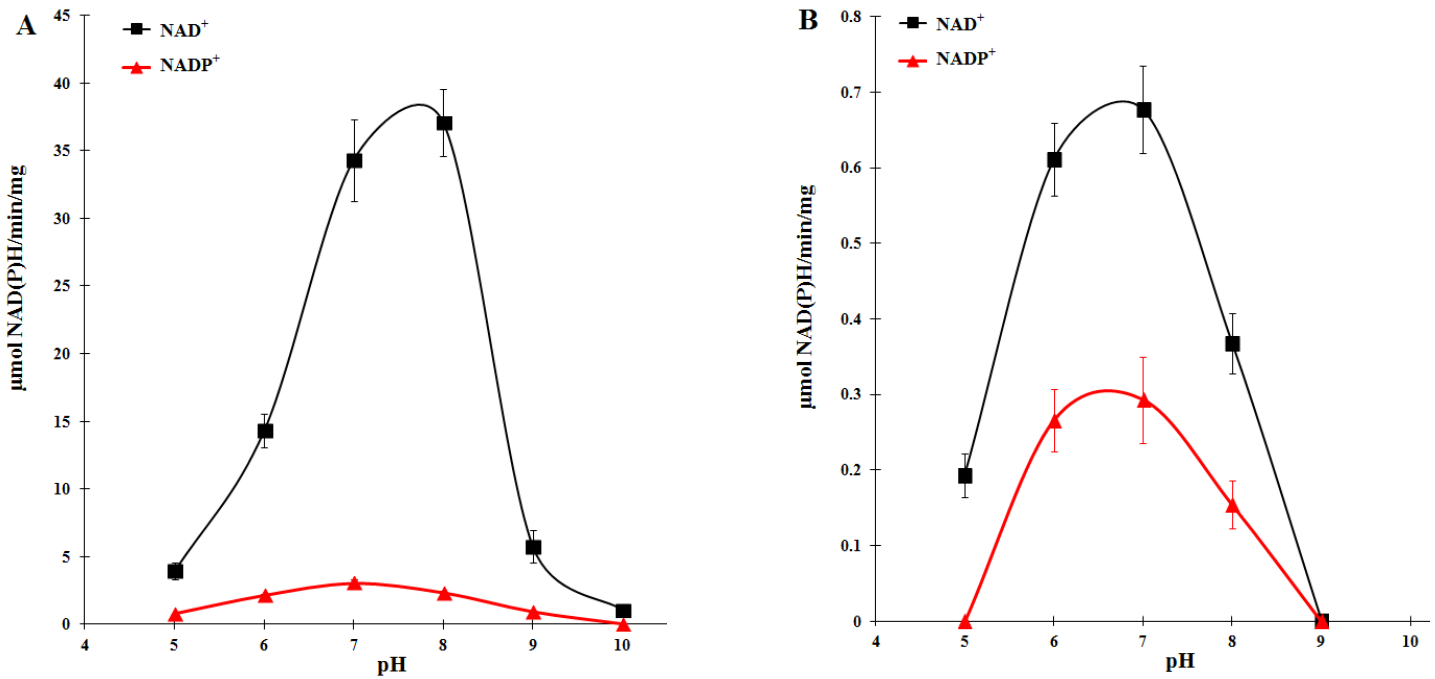

Figure 22 Malic enzyme activities of AZC3656 and AZC0119 proteins at various pHs

(A) AZC3656 protein malic enzyme activity (S.A) at various pHs. (B) AZC0119 protein malic enzyme activity (S.A) at various pHs. Buffers (100mM) used were as follows: 2-(*N*-morpholino) ethanesulfonic acid (MES), pH 5-6; tris (hydroxymethyl) aminomethane (Tris), pH 7-8; and 1,3-bis (tris(hydroxymethyl)methylamino) propane (BTP), pH 9-10. Malic enzyme activities were measured using substrate: 30 mM L-malate, cofactor: 1.5 mM NAD^+ (■) or $NADP^+$ (▲). Specific activity (S.A.) is shown as µmol NAD (P)H/minute/mg protein. Error bars represent standard error of the mean of triplicate samples.

Table 11 Summary of kinetic analyses of *A. caulinodans* AZC3656 protein with respect to malic enzyme activity

Varied compound[1]	Analysis[2]	K_m	V_{max} (μmol/min/mg)
L-malate	M-M	2.8 mM	51.1
	L-B	2.7 mM	46.1
	H-W	2.6 mM	49.1
NAD^+	M-M	94.6 μM	41.8
	L-B	103.8 μM	47.2
	H-W	97.6 μM	40.7
$NADP^+$	M-M	2.1 mM	22.3
	L-B	2.1 mM	21.6
	H-W	2.2 mM	22.1

Malic enzyme activities were measured by following the formation of NAD(P)H at 340 nm as mentioned in Materials and methods (chapter 2). [1] For kinetic experiments, malic enzyme was determined as the concentration of one of the substrate or coenzyme was varied: L-malate (0.1-90 mM), NAD^+ (0.01-8 mM), and $NADP^+$ (0.01-8 mM).[2] Data were calculated by using three different methods: Michaelis–Menten equation (M-M), $v = V_{max}[S]/(K_m+[S])$; Lineweaver-Burk plot (L-B), X: 1/ [S] vs. Y: 1/v; and Hanes–Woolf plot (H-W), X: [S] vs. Y: [S]/v ([S] = L-malate or $NAD(P)^+$ concentration, mM; v = specific activity, μmol NAD(P)H/min/mg protein)

AZC3656 protein showed high NAD^+ - dependent malic enzyme activity at pH 7.8, with Michaelis-Menten-like kinetics, at various concentrations of L-malate (Figure 23A). L-malate appeared to be saturated at concentrations between 20 and 40 mM and a slight decrease in NAD^+-dependent activity was observed at 70 and 90 mM malate. The K_m of AZC3656 for L-malate was 2.57 mM with a theoretical V_{max} of 49.1μmol/min/mg protein (Figure 23B &Table 11). As shown in Michaelis-Menten plot (Figure 23A), the AZC3656 NAD^+-dependent malic enzyme activity exhibited a hyperbolic function with respect to L-malate. Its Hill plot (Figure 23C), X: log[S] versus Y: $\log[v/(V_{max}-v)]$ ([S] = L-malate concentration, mM; V = enzyme specific activity, μmol NAD(P)H/min/mg), was linear up to an L-malate concentration of 15 mM. A Hill coefficient calculated from this Hill plot was close to 1 (1.1), which suggested that the AZC3656 protein had only a very limited positive cooperativity with respect to malate. It indicated that L-malate binding at one active site does not facilitate biding at other active sites of this malic enzyme.

AZC3656 protein also exhibited Michaelis-Menten type behavior with varying cofactor (NAD^+ and $NADP^+$) concentration. Plots of enzyme activity versus cofactor (NAD^+ and $NADP^+$) concentration showed malic enzyme activity with NAD^+ as well as $NADP^+$ (Figure 24A). The K_m of AZC3656 protein for NAD^+ was found to be 97.6 μM with a theoretical V_{max} of 40.7 μmol/min/mg protein (Figure 24B & Table 11), while the K_m and theoretical V_{max} values for this protein with $NADP^+$ as cofactor were 2.17 mM and 22.1 μmol/min/mg protein, respectively. (Figure 24B & Table 11).

Figure 23 NAD^+-dependent malic enzyme activity of AZC3656 protein in response to various concentrations of L-malate

(A) **Michaelis-Menten plot** of malic enzyme specific activity (S.A.: μmol/min/mg protein) in response to L-malate at an NAD^+ concentration of 1.5 mM.; (B) Analysis of the above data by using **Hanes–Woolf plot, [S]/v** = **[S]**/V_{max} + K_m/V_{max} (Y axis: **[S]/*v*,** X axis: **[S]**; When Y=0, K_m = -X; When X=0, V_{max} = K_m / Y)**,** to determine the K_m and V_{max} with respect to L-malate; (C) Analysis of the above data by using **Hill plot,** X: log[S] versus Y: log[$v/(V_{max}-v)$], to determine Hill coefficient with respect to L-malate ([S] = L-malate concentration, mM; v = specific activity, μmol NAD(P)H/min/mg protein). Malic enzyme activities were measured by following the formation of NAD(P)H at 340 nm as mentioned in Materials and methods (chapter2). Enzyme assay mixtures contained 1.1 μg purified AZC3656 protein, 100mM Tris (pH 7.8), 3mM $MnCl_2$, 5mM NH_4Cl, and 1.5mM NAD^+ in a final volume of 1 ml. Error bars represent standard errors of the means for triplicate samples.

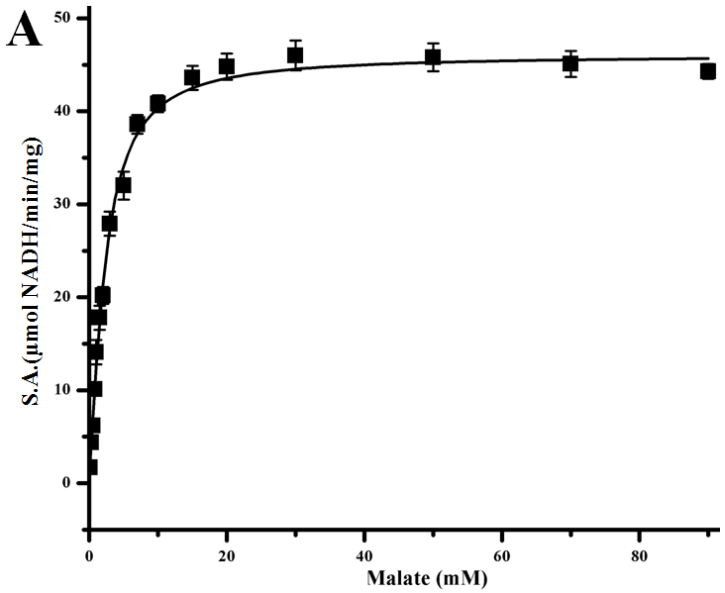
A
S.A.(µmol NADH/min/mg)
Malate (mM)
0
10
20
30
40
50
0
20
40
60
80

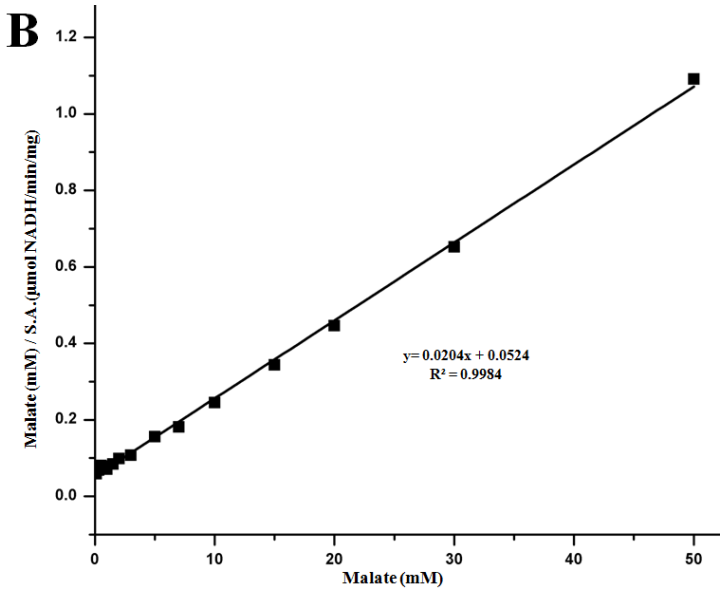
B
Malate (mM) / S.A.(µmol NADH/min/mg)
Malate (mM)
y= 0.0204x + 0.0524
R² = 0.9984
0.0
0.2
0.4
0.6
0.8
1.0
1.2
0
10
20
30
40
50

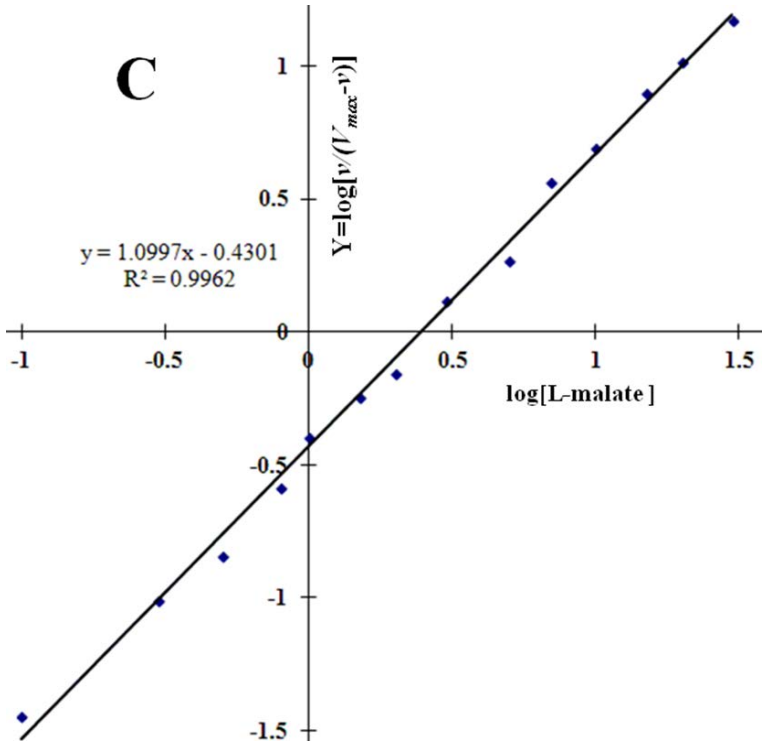
C
Y=log[v/(Vmax-v)]
log[L-malate]
y = 1.0997x - 0.4301
R² = 0.9962
-1.5
-1
-0.5
0
0.5
1
-1
-0.5
0
0.5
1
1.5

Figure 24 Malic enzyme activity of AZC3656 protein in response to various concentrations of the cofactors NAD^+ and $NADP^+$

(A) **Michaelis-Menten plots** of malic enzyme specific activity (S.A.: μmol/min/mg protein) in response to NAD^+ (squares) and $NADP^+$ (triangles) measured at an concentration of 30 mM L-malate ; (B) Analysis of the above data by using **Hanes–Woolf plot, [S]/*v*** = **[S]**/V_{max} + K_m/V_{max} (Y axis: **[S]/*v*,** X axis: **[S]**; When Y=0, K_m = -X; When X=0, V_{max} = K_m / Y)**,** to determine the K_m and V_{max} with respect to NAD^+ (squares) and $NADP^+$ (triangles). Malic enzyme activities were measured by following the formation of NAD(P)H at 340 nm as mentioned in Materials and Methods (Chapter2). Enzyme assay mixtures contained 1.1 μg purified AZC3656 protein, 100mM Tris (pH 7.8), 3mM $MnCl_2$, 5mM NH_4Cl, and 30 mM L-malate in a final volume of 1 ml. Error bars represent standard errors of the means for triplicate samples.

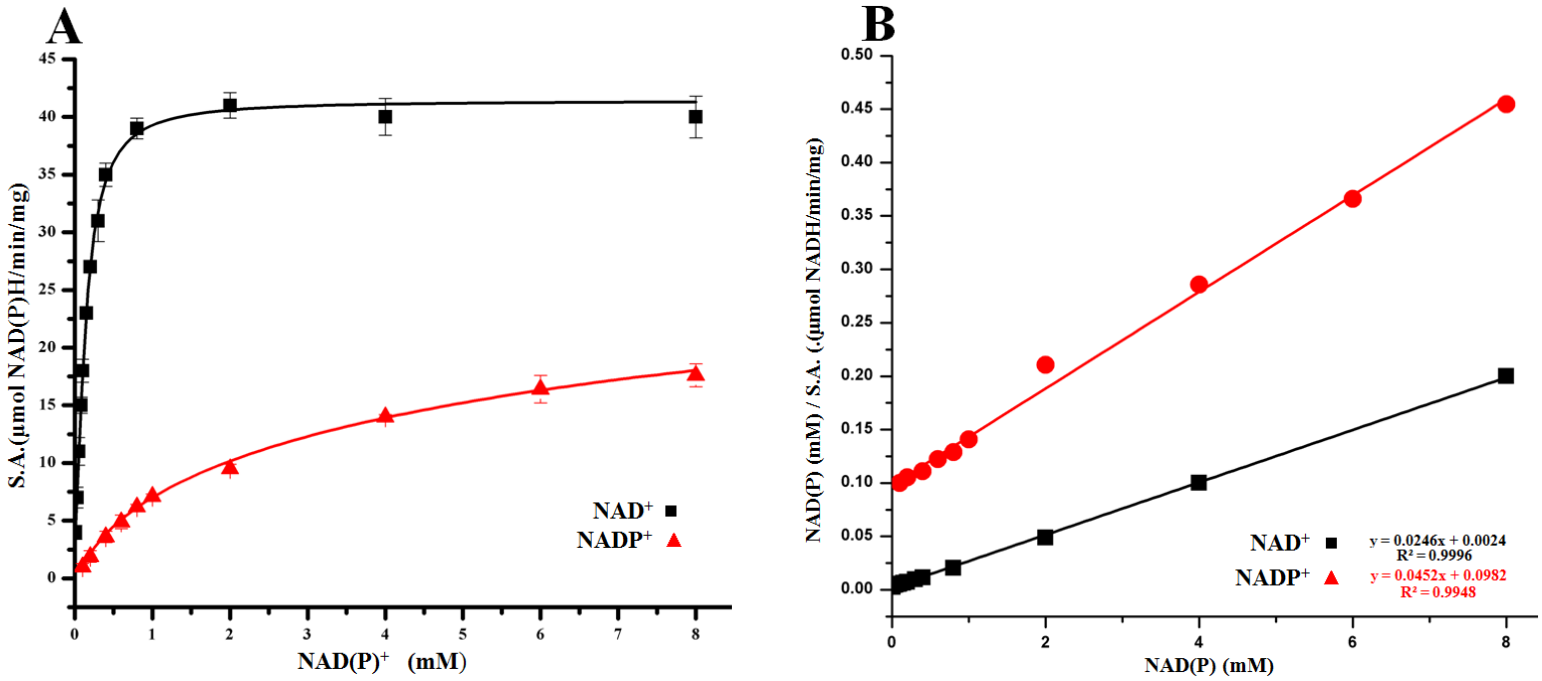
A
S.A.(μmol NAD(P)H/min/mg)
NAD(P)+ (mM)
NAD+
NADP+
B
NAD(P) (mM) / S.A. (.(μmol NADH/min/mg)
NAD(P) (mM)
NAD+
y = 0.0246x + 0.0024
R² = 0.9996
NADP+
y = 0.0452x + 0.0982
R² = 0.9948

Based on its specificity for NAD^+ and $NADP^+$ as cofactors, the AZC3656 protein belongs to the EC 1.1.1.39 class of malic enzyme, which is NAD^+- dependent, but generally shows some activity with $NADP^+$.

4.3.4 Fumarate and Succinate Stimulation of AZC3656 Malic Enzyme Activity

Succinate and fumarate are precursors of malate in the TCA cycle (Figure 6) and these significantly stimulated the activity of *S. meliloti* DME. The AZC3656 protein was proved to be a NAD^+-dependent malic enzyme and essential for symbiotic nitrogen fixation in *Azorhizobium caulinodans* ORS571. Hence, we hypothesized that NAD^+-dependent malic enzyme activity of AZC3656 protein would be stimulated by fumarate and succinate. 0.1 mM and 1mM fumarate stimulated malic enzyme activity of AZC3656 protein by 41% and 53%, respectively, at the malate concentration of 1mM.

According to the Michaelis-Menten plots presented in Figure 25A, the addition of fumarate shifted the curve to the left, which means fumarate increased the affinity of AZC3656 protein for malate. The Hanes–Woolf plots presented in B showed that the K_m for malate dropped from an apparent value of 2.9 mM to 0.79 mM with a slight increase (~15%) in the theoretical V_{max} at a fumarate concentration of 1mM (Table 12).

The addition of succinate had similar effects on malic activity of AZC3656 protein as the addition of fumarate (Figure 26). 1mM and 10mM succinate increased malic enzyme activity of AZC3656 protein by 45% and 61% respectively at the malate concentration of 1mM. As showed in Figure 26A, the addition of succinate shifted the Michaelis-Menten curve to the left, which indicated that succinate enhanced the affinity of AZC3656 protein for malate.

Table 12 Kinetic parameters of purified AZC3656 protein to L-malate in response to allosteric effectors.

Allosteric effectors	Concentrations	Kinetic parameters	
		K_m (mM)	V_{max} (μmol/min/mg)
Fumarate	0 mM	2.9	55
	0.1 mM	1.1	60
	1 mM	0.8	62
Succinate	0 mM	2.9	55
	1mM	1.5	62
	10 mM	1	64
Acetyl-CoA	0 μM	2.6	46
	25 μM	10.6	47
	50 μM	27.3	50
	100 μM	50	45

Malic enzyme activities were measured by following the formation of NADH at 340 nm as mentioned in Materials and methods (chapter2). For kinetic experiments, malic enzyme activity was determined at various concentrations of L-malate (0.1-40 mM). Data were calculated by Hanes–Woolf plot, $\mathbf{[S]}/\boldsymbol{v} = \mathbf{[S]}/V_{max} + K_m/V_{max}$ ([S] = L-malate concentration, mM; v = specific activity, μmol NADH/min/mg protein)**;** Y=0, K_m = -X; X=0, $V_{max} = K_m /$ Y (X axis: [S] vs. Y axis: [S]/v).

Figure 25 Malic enzyme activity of AZC3656 protein is stimulated by fumarate

(A) **Michaelis-Menten plots** of NAD^+-dependent malic enzyme specific activity (S.A.: µmol/min/mg protein) with 0 mM (squares), 0.1 mM (circles), or 1 mM (triangles) fumarate; (B) Analysis of the above data by using **Hanes–Woolf plot** ([S] vs.[S]/*v*), to determine the K_m and V_{max} for L-malate with response to 0 mM (squares), 0.1 mM (circles), or 1 mM (triangles) fumarate; Malic enzyme activity was determined by following the formation of NAD(P)H at 340 nm (Materials and methods, chapter2) as the concentration of L-malate was varied from 0.1 to 30 mM. Enzyme assay mixtures contained 1 µg purified AZC3656 protein, 100 mM Tris (pH 7.8), 3 mM $MnCl_2$, 5 mM NH_4Cl, and 1.5 mM NAD^+ in a final volume of 1 ml. Error bars represent standard errors of the means for triplicate samples.

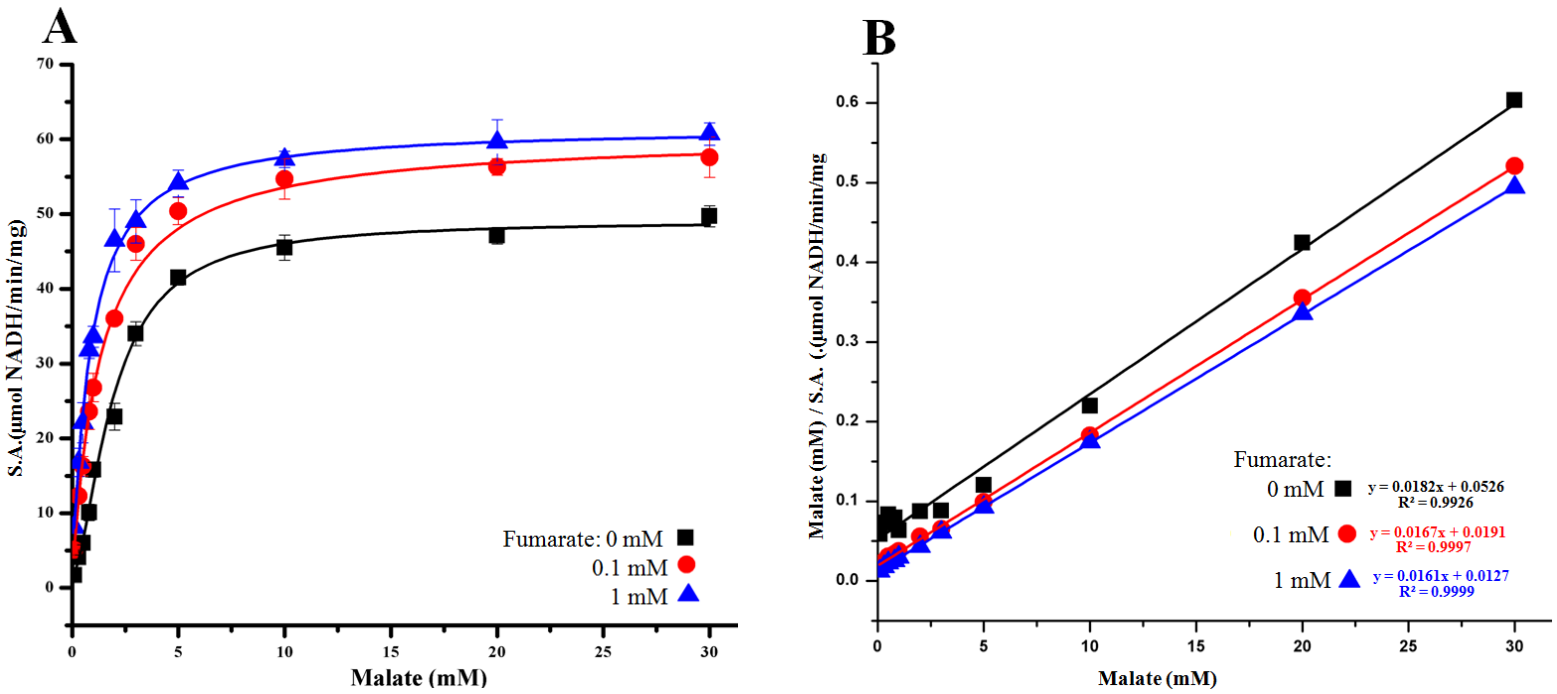
A
S.A.(µmol NADH/min/mg)
Malate (mM)
Fumarate: 0 mM
0.1 mM
1 mM
B
Malate (mM) / S.A. (.(µmol NADH/min/mg
Malate (mM)
Fumarate:
0 mM
y = 0.0182x + 0.0526
R² = 0.9926
0.1 mM
y = 0.0167x + 0.0191
R² = 0.9997
1 mM
y = 0.0161x + 0.0127
R² = 0.9999

Figure 26 Malic enzyme activity of AZC3656 protein is stimulated by succinate

(A) **Michaelis-Menten plots** of NAD^+-dependent malic enzyme specific activity (S.A.: μmol/min/mg protein) with 0 mM (squares), 1 mM (circles), or 10 mM (triangles) succinate; (B) Analysis of the above data by using **Hanes–Woolf plot** ([S] vs.[S]/*v*)**,** to determine the variation of K_m and V_{max} for L-malate with response to 0 mM (squares), 0.1 mM (circles), or 1 mM (triangles) succinate. Malic enzyme activity was determined by following the formation of NAD(P)H at 340 nm (Materials and methods, chapter2) as the concentration of L-malate was varied from 0.1 to 30 mM. Enzyme assay mixtures contained 1 μg purified AZC3656 protein, 100 mM Tris (pH 7.8), 3 mM $MnCl_2$, 5 mM NH_4Cl, and 1.5 mM NAD^+ in a final volume of 1 ml. Error bars represent standard errors of the means for triplicate samples.

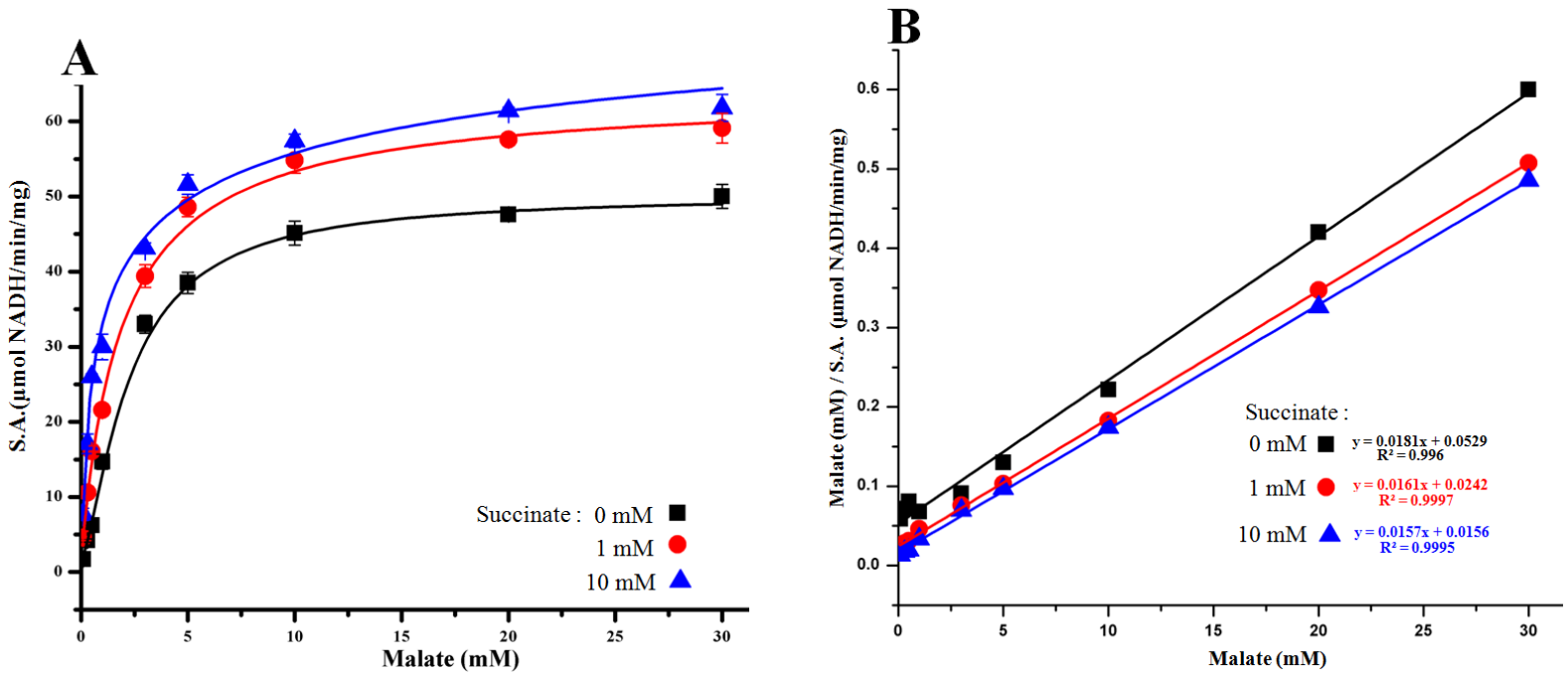
A
S.A.(μmol NADH/min/mg)
Malate (mM)
Succinate : 0 mM
1 mM
10 mM
B
Malate (mM) / S.A. (μmol NADH/min/mg)
Malate (mM)
Succinate :
0 mM y = 0.0181x + 0.0529 R² = 0.996
1 mM y = 0.0161x + 0.0242 R² = 0.9997
10 mM y = 0.0157x + 0.0156 R² = 0.9995

The Hanes–Woolf plots presented in Figure 26B revealed that the K_m of AZC3656 protein for malate reduced from an apparent value of 2.9 mM to 0.99 mM with a modest increase (~20%) in the theoretical V_{max} at a succinate concentration of 10mM (Table 12).

4.3.5 Acetyl-CoA inhibition of AZC3656 malic enzyme activity

Malic enzyme together with pyruvate dehydrogenase provides an important pathway to generate acetyl-CoA required to maintain flux through the TCA cycle (Figure 6). 25µM and 50µM acetyl-CoA was found to reduce NAD^+-dependent malic enzyme activity of AZC3656 protein by 69% and 88%, respectively, at the malate concentration of 1mM.

The Michaelis-Menten plots presented in Figure 27(A) showed that addition of acetyl-coA (25-100 µM) caused the curve shift to the right, indicating that acetyl-CoA reduced the affinity of AZC3656 protein for malate. The Hanes–Woolf plots (Figure 27B) revealed that the K_m of AZC3656 for malate increased almost 10 fold from 2.6 mM to 27.3 mM at the acetyl-CoA concentration of 50µM, but the V_{max} seemed to be unaffected (Table 12). The results obtained at various concentrations of acetyl-CoA suggested that acetyl-CoA affected the K_m of AZC3656 protein, and not its V_{max} (Table 12). Hence, acetyl-CoA exhibited competitive inhibition of AZC3656 protein with respect to NAD^+-dependent malic enzyme activity.

Figure 27 Malic enzyme activity of AZC3656 protein is inhibited by acetyl-CoA

(A) **Michaelis-Menten plots** of NAD^+-dependent malic enzyme specific activity (S.A.: μmol/min/mg protein) with 0 M (squares), 25 μM (circles), 50 μM (triangles), or 100 μM (stars) acetyl-CoA; (B) Analysis of the above data by using **Hanes–Woolf plot** ([S] vs.[S]/*v*)**,** to determine the K_m and V_{max} for L-malate with response to 0 M (squares), 25 μM (circles), 50 μM (triangles), or 100 μM (stars) acetyl-CoA. Malic enzyme activity was determined by following the formation of NAD(P)H at 340 nm (Materials and methods, chapter2) as the concentration of L-malate was varied from 0.1 to 30 mM. Enzyme assay mixtures contained 1 μg purified AZC3656 protein, 100 mM Tris (pH 7.8), 3 mM $MnCl_2$, 5 mM NH_4Cl, and 1.5 mM NAD^+ in a final volume of 1 ml. Error bars represent standard errors of the means for triplicate samples.

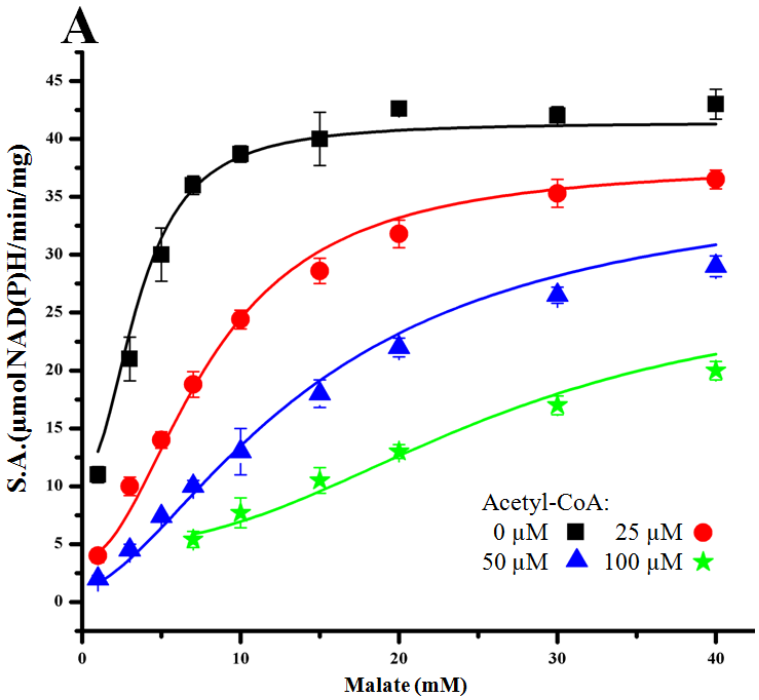
A
S.A.(μmol NAD(P)H/min/mg)
Malate (mM)
Acetyl-CoA:
0 μM
25 μM
50 μM
100 μM

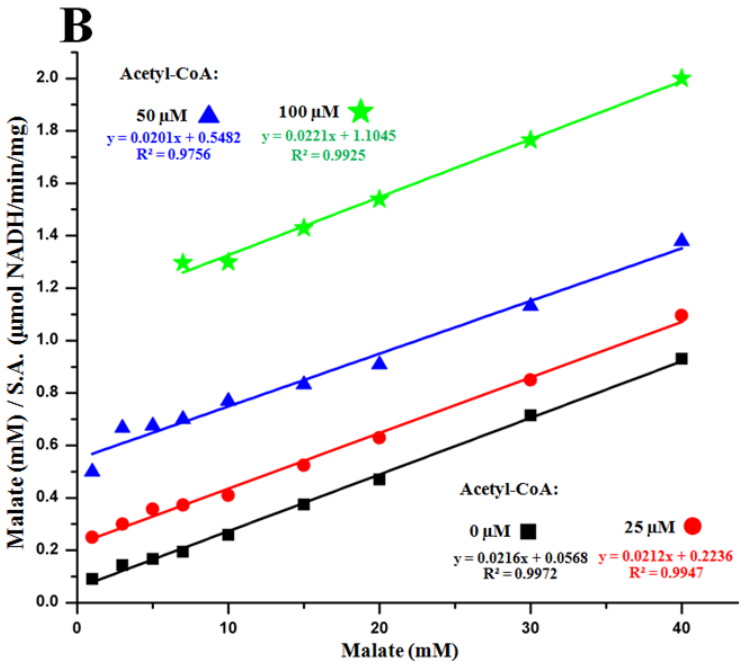
B
Malate (mM) / S.A. (μmol NADH/min/mg)
Malate (mM)
Acetyl-CoA:
50 μM
y = 0.0201x + 0.5482
R² = 0.9756
100 μM
y = 0.0221x + 1.1045
R² = 0.9925
Acetyl-CoA:
0 μM
y = 0.0216x + 0.0568
R² = 0.9972
25 μM
y = 0.0212x + 0.2236
R² = 0.9947

4.3.6 Malic Enzyme Activities in *A. caulinodans*

The results above showed that AZC3656 is an NAD(P)$^+$-dependent malic enzyme. To investigate whether *A. caulinodans* contains a NADP$^+$-dependent malic enzyme (EC1.1.1.40), like TME in *S. meliloti*, we assayed for NADP$^+$-dependent malic enzyme in crude extracts of wild-type *A. caulinodans* (RmP2649) and *A. caulinodans azc3656* mutant strains (RmP2662 & RmP2663), which were grown in TY liquid medium. As shown in Table 13, apparent NAD$^+$- dependent malic enzyme activities were detected in the two *A. caulinodans azc3656* mutants RmP2662 and RmP2663 (52 ± 7 and 43 ± 7 nmol/min/mg protein) and this activity was one-fourth of the activity detected in the wild type extracts (201 ± 9 nmol/min/mg protein). This "background" activity is similar to the level of NAD$^+$-dependent activity detected in the extract of *S. meliloti dme tme* double mutant RmG994 (51 ± 5 nmol/min/mg protein). The NADP$^+$-dependent malic enzyme activity detected in the wild type *A. caulinodans* was 30 nmol/min/mg protein, while it was almost undetectable (~2 nmol/min/mg protein) in both of the *A. caulinodans azc3656* mutants RmP2662 and RmP2663 (Table 13). Malate dehydrogenase activity was present in both of the *azc3656* mutants at slightly higher levels than in the wild type *A. caulinodans* (Table 13). This observation is similar to those reported for *dme* mutants of *S. meliloti* and *R. leguminosarum* (Driscoll and Finan 1993;Mulley *et al*. 2010). We conclude that the apparent NADP$^+$- malic enzyme activity detected in the wild-type *A. caulinodans* originates from the AZC3656 protein, and that *A. caulinodans* does not contain an NADP$^+$- dependent malic enzyme.

Table 13 Enzyme activities of *A. caulinodans* wild type and *azc3656* mutant bacteroids and free-living cells

Strains & Genotypes	Enzyme	Enzyme specific activity [a]	
		Free-living cells [c]	Bacteroids [b]
RmP2649 *A. caulinodans* wild type	DME	201 ± 9	157 ± 7
	TME	29 ± 3	15 ± 4
	MDH	598 ± 40	2,169 ± 140
	PCK	44 ± 7	15 ± 3
RmP2662 *A. caulinodans azc3656::Tn5*	DME	52 ± 7	ND
	TME	3 ± 1	ND
	MDH	660 ± 30	ND
RmP2663 *A. caulinodans azc3656::Tn5*	DME	43 ± 7	ND
	TME	2 ± 2	ND
	MDH	691± 48	ND
RmP110 *S. meliloti* wild type	DME	89 ± 5	184 ± 7
	TME	65± 3	37 ± 6
	MDH	1,184 ± 37	5,078 ± 109
	PCK	35 ± 4	12 ± 3
RmG994 *S. meliloti dme-3*::Tn5 & *tme-4*:: ΩSp^r	DME	51 ± 5	ND
	TME	0	ND
	MDH	1,317 ± 63	ND
RmG694*pckA* NGR234 *pckA*::ΩSp^r	PCK	10 ± 2	ND

[a] Values are means ± standard error for triplicate samples. For DME (NAD-dependent malic enzyme), specific activity is shown as nanomoles of pyruvate formed/minute/mg protein; for TME (NADP-dependent malic enzyme), specific activity is shown as nanomoles of pyruvate formed/minute/mg protein; for PCK (phosphoenolpyruvate carboxykinase), specific activity is shown as nanomoles of NADH oxidized/minute/mg protein; and for MDH (malate dehydrogenase), specific activity is shown as nanomoles of NADH formed/minute/mg protein. N.D.: not determined. **[b]** Bacteroids were isolated from nodules of 5-week-old *Sesbania rostrata* plants and 5-week-old alfalfa plants. Bacteroid extracts were prepared as described (Chapter 2 Material and Method).**[c]** Free-living cells of NGR234 and *A. caulinodans* strains were grown in TY liquid medium, *S. meliloti* strains were grown in LBmc liquid medium, and cell extracts were prepared as described (Chapter 2 Material and Method).

4.4 Discussion

In this study, we found that the purified AZC0119 protein is not a malic enzyme and that purified AZC3656 protein is an $NAD(P)^+$-dependent malic enzyme. The properties of AZC3656 are remarkably similar to those of DME from *S. meliloti* except for the apparent lack of positive cooperativity with respect to L-malate. Positive cooperativity with respect to L-Malate was obvious in the case of the *S. meliloti* DME protein with a Hill coefficient of 2.6 (Voegele *et al*. 1999), but was very limited for the AZC3656 protein with a Hill coefficient of 1.1 (Figure 23C). Both proteins share similar apparent K_m for L-malate, NAD^+, and $NADP^+$, and both activities were allosterically regulated by negative effector acetyl-CoA (Figure 27) and positive effectors succinate and fumarate (Figure 25 & Figure 26) (Voegele *et al*. 1999). The Fix^- phenotype of *A. caulinodans azc3656* insertion mutants on *Sesbania rostrata* appears to be identical to the Fix^- phenotype of *S. meliloti dme* mutants.

The Fix^- phenotype of *A. caulinodans azc3656* (*dme*) insertion mutants suggested that phosphoenolpyruvate carboxykinase (PCK) activity might not be involved in the formation of acetyl-CoA in *A. caulinodans* bacteroids. We have not found any report where the PCK activity of *A. caulinodans* bacteroids has been measured. However, data from a comprehensive microarray-transcriptome analysis of *A. caulinodans* suggest that *pckA* (*azc4063*) is transcribed in bacteroids. Transcript signal data from bacteroids, free-living cells grown in TY, and free-living cells grown with succinate plus lactate were 468 ± 33, 135 ± 37, and 75 ± 9, respectively (Tsukada *et al*. 2009). Thus, we assayed

PCK activity in crude extracts of *A. caulinodans* wild-type bacteroids from *Sesbania rostrata* nodules. The wild-type *A. caulinodans* (RmP2649) bacteroids had very low PCK activity (15 ± 3 nmol/minute/mg), which was at the similar level of the PCK activity detected in *S. meliloti* wild-type bacteroid from alfalfa (12 ± 3 nmol/min/mg protein) and slightly higher than the background level of the PCK activity detected in NGR234 *pck* mutant (10 ± 2 nmol/minute/mg) (Table 13).

These results indicate that the combined activities of $NAD(P)^+$-dependent malic enzyme (AZC3656 protein) and pyruvate dehydrogenase provide the only pathway to generate acetyl-CoA from malate in *A. caulinodans* bacteroids. This interpretation appears to be entirely consistent with the results showing that the malic enzyme activity of AZC3656 is stimulated by succinate and fumarate and inhibited by acetyl-CoA. Thus, when the concentration of acetyl-CoA is not high enough for the maintenance of metabolic flux through the TCA cycle, the accumulation of TCA cycle intermediates such as succinate and fumarate stimulates malic enzyme activity of AZC3656 protein, thus generating more acetyl-CoA for consumption by the TCA cycle. On the other side, the feedback inhibition of AZC3656 protein with respect to malic enzyme activity caused by a high concentration of acetyl-CoA might keep the level of malate concentration available for malate dehydrogenase (MDH). We also note that in bacterial cells the concentrations of acetyl-CoA normally range from 60 to 300 μM (Vallari *et al*. 1987), which is high enough to down-regulate malic enzyme activity of AZC3656 protein.

Furthermore, as shown in Table 13, activity of malate dehydrogenase (MDH) detected in wild-type *A. caulinodans* bacteroids (2169 ± 140 nmol/minute/mg) was

roughly half of that measured in *S. meliloti* bacteroids (5,078 ± 109 nmol/minute/mg). One possible explanation for this is that *A. caulinodans* bacteroids might also use oxaloacetate (OAA) as carbon source, in addition to malate, succinate, or fumarate, during symbiotic nitrogen fixation. The oxaloacetate (OAA) supplied by *Sesbania rostrata* directly enters TCA cycle for the synthesis of citrate (Figure 6), which reduces the conversion of malate to oxaloacetate (OAA) via malate dehydrogenase activity in *A. caulinodans* bacteroids.

The amino acid sequence of the *A. caulinodans* AZC3656 protein revealed a 400-amino-acid long N-terminal region similar to previously characterized malic enzymes and a 300-amino-acid domain at the C-terminus similar in sequence to previously characterized phosphotransacetylases (PTA, EC2.3.1.8). The presence of the PTA-like region prompted us to further examine the phosphotransacetylase-related activity of AZC3656 protein. Phosphotransacetylase (PTA) catalyses the reaction: CoA + Acetyl-phosphate $\rightleftharpoons$ Acetyl-CoA + Pi. Phosphotransacetylase (PTA) activity was measured following the formation of acetyl-CoA at 233nm (Klotzsch. 1969). However, under the conditions employed in our assays, the purified AZC3656 protein did not have any phosphotransacetylase (PTA) activity and hence the function of this domain remains to be determined.

Chapter 5 Does a high NADPH/NADP$^+$ ratio in *S. meliloti* bacteroids limit TME activity?

5.1 Introduction

S. meliloti contains two distinct malic enzymes: DME (EC 1.1.1.39) is NAD(P)$^+$-dependent, and TME (EC 1.1.1.40) is strictly NADP$^+$- dependent (Voegele *et al*. 1999). Based on the biochemical characterization of DME and TME, they have similar affinities for L-malate and their cofactors NAD$^+$ (DME) and NADP$^+$ (TME) suggesting that they should share similar catalytic rates (Driscoll and Finan 1997;Mitsch *et al*. 2007;Voegele *et al*. 1999). However, *S. meliloti dme* mutants form alfalfa root nodules that fail to fix nitrogen (Fix$^-$), while *tme* mutants induce wild-type, nitrogen-fixing root nodules (Fix$^+$) (Driscoll and Finan 1996;Driscoll and Finan 1997). Moreover the expression of TME in *dme* mutant nodules failed to rescue N_2-fixation even to a limited extent (Mitsch *et al*. 2007). The reason why DME, and not TME, is essential for symbiotic nitrogen fixation is unknown. We postulated that *S. meliloti* bacteroids might have a high NADPH/NADP$^+$ ratio, and that this ratio results in the complete inhibition of TME activity. However, we have not found any report where the ratios of NADPH/NADP$^+$ in *S. meliloti* bacteroids have been measured. To investigate this hypothesis, we attempted to lower the ratio of NADPH/NADP$^+$ *in vivo* by expressing a soluble pyridine nucleotide transhydrogenase (STH, EC 1.6.1.1) from *Pseudomonas aeruginosa* PAO1.

Pyridine nucleotide transhydrogenase catalyze the reversible transfer of reducing equivalents between the two co-enzyme systems of NADH/NAD$^+$ and NADPH/NADP$^+$

according to the following equation: NADPH + NAD^+ <=> $NADP^+$ + NADH (Arkblad *et al*. 1996). Two types of transhydrogenases have been defined on the basis of the stereospecificity of the transfer. AB-specific transhydrogenases (EC 1.6.1.2) are membrane-bound proteins and specific for the 4A proton of NADH and the 4B proton of NADPH. These enzymes utilize the electrochemical proton gradient for the transfer of reducing equivalents from NADH to $NADP^+$, and their physiological role appears to be NADPH regeneration for reductive biosynthesis (Rydstrom 2006). BB-specific transhydrogenases (EC 1.6.1.1) are soluble proteins and specific for the 4B proton of both NADH and NADPH (Rydstrom *et al*. 1976). Purification and properties of the soluble pyridine nucleotide transhydrogenases (STH) have been reported in *Escherichia coli* (Boonstra *et al*. 1999), *Pseudomonas fluorescens* (French *et al*. 1997) , *Pseudomonas aeruginosa* (Cohen and Kaplan 1970a;Cohen and Kaplan 1970b), *and Azotobacter vinelandii* (Voordouw *et al*. 1979;Voordouw *et al*. 1980). STH activity is strongly inhibited by $NADP^+$ and activated by NADPH and 2'-AMP, suggesting that its physiological role is NADH generation coupled with NADPH oxidation (Voordouw *et al*. 1980;Voordouw *et al*. 1983;Widmer and Kaplan 1977). Moreover, STH from *P. fluorescens* and *A. vinelandii* had been successfully used to enhance the conversion of NAD^+ and NADPH to NADH and $NADP^+$ in vivo (Boonstra *et al*. 2000;Nissen *et al*. 2001).

In this chapter, the soluble pyridine nucleotide transhydrogenase (STH, EC 1.6.1.1) of *Pseudomonas aeruginosa* PAO1was expressed in *S. meliloti*. However, STH activity in bacteroids failed to rescue the symbiotic N_2-fixation deficiency of *S. meliloti*

dme mutants. Furthermore, the concentrations of NAD^+, NADH, $NADP^+$, and NADPH were measured in *S. meliloti* free-living cells and bacteroids using reverse-phase high-performance liquid chromatography (HPLC). We found that STH activity did not reduce the ratio of NADPH/$NADP^+$, but it increased the ratio of NADH/NAD^+.

5.2 Materials and Methods

Bacterial strains, plasmids and primers used in this work are listed in Table 3 and Table 4. Primers were from Sigma-Aldrich or Integrated DNA Technologies. Methods other than those outlined below are summarized in Chapter 2 of this thesis.

5.2.1 Expression of STH in *S. meliloti* Strains

The vectors used for constitutively expressing a soluble pyridine nucleotide transhydrogenase (STH) in *S. meliloti* strains were constructed as follows (Figure 29). A 250-bp PCR fragment carrying promoter (Pneo) was amplified from pTH1937 (using the primers FP001 and RP001, Figure 28) and inserted into a broad-host-range plasmid pTH1582 (Figure 13), via *HindIII* and *NsiI*. The resulting plasmid pTH2632 carries promoter (Pneo) fused with a *gusA* gene (encoding β–glucuronidase reporter enzyme). A PCR fragment carrying a 1.5-kb STH-like gene and a 12-bp *S. meliloti* ribosome-binding site (in front of the ATG *sth* start codon) was amplified from genomic DNA using primers FP002/RP002 (*S. meliloti* 1021) or FP002/RP003 (*Pseudomonas aeruginosa* PAO1), and cloned into pTH2632 between promoter (Pneo) and *gusA* gene via *NsiI* and *SacI*, generating plasmids pTH2638 and pTH2639 (carrying *pa2991* from *P. aeruginosa* PAO1 and *smc00300* from *S. meliloti* 1021, respectively).

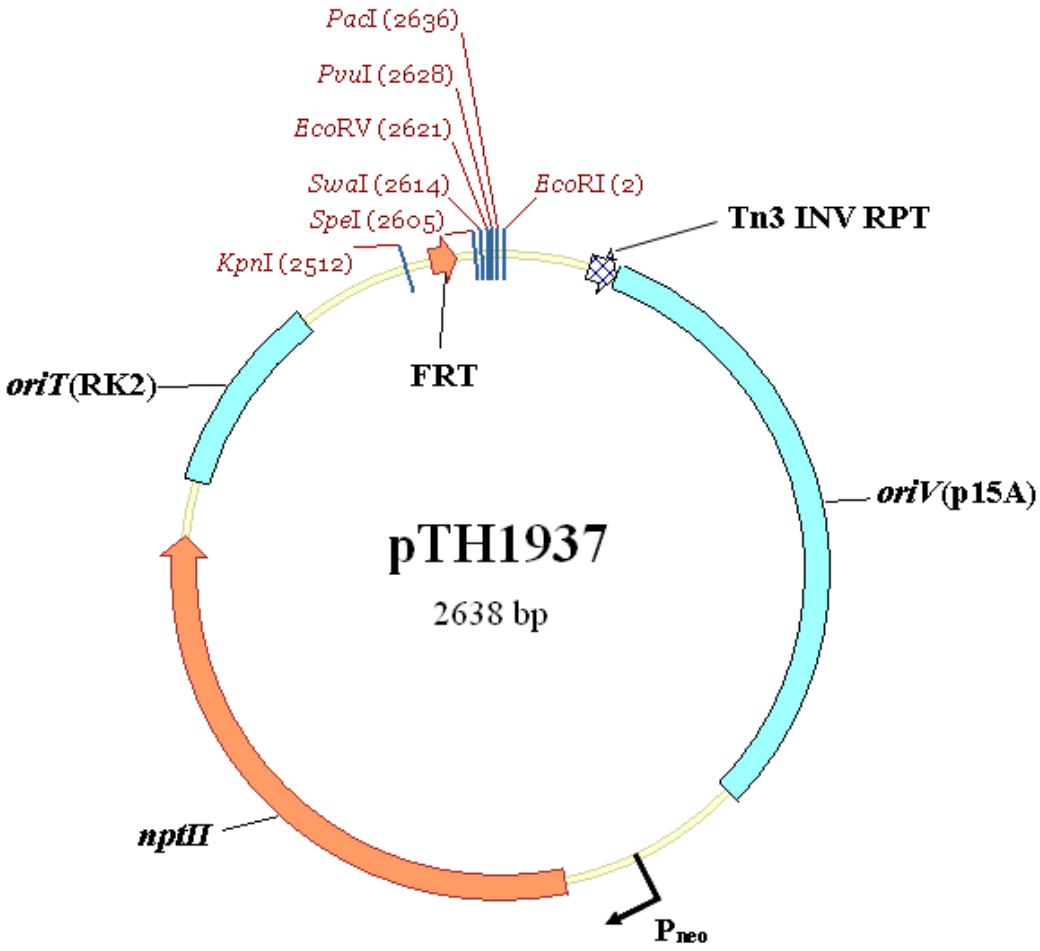

Figure 28 Schematic vector map of pTH1937

Plasmid pTH1937 is a derivative of plasmid pACYC177 (Chang and Cohen 1978) and was constructed by B. Milunovic (2011, Ph.D. Thesis). The important elements of this vector are: (1) *oriV*(p15A): p15A origin of replication (low copy: ~10/cell), which restricts plasmid replication only in enterobacteria (Chang and Cohen 1978); (2) *oriT* (RK2): RK2 origin of transfer, which allows the plasmid to mobilize into a wide range of Gram negative bacteria; (3) *nptII*: kanamycin (Km)/neomycin (Nm) resistance gene from Tn5; (4) Pneo: promoter from Tn5 controls the expression of *nptII*; (5)Tn3 INV RPT: Tn3 inverted repeat; (6) FRT: recognition target for FLP recombinase of yeast.

Figure 29 Schematic diagram illustrating the construction of plasmids constitutively expressing *sth* gene in *S. meliloti* bacteroids.

pTH1582: a broad-host range plasmid stable without selection of antibiotics (Figure 13) and constructed by Yuan *et al* (2005); Pneo: a promoter PCR amplified from pTH1937 (Figure 28); RBS: a 12-bp *S. meliloti* ribosome-binding site; *sth*: soluble pyridine nucleotide transhydrogenase-encoding gene; Tc^r: tetracycline resistance; Amp^r: ampicillin resistance; pTH2638: carrying a STH-like gene, *pa2991* from *P. aeruginosa* (NP_251681.1); pTH2639: carrying a STH-like gene, *smc00300* from *S. meliloti* 1021 (CAC46308.1).

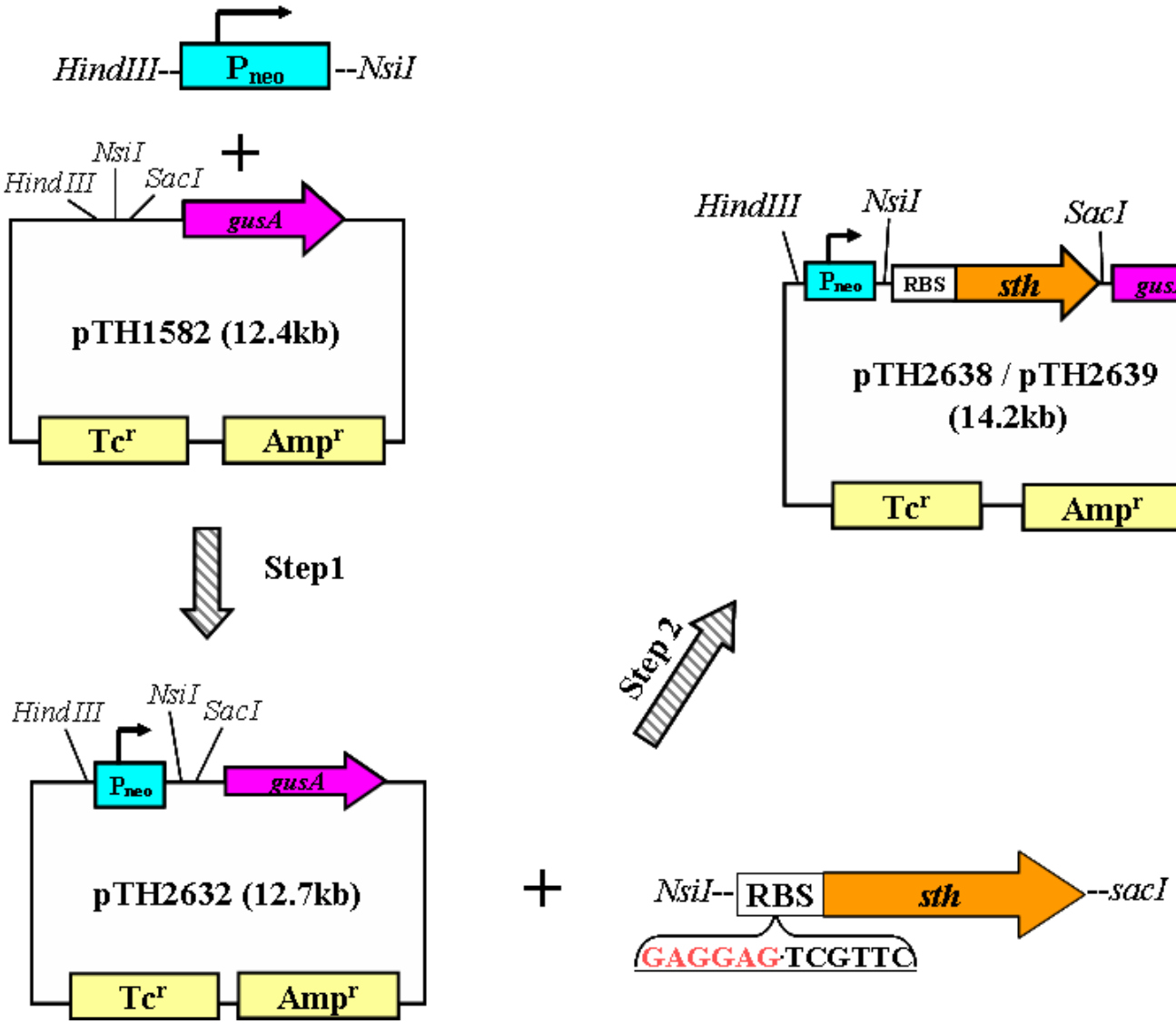
HindIII--
Pneo
--NsiI
NsiI
HindIII
SacI
gusA
pTH1582 (12.4kb)
Tcr
Ampr
Step1
HindIII
NsiI
SacI
Pneo
gusA
pTH2632 (12.7kb)
Tcr
Ampr
Step 2
HindIII
NsiI
SacI
Pneo
RBS
sth
gusA
pTH2638 / pTH2639
(14.2kb)
Tcr
Ampr
NsiI--
RBS
sth
--sacI
GAGGAG
TCGTTC

DNA sequencing of the cloned regions confirmed the absence of mutation with the 250 – bp promoter (Pneo) and 1.5-kb STH-like gene fragments. The expression of STH-like proteins and their STH activities were verified by measuring activities of GusA and STH. The plasmid pTH2638, carrying a functional *sth* gene from *P. aeruginosa* PAO1, was then transferred from *E.coli* into following *S. meliloti* strains: Rm1021 (wild type), RmG455 (Rm1021, *dme-3*::Tn5), and RmH879 (Rm1021, *dme-3*::Tn5, *tme-4*:: Ω Sp^r, P_{dme}-tme^+).

5.3 Results

5.3.1 Cloning of the Gene Encoding the Soluble Pyridine Nucleotide Transhydrogenase (STH)

The soluble pyridine nucleotide transhydrogenase (EC 1.6.1.1)-like genes *pa2991*from *P. aeruginosa* PAO1 (NP_251681.1) and *smc00300* from *S. meliloti* 1021 (CAC46308.1) were cloned into broad-host range plasmids (pTH2638 and pTH2639, respectively) and expressed under the control of promoter (Pneo) as mentioned in Materials and Methods (5.2.1). The expression of the *S. meliloti* 1021 and the *P. aeruginosa* PAO1 STH proteins in *E.coli* was investigated by assaying STH enzyme activities. Since the expression of *gusA* and STH-like genes were controlled by the same promoter Pneo in the constructed plasmid (pTH2638 and pTH2639), we were able to monitor the expression levels of STH-like genes in *E. coli* strains via β–Glucuronidase (GusA) activities. As shown in Table 14, the β–glucuronidase activity (1,216 ± 78, 1,118 ± 54, and 1,012 ± 62 nmol/min/OD_{600} unit) detected in *E.coli* strains with the Pneo plasmids (pTH2632, pTH2638, and pTH2639) were much higher than that detected in the

E. coli carrying the parent plasmid (pTH1582) (110 ± 23 nmol/min/OD_{600} unit) without the Pneo promoter. Thus, the Pneo acts as a strong promoter. STH activities were also measured in *E.coli* extracts the presence of plasmid (pTH2638) with the *P. aeruginosa pa2991* had high STH activity (569 ± 21 nmol/minute /mg), while STH activity was almost undetectable in *E. coli* (2.8 ± 2 nmol/minute /mg) carrying the *S. meliloti smc00300* gene (pTH2639). In fact this activity was similar to the *E. coli* strains carrying the empty plasmid or the Pneo promoter alone (3.4 ± 1 and 2.1 ± 2 nmol/minute /mg) (Table 14). Thus, the data suggested that the protein encoded by *P. aeruginosa pa2991* had STH (EC 1.6.1.1) activity, while the protein encoded by *S. meliloti smc00300* did not appear to be a STH (EC 1.6.1.1).

5.3.2 Expression of the *pa2991* gene (*P. aeruginosa*) in *S. meliloti* Cells

Plasmid pTH2638 carrying the *P. aeruginosa* PAO1 *pa2991* was transferred to *S. meliloti* wild type Rm1021, the Rm1021 *dme* mutant RmG455, and RmH897 which is a *dme tme* double mutant carrying the *tme* gene fusion to *dme* promoter in chromosome (Mitsch *et al*. 2007). The expression of STH in *S. meliloti* was assessed via enzyme assays (Table 15). β–glucuronidase activities were much higher in strains carrying the Pneo promoter than in those carrying the empty parent plasmid pTH1582. Thus Pneo is a strong promoter in *S. meliloti*. The STH activity data also showed that all strains carrying the *P. aeruginosa sth* gene had very high STH activity (1,687 ± 60, 1,668 ± 47, and 1,645 ± 32 nmol/minute/mg).

Table 14 Enzyme assays of *E. coli* strains expressing STH-like genes

E.coli strains	Plasmids	Enzyme specific activity	
		GusA	STH
M462	pTH1582	110 ± 23	3.4 ± 1
M1735	pTH2632 (pTH1582, Pneo::*gusA*)	1,216 ± 78	2.1 ± 2
M1747	pTH2638 (pTH1582, Pneo::*pa2991*::*gusA*)	1,118 ± 54	569 ± 21
M1748	pTH2639 (pTH1582, Pneo::*smc00300*::*gusA*)	1,012 ± 62	2.8 ± 2

Values are means ± standard error for triplicate samples. For GusA (β-glucuronidase), specific activity is shown as nmol *p*NP liberated/min/(OD_{600} unit); for STH (soluble pyridine nucleotide transhydrogenase) specific activity is shown as nmol of thio-NADH produced/minute/mg protein. STH –like genes: *pa2991* (*P. aeruginosa* PAO1) and *smc00300* (*S. meliloti*1021). *E.coli* strains were grown in 20 ml of LB to an OD_{600} of approximately 1. Cell extracts were prepared by sonication and STH activities were measured via observing the change in absorbance at 400 nm due to the reduction of thio-NAD^+ (see Chapter 2 Material and Methods).

Table 15 β-glucuronidase and pyridine nucleotide transhydrogenase activities of *S. meliloti* strains expressing the *P. aeruginosa* STH protein

Strains	Genotypes	Enzyme specific activity				
		DME	TME	MDH	GusA	STH
Rm1021	*S. meliloti* wild type	84 ± 3	62 ± 6	1,114 ± 23	ND	4 ± 2
RmG994	*S. meliloti dme-3*::Tn*5*, *tme-4*:: Ω Sp^r	44 ± 7	0	1,297 ± 41	ND	ND
RmG455	*S. meliloti dme-3*::Tn5	47 ± 6	48 ± 3	1,305 ± 27	ND	3 ± 2
RmH897	*S. meliloti dme-3*::Tn*5*, *tme-4*:: Ω Sp^r, P*dme-tme*$^+$	42 ± 3	98 ± 6	1,219 ± 35	ND	2 ± 1
RmP2312	*S. meliloti dme-3*::Tn5, pTH1582	22 ± 1	51 ± 3	1,272 ± 41	392 ± 22	4 ± 2
RmP2313	*S. meliloti dme-3*::Tn5, *sth*$^+$	21 ± 5	50 ± 7	1,340 ± 63	6,810 ± 487	1,687 ± 60
RmP2314	*S. meliloti dme-3*::Tn*5*, *tme-4*:: Ω Sp^r, P*dme-tme*$^+$, pTH1582	20 ± 4	105 ± 11	1,301 ± 47	414 ± 62	5 ± 3
RmP2315	*S. meliloti dme-3*::Tn*5*, *tme-4*:: Ω Sp^r, P*dme-tme*$^+$, *sth*$^+$	16 ± 5	113 ± 8	1,246 ± 62	7,260 ± 395	1,668 ± 47
RmP2333	*S. meliloti* wild type, pTH1582	79 ± 5	60 ± 2	1,078 ± 30	351 ± 34	6 ± 3
RmP2334	*S. meliloti* wild type, *sth*$^+$	55 ± 4	64 ± 6	1,169 ± 58	7,749 ± 438	1,645 ± 32

S. meliloti strains were grown in 20 ml of LBmc to an OD_{600} of approximately 1. Cell extracts were prepared by sonication and STH activities were measured via observing the change in absorbance at 400 nm due to the reduction of thio-NAD^+ (see Chapter 2 Material and Methods). For GusA (β-glucuronidase), specific activity is shown as nmol *p*NP liberated/min/ (OD_{600} unit); for STH (soluble pyridine nucleotide transhydrogenase) specific activity is shown as nmol of thio-NADH produced/minute /mg protein; for DME (NAD^+-dependent malic enzyme) and TME ($NADP^+$-dependent malic enzyme), specific activity is shown as nanomoles of pyruvate formed/minute/mg protein; for MDH (malate dehydrogenase) specific activity is shown as nanomoles of NADH formed/minute/mg protein. *sth*$^+$: pTH2638 carrying Pneo::*pa2991*::*gusA* (Pneo: promoter from Tn5; *pa2991*: *sth* gene from *P. aeruginosa*; and *gusA*: gene encoding β–glucuronidase reporter enzyme) (Figure 28 & Figure 29). pTH1582: parent plasmid. ND: not determined. Values are means ± standard error for triplicate samples

In contrast, STH activity was almost undetectable in strains such as Rm1021, RmG455, RmH897, RmP2312, RmP2314, and RmP2333 (2 to 6 nmol/minute /mg), which did not carry the *pa2991* gene from *P. aeruginosa* (Table 15). Thus the *pa2991* gene (*P. aeruginosa*) appeared to be highly-expressed and its protein product was functional in *S. meliloti*.

DME, TME, and MDH activities were measured in *S. meliloti* strains with the over-expressed STH protein. TME and MDH activities were not significantly different from those detected in *S. meliloti* strains without STH activity (Table 15). However, DME activity was found to be lower in a *S. meliloti* wild-type strain with the over-expressed STH, RmP2334 (55 ± 4 nmol/minute /mg), than in *S. meliloti* wild-type strains without STH activity, Rm1021 and Rm2333 (84 ± 3 and 79 ± 5 nmol/minute /mg) (Table 15). Strains in which STH was overproduced appeared to grow more slowly than those without STH activity and to quantify this difference, the OD_{600} of *S. meliloti* strains carrying plasmid pTH1582 (without STH activity) or pTH2638 (over-expressed STH) growing in LBmc liquid medium was monitored every two hours (Figure 30). The growth rate for strains with the over-expressed STH (RmP2313, RmP2315, and RmP2334) was lower than that for strains without STH activity (RmP2312, RmP2314, and RmP2333).

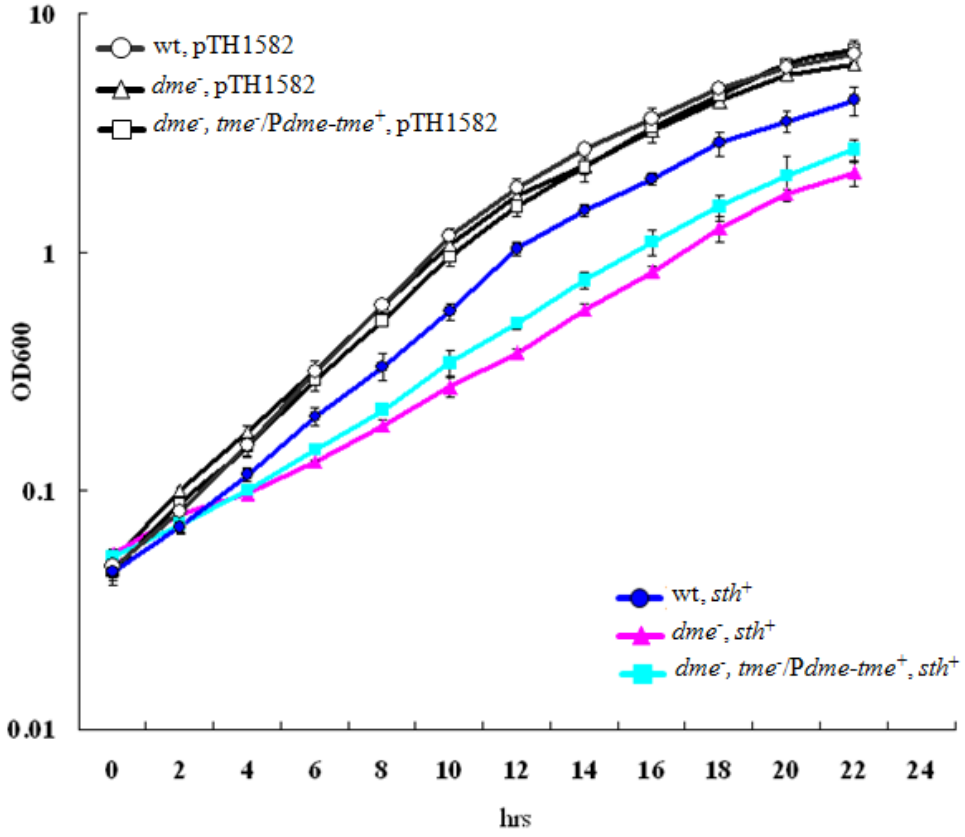

Figure 30 Growth of *S. meliloti* strains with the over-produced STH grown in LBmc

S. meliloti strains with the over-produced STH (sth^+) are marked by closed symbols. *S. meliloti* strains without STH activity (carrying pTH1582) are marked by opened symbols. Circle, wt; triangle, dme^-; and square, dme^-&tme^-/P*dme-tme*$^+$. Strains: RmP2312 (*dme-3*::Tn5, pTH1582), RmP2313 (*dme-3*::Tn5, sth^+), RmP2314 (*dme-3*::Tn5, *tme-4*:: Ω Sp^r, P*dme-tme*$^+$, pTH1582), RmP2315 (*dme-3*::Tn5, *tme-4*:: Ω Sp^r, P*dme-tme*$^+$, sth^+), RmP2333 (wt, pTH1582), and RmP2334 (wt, sth^+). sth^+: pTH2638 carrying Pneo::*pa2991*::*gusA* (Pneo: promoter from Tn5; *pa2991*: *sth* gene from *P. aeruginosa*; and *gusA*: gene encoding β–glucuronidase reporter enzyme) (Figure 28 & Figure 29). pTH1582: parent plasmid. STH: soluble pyridine nucleotide transhydrogenase. wt: wild type. Values are means for triplicate samples ± standard errors.

5.3.3 Symbiotic Phenotype of *S. meliloti* Strains with the Over-expressed STH.

The symbiotic phenotype of *S. meliloti* strains with the over-expressed STH were determined on alfalfa plants grown in plant nutrient solution without added nitrogen. N_2-fixation was assessed by measuring the plant dry weights and root-nodule acetylene-reducing (nitrogenase) activities 5-weeks after inoculation. The plants inoculated with the *dme* mutant strains with the over-expressed STH protein (RmP2313 and RmP2315) were stunted, chlorotic, and indistinguishable in appearance from the uninoculated controls (Figure 31A & B) and failed to fix N_2 (Fix^-) (Table 16). Thus over-expression of STH was not sufficient to allow TME to restore N_2-fixation to *S. meliloti dme* mutants. Moreover, we observed that the over-expression of *sth* in wild-type *S. meliloti* (RmP2334) resulted in a ~ 40% reduction in symbiotic N_2-fixation (Figure 31C, Table 16).

5.3.4 Intracellular Pyridine Nucleotide Levels

To determine whether the ratio of NADPH/$NADP^+$ in *S. meliloti* bacteroids was lowered upon over-expression of STH, the intracellular concentrations of NAD(H) and NDAP(H) in *S. meliloti* free-living cells and bacteroids were measured using reverse-phase HPLC (Materials and Methods, Chapter 2). Nucleotide extracts were prepared as alkaline extracts using the procedure of Sanchez *et al* (2006).

Figure 31 Effect of over-expression of the *sth* gene on symbiotic N_2-fixation by *S. meliloti* in alfalfa-root-nodules

Photographs were taken at 35 Days after inoculation, at which time the uninoculated plants displayed clear symptoms of nitrogen deficiency (yellowing of leaves and stunted growth). Eight seedlings per pot were planted in Leonard assemblies with Jensens medium (nitrogen free) and watered with sterile ddH_2O as required. Plants were incubated at 20ºC with a 18-hour light and 6-hour dark cycle. Stains: Rm102 (wt), RmG455 (*dme-3*::Tn5), RmH897 (*dme-3*::Tn*5, tme-4*:: Ω Sp^r, P*dme-tme*$^+$), RmP2312 (*dme-3*::Tn5, pTH1582), RmP2313 (*dme-3*::Tn5, *sth*$^+$), RmP2314 (*dme-3*::Tn*5, tme-4*:: Ω Sp^r, P*dme-tme*$^+$, pTH1582), RmP2315 (*dme-3*::Tn*5, tme-4*:: Ω Sp^r, P*dme-tme*$^+$, *sth*$^+$), RmP2333 (wt, pTH1582), and RmP2334 (wt, *sth*$^+$). *sth*$^+$: pTH2638 carrying Pneo::*pa2991*::*gusA* (Pneo: promoter from Tn5; *pa2991*: *sth* gene from *P. aeruginosa*; and *gusA*: gene encoding β–glucuronidase reporter enzyme) (Figure 28 & Figure 29). pTH1582: parent plasmid. Uni.: uninoculated control. wt: wild type.

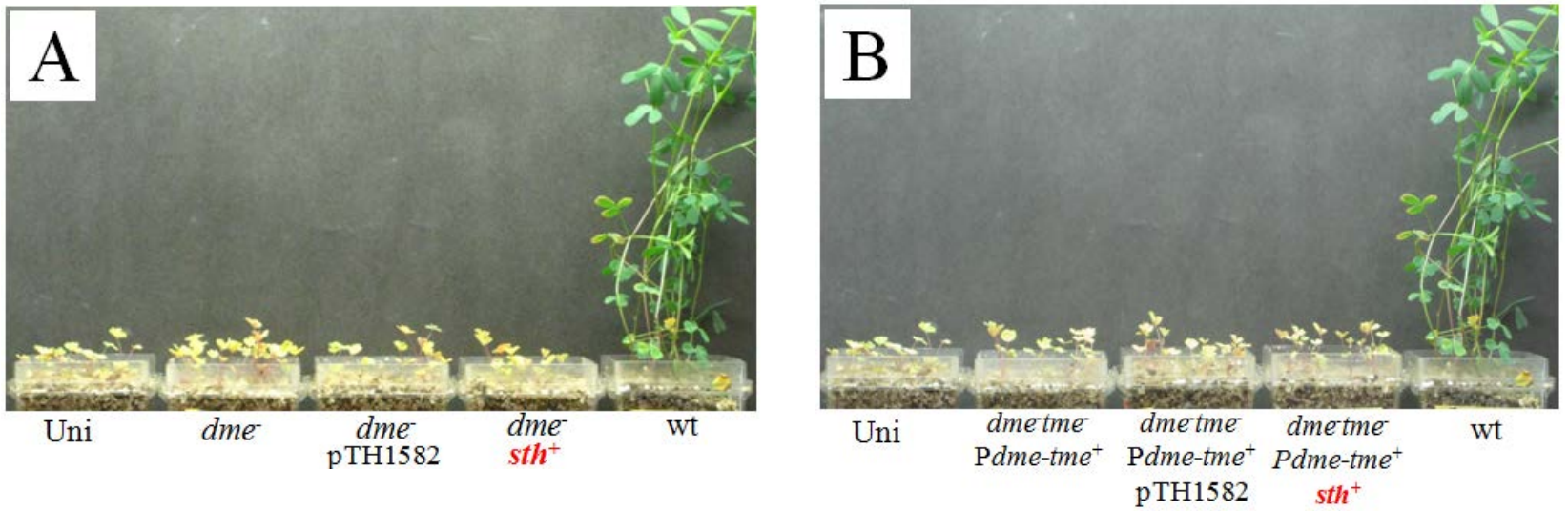
A
Uni
dme-
dme-
pTH1582
dme-
sth+
wt
B
Uni
dme-tme-
Pdme-tme+
dme-tme-
Pdme-tme+
pTH1582
dme-tme-
Pdme-tme+
sth+
wt
C
Uni
wt
sth+
wt
pTH1582
wt

Table 16 Symbiotic phenotypes of *S. meliloti* strains with the over-expressed STH

Strains	Genotype	Shoot dry weight per plant (mg)	Fix%[a]	AR activity[b] (per plant)	Fix%[c]
Uninoculated control	-	5.6 ± 1.1	-	0	-
Rm1021	*S. meliloti* wild type	64.4 ± 5.1	100%	1.3 ± 0.1	100%
RmG455	*S. meliloti dme-3*::Tn5	7.7 ± 0.6	3.6%	0	0
RmH897	*S. meliloti dme-3*::Tn*5*, *tme-4*:: Ω Sp^r, *Pdme-tme*$^+$	8.2 ± 1.7	4.4%	0	0
RmP2312	*S. meliloti dme-3*::Tn5, pTH1582	6.7 ± 1.2	1.9%	0	0
RmP2313	*S. meliloti dme-3*::Tn5, *sth*$^+$	9 ± 1	5.8%	0	0
RmP2314	*S. meliloti dme-3*::Tn*5*, *tme-4*:: Ω Sp^r, P*dme-tme*$^+$, pTH1582	7.6 ±1.5	3.4%	0	0
RmP2315	*S. meliloti dme-3*::Tn*5*, *tme-4*:: Ω Sp^r, P*dme-tme*$^+$, *sth*$^+$	8.5 ± 0.6	4.9%	0	0
RmP2333	*S. meliloti* wild type, pTH1582	68 ± 4.8	106%	1.36 ± 0.06	104.6%
RmP2334	*S. meliloti* wild type, *sth*$^+$	41.4 ± 4.7	60.9%	0.97 ± 0.06	74.6%

[a] Calculated by shoot dry weight per plant: (test-uninoculated)/(wild type-uninoculated). [b] Nitrogenase activity assayed by acetylene reduction activity (μmol C_2H_4 produced/hour/plant). [c] Calculated as the amount of acetylene reduced per plant: test/wild type. Each sample consisted of 8 plants. Values are means for triplicate samples ± standard errors. *sth*$^+$: pTH2638 carrying Pneo::*pa2991*::*gusA* (Pneo: promoter from Tn5; *pa2991*: *sth* gene from *P. aeruginosa*; and *gusA*: gene encoding β–glucuronidase reporter enzyme) (Figure 28 & Figure 29). STH: soluble pyridine nucleotide transhydrogenase.

The separation of various nucleotides in the alkaline extracts is shown in HPLC profiles (Figure 32), profiles for free-living cells were not included). The peaks of ATP, NAD^+, NADH, $NADP^+$, and NADPH were identified by their retention times (Figure 7) and coelution with added standards (80μM of each compound) (Figure 32C). The concentrations of the pyridine nucleotides (Materials and Methods, Chapter 2) and the ratios of NADH/NAD^+ and NADPH/$NADP^+$ were determined as shown in Table 17. In free-living cells, ratios of NADPH/$NADP^+$ and NADH/NAD^+ were significantly higher in *S. meliloti* strains with the over-expressed STH (5.59-6.4 and 0.99-1.26, respectively) than *in S. meliloti* strains without STH activity (2.88-3.38 and 0.6-0.66, respectively). In bacteroids, the ratio of NADH/NAD^+ showed a remarkable increase in *S. meliloti* wild type with the overexpressed STH, RmP2334 (2.99) compared with *S. meliloti* wild-type strains without STH activity, Rm1021 (1.9) and RmP2333 (1.82). The ratio of NADPH/$NADP^+$ in *S. meliloti* wild type with the overexpressed STH, RmP2334 (1.53 ± 0.15) was not significantly different from that in *S. meliloti* wild-type strains without STH activity, Rm1021 (1.35 ± 0.06) and RmP2333 (1.39 ± 0.04). Thus, the data suggested that *P. aeruginosa* STH activity increased the ratio of NADH/NAD^+ but failed to decrease the ratio of NADPH/$NADP^+$ in *S. meliloti* free-living cells and bacteroids from alfalfa root nodules.

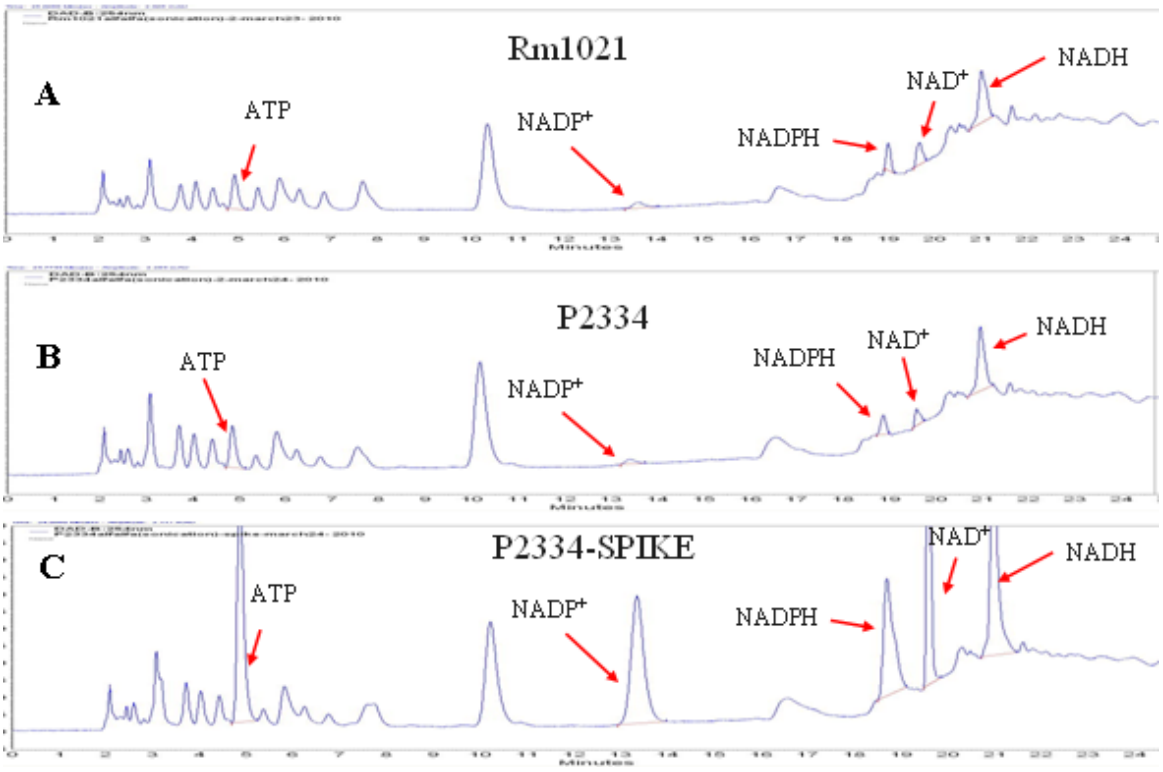

Figure 32 HPLC chromatogram of nucleotide extracts from *S. meliloti* alfalfa bacteroids

(A) nucleotides from Rm1021 bacteroids. (B) nucleotides from RmP2334 bacteroids. (C) nucleotides from RmP2334 bacteroids spiked by a standard mixture of ATP, NAD^+, NADH, $NADP^+$, and NADPH (80µM of each compound). Strains: Rm1021 (wt) and RmP2334 (wt, sth^+). wt: wild type. sth^+: pTH2638 carrying Pneo::*pa2991*::*gusA* (Pneo: promoter from Tn5; *pa2991*: *sth* gene from *P. aeruginosa*; and *gusA*: gene encoding β–glucuronidase reporter enzyme) (Figure 28 & Figure 29). Chromatographic conditions were as in Figure 7.

Table 17 The ratios of NADH/NAD$^+$ and NADPH/NADP$^+$ in *S. meliloti* free-living cells and bacteroids from alfalfa

	Strains	Genotypes	Ratios	
			NADPH/NADP$^+$	NADH/NAD$^+$
Free-living cells (LBmc)	Rm1021	*S. meliloti* wild type	3.1 ± 0.1	0.6 ± 0.03
	RmG455	*S. meliloti dme-3*::Tn5	2.96 ± 0.25	0.61 ± 0.02
	RmH897	*S. meliloti dme-3*::Tn*5*, *tme-4*:: Ω Sp^r, *pdme-tme*$^+$	3.28 ± 0.18	0.59± 0.05
	RmP2312	*S. meliloti dme-3*::Tn5, pTH1582	3.38 ± 0.22	0.66 ± 0.04
	RmP2313	*S. meliloti dme-3*::Tn5, *sth*$^+$	5.79 ± 0.66	1.24 ± 0.13
	RmP2314	*S. meliloti dme-3*::Tn*5*, *tme-4*:: Ω Sp^r, P*dme-tme*$^+$, pTH1582	2.93 ± 0.18	0.65 ± 0.04
	RmP2315	*S. meliloti dme-3*::Tn*5*, *tme-4*:: Ω Sp^r, P*dme-tme*$^+$, *sth*$^+$	5.59 ± 0.56	1.26 ± 0.11
	RmP2333	*S. meliloti* wild type, pTH1582	2.88 ± 0.07	0.64 ± 0.04
	RmP2334	*S. meliloti* wild type, *sth*$^+$	6.4 ± 0.28	0.99 ± 0.09
Bacteroids (alfalfa)	Rm1021	wild type	1.35 ± 0.06	1.9 ± 0.13
	RmP2333	*S. meliloti* wild type, pTH1582	1.39 ± 0.04	1.82 ± 0.12
	RmP2334	*S. meliloti* wild type, *sth*$^+$	1.53 ± 0.15	2.99 ± 0.07

Total nucleotide extracts were prepared from free-living cells grown in LBmc or bacteroids isolated from 5-week alfalfa nodules as alkaline extracts (Materials and Methods, Chapter 2). The concentration of NAD(P)$^+$ and NAD(P)H (mM) was calculated with the equation: (Area of peak * 10^{-4})/(slope of standard curve * Vol of injection in µl). Values are means for triplicate samples ± standard errors. *sth*$^+$: pTH2638 carrying Pneo::*pa2991*::*gusA* (Pneo: promoter from Tn5; *pa2991*: *sth* gene from *P. aeruginosa*; and *gusA*: gene encoding β–glucuronidase reporter enzyme) (Figure 28 & Figure 29)

5.4 Discussion

Previous work in this laboratory showed expression of the TME protein failed to functionally replace the requirement of DME for *S. meliloti* symbiotic nitrogen fixation. One possible explanation for this is that the ratio of NADPH/$NADP^+$ in bacteroids is high enough to prevent TME from functioning in nodules i.e. a high NADPH/$NADP^+$ ratio would not allow the reaction $NADP^+$ + Malate → NADPH + Pyruvate + CO_2. We therefore sought to lower the ratio of NADPH/$NADP^+$ in bacteroids by overexpressing a soluble pyridine nucleotide transhydrogenase (STH), which catalyzes the transfer of reducing equivalents from NADPH to NADH. However, STH activity in bacteroids failed to rescue the symbiotic N_2-fixation deficiency of *S. meliloti dme* mutants.

It was well known that $NADP^+$ acts as co-enzyme in cellular electron transfer reactions. Perhaps, the most important role of $NADP^+$ is to maintain the cellular NADPH pool (Pollak *et al*. 2007). Its reduced form, NADPH, mainly plays a role as the universal electron donor in reductive biosynthesis such as synthesis of fatty acid and the reduction of ribonucleotides to deoxyribonucleotides (Nakamura *et al*. 2012). Moreover, NADPH, which acts as the unique provider of reducing equivalents, is essential for cellular detoxification and is important for the cellular antioxidative defense systems to counteract oxidative damage caused by reactive oxygen species (ROS) such as oxygen ions and peroxides (Agledal *et al*. 2010). To maintain sufficient reducing equivalents, the NADP pool is normally kept in the reduced state using various $NADP^+$-dependent enzymes such as glucose-6-phosphate dehydrogenase (G6PD), isocitrate dehydrogenase (IDP), malic enzyme (TME), and aldehyde dehydrogenase (ALDH) (Marchler-Bauer *et al*. 2011).

Among them, glucose-6-phosphate dehydrogenase (G6PD), catalyzing the first and rate-limiting step of the pentose phosphate pathway, is constitutively expressed in most organisms and considered as the major source of NADPH generation (Pollak *et al*. 2007).

In this study, HPLC data (Table 17) showed that *P. aeruginosa* STH activity did increase the ratio of $NADH/NAD^+$ in *S. meliloti*, which suggested that the STH functioned well and the NADH pool received reducing equivalents from NADPH. However, it failed to lower the ratio of $NADPH/NADP^+$. One possible explanation for this maybe that *P. aeruginosa* STH activity is not sufficient to overcome the formation of NADPH via $NADP^+$- dependent enzymes in *S. meliloti*. Moreover, a ~ 40% reduction in symbiotic N_2-fixation was observed in wild-type *S. meliloti* with the over-expressed *sth* (Figure 31C, Table 16). We assumed that activities of some NAD^+- dependent TCA cycle enzymes such as DME and MDH might be inhibited by the increased ratio of $NADH/NAD^+$ in *S. meliloti* with the over-produced STH (Table 17), which may lead to the loss of energy and reducing power required for symbiotic nitrogen fixation. This result appears to be consistent with the lower growth rate of *S. meliloti* with the over-expressed STH (Figure 30).

In view of the failure of soluble pyridine nucleotide transhydrogenase (STH) to lower the ratio of $NADPH/NADP^+$ in *S. meliloti* bacteroids, one recent report regarding modification of the cofactor specificities of the human malic enzymes is worth noting. Mammals contain three malic enzyme isoforms: the cytosolic and mitochondrial $NADP^+$-malic enzymes (EC 1.1.1.40) are strictly $NADP^+$ dependent (Loeber *et al*. 1994a; Loeber *et al*. 1994b), and mitochondrial $NAD(P)^+$-dependent malic enzyme (EC 1.1.1.39) is

NAD^+ dependent, but generally shows some activity with $NADP^+$ (Loeber *et al*. 1991; Sauer *et al*. 1980). The conserved residue 362 in mammalian malic enzymes, Gln (Q) for $NAD(P)^+$-dependent malic enzyme and Lys (K) for $NADP^+$-dependent malic enzyme, was identified as the decisive factor which determined the cofactor specificity of human malic enzymes (Hsieh and Hung 2009). Furthermore, a human $NAD(P)^+$-dependent malic enzyme mutant carrying triple amino acid substitutions K346S, Y347K, and Q362K was reported to switch its cofactor specificity from NAD^+ to $NADP^+$, and became a $NADP^+$ specific malic enzyme (Hsieh and Hung 2009). The substitution of resides responsible for determining the cofactor specificity of the *S. meliloti* malic enzymes might be able to shift the cofactor specificity of TME and turn it into a NAD^+-dependent malic enzyme. This would make it possible to investigate whether the failure of TME to support symbiotic nitrogen fixation in *S. meliloti dme* mutants is due to a high ratio of $NADPH/NADP^+$ in bacteroids.

To search for the residues which are critical for the cofactor specificity of *S. meliloti* malic enzymes, we conducted a multiple sequence alignment of 15 malic enzyme proteins from 8 related strains belonging to proteobacteria (*S. meliloti, S. medicae, Sinorhizobium sp. NGR234, R. leguminosarum, R. etli, M. loti, Agrobacterium radiobacter,* and *E.coli).* The multiple sequence alignment (Figure 33) revealed that the cofactor binding domain (approximately 200 amino acids) following the N-terminal malic enzyme domain, was not conserved between $NAD(P)^+$- and $NADP^+$- dependent malic enzymes. Within the cofactor binding region, six amino acid residues at the positions (based on the sequence of *S. meliloti* TME protein) 283(Met/Leu), 316 (Ile/Met), 324

(Tyr/Phe), 344 (Val/Cys), 373 (Val/Ala), and 389 (Ile/Leu) were found to have the distribution tightly related with the cofactor specificity of malic enzymes. It suggested that these might be the residues responsible for determining the cofactor preference of the malic enzymes.

Figure 33 Sequence alignment of the cofactor binding region for *S. meliloti* malic enzymes

Alignments of 15 malic enzymes with amino acid sequences of the cofactor binding regions are shown from residues 276 to 391. The NCBI reference sequences used for alignments are as follows: *S. meliloti* DME (AAB82459.1), *S. meliloti* TME (NP_384500.1), *S. medicae* DME (YP_001327235.1), *S. medicae* TME (YP_001325724.1), *Sinorhizobium sp.* NGR234 DME (YP_002826206.1), *Sinorhizobium sp.* NGR234 TME (YP_002824587.1), *R. leguminosarum* DME (YP_002281503.1), *R. leguminosarum* TME (YP_002279562.1), *R. etli* DME (YP_001978584.1), *R. etli* TME (YP_001976602.1), *M. loti* DME (NP_102533.1) , *M. loti* TME (NP_106015.1), *Agrobacterium radiobacter* DME (P_002544735.1), *A. radiobacter* TME (YP_002543208.1) and *E.coli* TME (NP_311352.1). Alignments were created using DNAMAN 6.0 program.

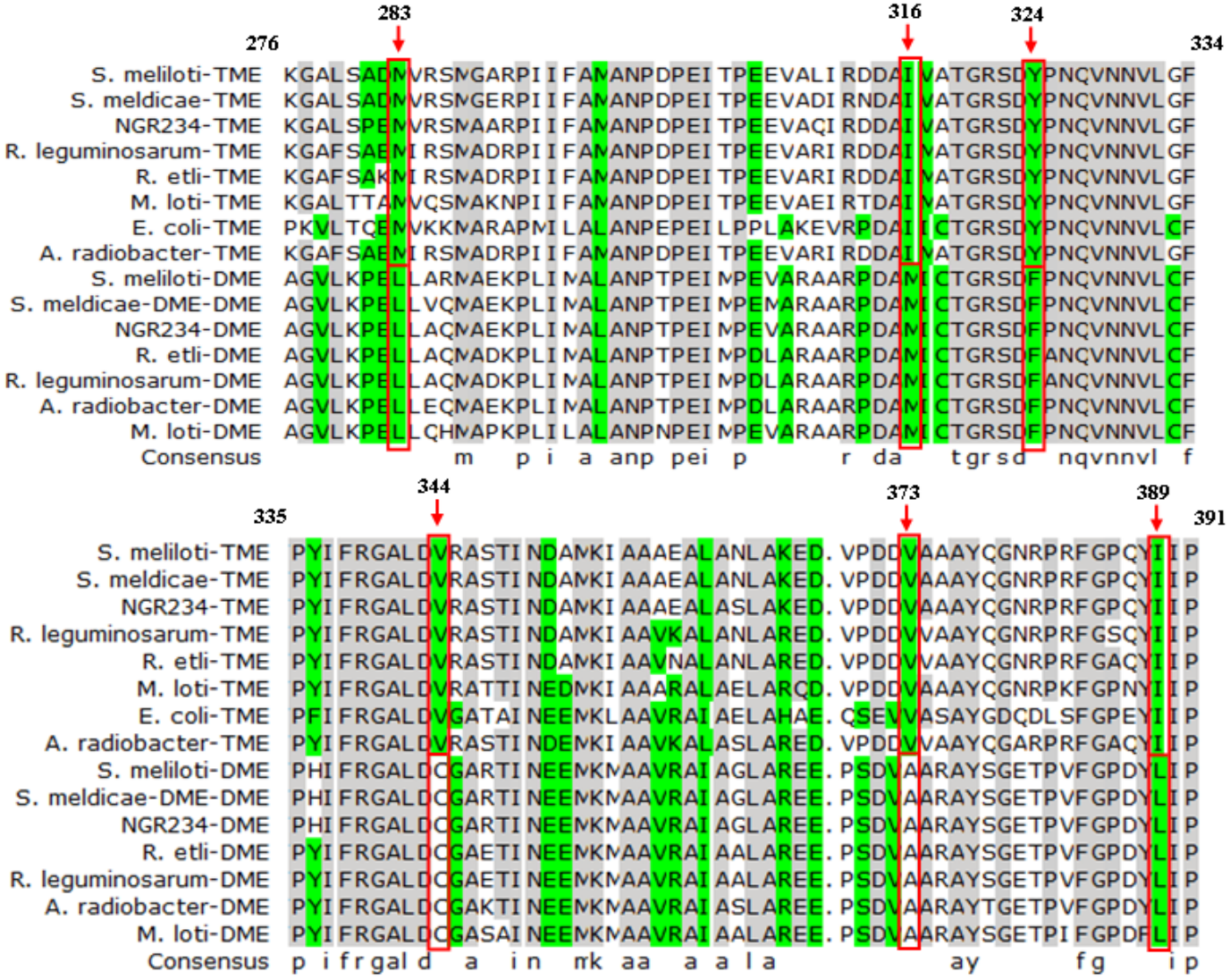
276
283
316
324
334
S. meliloti-TME KGALSADMVRSMGARPIIFAMANPDPEITPEEVALIRDDAIMATGRSDYPNQVNNVLGF
S. meldicae-TME KGALSADMVRSMGERPIIFAMANPDPEITPEEVADIRNDAIMATGRSDYPNQVNNVLGF
NGR234-TME KGALSPEMVRSMAARPIIFAMANPDPEITPEEVAQIRDDAIMATGRSDYPNQVNNVLGF
R. leguminosarum-TME KGAFSAEMIRSMADRPIIFAMANPDPEITPEEVARIRDDAIMATGRSDYPNQVNNVLGF
R. etli-TME KGAFSAKMIRSMADRPIIFAMANPDPEITPEEVARIRDDAIMATGRSDYPNQVNNVLGF
M. loti-TME KGALTTAMVQSMAKNPIIFAMANPDPEITPEEVAEIRTDAIMATGRSDYPNQVNNVLGF
E. coli-TME PKVLTQEMVKKMARAPMILALANPEPEILPPLAKEVRPDAIICTGRSDYPNQVNNVLCF
A. radiobacter-TME KGAFSAEMIRSMADRPIIFAMANPDPEITPEEVARIRDDAIMATGRSDYPNQVNNVLGF
S. meliloti-DME AGVLKPELLARMAEKPLIMALANPTPEIMPEVARAARPDAMICTGRSDFPNQVNNVLCF
S. meldicae-DME-DME AGVLKPELLVQMAEKPLIMALANPTPEIMPEMARAARPDAMICTGRSDFPNQVNNVLCF
NGR234-DME AGVLKPELLAQMAEKPLIMALANPTPEIMPEVARAARPDAMICTGRSDFPNQVNNVLCF
R. etli-DME AGVLKPELLAQMADKPLIMALANPTPEIMPDLARAARPDAMICTGRSDFANQVNNVLCF
R. leguminosarum-DME AGVLKPELLAQMADKPLIMALANPTPEIMPDLARAARPDAMICTGRSDFANQVNNVLCF
A. radiobacter-DME AGVLKPELLEQMAEKPLIMALANPTPEIMPDLARAARPDAMICTGRSDFPNQVNNVLCF
M. loti-DME AGVLKPELLQHMAPKPLILALANPNPEIMPEVARAARPDAMICTGRSDFPNQVNNVLCF
Consensus m p i a anp pei p r da tgrsd nqvnnvl f
335
344
373
389
391
S. meliloti-TME PYIFRGALDVRASTINDAMKIAAAEALANLAKED.VPDDVAAAYQGNRPRFGPQYIIP
S. meldicae-TME PYIFRGALDVRASTINDAMKIAAAEALANLAKED.VPDDVAAAYQGNRPRFGPQYIIP
NGR234-TME PYIFRGALDVRASTINDAMKIAAAEALASLAKED.VPDDVAAAYQGNRPRFGPQYIIP
R. leguminosarum-TME PYIFRGALDVRASTINDAMKIAAVKALANLARED.VPDDVVAAYQGNRPRFGSQYIIP
R. etli-TME PYIFRGALDVRASTINDAMKIAAVNALANLARED.VPDDVVAAYQGNRPRFGAQYIIP
M. loti-TME PYIFRGALDVRATTINEDMKIAAARALAELARQD.VPDDVAAAYQGNRPKFGPNYIIP
E. coli-TME PFIFRGALDVGATAINEEMKLAAVRAIAELAHAE.QSEVVASAYGDQDLSFGPEYIIP
A. radiobacter-TME PYIFRGALDVRASTINDEMKIAAVKALASLARED.VPDDVVAAYQGARPRFGAQYIIP
S. meliloti-DME PHIFRGALDCGARTINEEMKMAAVRAIAGLAREE.PSDVAARAYSGETPVFGPDYLIP
S. meldicae-DME-DME PHIFRGALDCGARTINEEMKMAAVRAIAGLAREE.PSDVAARAYSGETPVFGPDYLIP
NGR234-DME PHIFRGALDCGARTINEEMKMAAVRAIAGLAREE.PSDVAARAYSGETPVFGPDYLIP
R. etli-DME PYIFRGALDCGAETINEEMKMAAVRAIAALAREE.PSDVAARAYSGETPVFGPDYLIP
R. leguminosarum-DME PYIFRGALDCGAETINEEMKMAAVRAIAALAREE.PSDVAARAYSGETPVFGPDYLIP
A. radiobacter-DME PYIFRGALDCGAKTINEEMKMAAVRAIASLAREE.PSDVAARAYTGETPVFGPDYLIP
M. loti-DME PYIFRGALDCGASAINEEMKMAAVRAIAALAREE.PSDVAARAYSGETPIFGPDFLIP
Consensus p ifrgald a in mk aa a a l a ay fg ip

Chapter 6 Microarray analysis of *S. meliloti* single *dme* and single *tme* mutants grown in minimal medium with glucose or succinate

6.1 Introduction

Malic enzymes belong to a family of divalent metal ion (Mg^{2+}) dependent oxidative decarboxylases, that catalyzes the conversion of L-malate to pyruvate coupled with the reduction of NAD^+ or $NADP^+$ (Wedding 1989). *S. meliloti* has two distinct malic enzymes, $NAD(P)^+$ -dependent malic enzyme (DME) and $NADP^+$-dependent malic enzyme (TME) (Voegele *et al*. 1999). Previous studies in our laboratory found that DME activity is essential for symbiotic nitrogen fixation in *S. meliloti* whereas TME activity is not (Driscoll and Finan 1996;Driscoll and Finan 1997) and the reason for this difference has not been clearly defined. The different growth rate of *S. meliloti* single *dme* and single *tme* mutants in M9 minimal medium with glucose and succinate, demonstrated by Smallbone (2006), reflected the different roles played by DME and TME in carbon metabolism. DME and TME were found to share similar apparent K_m and V_{max} values for substrate and cofactors, however, it was noted that DME activity was allosterically stimulated by succinate and fumarate and inhibited by acetyl-CoA, and TME activity was not allosterically regulated by TCA cycle intermediates (Voegele *et al*. 1999). It suggested that DME activity might be important for regulating the levels of TCA cycle intermediates.

Previous studies conducted by Smallbone (2006) showed differences in the polar metabolite profiles from *S. meliloti dme* and *tme* mutants grown in M9-succinate media. This suggested that the physiological role of DME in *S. meliloti* might be the regulation of the metabolic flux through the TCA cycle during C_4-dicarboxylate oxidation by converting malate to pyruvate and then to acetyl-CoA. To further investigate the physiological functions of DME and TME, we conducted a genome-wide microarray analysis of gene expression in *S. meliloti* wild type, *dme* and *tme* mutants grown in medium containing glucose or succinate as a carbon source. The gene expression differences observed in *S. meliloti dme* mutants grown on succinate hinted that a disturbance in the central carbon metabolism was caused by the *dme* mutation. This suggested that DME activity is important for the maintenance of metabolic flux through TCA cycle during C_4-dicarboxylate oxidation. However, changes of gene expression found in *tme* mutants were so limited that it was impossible to predict the physiological functions of TME protein in central carbon metabolism.

6.2 Materials and Methods

Bacterial strains, plasmids and primers used in this work are listed in Table 3 and Table 4. Primers were from Sigma-Aldrich or Integrated DNA Technologies. Methods other than those outlined below are summarized in Chapter 2 of this thesis.

6.2.1 Construction of *S. meliloti* single *dme* and single *tme* Mutants with Insertion of ΩSp^r Cassette

S. meliloti tme mutant, RmP2179 (RmP110, *tme*::Ω Sp^r) was constructed by transducing Sp^r from RmG994 (Rm1021, *dme-3*::Tn*5* *tme-4*:: Ω Sp^r) to the wild type

RmP110. The structure of the *tme* mutation in RmP2179 (RmP110, *tme*::Ω Sp^r) was verified by restriction analysis following PCR amplification of the *tme* region by use of primers Tme-Sm-F2v (bp267 at *tme*) and Tme-Sm-R2v (bp 967 at *tme*). Western Blot analysis also confirmed the absence of the TME protein in RmP2179 (data not show).

The *S. meliloti dme* mutant strain was constructed by introducing the ΩSp^r/Sm^r cassette (Blondelet-Rouault *et al*. 1997) into the *dme* gene as outlined in Material and Methods (Chapter 2). Plasmid pTH2576 was constructed by inserting the *S. meliloti dme* gene region from positions -534 to 1019 (amplified using the primers DME-Sm-F1 and DME-Sm-R2) into the Gm^r plasmid pJQ200-mp18 (Figure 10) via *SacI* and *Pst*I. Plasmid pTH2578, carrying a 2-kb ΩSp^r Sm^r cassette inserted at the *SmaI* site at position bp 161 relative to the ATG *dme* start codon (the *dme*::ΩSp^r Sm^r allele), was transferred from *E. coli* to the wild type *S. meliloti* strain RmP110. The transconjugants, RmP2189 (RmP110, *dme*::Ω Sp^r), were identified as Sm^r Sp^r Gm^s colonies growing with 5% sucrose. The structure of the *dme* mutation in RmP2189 was verified by restriction analysis following PCR amplification of the *dme* region by use of primers from outside the region employed for mutant construction, DME-Sm-F6v (bp -842 upstream) and DME-Sm-R6v (bp 1069). Western Blot analysis also confirmed the absence of the DME protein in RmP2189 (data not show).

6.2.2 Construction of Reporter Gene Fusion Strains

To construct promoter fusions to the reporter genes (*gfp-lacZ* and *gusA-tdimer2*), a 0.5-1 kb DNA fragment carrying the promoter region plus part of the target gene open reading frame (ORF) was PCR amplified and then cloned into the BglII-NsiI sites in

reporter plasmid pTH1703 (Figure 34). The resulting plasmids were transferred from *E. coli* into *S. meliloti* RmP110, RmP2189 (*dme*), and RmP2179 (*tme*). Transconjugants obtained via single-crossover homologous recombination of reporter plasmids into the *S. meliloti* genome were identified as Sm^r and Gm^r colonies. Resultant strains carried the fusion of target promoter region to *gfp-lacZ* or *gusA-tdimer2* and preserved a functional copy of the promoter and all genes at this locus (Figure 35).

6.2.3 *S. meliloti* DNA Microarray

Bacteria were grown in 250 ml of minimal medium up to an optical density at 600 nm of 0.4 – 0.7 (log phase). Cells were harvested by centrifugation and total RNAs were extracted. A total of 12 RNA samples were prepared from three *S. meliloti* strains, RmP110 (wild type), RmP2179 (*tme*::Ω Sp^r), and RmP2189 (*dme*::Ω Sp^r), grown in two different minimal media (MOPS-P2 plus 15 mM glucose and MOPS-P2 plus 15 mM succinate) in duplicate. Microarray chips used in this study were purchased from NimbleGen Systems Inc., Madison, WI. Each microarray carried 385,298 24-mer oligonucleotide probes representative of the 6269 predicted open reading frame (ORF) of *S. meliloti* 1021 (mostly protein coding genes).Synthesis of cDNAs, end-labeling, hybridization, and probe intensity analysis were performed by NimbleGen, following company procedures.

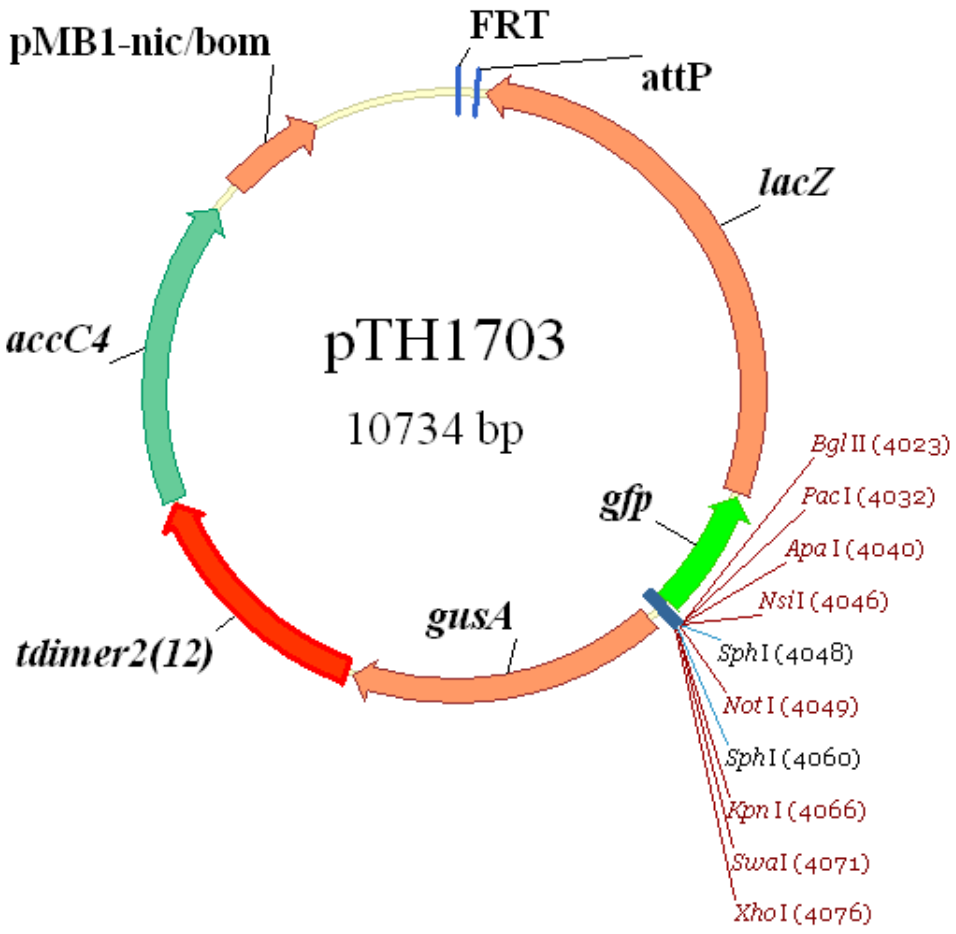

Figure 34 Schematic vector map of reporter plasmid pTH1703

Plasmid pTH1703 (Cowie *et al*. 2006), with reporter genes *gfp*+, *lacZ*, *gusA*, and *tdimer2(12)* shown as divergent operons from the multiple cloning site. Also indicated is the position of the FRT site, *attP* site and gentamicin resistance gene (*accC4*) and the locations of stop codons either side of the cloning site to prevent translational read-through.

Figure 35 Schematic illustrating the strategy to construct reporter gene fusion strains

(1) Reporter plasmid carrying a 0.5-1 kb DNA fragment which contains the whole promoter region (red) and part of the first gene (red) in the operon. (2) Region of *S. meliloti* genome carrying target gene and it promoter. (3) Single –crossover homologous recombination between reporter plasmid and *S. meliloti* genome formed the fusion of promoter region (red) to reporter genes and a functional copy of the promoter (black) and all genes at this locus in the fusion strains.

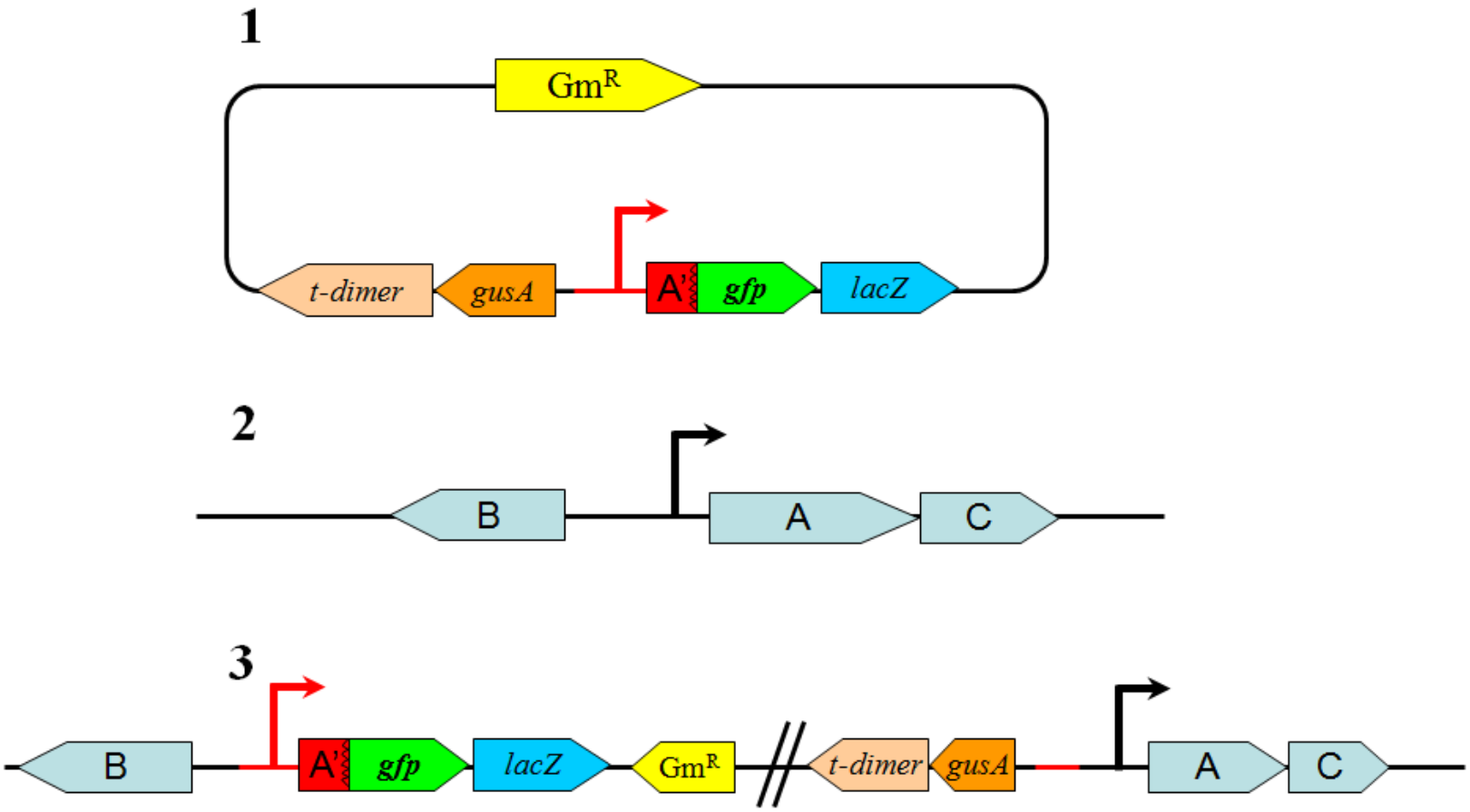
1
Gm^R
t-dimer
gusA
A'
gfp
lacZ
2
B
A
C
3
B
A'
gfp
lacZ
Gm^R
t-dimer
gusA
A
C

Signal intensities in the raw data were quantile normalized across all experimental replicates with help of Dr. Dick Morton. For each experiment, the median intensity of all probes within the predicted open reading frame (ORF) was used as an uncorrected measure of gene expression. Background expression was estimated for each experiment by simulating a gene through 10,000 random samples drawn from the normalized intensities of a null probe set of randomly generated sequences.

Normalized data were then processed using Microsoft Excel. Genes were considered differentially expressed if FC $\geq$ 3 [fold change: the ratio of treatment to control]. The difference in gene expression was considered to be significant if the *P* value from a Student's *t* test was $\leq$ 0.05.

6.3 Results

In the current study, genome-wide transcriptional analysis of *S. meliloti* 1021 was conducted in the free-living cells of the wild-type strain, *dme*, and *tme* mutants grown in MOPS-buffered minimal media supplemented with 15 mM succinate or15 mM glucose. Two replicates were applied in all six different conditions. These samples will hereafter be referred to as WS (wild-type strain RmP110 grown in MOP-P2-succinate), WG (wild-type strain RmP110 grown in MOP-P2-glucose), DS (*dme* mutant RmP2189 grown in MOP-P2-succinate), DG (*dme* mutant RmP2189 grown in MOP-P2-glucose), TS (*tme* mutant RmP2189 grown in MOP-P2-succinate), and TG (*tme* mutant RmP2189 grown in MOPS-P2-glucose). To monitor gene expression across the genome, the custom-made arrays (NimbleGen) that carries 385,298 24-mer oligonucleotide probes, representing 6,269 annotated *S. meliloti* features was used. Microarray data were processed and

normalized as described in Methods (6.2.3). We evaluated the variation of expression of genes by using the fold change (FC) and the *P*-value from a Student's *t* test. Gene expression was considered to be significantly different only if the fold change (FC) was great than or equal to 3 and the *P*-value was less than or equal to 0.05.

6.3.1 Global Expression Patterns

In order to gain an overview of the largest source of similarities and differences among the transcriptional profiles from twelve *S. meliloti* cultures, two complementary methods, principal component analysis (PCA) and hierarchical clustering, were performed to analyze global gene expression patterns using all probe sets present on the arrays. The result of PCA is shown in Figure 36. This yielded a model that two main axes of principal components PC1 and PC2 explained 36.3% and 26.1% of the total variability respectively. The two replicates for each condition grouped closely to each other, indicating that both replicates shared highly similar expression patterns and microarray data for all six different conditions were repeatable. As expected, PC1 (abscissa) separated the wild-type strain RmP110 from the *dme* and *tme* mutants (RmP2189 and RmP2179). The PC2 (ordinate), on the other hand, separated *S. meliloti* cultures grown with glucose from those grown with succinate as carbon source. This indicated that the deletion of *dme* or *tme* genes and the different carbon sources in minimal media resulted in differential expression of many genes in *S. meliloti* genome. The *S. meliloti dme* and *tme* mutants grown in minimal media supplemented with glucose grouped tightly together and therefore their transcriptional profiles were very much alike. This suggests that the

effect of *dme* or *tme* mutations on the expression patterns of *S meliloti* are similar when cultures were grown in minimal medium with glucose as sole carbon.

The result of hierarchical clustering of transcriptional profiles from 12 *S. meliloti* cultures was shown in Figure 37. It was entirely consistent with the conclusions of principal component analysis. The two replicates of each condition were paired together with a high similarity over 95%. The dendrogram revealed that all 12 samples divided into two major groups, sharing 62% similarity. One group consists of cultures grown with glucose (WG, DG, and TG), while the other group contains cultures grown with succinate (WS, DS, and TS). In both groups, expression patterns of *S. meliloti* wild-type strain (WS or WG) are further separated from those of *dme* and *tme* mutants (DS&TS or DG&TG). The *dme* and *tme* mutants grown with succinate (DS and TS) are further divided into two different subgroups, sharing 86% similarity, while expression patterns corresponding to *dme* and *tme* mutants grown with glucose (DG and TG) are highly similar (> 95%) and belong to the same subgroup.

6.3.2 Gene Expression Validation

To assess the overall validity of our microarray data, we first compared transcriptional profiles of *S. meliloti* cultures grown in glucose and succinate. In total the expression levels of 101 genes were found as significantly modulated (Fold change (FC) ≥ 3 and $P \leq 0.05$) in the wild type RmP110. 64 genes were up-regulated in response to glucose and 47 genes were up-regulated in response to succinate (Table 18).

Figure 36 Principal component analysis of transcriptional profiles from *S. meliloti* cultures grown in minimal media

PCA scores of transcriptional profiles from 12 *S. meliloti* cultures were projected on two main axes, PC1 vs. PC2. PC1 accounted for 36.3% of total variation in the dataset, whereas PC2 captured another 26.1% of the variance present in the dataset. Sample labels include the type of strain (W, wild type RmP110; D, *dme* mutant RmP2189; and T, *tme* mutant RmP2179) and the carbon source supplied to MOPS-P2 medium (S, succinate and G, glucose). For example, WS was wild type RmP110 grown in minimal medium MOPS-P2 supplemented with succinate. Labels marked with 1 or 2 indicate replicate samples for each condition.

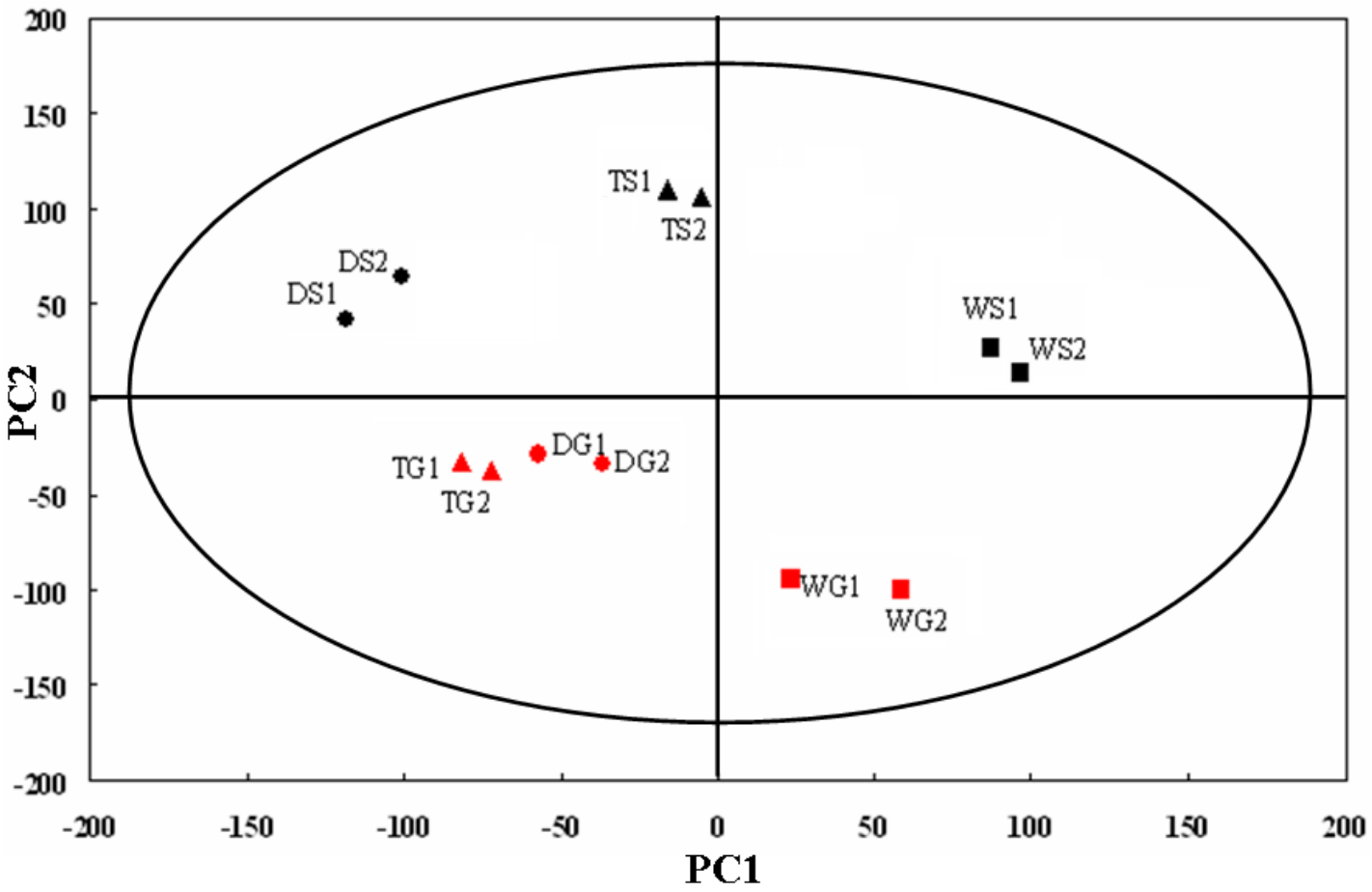
200
150
100
50
0
-50
-100
-150
-200
PC2
-200
-150
-100
-50
0
50
100
150
200
PC1
TS1
TS2
DS2
DS1
WS1
WS2
TG1
TG2
DG1
DG2
WG1
WG2

Figure 37 Hierarchical cluster analysis of transcriptional profiles from *S. meliloti* cultures grown in minimal media

Transcriptional profiles of 12 *S. meliloti* cultures were clustered using Mintab14 with Ward Linkage and Absolute Correlation Distance. Sample labels at the branch termini include the type of strains (W, wild type RmP110; D, *dme* mutant RmP2189; and T, *tme* mutant RmP2179) and the carbon source supplied to MOPS-P2 medium (S, succinate and G, glucose). For example, WS was wild type RmP110 grown in minimal medium MOPS-P2 supplemented with succinate. Labels marked with 1 or 2 indicate replicate samples for each condition.

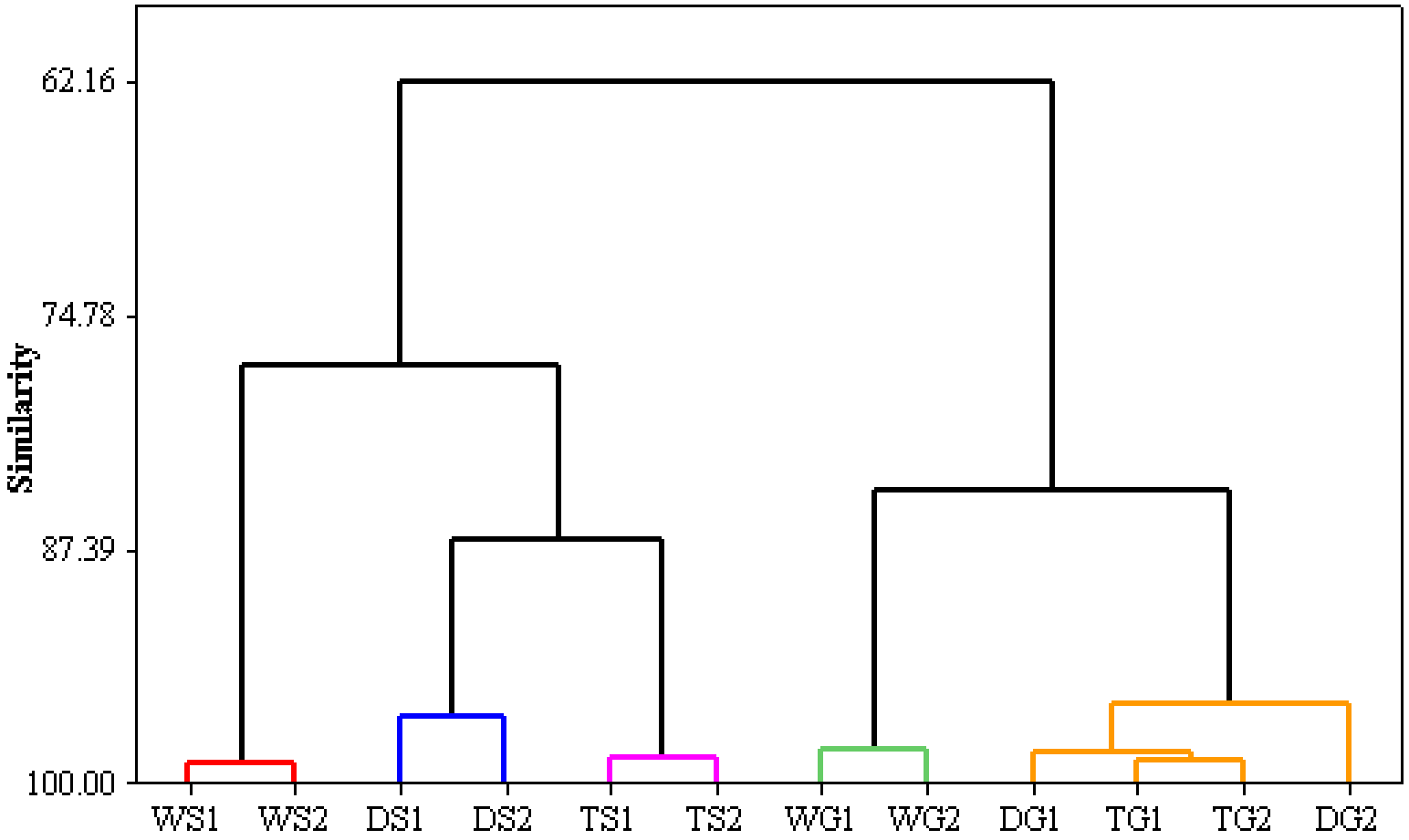
Similarity
62.16
74.78
87.39
100.00
WS1
WS2
DS1
DS2
TS1
TS2
WG1
WG2
DG1
TG1
TG2
DG2

As shown in Table 20, the most highly up-regulated gene found in succinate-grown cells of *S. meliloti* wild type RmP110 compared with glucose-grown cells was *dctA* (SM_b 20611) (98-fold), which encodes the C_4-dicarboxylate transport protein, responsible for succinate uptake. The next most highly up-regulated genes were *pckA* (SMc02560), encoding phosphoenolpyruvate carboxykinase (18-fold), and *fbaB* (SMc03983), encoding fructose-bisphosphate aldolase (7.8-fold). Both PckA and FbaB are the gluconeogenic enzymes and essential for the synthesis of hexose sugars when TCA cycle intermediates such as succinate, fumarate, and malate are supplied as sole carbon source (Figure 38). The expression levels of these three genes also showed strong upregulation in succinate-grown cells of the *dme* and *tme* mutants (Table 20). These results were entirely consistent with previous studies showing the failure of *dctA* and *pckA* mutants to grow on succinate and highly increased PckA activity in succinate-grown cells (Finan *et al*. 1988), and the elevated expression of these genes were reported previously for succinate-grown cultures of *S. meliloti* (Barnett *et al*. 2004; Smallbone, L.A., 2006, M.Sc thesis) and *R. leguminosarum* (Karunakaran *et al*. 2009).

As expected, genes encoding components of putative sugar ABC transport systems were found to be highly induced by growth on glucose (Table 20). The most highly up-regulated of all the genes was a set of three genes adjacent to each other on pSymB: SM_b20902 (30-fold), SM_b20903 (28-fold), and SM_b20904 (12-fold), which encode a sugar uptake ABC transport system. Three genes were also found to be strongly up-regulated in glucose-grown cells of the *dme* and *tme* mutants (Table 20).

Table 18 Overview of differential expression patterns based on gene functional categories

Gene category	No. of genes significantly regulated [a] (increased/decreased)				
	glucose vs succinate (wt) [b]	*dme* vs wt (succinate) [c]	*tme* vs wt (succinate) [d]	*dme* vs wt (glucose) [e]	*dme* vs wt (glucose) [f]
Amino acid metabolism	3/0	17/0	4/0	3/2	2/0
Cofactor and vitamin metabolism	3/0	12/0	1/0	0/0	0/0
Fatty acid, ester, and phospholipid metabolism	1/1	4/0	2/0	0/0	1/0
Carbohydrate metabolism	13/3	15/0	2/0	0/0	0/0
Purine, pyrimidine, and nucleotide metabolism	0/1	1/0	3/0	1/0	1/1
Regulatory function	7/0	3/0	2/3	3/1	1/1
DNA replication and repair	1/1	4/0	1/1	0/0	0/1
Transport system	16/5	55/0	9/0	3/5	3/5
Energy metabolism	2/2	17/0	8/0	0/3	2/3
Other categories	4/3	7/3	3/2	2/2	5/0
Hypothetical protein	14/31	47/16	21/8	11/4	12/8
Total (6269)	64/47	182/19	56/14	23/17	27/19

[a] Genes found as significantly regulated have a fold change of ≥ 3 and a *P*-value (Student's *t* test) of ≤ 0.05. [b] Comparing *S. meliloti* wild type grown in glucose and succinate. [c] Comparing *dme* mutant and wild type grown in succinate. [d] Comparing *tme* mutant and wild type grown in succinate. [e] Comparing *dme* mutant and wild type grown in glucose. [f] Comparing *tme* mutant and wild type grown in glucose.

Figure 38 Schematic diagram illustrating genes involved in *S. meliloti* gluconeogenesis

Genes that were upregulated in *S. meliloti* wild type grown on succinate compared with glucose are colored in red and the numbers in green are the fold change of the indicated genes. Metabolic enzymes encoded by the listed genes: *cbbA*(SM_b20199)/*cbbA2* (SM_b21192)/*fbaB*(SMc03983), fructose-1,6-bisphosphate aldolase; *cbbF*(SM_b20202), fructose-1,6-bisphosphatase; *eno*(SMc01028), phosphopyruvate hydratase; *gap*(SMc03979), glyceraldehyde-3-phosphate dehydrogenase; *gpmA*(SMc02838)/*gpmB* (SMc00006)/SMa0527, phosphoglyceromutase; *manB*(SM_b21081)/*pgm*(SMc03925), phosphoglucomutase; *pckA*(SMc02562), phosphoenolpyruvate carboxykinase; *pgi*(SMc02163)/*pgiA1*(SMc02042)/*pgiA2*(SM_b20857), glucose-6-phosphate isomerase; *pgk*(SMc03981), phosphoglycerate kinase; and *tpiA*(SMc01023)/*tpiB*(SMc01614), triosephosphate isomerase.

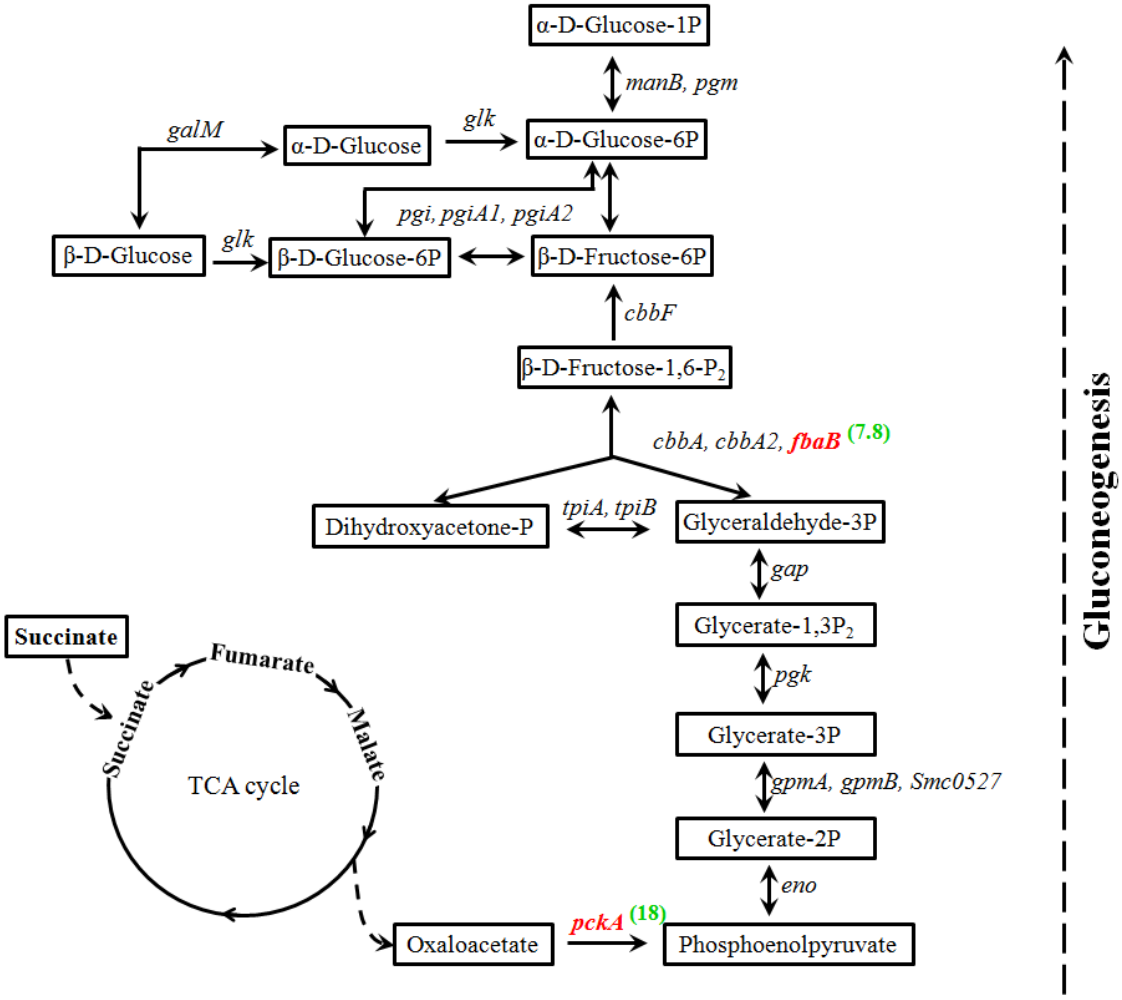
α-D-Glucose-1P
manB, pgm
galM
α-D-Glucose
glk
α-D-Glucose-6P
pgi, pgiA1, pgiA2
β-D-Glucose
glk
β-D-Glucose-6P
β-D-Fructose-6P
cbbF
β-D-Fructose-1,6-P2
cbbA, cbbA2, fbaB (7.8)
Dihydroxyacetone-P
tpiA, tpiB
Glyceraldehyde-3P
gap
Glycerate-1,3P2
pgk
Glycerate-3P
gpmA, gpmB, Smc0527
Glycerate-2P
eno
Phosphoenolpyruvate
pckA (18)
Oxaloacetate
Succinate
Fumarate
Malate
Succinate
TCA cycle
Gluconeogenesis

Similarly, genes related to the Entner-Doudoroff (ED) pathway were highly induced in wild type cells (Figure 39 and Table 20). These genes were *eda1*(SMc02043)/*eda2* (SMc03153), encoding 2-dehydro-3-deoxy-phosphogluconate aldolase (up to 5.7-fold); *glk* (SMc02835), encoding glucokinase (2-fold); *edd* (SMc03068), encoding phosphogluconate dehydratase (4.8-fold); *pgl* (SMc03069), encoding 6-phosphogluconolactonase (4.4-fold); *zwf* (SMc03070), encoding glucose-6-phosphate 1-dehydrogenase (5.5-fold); *pdhABC* (SMc01030 to SMc01032), encoding pyruvate dehydrogenase (~3-fold); and *pykA* (SMc04005), encoding pyruvate kinase (4.1-fold). Except for *glk* and *eda1*, the expression levels of these genes also showed strong upregulation in glucose-grown cells of the *dme* and *tme* mutants (Table 20). These results were entirely consistent with previous studies showing that rhizobia metabolize glucose through the Entner-Doudoroff (ED) pathway (Finan *et al.* 1988), and the elevated expression of these genes were reported previously for glucose-grown cultures of *S. meliloti* (Barnett *et al*. 2004; Smallbone, L.A., 2006, M.Sc thesis) and *R. leguminosarum* (Karunakaran *et al*. 2009).

The microarray results were validated using transcriptional gene fusions where the first gene in a putative operon was fused to the *gusA* or *gfp* reporter genes. Fifteen genes, belonging to nine operons were examined in wild type, *dme*, and *tme* mutants (see Methods 6.2.2). All *S. meliloti* fusion strains were grown in MOP-P2 minimal media with glucose or succinate as the sole carbon source and GusA specific activity or GFP relative fluorescence were measured as described in Methods (2.19).

Figure 39 Schematic diagram illustrating genes involved in *S. meliloti* Entner-Doudoroff pathway

Genes that were upregulated in *S. meliloti* wild type grown on glucose compared with succinate are colored in red and the numbers in green are the fold change (FC) of the indicated genes. Only genes with FC ≥ 3 were listed in Table 20. Metabolic enzymes encoded by the listed genes: *eda*(SMc02043)/*eda2*(SMc03153), 2-dehydro-3-deoxyphosphogluconate aldolase; *edd*(SMc03068), phosphogluconate dehydratase; *eno*(SMc01028), phosphopyruvate hydratase; *galM*(SMc03798), aldose 1-epimerase; *gap*(SMc03979), glyceraldehyde-3-phosphate dehydrogenase; *glk*(SMc02835), glucokinase; *gpmA*(SMc02838)/*gpmB*(SMc00006)/Sma0527, phosphoglyceromutase; *manB*(SM_b21081)/*pgm*(SMc03925), phosphoglucomutase; *pdhABC*(SMc01030 to SMc01032), pyruvate dehydrogenase; *pgi*(SMc02163)/*pgiA1*(SMc02042)/*pgiA2* (SM_b20857), glucose-6-phosphate isomerase; *pgk*(SMc03981), phosphoglycerate kinase; *pgl*(SMc03069), 6-phosphogluconolactonase; *pykA*(SMc04005): pyruvate kinase; and *zwf* (SMc03070), glucose-6-phosphate 1-dehydrogenase.

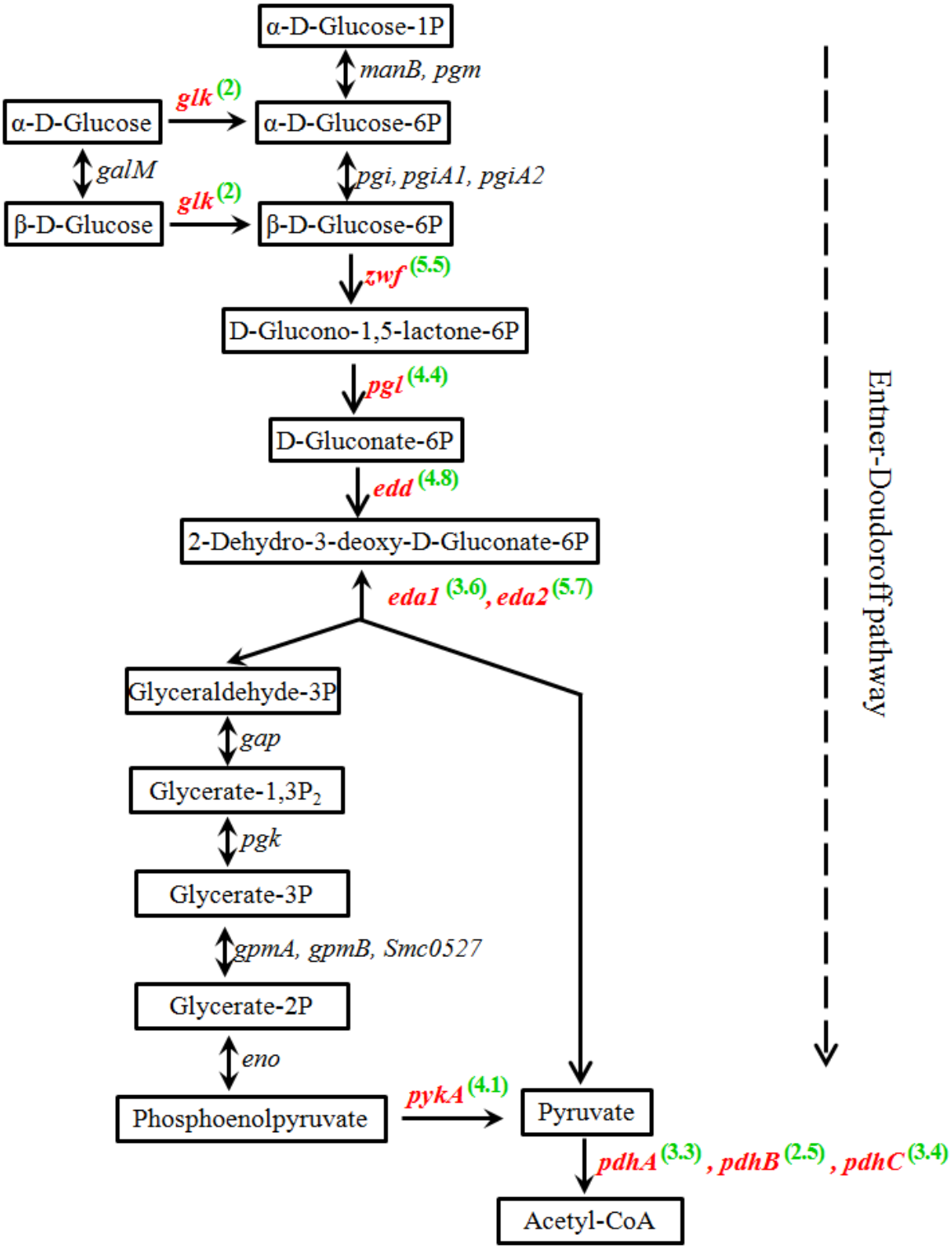
α-D-Glucose-1P
manB, pgm
α-D-Glucose
glk (2)
α-D-Glucose-6P
galM
pgi, pgiA1, pgiA2
β-D-Glucose
glk (2)
β-D-Glucose-6P
zwf (5.5)
D-Glucono-1,5-lactone-6P
pgl (4.4)
D-Gluconate-6P
edd (4.8)
2-Dehydro-3-deoxy-D-Gluconate-6P
eda1 (3.6), eda2 (5.7)
Glyceraldehyde-3P
gap
Glycerate-1,3P2
pgk
Glycerate-3P
gpmA, gpmB, Smc0527
Glycerate-2P
eno
Phosphoenolpyruvate
pykA (4.1)
Pyruvate
pdhA (3.3), pdhB (2.5), pdhC (3.4)
Acetyl-CoA
Entner-Doudoroff pathway

In general, the results of reporter gene fusions showed very close agreement with those of microarrays (Table 19). However, several differences were observed; for example, the relative expression of Sm_b20206, Sm_b20282, and Sm_b21441 in succinate-grown *tme* mutant and Sm_b20418 in glucose-grown *tme* mutant was up-regulated in microarray (3-, 2.1-, 1.8-, and 2.3-fold respectively) but was almost no change in the equivalent report gene fusion experiment.

6.3.3 Gene Expression Patterns in *S. meliloti dme* Mutant Grown on Succinate Compared with the Wild Type

To gain insights to the role of DME in succinate metabolism we compared expression of the wild type vs the *dme* mutant in succinate grown cells (Table 21). With succinate as the carbon source, the expression of 182 genes higher and 19 genes lower in the *dme* mutant vs the wild type (fold change $\geq$ 3 and *P*-value $\leq$ 0.05). Of the 19 genes that are $\geq$ 3-fold downregulated (Table 21), only 3 genes are found in operons of 2 or more genes, 16 genes encode hypothetical proteins whose functions are not known, and the rest include two genes encoding ribosomal proteins (SMc00323: *rpsO* and SMc01369: *rpmG*) and one gene encoding putative methyl viologen/ethidium resistance transmembrane protein (SMc01523: *emrE*).

Table 19 The relative expression levels of selected genes under different conditions determined by microarray and transcriptional fusion reporter

Expression levels of selected genes were determined for *S. meliloti* wild type, *dme*, and *tme* mutants grown in MOPS-buffered minimal media supplemented with 15 mM succinate or15 mM glucose using transcriptional reporter gene fusions, and each reaction was made in triplicate. Values marked by * were significant at $P \leq 0.05$, calculated using Student's *t* test. FC, fold change. -, changes in gene expression between two conditions were not statistical significance ($P > 0.05$). N.D., not detected. [a] *gfp* or *gusA* fusion to the first gene in a putative operon which is in boldface. [b] Comparing *S. meliloti* wild type grown in glucose and succinate. [c] Comparing *dme* mutant and wild type grown in succinate. [d] Comparing *tme* mutant and wild type grown in succinate. [e] Comparing *dme* mutant and wild type grown in glucose. [f] Comparing *tme* mutant and wild type grown in glucose.

Fusion strains	Gene ID	Glucose/Succinate (wt) [b]		*dme*/wt (succinate) [c]		*tme*/wt (succinate) [d]		*dme*/wt (glucose) [e]		*tme*/wt (glucose) [f]	
		Microarray FC	Fusion FC	Microarray FC	Fusion FC	Microarray FC	Fusion FC	Microarray FC	Fusion FC	Microarray FC	Fusion FC
SmFL5233 (*gfp*) [a]	**SMc02047**	-	N.D.	-	N.D.	3.8*	2.2*	-	N.D.	-	N.D.
SmFL4290 (*gfp*) [a]	**SM_b20171**	-	N.D.	12.5*	4.7*	3.8*	1.9*	-	N.D.	-	N.D.
	SM_b20172	-		10.4*		3.1*		-		-	
RmP2473 (*gusA*) [a]	**SM_b20173**	-	N.D.	41.9*	6.3*	9.8*	2.5*	-	N.D.	-	N.D.
SmFL6081 (*gusA*) [a]	**SM_b20174**	-	N.D.	16.5*	5.3*	4.4*	2.0*	-	N.D.	-	N.D.
	SM_b20175	-		17.8*		6.6*		-		-	
SmFL673 (*gusA*) [a]	**SM_b20204**	-	N.D.	3.2*	2.4*	-	0.9	-	N.D.	-	N.D.
	SM_b20205	-		5.0*		-		-		-	
	SM_b20206	-		4.7*		3.0*		-		-	
	SM_b20207	-		3.8*		-		-		-	
	SM_b20208	-		4.9*		-		-		-	
RmP2479 (*gusA*) [a]	**SM_b20280**	-	N.D.	3.4*	2.2*	-	N.D.	1.6*	1.0	1.6*	1.1
SmFL1445 (*gusA*) [a]	**SM_b20282**	2.6*	2.2*	3.0*	2.8*	2.1*	1.2	-	N.D.	-	N.D.
SmFL1913 (*gfp*) [a]	**SM_b20481**	-	N.D.	4.0*	2.2*	-	N.D.	-	N.D.	2.3*	1.1
SmFL1896 (*gusA*) [a]	**SM_b21441**	0.3*	0.3*	-	N.D.	1.8*	1.1	3.6*	2.1*	3.2*	2.6*

Among the 182 genes that are ≥ 3-fold upregulated in succinate-grown *dme* mutant strain grown on succinate, 109 genes are found in putative operons containing two or more genes. Most of these genes that are ≥ 3-fold upregulated in the *dme* mutant strain grown on succinate belong to different functional categories as following (Table 18 and Table 21).

A. 47 genes (~26%) encode hypothetical proteins and their functions are not known. Of these, 14 genes were ≥ fivefold upregulated (Table 21). They are SMc00769 (6-fold), SMc01036 (5-fold), SMc00706 (7-fold), SMa1294 (5-fold), SMa2361 (5-fold), **SM_b20165** (6-fold), **SM_b20166** (5-fold), **SM_b20169** (5-fold), **SM_b20175** (18-fold), **SM_b20177** (7-fold), **SM_b20179** (5-fold), SM_b20385 (6-fold), SM_b21226 (5-fold), and SM_b21182 (11-fold). Six of these, with Gene ID shown in boldface, are adjacent to a strongly upregulated gene cluster (SM_b20171 to SM _b20174) which is involved in methanol metabolism according to the KEGG PATHWAY Database (Figure 40) (http://www.genome.jp/kegg/pathway.html).

B. 55 genes (~30%) are involved in transport. They mainly relate to uptake and utilization of spermidine/putrescine (9 genes), peptides/oligopeptids (7 genes), amino acids (11 genes), simple/multiple sugars ABC (12 genes), iron (3 genes), and dicarboxylates (2 gene). Of these, 18 genes were ≥ fivefold upregulated (Table 21). They are SMa0070, encoding simple sugar permease protein (28-fold); SM_b20036, encoding periplasmic quinic acid-binding protein (8-fold); SMc04396, encoding periplasmic multiple sugar-binding protein (5-fold); SMc03131, encoding periplasmic polar amino acid-binding protein (14-fold); *ehuC* (SM_b20429), encoding polar amino acid permease protein (9-

fold); SMa1650, encoding peptide/nickel permease protein (8-fold); SM_b20383, encoding periplasmic spermidine/putrescine-binding protein (7-fold); SMa0396, SMa0800, and SM_b21275 encoding spermidine/putrescine permease proteins (6-, 5-, and 5-folds respectively); *choW* (SMc02738), encoding glycine betaine/proline permease protein (5-fold); SMc02356, encoding periplasmic branched-chain amino acid-binding protein (6-fold); SM_b20322, encoding hydroxyproline permease protein (6-fold); *hisW* (SMc00671), encoding histidine permease protein (5-fold); SM_b20365, encoding periplasmic iron(III)-binding protein (6-fold); *cbtK* (SM_b20057), encoding cobalt(II) permease protein (9-fold); and two clustered genes: SM_b20373, encoding dicarboxylate permease protein (6-fold), and SM_b20374, encoding periplasmic dicarboxylate-binding protein (5-fold).

C. 17 genes (~10%) are involved in amino acid metabolism. Of these, 4 genes were ≥ fivefold upregulated (Table 21). They are *aspC* (SMc0226; 5-fold), encoding aspartate transaminase which catalyzes the interconversion of aspartate and α-ketoglutarate to oxaloacetate and glutamate; *leuA2* (SMc02546; 5-fold), encoding 2-isopropylmalate synthase which participates in biosynthesis of Val, Leu, and Ile via pyruvate metabolism; *ttuD3* (SMa1406; 15-fold), encoding hydroxypyruvate reductase which participates in Gly, Ser and Thr metabolism and glyoxylate and dicarboxylate metabolism; and *argH2* (SM_b21094), encoding argininosuccinate lyase which catalyzes the reversible breakdown of argininosuccinate (ASA) producing the amino acid Arg and dicarboxylic acid fumarate.

D. 15 genes (~8%) belong to the functional category “carbohydrate metabolism” and are mainly involved in metabolism of various simple sugars (Table 21). Of these, 3 genes were ≥ fivefold upregulated (Table 21). They are SMc02384 (5-fold), encoding glycosyltransferase transmembrane protein which are responsible for the biosynthesis of disaccharides, oligosaccharides and polysaccharides; SMc01992 (6-fold), encoding D-xylulose reductase which participates in pentose and glucuronate interconversions; and *sucD* (SMc02481; 11-fold), encoding succinyl-CoA synthetase, which is a key TCA cycle enzyme catalyzing the reversible reaction of succinyl-CoA to succinate.

E. 17 genes (~10%) are related to energy metabolism and products of these genes mainly consist of dehydrogenases, oxidoreductases, and cytochrome c proteins. As shown in Table 21, six of these genes were ≥ fivefold upregulated. They are SMa1410 (8-fold), encoding oxidoreductase; *gfa* (SM_b20186; 12-fold), encoding glutathione-dependent formaldehyde-activating enzyme; and a gene cluster, SM_b20171 to SM _b20174, encoding S-formylglutathione hydrolase (13-fold), cytochrome c protein (10-fold), methanol dehydrogenase (42-fold), and cytochrome c protein (17-fold). As shown in Figure 40, *gfa* (SM_b20186) and the cluster SM_b20171 to SM _b20174 are involved in methanol metabolism. The upregulated expression of cluster SM_b20171 to SM _b20174 was verified using transcriptional fusion reporter (GusA or GFP) (Table 19)

Figure 40 Schematic diagram illustrating genes involved in *S. meliloti* methonal metabolism

Genes that were upregulated in *S. meliloti dme* mutant grown on succinate compared with the wild type are colored in red and the numbers in green are the fold change (FC) of the indicated genes. Only genes with FC ≥ 3 were listed in Table 21. Metabolic enzymes encoded by the listed genes: *adhC2*(SMa2113)/*fdh*(SM_b20170), S-(hydroxymethyl)glutathione dehydrogenase; *fdhE*(SMa0009), formate dehydrogenase; *gfa*(SM_b20186), S-(hydroxymethyl)glutathione synthase; *katB*(SMa2379), KatB catalase/peroxidase; SM_b20173, methanol dehydrogenase; and SM_b20171/SMc01273, S-formylglutathione hydrolase.

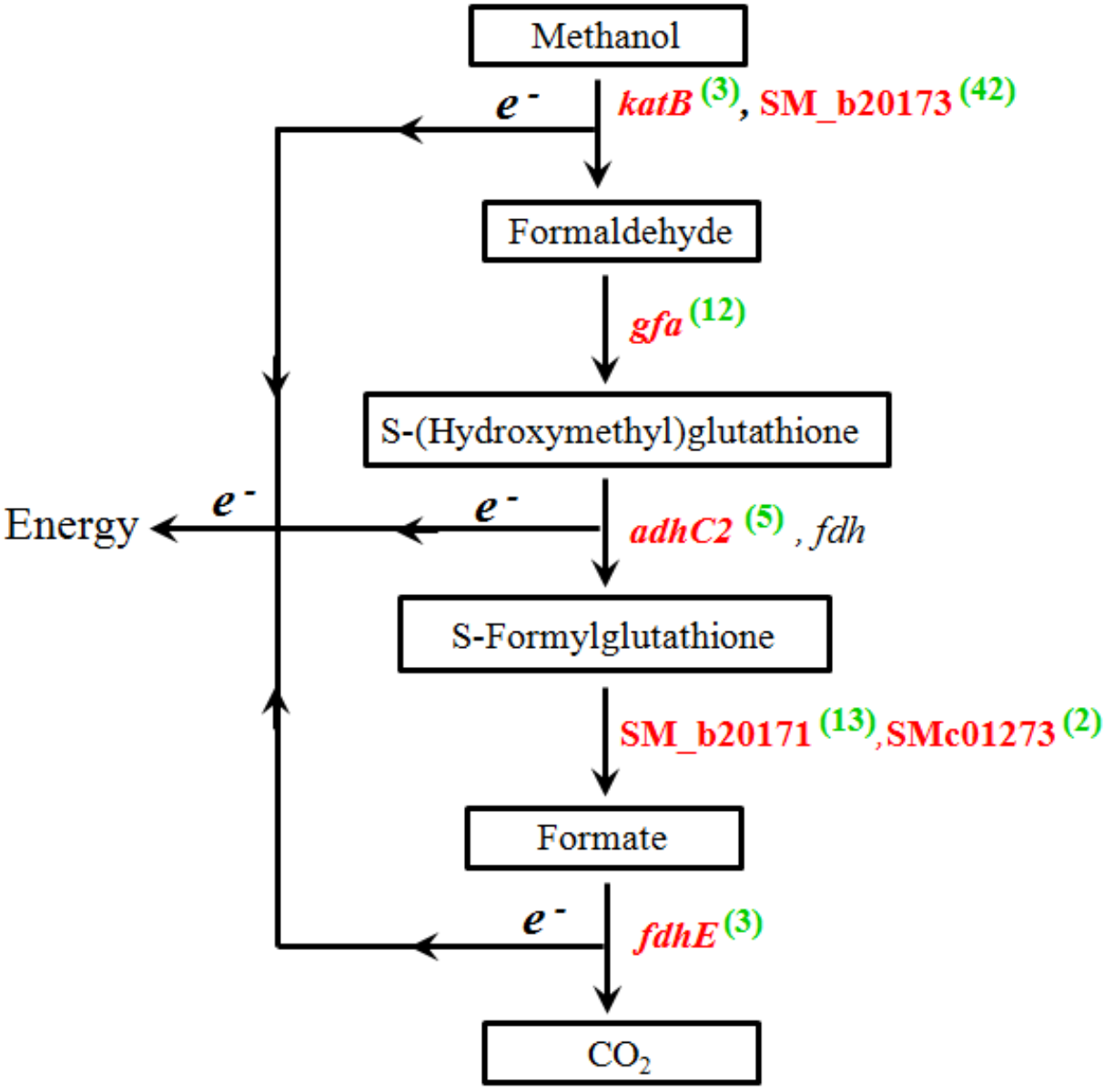
Methanol
e -
katB (3), SM_b20173 (42)
Formaldehyde
gfa (12)
S-(Hydroxymethyl)glutathione
Energy
e -
e -
adhC2 (5) , fdh
S-Formylglutathione
SM_b20171 (13),SMc01273 (2)
Formate
e -
fdhE (3)
CO2

F. 12 genes (~7%) are involved in metabolism of cofactors and vitamins. As showed in Table 21, enzymes encoded by these genes mainly participate in the biosynthesis of cobalamin (*cobU*: SMc04305 and *cob*: SMc04282) (4-fold), thiamine (*thiOG*: SM_b20616 & SM_b20617) (approximately 3 to 4-fold), and pyrroloquinoline quinine (*pqqABCDE*: SM_b20204-SM_b20208) (approximately 3 to 5-fold) and regeneration of $NAD(P)^+$ (*pntAaAbB*: SMc3950 & SMc3938-SMc03939) (approximately 3 to 5-fold).

G. The remaining 19 genes belong to several other functional categories such as metabolism of fatty acid and nucleotide, transcriptional regulation, DNA replication and repair, and so on.

6.3.4 Gene Expression Patterns in *S. meliloti dme* Mutant Grown on Glucose Compared with the Wild Type

To gain insights to the role of DME in glucose metabolism we compared expression of the wildtype vs the *dme* mutant in glucose grown cells (Table 22). With glucose as the carbon source, the expression of 23 genes was higher and 17 genes was lower in the *dme* mutant vs the wild type (fold change ≥ 3 and *P*-value ≤ 0.05). Of the 17 genes that are ≥ 3-fold downregulated, eight genes are found in operons of 2 or more genes. As shown in Table 18 and Table 22, four genes (~24%) encode hypothetical proteins of unknown function and 2 of these were ≥ fivefold downregulated: SMc03107 (17-fold) and SM_b21154 (5-fold). Among the ≥ 3-fold downregulated genes, five genes (~20%) encode transport proteins and three genes (~17%) encode proteins involved in

energy metabolism (Table 18). The downregulated transport proteins include two putative MFS proteins encoded by SMc02372 (4-fold) and SM_b21162 (6-fold), one peptide/nickel ABC transporter permease encoded by SMc02028 (4-fold), one multiple sugar ABC transport substrate-binding protein encoded by SM_b20231 (9-fold), and one simple sugar ABC transport ATP-binding protein encoded by SM_b20622 (5-fold) (Table 22). The downregulated proteins responsible for energy metabolism are listed as follows: two oxidoreductases encoded by SMc02035 (4-fold) and SMa1386 (4-fold) and NAD-dependent formate dehydrogenase encoded by *fdsB* (SMc02525, 4-fold) (Table 22). The remaining 5 genes ≥ 3-fold downregulated encode proteins involved in amino acid metabolism (SM_b20668 & SM_b21633, up to 4-fold), transcriptional regulation (SM_b21079, 6-fold), and plasmid stability (SM_b21509-SM_b21510, up to 8-fold) (Table 22).

Of the 23 genes that are ≥ 3-fold upregulated in the *dme* mutant grown on glucose, 12 genes are found in operons of 2 or more genes. As shown in Table 18, eleven genes (~49%) encode hypothetical proteins of unknown function and 3 of these were ≥ fivefold upregulated: SMc01509 (5-fold), SMa0747 (6-fold), and SM_b20414 (6-fold) (Table 22). Among the ≥ 3-fold upregulated genes, three genes encode transport proteins and three genes encode proteins involved in amino acid metabolism (Table 18). The upregulated transport proteins include one periplasmic simple sugar-binding protein encoded by SMa1427 (5-fold), one multiple sugar ABC transport permease encoded by SMc01626 (4-fold), and one multiple sugar ABC transport ATP-binding protein encoded by SMa0714 (4-fold) (Table 22). The upregulated genes involved in amino acid

metabolism are listed as follows: *hipO1* (SMc00682, 3-fold), encoding hippurate hydrolase which participates in phenylalanine metabolism; *gltB* (SMc04028, 4-fold), encoding glutamate synthase which catalyzes the conversion of 2-oxoglutarate to glutamine; and SMa1711 (4-fold), encoding arginase which is responsible for arginine metabolism (Table 22). The remaining 6 genes ≥ 3-fold upregulated are: SM_b21115, SM_b20467, and SMc04220 (up to 4-fold), encoding proteins responsible for transcriptional regulation; SM_b21441 (4-fold), encoding inosine-5′-monophosphate dehydrogenase which catalyzes the first and rate-limiting step towards the biosynthesis of guanosine triphosphate (GTP) from inosine monophosphate (IMP); *katC* (SM_b20007, 3-fold), encoding catalase which is responsible for decomposition of hydrogen peroxide to water and oxygen; and *ndiA-1* (SM_b20227**,** 4-fold), encoding a nutrient deprivation-induced protein (Table 22).

6.3.5 Gene Expression Patterns in *S. meliloti tme* Mutant Grown on Succinate Compared with Wild Type

To gain insights to the role of TME in succinate metabolism we compared expression of the wildtype vs the *tme* mutant in succinate grown cells (Table 23). With succinate as the carbon source, the expression of 56 genes was higher and 14 genes was lower in the *tme* mutant vs the wild type (fold change ≥ 3 and *P*-value ≤ 0.05). Of the 14 genes that are ≥ 3-fold downregulated, seven genes are found in operons of 2 or more genes. As shown in Table 18, eight genes (~57%) encode hypothetical proteins of unknown function and 6 of these were ≥ fivefold downregulated: SMc00397 (5-fold), SMc01009 (10-fold), SMa5000 (12-fold), SMa1101 (5-fold), SMa1643 (7-fold), and

SM_b20876 (6-fold) (Table 23). The remaining 4 genes ≥ 3-fold downregulated are *helO* (SMc02586, 4-fold) and *mutT* (SMc02448, 6-fold), encoding ATP-dependent helicase and 7,8-dihydro-8-oxoguanine-triphosphatase involved in DNA replication, transcription, and repair; *fliI* (SMc03025, 11-fold), encoding flagellum-specific ATP synthase responsible for cell motility; and *cyaM* (SM_b20257, 10-fold), encoding adenylate cyclase catalyzing the conversion of ATP to cAMP (a regulatory signal) (Table 23).

Among the 56 genes that are ≥ 3-fold upregulated in the *tme* mutant grown on succinate, thirty-four genes are found in operons of 2 or more genes and 29 genes (~52%) are also highly induced (≥ 3-fold) in *dme* mutant grown on succinate (Table 23). Genes, ≥ 3-fold upregulated in both mutant *tme* and *dme* mutant grown on succinate, are labeled by * in this section (6.3.5). As shown in Table 18, twenty-one genes (~38%) encode hypothetical proteins of unknown function and 9 of these were ≥ fivefold upregulated: SMc00559 (6-fold), SMc00569 (27-fold), SMc01508 (8-fold), SMc02515 (7-fold), SMa1394 (5-fold), SMa2269 (9-fold), SM_b20175* (7-fold), SM_b20275 (6-fold), and SM_b21182* (6-fold) (Table 23). Among the ≥ 3-fold upregulated genes, nine genes (~16%) encode transport proteins, eight genes (~14%) encode proteins involved in energy metabolism, and 4 genes (~7%) encode proteins responsible for amino acid metabolism (Table 18). The upregulated transport proteins mainly relate to uptake and utilization of dicarboxylates (SM_b20373*, 6-fold), simple sugars (SMa0070* & SM_b20036*; 11- & 5- fold), peptides (SMa1863*, 3-fold), spermidine/putrescine (SMa0800*, 5-fold), amino acids (SMc03131*, 12-fold), and irons (SMc01658*, 3-fold) (Table 23). The upregulated genes involved in energy metabolism are listed as follows: *cycF* (SMc00045),

SM_b20172*, and SM_b20174* (up to 4-fold), encoding cytochrome C protein; SM_b20100 and SMa0237* (up to 4-fold), encoding dehydrogenase; SM_b20171* (4-fold), encoding S-formylglutathione hydrolase; SM_b20173* (10-fold), encoding methanol dehydrogenase, and SM_b20342* (3-fold), encoding isoquinoline 1-oxidoreductase (Table 23). The upregulated genes involved in amino acid metabolism are listed as follows: *gcvT* (SMc02047, 4-fold), encoding aminomethyltransferase which participates in Gly, Ser, and Thr metabolism; *pheAa* (SMc03858, 3-fold), encoding chorismate mutase responsible for Phe, Tyr, and Trp biosynthesis; *nthA* (SMc01424*, 4-fold), encoding nitrile hydratase involved in Trp metabolism; and *ttuD3* (SMa1406*, 21-fold), encoding hydroxypyruvate reductase which participates in Gly, Ser and Thr metabolism and glyoxylate and dicarboxylate metabolism (Table 23). Other genes ≥ 3-fold upregulated genes mainly participate in simple sugar metabolism (SMc01992* and SMc02874, 5-fold), fatty acid metabolism (SMc01093 and SMc02229*, 3-fold), pyrroloquinoline quinine biosynthesis (*pqqC*; SM_b20206*) (3-fold), purine metabolism (SMa2349*, SMa2351, and SMa2353) (up to 5-fold), transcriptional regulation (SMc01954 and SMa1882*, up to 5-fold), and DNA repair (SM_b20708*, 6-fold) (Table 23).

6.3.6 Gene Expression Patterns in *S. meliloti tme* Mutant Grown on Glucose Compared with Wild Type

To gain insights to the role of TME in glucose metabolism we compared expression of the wildtype vs the *tme* mutant in glucose grown cells (Table 24). With glucose as the carbon source, the expression of 27 genes was higher and 19 genes was

lower in the *tme* mutant vs the wild type (fold change ≥ 3 and *P*-value ≤ 0.05). Of the 19 genes that are ≥ 3-fold downregulated, seven genes are found in operons of 2 or more genes. As shown in Table 18, eight genes (~42%) encode hypothetical proteins of unknown function and 3 of these were ≥ fivefold downregulated: SMc00613 (7-fold), SMa2347 (5-fold), and SM_b20518 (5-fold) (Table 24). Among the ≥ 3-fold downregulated genes, five genes encode transport proteins and 3 genes encode proteins involved in energy metabolism (Table 18). The downregulated transport proteins include one MFS permease protein encoded by SMc02372 (3-fold), one peptide/nickel ABC transporter permease encoded by SMc02028 (3-fold), one molybdenum transport associated protein encoded by SMc03199 (4-fold), one multiple sugar ABC transport permease protein encoded by SMa1339 (4-fold), and one simple sugar ABC transport ATP-binding protein encoded by SM_b20673 (4-fold) (Table 24). The downregulated proteins responsible for energy metabolism are listed as follows: *nuoM2* (SMa1536; 5-fold), encoding NADH-quinone oxidoreductase, SM_b20403 (4-fold), encoding putative oxidoreductase, and SM_b21368 (4-fold), encoding cytochrome c oxidase (Table 24). The remaining 3 genes ≥ 3-fold downregulated are SMc01570 (6-fold), encoding transcriptional regulator; SMc02416 (4-fold), encoding putative guanine deaminase; and SM_b21044 (4-fold), encoding ATP-dependent DNA ligase (Table 24).

Of the 27 genes that are ≥ 3-fold upregulated in the *tme* mutant grown on glucose, ten genes are found in operons of 2 or more genes and 9 genes (~33%) are also highly induced (≥ 3-fold) in *dme* mutant grown on glucose (Table 24). Genes, ≥ 3-fold upregulated in both mutant *tme* and *dme* mutant grown on glucose, are labeled by # in this

section (6.3.6). As shown in Table 18, twelve genes (~45%) encode hypothetical proteins of unknown function and 3 of these were ≥ fivefold upregulated: SM_b20251 (6-fold), SM_b20331 (6-fold), and SMc01509[#] (6-fold) (Table 24). Among the ≥ 3-fold upregulated genes, three genes encode transport proteins, two genes encode proteins involved in energy metabolism, and two genes encode proteins involved in amino acid metabolism (Table 18). The upregulated transport proteins include periplasmic simple sugar-binding protein encoded by SMa1427[#] (5-fold), periplasmic hydroxyproline-binding protein encoded by SM_b20263 (3-fold), and putative permease encoded by SM_b21486 (3-fold) (Table 24). The upregulated genes involved in amino acid metabolism are *hipO1* (SMc00682[#], 4-fold) encoding hippurate hydrolase which participates in phenylalanine metabolism and *gltB* (SMc04028[#], 4-fold) encoding glutamate synthase which catalyzes the conversion of 2-oxoglutarate to glutamine (Table 24). The upregulated proteins responsible for energy metabolism are SMc01159 (4-fold) encoding oxidoreductase and SMc04385 (3-fold) encoding aldehyde dehydrogenase (Table 24). The remaining genes ≥ 3-fold upregulated genes belong to several other functional categories such as fatty acid metabolism (SM_b20752, 3-fold), purine metabolism (SM_b21441[#], 3-fold), transcriptional regulation (SMc04220[#], 10-fold**),** and so on (Table 24).

6.4 Discussion

In this study, we report on a whole genome transcriptomic study of *S. meliloti dme* and *tme* mutants grown in MOPS-buffered minimal media supplemented with 15 mM succinate or15 mM glucose, the objective of which was to explore the physiological

roles of DME and TME in *S. meliloti* central carbon metabolism. For this purpose, we compared the transcriptome profiles of *S. meliloti* wild type to *dme* and *tme* mutants, grown in minimal media (MOPS-P2) with succinate or glucose as the sole carbon source. Global analysis of gene expression patterns (principal component analysis and hierarchical clustering) showed that the transcriptome profiles of *dme* mutant were clearly separated from those of *tme* mutant when cultures were grown with succinate. The transcriptome profiles of *dme* and *tme* mutants grouped tightly when cultures were grown with glucose (Figure 36 & Figure 37). This indicated that the expression patterns of the *dme* and *tme* mutants were significantly different in succinate-grown cells, whereas they were highly similar in glucose-grown cells. Hence, the physiological functions of DME and TME are equivalent in free-living cells grown on glucose, but different in cells grown on succinate.

Compared to the wild type, 182 genes were ≥ 3-fold upregulated in the *dme* mutant, whereas 56 genes in the *tme* mutant were upregulated when cells were grown on succinate. Equivalent figures for cells grown with glucose were 23 and 27 respectively (Table 18). The number of genes ≥ 3-fold upregulated in *dme* mutant grown on succinate (182 genes) was roughly 3-, 6-, and 8-fold that in *tme* mutant grown on succinate (56 genes), *tme* mutant grown on glucose (27 genes), and *dme* mutant grown on glucose (23 genes), respectively (Table 18). Among the ≥ 3-fold upregulated genes, the numbers of genes involved in transport across membranes, amino acid and carbohydrate metabolism, and cofactor and energy metabolism in *dme* mutant grown on succinate (55, 32, and 29 genes, respectively) was larger than those in *tme* mutant grown on succinate (9, 6, and 9

genes, respectively), and most significantly, much larger than those in *tme* mutant grown on glucose (3, 2, and 2 genes, respectively), and *dme* mutant grown on glucose (3, 3, and 0 genes, respectively) (Table 18). On the other side, only a low number of genes was found to be ≥ 3-fold downregulated in succinate-grown *dme* mutant (19 genes), succinate-grown *tme* mutant (14 genes), glucose-grown *dme* mutant (17 genes), and glucose-grown *tme* mutant (19 genes) (Table 18). Among the ≥ 3-fold downregulated genes, only a few were involved in transport across membranes, amino acid and carbohydrate metabolism, and cofactor and energy metabolism: the *dme* and *tme* mutants grown on succinate (none), glucose-grown *dme* mutant (11 genes), and glucose-grown mutant (9 genes). Since the differences of gene expression in *S. meliloti* caused by the *dme* or *tme* mutation were much more striking in succinate-grown cells compared with glucose-grown cells, we reasoned that the physiological roles of DME and TME in *S. meliloti* could be linked to efficient utilization of C_4-dicarboxylates such as malate rather than metabolism of glucose. Furthermore, we could also argue that DME is more important for central carbon metabolism in *S. meliloti* free-living cells than TME on the basis of the number of ≥ 3-fold upregulated genes observed in the *dme* and *tme* mutants grown on succinate (182 and 56 genes, respectively).

Smallbone, L.A (2006, M.Sc. thesis) conducted an analysis of the polar metabolome of *S. meliloti* malic enzyme mutants using gas chromatography-mass spectrometry (GC-MS). The major differences in the metabolite profiles noted between the *dme* mutant and the wild type in succinate grown cells showed that the *dme* mutant accumulated the 6-phosphate sugars (6PS) intracellularly, such as fructose-6-phosphate,

mannose-6-phosphate, glucose-6-phosphate, and it also excreted malate and fumarate into extracellular environment. On the basis of these results, Smallbone (2006, M.Sc. thesis) hypothesized that the *dme* mutation blocked the conversion of malate to pyruvate and caused a disturbance in the central metabolism in succinate grown cells. The accumulated TCA cycle intermediates were excreted, such as fumarate and malate, or increased the flux through gluconeogenic pathway (the conversion of oxaloacetate to phosphoenolpyruvate, phosphoenolpyruvate to glycerate-2P and so on) to generate excess 6-phosphate sugars leading to their accumulation within the cells.

The genome-wide microarray results reported here are consistent with Smallbone's hypothesis (2006, M.Sc. thesis). Of the 182 genes that were ≥ 3-fold upregulated in the *dme* mutant grown with succinate, 116 genes (~65%) encode proteins involved in transport across membranes, amino acid and carbohydrate metabolism, and cofactor and energy metabolism, and the functions of the remaining genes are mainly unknown (Table 18). In succinate-grown cells, expression of five genes involved in the TCA cycles was found to be upregulated in the *dme* mutant relative to the wild type (Figure 41and Table 21). They are *sucAB* (SMc02482 and SMc02483), encoding 2-oxoglutarate dehydrogenase which catalyzes the reversible conversion of 2-oxoglutarate to succinyl-CoA (3- and 2.3- fold); *sucCD* (SMc02480 and SMc02481), encoding succinyl-CoA synthetase which catalyzes the reversible reaction of succinyl-CoA to succinate (2.4- and 11- fold); and *mdh* (SMc02479), encoding malate dehydrogenase which reversibly catalyzes the oxidation of malate to oxaloacetate (1.5-fold). These

results suggest that *dme* mutation might lead to an intracellular accumulation of TCA cycle intermediates such as 2-oxoglutarate, succinyl-CoA, and malate (Figure 41).

Among the upregulated genes in succinate-grown cells of the *dme* mutant, ten genes encoding enzymes in the Entner-Doudoroff (ED) pathway were induced (Figure 41 and Table 21). They are *zwf* (SMc03070; 2-fold), *pgl* (SMc03069; 2-fold), *eda1* (SMc02043; 1.9-fold), *eda2* (SMc03153; 2.9-fold), *gap* (SMc03979; 1.5-fold), *pgk* (SMc03981; 2.3-fold), *eno* (SMc01028; 4-fold), *pykA* (SMc04005; 2.1-fold), *pdhB* (SMc01031; 1.5-fold), and *pdhB* (SMc01031; 3.1-fold). The upregulated Entner-Doudoroff (ED) pathway may suggest that the 6-phosphate sugars (6PS) such as fructose-6-phosphate and glucose-6-phosphate were accumulated in succinate-grown cells of the *dme* mutant (Figure 41). Similarly, expression of ten genes encoding enzymes responsible for the interconversion of various sugars was elevated in succinate-grown cells of the *dme* mutant, which hinted an accumulation of the 6-phosphate sugars (6PS) within cells (Figure 41 and Table 21). For example, SMc00430 (3.4-fold) and *exoB* (SM_b20942; 1.7-fold) encode UDP glucose 4-epimerase which catalyze the reversible conversion of UDP-galactose to UDP-glucose; *tkt2* (SMc03978; 3.8-fold) encodes transketolase which catalyzes the reversible reaction of D-sedoheptulose-7P and glyceraldehyde-3P to D-ribose-5P and D-xylulose-5P and the reversible reaction of β-D-fructose-6P and glyceraldehyde-3P to D-xylulose-5P and D-erythrose-4P; SMc02877 (3.5-fold) encodes glucosamine-6-phosphate isomerase which catalyzes the reversible conversion of D-glucosamine-6P to β-D-fructose-6P;

Figure 41 Schematic diagram illustrating genes involved in *S. meliloti* 6-phosphate sugar metabolism.

Genes that were upregulated in *S. meliloti dme* mutant grown on succinate compared with the wild type are colored in red and the numbers in green are the fold change (FC) of the indicated genes. Only genes with FC ≥ 3 were listed in Table 21. Metabolic enzymes encoded by the listed genes: *acnA*(SMc03846), aconitate hydratase; *gltA*(SMc02087), citrate synthase; *edd*(SMc03068), phosphogluconate dehydratase; *eda1*(SMc02043)/*eda2*(SMc03153), 2-dehydro-3-deoxyphosphogluconate aldolase; *eno*(SMc01028), phosphopyruvate hydratase; *exoB*(SM_b20942)/SMc00430, UDP-glucose 4-epimerase; *fumC*(SMc00149), fumarate hydratase; *gap*(SMc03979), glyceraldehyde-3-phosphate dehydrogenase; *gntK*(SM_b21119), gluconokinase; *gpmA*(SMc02838)/*gpmB*(SMc00006)/Sma0527, phosphoglyceromutase; *icd*(SMc00480), isocitrate dehydrogenase; *manB*(SM_b21081)/*pgm*(SMc03925), phosphoglucomutase; *mdh*(SMc02479), malate dehydrogenase; *pdhABC*(SMc01030 to SMc01032), pyruvate dehydrogenase; *pgi*(SMc02163), glucose-6-phosphate isomerase; *pgk*(SMc03981), phosphoglycerate kinase; *pgl*(SMc03069), 6-phosphogluconolactonase; *pykA*(SMc04005), pyruvate kinase; *sdhABCD*(SMc02463 to SMc02466), succinate dehydrogenase; *sucAB*(SMc02482&SMc02483), 2-oxoglutarate dehydrogenase; *sucCD*(SMc02480&SMc02481), succinyl-CoA synthetase; *tkt2*(SMc03978), transketolase; *xlyA*(SMc03163), xylose isomerase; *xylB*(SMc03164), xylulose kinase; *zwf*(SMc03070), glucose-6-phosphate 1-dehydrogenase; SM_b20453, gluconolactonase; SMc01992, D-xylulose reductase; and SMc02877, glucosamine-6-phosphate isomerase.

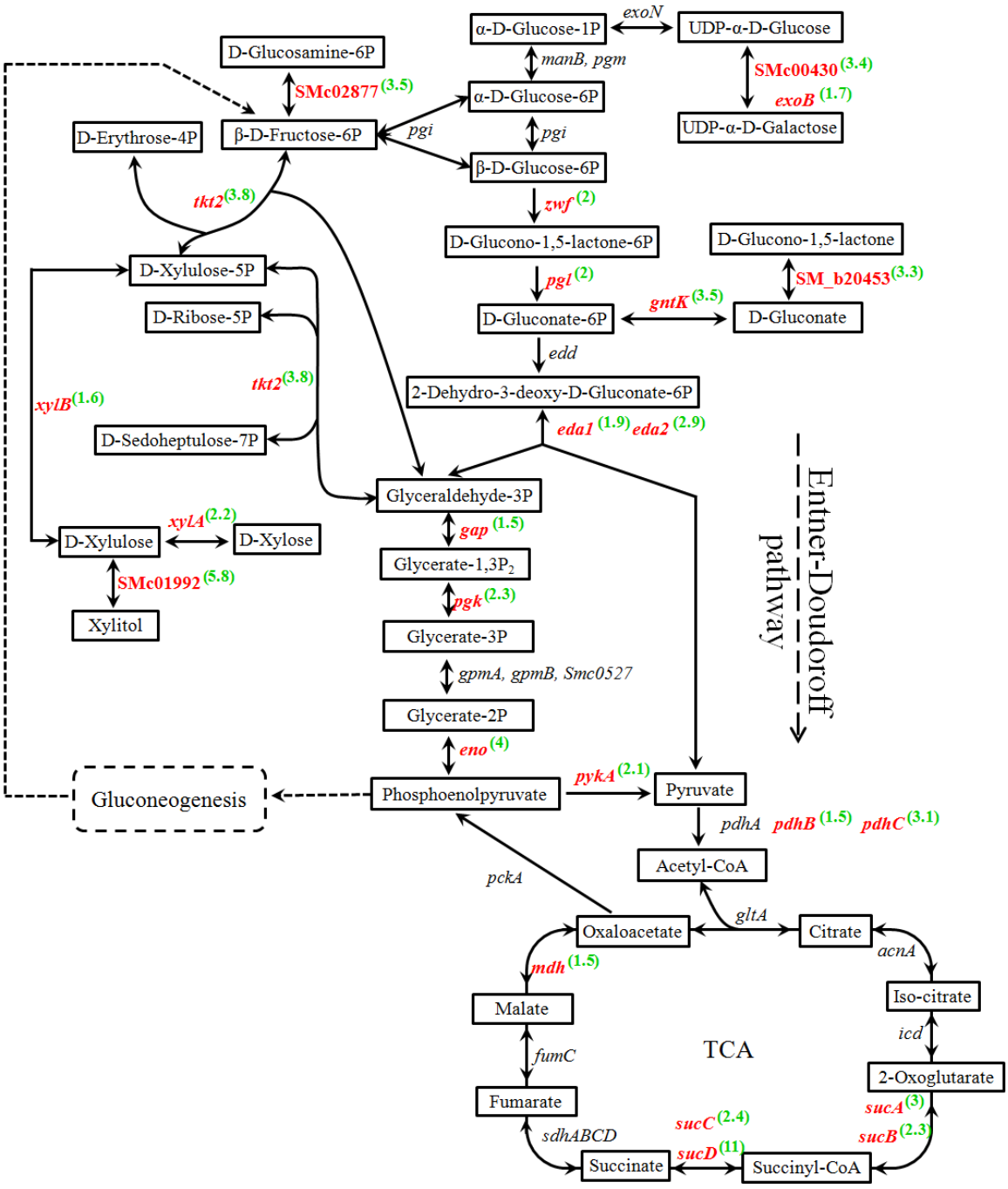
α-D-Glucose-1P
exoN
UDP-α-D-Glucose
manB, pgm
SMc00430 (3.4)
exoB (1.7)
α-D-Glucose-6P
UDP-α-D-Galactose
D-Glucosamine-6P
SMc02877 (3.5)
D-Erythrose-4P
β-D-Fructose-6P
pgi
pgi
β-D-Glucose-6P
tkt2 (3.8)
zwf (2)
D-Glucono-1,5-lactone-6P
D-Glucono-1,5-lactone
D-Xylulose-5P
pgl (2)
SM_b20453 (3.3)
D-Ribose-5P
D-Gluconate-6P
gntK (3.5)
D-Gluconate
edd
tkt2 (3.8)
2-Dehydro-3-deoxy-D-Gluconate-6P
xylB (1.6)
eda1 (1.9) eda2 (2.9)
D-Sedoheptulose-7P
Entner-Doudoroff pathway
Glyceraldehyde-3P
xylA (2.2)
D-Xylulose
D-Xylose
gap (1.5)
Glycerate-1,3P2
SMc01992 (5.8)
pgk (2.3)
Xylitol
Glycerate-3P
gpmA, gpmB, Smc0527
Glycerate-2P
eno (4)
pykA (2.1)
Gluconeogenesis
Phosphoenolpyruvate
Pyruvate
pdhA pdhB (1.5) pdhC (3.1)
Acetyl-CoA
pckA
gltA
Oxaloacetate
Citrate
acnA
mdh (1.5)
Iso-citrate
Malate
icd
fumC
TCA
2-Oxoglutarate
Fumarate
sucA (3)
sucC (2.4)
sucB (2.3)
sdhABCD
sucD (11)
Succinate
Succinyl-CoA

SM_b20453 (3.3-fold) encodes gluconolactonase which catalyze the reaction of D-glucono-1,5-lactone to D-gluconate; and *gntK* (SM_b21119; 3.5-fold) encodes gluconokinase which catalyzes the reaction of D-gluconate to D-gluconate-6P.

Furthermore, 14 genes involved in the transport of various sugars were found to be highly induced in succinate-grown cells of the *dme* mutant (Table 21). For example, SMa0070 encoding simple sugar permease protein was induced 28-fold, SMc04396 encoding periplasmic multiple sugar-binding protein was induced 5-fold, and SM_b20036 encoding periplasmic quinic acid-binding protein was induced 8-fold. This may suggest that the accumulated sugars are exported and the sugars in the external environment induce the transporters - or the transporters are induced to export the accumulated sugars.

Among the upregulated genes in succinate-grown cells of the *dme* mutant, 20 genes encode enzymes catalyzing the synthesis of various amino acids from pyruvate, fumarate, oxaloacetate, and 2-oxoglutarate (Figure 42 and Table 21). For example, *aspC* (SMc02262; 5-fold) and *aatB* (SMc04386; 1.9-fold) encode aspartate aminotransferase which catalyzes interconversion of aspartate and 2-oxoglutarate to oxaloacetate and glutamate; *gltB* (SMc04028; 6.7-fold) and *argD* (SMc02138, 4-fold) encode glutamate synthase and acetylornithine transaminase respectively which catalyze the reaction of 2-oxoglutarate to glutamate; *argH1* (SMc00725, 1.5-fold) and *argH2* (SM_b21094, 7.5-fold) encode argininosuccinate lyase which catalyzes the reversible breakdown of argininosuccinate producing the amino acid arginine and dicarboxylic acid fumarate; *asnO* (SM_b20481; 4-fold) encodes asparagine synthetase that generates asparagine from aspartate; SMc02352 (2-fold) and SMc01594 (1.8-fold) encode glutamine synthetase

which catalyzes the condensation of glutamate and ammonia to form glutamine; *sgaA* (SMa2139, 2.6-fold) encodes a transaminase which catalyzes the reversible conversion of pyruvate to alanine; and 10 genes encode enzymes which participate in the conversion of pyruvate to leucine, isoleucine and valine, such as acetolactate synthase (*ilvIG*, SMa0958, and SMa2211) (~2-fold), dihydroxy-acid dehydratase (*ilvD1D4*, *araF*, and SMa0235) (up to 3-fold), aminotransferase (*ilvE1*; SMc00042) (2.2-fold), 3-isopropylmalate dehydrogenase (*leuB*; SMc04405) (3.4-fold), and 2-isopropylmalate synthase (*leuA2*; SMc02546) (4.5-fold).

Furthermore, 27 genes that are involved in the transport of amino compounds such as spermidine/putrescine, peptides/oligopeptid, and amino acids were found to be highly induced in succinate-grown cells of the *dme* mutant (Table 21), which may suggest that the amino acids are exported and the amino acids in the external environment induce the transporters - or the transporters are induced to export the amino acids. For example, SMc03131 encoding periplasmic polar amino acid-binding protein was induced 14-fold, SMc00671 encoding histidine permease protein was induced 5-fold, SMa0800 encoding spermidine/putrescine permease protein was induced 5-fold, and SM_b20383 encoding periplasmic spermidine/putrescine -binding protein was induced 7-fold.

We also noticed that 10 genes involved in the biosynthesis of fatty acids from acetyl-CoA were induced in succinate-grown cells of the *dme* mutant (Figure 42). They are *accB* (SMc01344), encoding acetyl-CoA carboxylase (1.5-fold); *fabH* (SMc01785)/*fabF* (SMc00574)/SMc04273, encoding 3-oxoacyl-ACP synthase (up to 2.6-fold);

Figure 42 Schematic diagram illustrating genes involved in *S. meliloti* amino acid and fatty acid synthesis

Genes that were upregulated in *S. meliloti dme* mutant grown on succinate compared with the wild type are colored in red and the numbers in green are the fold change (FC) of the indicated genes. Only genes with FC ≥ 3 were listed in Table 21. Metabolic enzymes encoded by the listed genes: *accA*(SMc00690)/*accB*(SMc01344)/*accC* (SMc01345)/*accD* (SMc02764), acetyl-CoA carboxylase; *argG*(SMc03826), argininosuccinate synthase; *argH1*(SMc00725)/*argH2*(SM_b21094), argininosuccinate lyase; *asnO*(SM_b20481), asparagine synthetase; *aspC*(SMc02262)/*aatB*(SMc04386), aspartate aminotransferase; *fabA*(SMc00328)/SMc04277, 3-hydroxydecanoyl-ACP dehydratase; *fabD*(SMc00571), ACP S-malonyltransferase; *fabF*(SMc00574)/*fabH*(SMc01785)/SMc04273, 3-oxoacyl-ACP synthase; *fabG2*(SMc00880)/SMc01157, 3-oxoacyl-(acyl carrier protein) reductase; *fabI*(SMc00005/SMc00326), enoyl-ACP reductase; *gltB*(SMc04028)/*gltD* (SMc04026)/SMc01814, glutamate synthase; *ilvC*(SMc04346), ketol-acid reductoisomerase; *ilvD4*(SMb_20115)/*araF*(SM_b20890)/SMa0235, dihydroxy-acid dehydratase; *ilvE1*(SMc02896), branched-chain amino acid aminotransferase; *ilvI*(SMc01431)/*ilvG*(SMc04455)/SMa2211/SMa0958, acetolactate synthase; *leuA2*(SMc02546), 2-isopropylmalate synthase; *leuB*(SMc04405), 3-isopropylmalate dehydrogenase; *leuC*(SMc03823)/*leuD*(SMc03795), isopropylmalate isomerase; *sgaA*(SMa2139), SgaA serine-glyoxylate aminotransferase; and SMc01594/SMc02352, glutamine synthetase.

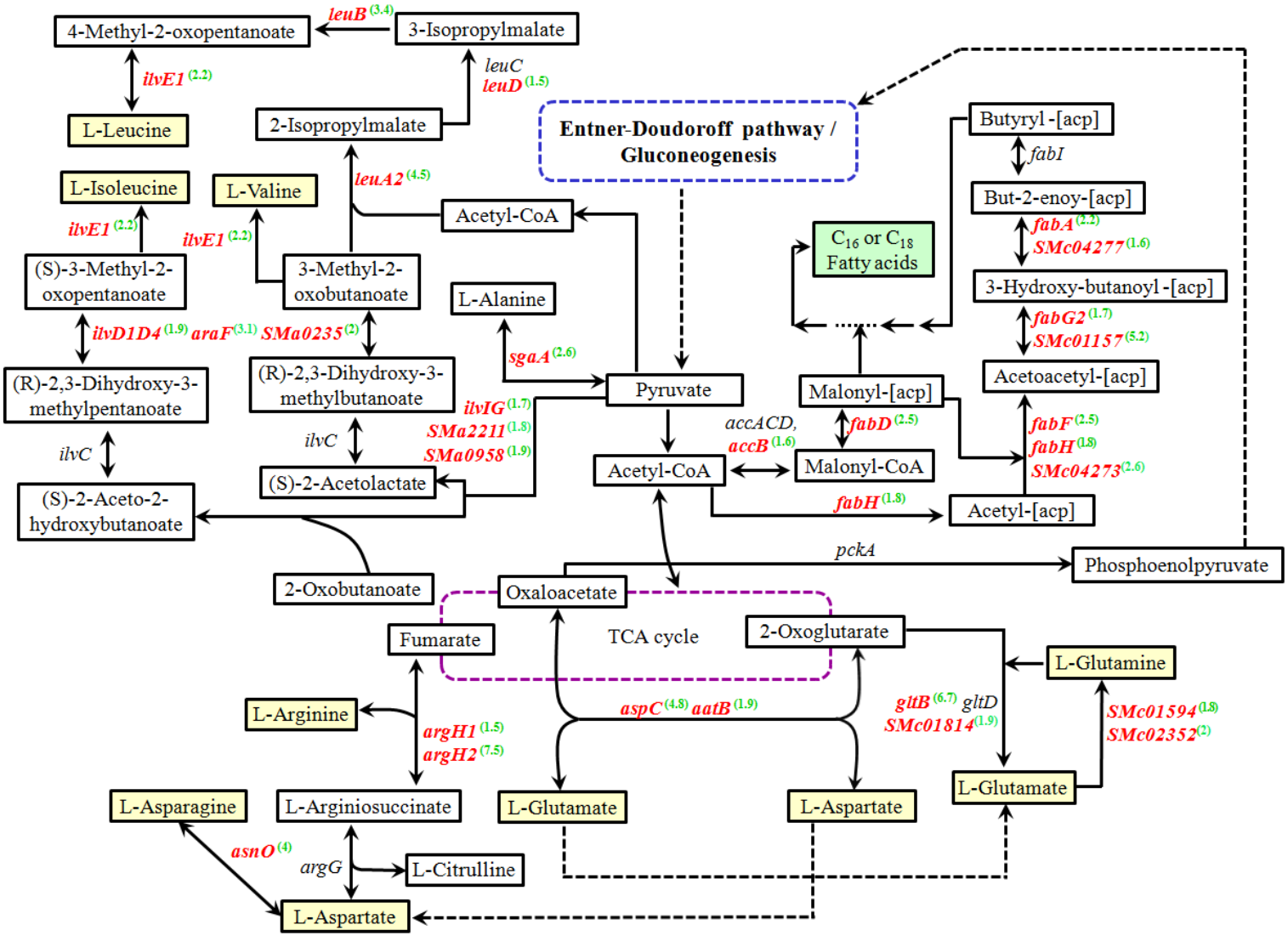
4-Methyl-2-oxopentanoate
leuB (3.4)
3-Isopropylmalate
ilvE1 (2.2)
leuC
leuD (1.5)
L-Leucine
2-Isopropylmalate
Entner-Doudoroff pathway / Gluconeogenesis
Butyryl -[acp]
fabI
But-2-enoy-[acp]
L-Isoleucine
L-Valine
leuA2 (4.5)
Acetyl-CoA
fabA (2.2)
SMc04277 (1.6)
C16 or C18 Fatty acids
3-Hydroxy-butanoyl -[acp]
ilvE1 (2.2)
ilvE1 (2.2)
(S)-3-Methyl-2-oxopentanoate
3-Methyl-2-oxobutanoate
L-Alanine
fabG2 (1.7)
SMc01157 (5.2)
ilvD1D4 (1.9) araF (3.1) SMa0235 (2)
sgaA (2.6)
Acetoacetyl-[acp]
(R)-2,3-Dihydroxy-3-methylpentanoate
(R)-2,3-Dihydroxy-3-methylbutanoate
Pyruvate
Malonyl-[acp]
ilvIG (1.7)
SMa2211 (1.8)
SMa0958 (1.9)
accACD, accB (1.6)
fabD (2.5)
fabF (2.5)
fabH (1.8)
SMc04273 (2.6)
ilvC
ilvC
(S)-2-Acetolactate
Acetyl-CoA
Malonyl-CoA
(S)-2-Aceto-2-hydroxybutanoate
fabH (1.8)
Acetyl-[acp]
pckA
Phosphoenolpyruvate
2-Oxobutanoate
Oxaloacetate
Fumarate
TCA cycle
2-Oxoglutarate
L-Glutamine
L-Arginine
aspC (4.8) aatB (1.9)
gltB (6.7) gltD
SMc01814 (1.9)
SMc01594 (1.8)
SMc02352 (2)
argH1 (1.5)
argH2 (7.5)
L-Asparagine
L-Arginiosuccinate
L-Glutamate
L-Aspartate
L-Glutamate
asnO (4)
argG
L-Citrulline
L-Aspartate

fabD (SMc00571), encoding ACP S-malonyltransferase (2.5-fold); *fabG2*(SMc00880)/SMc01157, encoding 3-oxoacyl-[acyl-carrier protein] reductase (up to 5.2-fold); and *fabA* (SMc00328)/SMc04227, encoding 3-hydroxydecanoyl-ACP dehydratase (up to 2.2-fold). Therefore, the up-regulation of these genes may reflect an increased flux through the pathways involved in amino acid and fatty acid synthesis.

The citric acid (TCA) cycle is a key pathway of the aerobic metabolism, which provides the majority of energy used by aerobic bacteria in conjunction with oxidative phosphorylation. So we suggest that the disturbance of central carbon metabolism may lead to an energy shortage in succinate-grown cells of the *dme* mutant. Consistent with such a hypothesis, seventeen genes related to energy metabolism were found to be highly upregulated in succinate-grown cells of the *dme* mutant. For example, seven genes encode enzymes involved in methanol metabolism (Figure 40 and Table 21), such as S-(hydroxymethyl) glutathione dehydrogenase (*adhC2*; SMa2113) (5-fold), formate dehydrogenase (*fdhE*; SMa0009) (5-fold); S-(hydroxymethyl) glutathione synthase (*gfa*; SM_b20186) (12-fold), methanol dehydrogenase (SM_b20173) (42-fold), and S-formylglutathione hydrolase (SM_b20171) (13-fold). Furthermore, eight genes related to redox cofactor metabolism were ≥ 3-fold upregulated in succinate-grown cells of the *dme* mutant (Table 21). They belong to two different operons. Operon *pntAabB* (SMc03938, SMc03939, and SMc03950) (up to 5-fold) encode $NAD(P)^+$ transhydrogenase which catalyzes the reversible conversion of $NADP^+$ and NADH to NADPH and NAD^+. Operon *pqqABCDE* (SM_b20204 to SM_b20208; up to 5-fold) encode proteins responsible for

the biosynthesis of pyrroloquinoline quinone (PQQ) and the upregulated expression of this operon was verified using transcriptional fusion reporter (GusA or GFP) (Table 19).

Together with previous metabolite analysis conducted by Smallbone, L.A (2006, M.Sc. thesis), the microarray data discussed above suggest that a *dme* mutation may lead to a disturbance of central carbon metabolism in *S. meliloti* succinate-grown cells resulting in an accumulation of 6-phosphate sugars, acetyl-CoA, pyruvate, and TCA cycle intermediates such as fumarate, malate, oxaloacetate, and 2-oxoglutarate (Figure 41 and Figure 42). Therefore, we hypothesize that DME plays an important role in regulating the levels of TCA cycle intermediates, which is essential for the maintenance of metabolic flux through the TCA cycle during C_4-dicarboxylate oxidation. This hypothesis appears to be entirely consistent with previous studies showing that DME enzyme was allosterically regulated by fumarate, succinate, and acetyl-CoA (Voegele *et al*. 1999;Zhang *et al*. 2012).

In the *S meliloti tme* mutant grown on succinate, among the 56 genes that were $\geq$ 3-fold upregulated, only very few of them encode proteins involved in uptake of amino compounds (3 genes) and carbohydrate (3 gene), metabolism of amino acids (4 genes), carbohydrate (2 genes), cofactors (1 gene), fatty acids (2 genes), and energy (8 genes), which is not significant enough to indicate the linkage between the physiological functions of TME and the central carbon metabolism in *S. meliloti* free-living cells. Since TME is strictly $NADP^+$-dependent malic enzyme, we assume that its physiological roles may be related to this property such as the contribution of NADPH for anabolic purposes.

Table 20 Differentially regulated genes in *S. meliloti* free-living cells grown in MOPS-P2-glucose compared with MOPS-P2 succinate

gene ID	Gene name	Production description	FC		
			wt	*dme*$^-$	*tme*$^-$
SMc02607	*soxD*	Sarcosine oxidase subunit delta, EC:1.5.3.1 (metabolism of amino acid: Gly, Ser, and Thr)	13.8	1.5	0.8
SMc02864	*moeB*	molybdopterin biosynthesis protein (metabolism of cofactors and vitamins)	10.5	0.8	2.9
SMc01158		Hypothetical protein	3.9	0.8	1.3
SMc03012	*cheD*	Chemoreceptor glutamine deamidase (Bacterial chemotaxis and Cell motility)	3	1.5	1.4
SMc03035	*fliL*	flagellar transmembrane protein (Cell motility)	4.9	1.9	1.7
SMc03069	*pgl*	6-phosphogluconolactonase, EC:3.1.1.31 (Entner-Doudoroff pathway)	4.4	2.2	1.9
SMc03070	*zwf*	glucose-6-phosphate 1-dehydrogenase, EC:1.1.1.49 (Entner-Doudoroff pathway)	5.5	2.8	3.2
SMc00773	*potI*	putrescine permease (ABC transport system)	3.5	1.3	2.6
SMc00874	*corA2*	magnesium/cobalt transporter CorA	3.4	0.7	0.9
SMc00098		Transcriptional regulator	5.5	0.6	1.5
SMc00457		hypothetical protein	4.6	1.2	1.3
SMc02646		Putative glycerophosphoryl diester phosphodiesterase, EC:3.1.4.46 (glycerophospholipid metabolism)	3	0.8	1.3
SMc01030	*pdhA*	pyruvate dehydrogenase alpha2 subunit protein, EC:1.2.4.1 (Entner-Doudoroff pathway)	3.3	2	2.9
SMc01031	*pdhB*	pyruvate dehydrogenase subunit beta (EC:1.2.4.1) (Entner-Doudoroff pathway)	2.5	2.1	4.5
SMc01032	*pdhC*	Dihydrolipoamide S-acetyltransferase, EC:2.3.1.12 (Entner-Doudoroff pathway)	3.4	2	3.9
SMc04210		Hypothetical protein	7.9	2.	0.9
SMc01412		Hypothetical protein	3.4	0.7	1.5
SMc01456		Hypothetical protein (signal peptide)	3.4	1.3	1.4
SMc01877	*recN*	DNA repair protein	4.4	4.7	1.9
SMc01861	*murE*	UDP-N-acetylmuramoylalanyl-D-glutamate--2,6-diaminopimelate ligase, EC:6.3.2.13 (Peptidoglycan biosynthesis)	9.9	2	1.9

Continued on following page

Table 20-Continued

gene ID	Gene name	Production description	FC		
			wt	*dme*$^-$	*tme*$^-$
SMc02032		ATP-binding protein (putative simple sugar ABC transport system)	5.3	1.7	10.4
SMc02043	*eda1*	KDPG aldolase, EC:4.1.2.14 (Entner-Doudoroff pathway)	3.6	1	1.9
SMc02835	*glk*	Glucokinase (Entner-Doudoroff pathway)	2	0.7	2.2
SMc03153	*eda2*	KDPG aldolase, EC:4.1.2.14 (Entner-Doudoroff pathway)	5.7	3	7.5
SMc03068	*edd*	phosphogluconate dehydratase (Entner-Doudoroff pathway)	4.8	3.4	4.4
SMc04005	*pykA*	pyruvate kinase, EC:2.7.1.40 (Entner-Doudoroff pathway)	4.1	2.7	2.5
SMc04031	*pip2*	proline iminopeptidase, EC:3.4.11.5 (metabolism of Arg and Pro)	11.5	1.1	1.6
SMa0067		periplasmic solute-binding protein (putative simple sugar ABC transport system)	3.6	1.0	1.5
SMa0078		LacI family transcriptional regulator	3.5	0.8	2.2
SMa0197		simple sugar permease (putative ABC transport system)	4.2	10.9	12.3
SMa0563		aldehyde or keto oxidase	3.3	0.9	1.2
SMa0594		hypothetical protein	5.4	1.6	1.9
SMa0599		hypothetical protein	6.7	1.6	1.0
SMa0849	*syrM*	SyrM transcriptional regulator	3	1.5	2.5
SMa0952		Mannopine Permease (ABC transport system)	3.3	1.7	1.6
SMa1050		Hypothetical protein	3.3	1.5	2.7
SMa1138		Hypothetical protein	3.0	1.5	1.8
SMa1141		FNR/CRP family transcriptional regulator	5.6	1.7	1.6
SMa1184	*nosF*	NosF ATPase (ABC-2 type transport system)	3.6	1.8	0.9
SMa1500		Oxidoreductase	3.7	1.4	1.9
SMa1882		Transcriptional activator	15	1.9	1.7

Continued on following page

Table 20-Continue

gene ID	Gene name	Production description	FC		
			wt	*dme*$^-$	*tme*$^-$
SMa2347		Hypothetical protein	5.6	1.4	2.1
SM_b20381		spermidine/putrescine permease (putative ABC transport system)	4.0	1.5	1.8
SM_b20383		substrate-binding protein (putative spermidine/putrescine ABC transport system)	3.6	1.3	1.8
SM_b20391		Cellulose synthase catalytic subunit protein, EC:2.4.1.12 (Starch and sucrose metabolism)	3.3	0.9	4.2
SM_b20505	*tfxG*	Trifolitoxin immunity protein	7.3	1.6	3.7
SM_b21094	*argH2*	argininosuccinate lyase, EC:4.3.2.1 (metabolism of Ala, Asp, Glu, Arg, and Pro)	3.1	0.8	4.3
SM_b21095		polar amino acid permease (putative ABC transport system)	3.5	1.2	2.5
SM_b21222		Transcriptional regulator	4.5	1.6	1.4
SM_b21226		Hypothetical protein	4.0	0.8	0.7
SM_b21313	*wgeB*	bifunctional glycosyltransferase (biosynthesis of polysaccharides)	3.1	0.9	2.1
SM_b21314	*wgdA*	RTX toxins and secreted calcium-binding protein	4.2	1.5	2.0
SM_b21531		Hypothetical protein	12.4	0.7	1.2
SM_b21535		LysR family transcriptional regulator	4.2	0.9	1.9
SM_b20930		ATP-binding protein (putative simple sugar uptake ABC transport system	3.4	0.8	1.3
SM_b20982		Hypothetical protein	5.6	5.5	0.9
SM_b20897		Hypothetical protein	3.7	2.2	1.2
SM_b20902		periplasmic solute-binding protein (sugar uptake ABC transporter system)	30.3	7.4	21.7
SM_b20903		permease (sugar uptake ABC transporter system)	28.4	11.2	14.1
SM_b20904		ATP-binding protein (sugar uptake ABC transporter system)	11.6	9.7	16.5
SM_b20916		Hypothetical protein	5.1	1.2	1.5

Continued on following page

Table 20-Continue

gene ID	Gene name	Production description	FC		
			wt	*dme*$^-$	*tme*$^-$
SM_b21510		plasmid stability protein	4.3	0.6	3.9
SM_b20615	*thiC*	thiamine biosynthesis protein	5.0	3.4	4.6
SM_b20617	*thiG*	thiazole synthase (biosynthesis of thiamine)	5.0	2.7	5.3
SM_b20630		ATP-binding protein (Putative multiple sugar uptake ABC transport system)	3.3	0.9	1.4
Smc02562	*pckA*	phosphoenolpyruvate carboxykinase , EC:4.1.1.49 (Gluconeogenesis)	-18.3	-10.7	-15.4
SMc00371		Hypothetical protein	-3.5	-1.6	-2.3
SMc00768	*aceA*	Isocitrate lyase, EC:4.1.3.1 (Glyoxylate and dicarboxylate metabolism)	-3.2	-1.7	-5.5
SMc00800		Hypothetical protein	-3	-1	-3.3
SMc00809		Hypothetical protein	-3.5	-1.2	-2.8
SMc00885		Hypothetical protein (signal peptide)	-3.9	-1.3	-3.4
SMc00063		Hypothetical protein	-3.3	-1.2	-2.4
SMc01788		Hypothetical protein	-3.8	-1.8	-2.3
SMc00252		Hypothetical protein (signal peptide)	-6.2	-1.9	-3.3
SMc04232		Putative glycine-rich transmembrane protein	-3.5	-1.3	-2.1
SMc04184		Hypothetical protein	-3.1	-1.2	-1.4
SMc04194		Putative transmembrane protein	-3.1	-0.8	-2.7
SMc01467		Hypothetical protein (signal peptide)	-4.5	-1.6	-4.7
SMc01611	*fhuA*	Ferrichrome-iron receptor protein (iron uptake)	-3.0	-3.8	-6.6
SMc01749		Replicative DNA helicase (DNA Replication and repair)	-4.3	-1.1	-1.0
SMc01509		Hypothetical transmembrane protein	-4.5	-1.2	-1.5
SMc03983	*fbaB*	Fructose-bisphosphate aldolase class I protein, EC:4.1.2.13 (Gluconeogenesis)	-7.8	-5.5	-4.8
SMc03146		HlyD family secretion protein	-3.1	-0.9	-0.7
SMa0134		Hypothetical protein	-4.8	-1.6	-3.5

Continued on following page

Table 20-Continue

gene ID	Gene name	Production description	FC		
			wt	*dme*$^-$	*tme*$^-$
SMa5002		Hypothetical protein	-3.4	-1.3	-2.5
SMa0187		Short chain dehydrogenase	-3.1	-1.8	-2.1
SMa0541		Hypothetical protein	-3.0	-1.4	-2.3
SMa2059		Hypothetical protein	-3.6	-1.6	-6.8
SMa2071		Hypothetical protein	-3.8	-1.1	-2.0
SMa2297		hypothetical protein	-3.1	-3.1	-2.3
SMa2406	*rhbD*	Rhizobactin siderophore biosynthesis protein (iron uptake)	-3.8	-2.2	-3.7
SM_b20065		Hypothetical protein	-3.0	-1.0	-2.1
SM_b20072		myo-inositol induced periplasmic solute-binding protein (simple sugar ABC transport system)	-3.7	-1.3	-4.6
SM_b20073		Oxidoreductase	-5.7	-1.2	-8.8
SM_b20074		Hypothetical protein	-5.2	-1.2	-2.3
SM_b20086		hypothetical protein	-3.3	-1.6	-3.8
SM_b20227	*ndiA-1*	Putative nutrient deprivation-induced protein	-6.1	-2.1	-3.9
SM_b20454		Hypothetical protein	-7.0	-1.4	-7.2
SM_b20465		Hypothetical protein	-3.0	-1.1	-2.6
SM_b21664		Hypothetical protein	-12.8	-3.9	-18.9
SM_b21330		Hypothetical protein	-4.8	-1.4	-2.6
SM_b21395		Hypothetical protein	-4.2	-0.8	-1.4
SM_b21406		Hypothetical protein	-3.5	-1.0	-1.5
SM_b21441		Inosine-5′-monophosphate dehydrogenase, EC:1.1.1.205 (synthesis of GTP from IMP)	-3.3	-1.3	-1.9
SM_b21442		hypothetical protein	-3.6	-1.2	-2.5
SM_b21444		Osmotic sensory protein	-4.1	-1.3	-4.7

Continued on following page

Table 20-Continue

gene ID	Gene name	Production description	FC		
			wt	*dme*$^-$	*tme*$^-$
SM_b21454		Hypothetical protein	-3.2	-0.9	-2.9
SM_b21456		Hypothetical protein	-4.3	-2.3	-4.6
SM_b21473		Hypothetical protein	-3.2	-0.7	-2.3
SM_b21474	*fabG*	3-ketoacyl-ACP reductase, EC:1.1.1.100 (fatty acid biosynthesis)	-3.6	-0.9	-2.1
SM_b21483		Hypothetical protein	-8.1	-1.6	-4.8
SM_b20611	*dctA*	C4-dicarboxylate transporter	-98	-139	-72

Genes are listed in order, FC is fold change of gene expression (*S. meliloti* cultures grown in glucose vs succinate). Significantly regulated genes: FC $\geq$ 3 and *P*-value (Student's *t* test) $\leq$ 0.05. Minus (-), genes significantly downregulated; wt, *S. meliloti* wild type strains RmP110; *dme*$^-$: *S. meliloti dme* mutant RmP2189; and *tme*$^-$: *S. meliloti tme* mutant RmP2189

Table 21 Differentially regulated genes in a succinate-grown *S. meliloti dme* mutant compared with wild-type strain

gene ID	Gene name	Production description (functions)	FC *dme*/wt
SMc02758		Putative nucleotidyl transferase (DNA repair)	3.3
SMc02610	*glxB*	Putative glutamine amidotransferase (amino acid metabolism)	3.8
SMc02825	*pepA2*	Aminopeptidase (glutathione metabolism)	3.0
SMc02877		Putative sugar isomerase (sugar metabolism)	3.5
SMc02907		amino acid efflux transmembrane protein	4.2
SMc00385		Hypothetical protein	3.0
SMc00389		Hypothetical protein	3.2
SMc00430		Putative UDP-glucose 4-epimerase, EC:5.1.3.2 (galactose, amino sugar, and nucleotide sugar metabolism)	3.4
SMc00433	*iolE*	Putative inosose dehydratase, EC:4.2.1.44 (myo-inositol metabolism)	3.3
SMc01157		Putative [acyl-carrier-protein] reductase, EC:1.1.1.100 (Biosynthesis of fatty acid and biotin)	5.1
SMc01167	*dnaA*	chromosomal replication initiation protein (DNA replicate)	3.1
SMc02138	*argD*	acetylornithine transaminase, EC:2.6.1.17 &2.6.1.11 (metabolism of Lys, Arg, and Pro)	3.7
SMc02229*		acyl-CoA dehydrogenase, EC:1.3.99.- (fatty acid metabolism)	3.4
SMc02262	*aspC*	Aspartate transaminase, EC: 2.6.1.1 (interconversion of Asp and α-ketoglutarate to OAA and Glu)	4.7
SMc02305	*murA*	UDP-N-acetylglucosamine 1-carboxyvinyltransferase, EC:2.5.1.7 (Amino sugar and nucleotide sugar metabolism and Peptidoglycan biosynthesis)	3.0
SMc02319		hypothetical protein	3.2
SMc03035	*fliL*	flagellar transmembrane protein (cell mobility)	4.2
SMc03061	*aglE*	periplasmic-binding protein (alpha-glucoside ABC transport system)	4.2
SMc00769		hypothetical protein	5.8
SMc00771	*potG*	ATP-binding protein (putrescine ABC transporter)	3.3
SMc00788	*dppC1*	dipeptide permeas (ABC transport system)	3.6
SMc00923	*tag*	DNA-3-methyladenine DNA glycosylase, EC:3.2.2.20 (DNA Replication and repair)	3.8

Continued on following page

Table 21-Continued

gene ID	Gene name	Production description (functions)	FC *dme*/wt
SMc00078	*livJ*	periplasmic solute-binding protein (branched-chain amino acid ABC transport system)	3.3
SMc02384		glycosyltransferase transmembrane protein (biosynthesis of polysaccharides)	4.6
SMc02653	*lepB*	signal peptidase I transmembrane protein, EC:3.4.21.89 (Protein export)	3.1
SMc02549		hypothetical protein	3.1
SMc02546	*leuA2*	Putative2-isopropylmalate synthase, EC:2.3.3.13 (pyruvate metabolism and biosynthesis of Val, Leu, and Ile)	4.5
SMc01779		MFS-type transporter	4.8
SMc01782		hypothetical protein	3.0
SMc01793		glycosyltransferase (biosynthesis of polysaccharides)	3.2
SMc01340		aminotransferase (interconversion between mino acid and an α-keto acid)	3.6
SMc01317*	*rpoB*	DNA-directed RNA polymerase, EC:2.7.7.6 (transcription)	4.6
SMc01274*	*crcB*	hypothetical protein (signal peptide)	3.1
SMc01028	*eno*	phosphopyruvate hydratase, EC:4.2.1.11 (Entner–Doudoroff pathway)	4.0
SMc01032	*pdhC*	Dihydrolipoamide S-acetyltransferase, EC:2.3.1.12 (pyruvate metabolism)	3.0
SMc01036*		hypothetical protein	4.7
SMc02120	*aapM*	general L-amino acid permease (ABC transport system)	3.3
SMc02103		hypothetical protein	3.8
SMc04305	*cobU*	adenosylcobinamide kinase/adenosylcobinamide-phosphate guanylyltransferase, EC:2.7.7.62& 2.7.1.156 (Porphyrin and V B12 metabolism)	3.6
SMc04264		transcriptional regulator	5.1
SMc04282	*cobB*	cobyrinic acid a,c-diamide synthase, EC:6.3.5.9 & 6.3.5.11 (Porphyrin and V B12 metabolism)	4.1

Continued on following page

Table 21-Continued

gene ID	Gene name	Production description (functions)	FC *dme*/wt
SMc01424*	*nthA*	nitrile hydratase subunit alpha protein, EC:4.2.1.84 (metabolism of Trp and Xenobiotics, Styrene, Aminobenzoate, and Fluorobenzoate)	3.6
SMc01469	*mcpW*	Probable methyl accepting chemotaxis transmembrane protein (cell mobility and Bacterial chemotaxis)	3.4
SMc01574		hypothetical protein	3.1
SMc01628		periplasmic solute-binding protein (multiple sugar ABC transport system)	3.8
SMc01639		acyl-CoA dehydrogenase, EC:1.3.99.3 (Metabolism of fatty acid)	6.9
SMc01658*		Ferrioxamine B specific ferric iron reductase (iron uptake)	3.5
SMc01660		hypothetical protein	3.2
SMc02684		hypothetical protein	3.3
SMc02738	*choW*	glycine betaine/proline permease (ABC transport system, protection against osmotic stress)	5.1
SMc01526	*dppB2*	peptide/nickel permease (ABC transport system)	3.8
SMc01820		hypothetical protein	3.0
SMc01946	*livK*	leucine-specific binding protein (Branched-chain amino acid ABC transport system)	3.4
SMc01947		hypothetical protein	3.4
SMc01950	*livM*	high-affinity branched-chain amino acid permease (ABC transport system)	3.4
SMc01965		ATP-binding protein (spermidine/putrescine ABC transport system)	3.1
SMc01967	*speB2*	agmatinase, EC:3.5.3.11 (metabolism of Arg and Pro,conversion of agmatine to putrescine)	3.5
SMc01992*		D-xylulose reductase, EC:1.1.1.9 (pentose and glucuronate interconversions)	5.8
SMc02350		hypothetical protein	3.1
SMc02356		periplasmic solute-binding protein (branched-chain amino acid ABC transport system)	5.7
SMc00706		hypothetical protein	6.9

Continued on following page

Table 21-Continued

gene ID	Gene name	Production description (functions)	FC *dme*/wt
SMc00696	*aroB*	3-dehydroquinate synthase, EC:4.2.3.4 (PEP involved biosynthesis of Phe, Tyr and Trp)	3.4
SMc00671	*hisW*	histidine permease (amino acid ABC transport system)	4.7
SMc03978	*tkt2*	transketolase, EC:2.2.1.1 (Pentose phosphate pathway)	3.8
SMc04048		cytochrome c protein (electron transport)	3.2
SMc03931	*soxA2*	sarcosine oxidase subunit alpha, EC:1.5.3.1 (metabolism of Gly, Ser, and Thr)	3.0
SMc03938	*pntB*	NAD(P) transhydrogenase subunit beta , EC:1.6.1.1 (recycling of NAD^+ and $NADP^+$)	4.8
SMc03939	*pntAb*	NAD(P) transhydrogenase subunit alpha, EC:1.6.1.1 (recycling of NAD^+ and $NADP^+$)	5.3
SMc03950	*pntAa*	NAD(P) transhydrogenase subunit alpha, EC:1.6.1.1 (recycling of NAD^+ and $NADP^+$)	3.2
SMc03943		hypothetical protein	3.0
SMc03162		hypothetical protein	3.1
SMc03207		hypothetical protein	3.3
SMc03131*		periplasmic solute-binding protein (polar amino acid ABC transport system)	13.8
SMc03117		branched-chain amino acid permease (ABC transport system)	2.9
SMc02482	*sucA*	2-oxoglutarate dehydrogenase E1 component, EC:1.2.4.2 (TCA cycle: coversion of 2-oxoglutarate to succinyl-coA)	3.0
SMc02481	*sucD*	succinyl-CoA synthetase subunit alpha, EC:6.2.1.5 (TCA cycle)	10.9
SMc04093	*acsA1*	acetyl-CoA synthetase (conversion of acetate to acetyl-coA)	3.2
SMc02469		oxidoreductase	4.0
SMc03822		hypothetical protein	4.3
SMc03829		putative ABC transport system permease	3.1

Continued on following page

Table 21-Continued

gene ID	Gene name	Production description (functions)	FC *dme*/wt
SMc03979	*gap*	glyceraldehyde-3-phosphate dehydrogenase,EC:1.2.1.12 (Entner–Doudoroff pathway)	1.5
SMc03981	*pgk*	phosphoglycerate kinase,EC:2.7.2.3 (Entner–Doudoroff pathway)	2.3
SMc04396		periplasmic solute-binding protein (multiple sugar ABC transport system)	5.4
SMc04405	*leuB*	3-isopropylmalate dehydrogenase, EC:1.1.1.85 (biosynthesis of Val, Leu and Ile from pyruvate and acetylcoA)	3.4
SMa0009	*fdhE*	formate dehydrogenase accessory protein (conversion of formate to bicarbonate, metabolism of C1 compounds such as methanol)	3.0
SMa0067		periplasmic solute-binding protein (simple sugar ABC transport system)	4.1
SMa0070*		simple sugar permease (ABC transport system)	27.5
SMa0087		hypothetical protein	3.3
SMa0105		permease protein (Peptides/nickel ABC transport system)	3.3
SMa0237*		dehydrogenase	3.8
SMa0396		permease protein (spermidine/putrescine ABC transport system)	6.2
SMa0525		permease protein (iron(III) ABC transport system)	3.8
SMa0800*		permease protein (spermidine/putrescine ABC transport system)	5.0
SMa1168		Dehydrogenase, FAD-dependent	4.3
SMa1259		hypothetical protein	3.2
SMa1294		hypothetical protein	5.3
SMa1406*	*ttuD3*	hydroxypyruvate reductase, EC:1.1.1.81 (Gly, Ser and Thr metabolism)	15.4
SMa1410		Oxidoreductase	8.3
SMa1500		oxidoreductase	4.2

Continued on following page

Table 21-Continued

gene ID	Gene name	Production description (functions)	FC *dme*/wt
SMa1650		permease protein (peptide/nickel ABC transport system)	7.7
SMa1664		HlyD-family protein (ABC export system)	4.3
SMa1787		transposase, fragment	3.1
SMa1817*		hypothetical protein	3.4
SMa1863*		permease protein (Peptides/nickel ABC transport system)	3.7
SMa1882*		transcriptional activator	5.0
SMa1913		Na+/H+ antiporter (Methane metabolism)	4.2
SMa2087		Desulfurization enzyme	3.4
SMa2117		oxidoreductase	3.2
SMa2119		hypothetical protein	3.2
SMa2203		permease protein (putative spermidine/putrescine ABC transport system)	3.3
SMa2361		hypothetical protein	4.9
SMa5034		hypothetical protein	3.5
SM_b20003		pyrroline-5-carboxylate reductase, EC:1.5.1.2 (metabolism of Arg and Pro)	4.0
SM_b20006		hypothetical protein	3.2
SM_b20036*		periplasmic solute-binding protein (Putative TRAP-type quinic acid transport ststem)	7.6
SM_b20057	*btuC*	Permease protein (Cobalt ABC transport system)	9.0
SM_b20071		efflux protein	3.6
SM_b20107		hypothetical protein	4.3
SM_b20108		periplasmic solute-binding protein (peptide/nickel ABC transport system)	3.1
SM_b20165		hypothetical protein	5.5
SM_b20166*		hypothetical protein	4.8
SM_b20169		hypothetical protein	4.6

Continued on following page

Table 21-Continued

gene ID	Gene name	Production description (functions)	FC *dme*/wt
SM_b20171*		Putative S-formylglutathione hydrolase, EC:3.1.2.12 (Methonal metabolism)	12.5
SM_b20172*		cytochrome c protein	10.4
SM_b20173*		methanol dehydrogenase large subunit (Methonal metabolism)	41.9
SM_b20174*		cytochrome c protein	16.5
SM_b20175*		hypothetical protein	17.8
SM_b20177		hypothetical protein	7.2
SM_b20178		hypothetical protein	2.4
SM_b20179		hypothetical protein	4.9
SM_b20180		hypothetical protein	2.2
SM_b20186	*gfa*	Glutathione-dependent formaldehyde-activating enzyme, EC:4.4.1.22 (methonal metabolism)	12.2
SM_b20204	*pqqA*	**P**yrrolo**q**uinoline **q**uinone(PQQ) synthesis protein (redox cofactor for methanol dehydrogenase)	3.2
SM_b20205	*pqqB*	PQQ biosynthesis protein (methonal metabolism)	5.0
SM_b20206*	*pqqC*	PQQ biosynthesis protein (methonal metabolism)	4.7
SM_b20207	*pqqD*	PQQ biosynthesis protein (methonal metabolism)	3.8
SM_b20208	*pqqE*	PQQ biosynthesis protein(methonal metabolism)	4.9
SM_b20262		NADP-semialdehyde dehydrogenase, EC:1.2.1.4 (biodegradation of caprolactam)	3.5
SM_b20280		hypothetical protein	3.4
SM_b20282		permease protein (putative spermidine/putrescine ABC transport system)	3.0
SM_b20322		permease protein (putative hydroxyproline trap-type transport system)	6.2
SM_b20342*		isoquinoline 1-oxidoreductase, EC:1.3.99.16	3.6
SM_b20365		periplasmic solute-binding protein (iron(III) ABC transport system)	6.0
SM_b20373*		permease protein (putative TRAP-type dicarboxylate transport system)	6.4

Continued on following page

Table 21-Continued

gene ID	Gene name	Production description (functions)	FC *dme*/wt
SM_b20374		periplasmic substrate-binding protein (putative TRAP-type dicarboxylate transport system)	5.1
SM_b20381		permease protein (putative spermidine/putrescine ABC transport system)	3.5
SM_b20383		periplasmic solute-binding protein (putative spermidine/putrescine transport system)	6.6
SM_b20385		hypothetical protein	5.5
SM_b20429	*ehuC*	permease protein (putative polar amino acid ABC transport system)	9.2
SM_b20453		gluconolactonase, EC:3.1.1.17 (Pentose phosphate pathway)	3.3
SM_b20481	*asnO*	asparagine synthetase, EC:6.3.5.4 (Ala, Asp, and Glu metabolism)	4.0
SM_b20484	*supA*	periplasmic sugar-binding protein (simple sugar ABC transport system)	3.6
SM_b21049		hypothetical protein	4.4
SM_b21094	*argH2*	argininosuccinate lyase, EC:4.3.2.1 (Ala, Asp, and Glu metabolism)	7.5
SM_b21111		oxidoreductase	3.5
SM_b21119	*gntK*	gluconokinase, EC:2.7.1.12 (Pentose phosphate pathway)	3.5
SM_b21131	*cysP2*	permease protein (sulfate ABC transport system)	2.9
SM_b21221		periplasmic solute-binding protein (Putative multiple sugar ABC transport system)	3.8
SM_b21226		hypothetical protein	4.8
SM_b21275		permease protein (putative spermidine/putrescine ABC transport system)	4.6
SM_b21181		glutaryl-CoA dehydrogenase, EC:1.3.99.7 (metabolism of Lys and Trp)	3.2
SM_b21182*		Hypothetical protein	10.5
SM_b21198		permease protein (oligopeptid ABC transport system)	3.7
SM_b21206		ATP-binding protein (ABC-2 type transport system for export of a variety of substrates)	4.5
SM_b21333		hypothetical protein	3.6

Continued on following page

Table 21-Continued

gene ID	Gene name	Production description (functions)	FC *dme*/wt
SM_b21535		LysR family transcriptional regulator	4.7
SM_b21550*		hypothetical protein	3.0
SM_b21558		aldehyde or xanthine dehydrogenase, iron-sulfur subunit protein (purine metabolism)	5.8
SM_b20930		ATP-binding protein (putative simple sugar ABC transport system)	3.3
SM_b21000		putative transport protein	5.5
SM_b21006		hypothetical protein	3.1
SM_b20865		hypothetical protein	3.5
SM_b20890	*araF*	dihydroxy-acid dehydratase, EC:4.2.1.9 (biosynthesis of Val, Leu, and Ile	3.1
SM_b20891	*araE*	2-oxoglutarate semialdehyde dehydrogenase, EC 1.2.1.26 (metabolism of ascorbate and aldarate, Vc, simple sugar)	3.8
SM_b20902		periplasmic solute-binding protein (simple sugar ABC transport system)	4.0
SM_b21420		L-arabinose isomerase (sugar metabolism)	3.1
SM_b21424		Putative acyl esterase (metabolism of ester)	3.2
SM_b21461		periplasmic solute-binding protein (putative trehalose/maltose ABC transport system)	3.2
SM_b21475*		hypothetical protein	4.3
SM_b21499		hypothetical protein	4.7
SM_b20708*		methylated-DNA--protein-cysteine methyltransferase, EC:2.1.1.63 (repair of alkylated DNA)	11.8
SM_b21691		Alkanesulfonate monooxygenase (amino acid metabolism)	3.9
SM_b20616	*thiO*	thiamine biosynthesis oxidoreductase (thiamine metabolism)	3.3
SM_b20617	*thiG*	thiazole synthase (thiamine metabolism)	3.8
SM_b20620		substrate-binding protein (simple sugar ABC transport system)	3.1

Continued on following page

Table 21-Continued

gene ID	Gene name	Production description (functions)	FC *dme*/wt
SMc00323	*rpsO*	30S ribosomal protein S15	-3.0
SMc00809		hypothetical protein	-3.2
SMc01791		hypothetical protein	-4.0
SMc01369	*rpmG*	50S ribosomal protein L33	-3.0
SMc00252		hypothetical protein	-4.1
SMc00198		hypothetical protein	-3.4
SMc04184		hypothetical protein	-4.6
SMc04186		hypothetical protein	-3.5
SMc04194		hypothetical protein	-3.1
SMc01551		hypothetical protein	-3.0
SMc01586		hypothetical protein	-3.2
SMc01523	*emrE*	Putative methyl viologen/ethidium resistance transmembrane protein	-3.8
SMa1678		hypothetical protein	-3.1
SM_b22008		hypothetical protein	-3.0
SM_b21329		hypothetical protein	-3.1
SM_b21574		hypothetical protein	-4.4
SM_b21685		hypothetical protein	-4.5
SM_b21456		hypothetical protein	-3.8
SM_b20711		hypothetical protein	-5.5

Genes are listed in order, FC (*dme*/wt) is fold change of gene expression (*S. meliloti* succinate-grown cells of the *dme* mutant vs wild type), and genes also found as significantly regulated in *tme* mutant grown on succinate are labeled by *. Significantly regulated genes: FC $\geq$ 3 and *P*-value (Student's *t* test) $\leq$ 0.05. Minus (-), genes significantly downregulated; wt, *S. meliloti* wild type strains RmP110; *dme*: *S. meliloti dme* mutant RmP2189.

Table 22 Differentially regulated genes in a glucose-grown *S. meliloti dme* mutant compared with wild-type strain

gene ID	Gene name	Production description (functions)	FC *dme*/wt
SMc00371		hypothetical protein	3.0
SMc00259		hypothetical protein	3.9
SMc00682#	*hipO1*	hippurate hydrolase, EC:3.5.1.32 (Phe metabolism)	3.1
SMc00703		hypothetical protein	3.1
SMc01509#		hypothetical protein	5.2
SMc01626		permease protein (putative multiple sugar ABC transport system)	3.5
SMc04028#	*gltB*	glutamate synthase, EC:1.4.1.13 (biosynthesis of Glu from 2-oxoglutarate)	3.9
SMc04220#		transcriptional regulator	13.0
SMa0134		hypothetical protein	3.6
SMa0714		ATP-binding protein (putative multiple sugar ABC transport system)	3.9
SMa0747		hypothetical protein	6.0
SMa1093#		hypothetical protein	5.9
SMa1427#		periplasmic solute-binding protein (putative simple sugar ABC transport system)	3.0
SMa1711		arginase, EC:3.5.3.1 (Arg and Pro metabolism)	3.9
SM_b20007	*katC*	catalase C protein, EC:1.11.1.6 (decomposition of hydrogen peroxide to water and oxygen)	3.4
SM_b20227#	*ndiA-1*	nutrient deprivation-induced protein	4.1
SM_b20414		hypothetical protein	5.8
SM_b20467		Putative sensor kinase (trancsriptional regulation)	4.0
SM_b21115		Putative response regulator (trancsriptional regulation)	3.3
SM_b21395		hypothetical protein	4.3
SM_b21441#		Inosine-*5′*-monophosphate dehydrogenase, EC:1.1.1.205 (synthesis of GTP from IMP)	3.6

Continued on following page

Table 22-Continued

gene ID	Gene name	Production description (functions)	FC *dme*/wt
SM_b21442		hypothetical protein	3.4
SM_b21483		hypothetical protein	3.0
SMc02180		hypothetical protein	-3.1
SMc02372#		Putative MFS permease	-3.7
SMc02028#		permease protein (peptide/nickel ABC transport system)	-4.2
SMc02035		Oxidoreductase	-3.7
SMc03107		hypothetical protein	-16.5
SMc02525	*fdsB*	NAD-dependent formate dehydrogenase subunit beta, EC:1.2.1.2 (Methonal metabolism)	-3.7
SMa1096		hypothetical protein	-4.2
SMa1386		Oxidoreductase	-4.0
SM_b20231		substrate-binding protein (putative multiple sugar transport system)	-9.2
SM_b21079		transcriptional regulator	-6.3
SM_b21154		hypothetical protein	-4.8
SM_b21162		Putative MFS permease	-5.7
SM_b21509		Putative plasmid stability protein	-6.1
SM_b21510		Putative plasmid stability protein	-7.8
SM_b20668		putative 3-hydroxyisobutyrate dehydrogenase, EC:1.1.1.31 (Val, Leu, and Ile metabolism)	-3.9
SM_b20622		ATP-binding protein (putative simple sugar ABC transport system)	-5.0
SM_b21633	*paaG*	Enoyl-CoA hydratase, EC:4.2.1.17 (metabolism of Phe to acetyl-CoA)	-3.1

Genes are listed in order, FC (*dme*/wt) is fold change of gene expression (*S. meliloti* glucose-grown cells of the *dme* mutant vs wild type), and genes also found as significantly regulated in *tme* mutant grown on glucose are labeled by #. Significantly regulated genes: FC $\geq$ 3 and *P*-value (Student's *t* test) $\leq$ 0.05. Minus (-), genes significantly downregulated; wt, *S. meliloti* wild type strains RmP110; *dme*$^-$: *S. meliloti dme* mutant RmP2189.

Table 23 Differentially regulated genes in a succinate-grown *S. meliloti tme* mutant compared with wild-type strain

gene ID	Gene name	Production description (functions)	FC *tme*/wt
SMc02874		N-acetylmuramic acid 6-phosphate etherase, EC:4.2.1.126 (Amino sugar and nucleotide sugar metabolism)	5.0
SMc01095	*mexF1*	multidrug-efflux system transmembrane protein (Bacterial efflux pumps)	3.4
SMc01093		Putative esterase/lipase (fatty acid metabolism)	3.4
SMc02224	*chaA*	calcium/proton antiporter transmembrane protein	3.2
SMc02229*		acyl-CoA dehydrogenase, EC:1.3.99.- (fatty acid metabolism)	3.1
SMc02328		hypothetical protein	3.0
SMc00045	*cycF*	Probable Cytochrome c556	3.5
SMc00559		hypothetical protein	5.7
SMc00569		hypothetical protein	26.8
SMc01317*	*rpoB*	DNA-directed RNA polymerase beta chain, EC:2.7.7.6 (transcription)	3.4
SMc01274*	*crcB*	signal peptide protein	3.1
SMc01036*		hypothetical protein	3.4
SMc02047	*gcvT*	glycine cleavage system aminomethyltransferase T, EC:2.1.2.10 (metabolism of Gly, Ser, and Thr)	3.8
SMc00253		signal peptide protein	3.4
SMc00478		hypothetical protein	3.6
SMc01424*	*nthA*	nitrile hydratase subunit alpha protein, EC:4.2.1.84 84 (metabolism of Trp and Xenobiotics, Styrene, Aminobenzoate, and Fluorobenzoate)	3.6
SMc01658*		Ferrioxamine B specific ferric iron reductase (iron uptake)	3.3
SMc01508		hypothetical protein	8.4
SMc01954		transcriptional regulator	3.4
SMc01992*		D-xylulose reductase, EC:1.1.1.9 (pentose and glucuronate interconversions)	4.6

Continued on following page

Table 23-Continued

gene ID	Gene name	Production description (functions)	FC *tme*/wt
SMc03131*		periplasmic solute-binding protein (polar amino acid ABC transport system)	12.7
SMc02515		hypothetical protein	7.2
SMc03858	*pheAa*	chorismate mutase, EC:5.4.99.5 (biosynthesis of Phe, Tyr, and Trp)	3.0
SMa0070*		simple sugar permease (ABC transport system)	11.1
SMa0171		hypothetical protein	3.1
SMa0237*		Dehydrogenase	3.3
SMa0631		hypothetical protein	3.4
SMa0800*		permease protein (spermidine/putrescine ABC transport system)	4.8
SMa1394		hypothetical protein	5.2
SMa1406*	*ttuD3*	hydroxypyruvate reductase, EC:1.1.1.81 (Gly, Ser and Thr metabolism)	21.2
SMa1817*		hypothetical protein	3.3
SMa1863*		permease protein (Peptides/nickel ABC transport system)	3.2
SMa1882*		transcriptional activator	5.1
SMa1907		hypothetical protein	3.8
SMa2269		hypothetical protein	8.8
SMa2349		xanthine dehydrogenase iron-sulfur-binding subunit (Purine metabolism)	5.3
SMa2351		xanthine dehydrogenase YagS FAD-binding subunit, EC:1.17.1.4 (Purine metabolism)	4.8
SMa2353		xanthine dehydrogenase YagR molybdenum-binding subunit, EC:1.17.1.4 (Purine metabolism)	3.6
SM_b20036*		periplasmic solute-binding protein (Putative TRAP-type quinic acid transport ststem)	5.2
SM_b20100		Putative dehydrogenase	3.2
SM_b20166*		hypothetical protein	3.1

Continued on following page

Table 23-Continued

gene ID	Gene name	Production description (functions)	FC *tme*/wt
SM_b20171*		Putative S-formylglutathione hydrolase, EC:3.1.2.12 (Methonal metabolism)	3.8
SM_b20172*		cytochrome c protein	3.1
SM_b20173*		methanol dehydrogenase large subunit (Methonal metabolism)	9.8
SM_b20174*		Putative cytochrome c	4.4
SM_b20175*		hypothetical protein	6.6
SM_b20206*	*pqqC*	PQQ biosynthesis protein (methonal metabolism)	3.0
SM_b20243		glycosyltransferase (biosynthesis polysaccharides)	3.8
SM_b20275		hypothetical protein	6.2
SM_b20342*		isoquinoline 1-oxidoreductase, EC:1.3.99.16	3.1
SM_b20373*		permease protein (putative TRAP-type dicarboxylate transport system)	6.1
SM_b21182*		hypothetical protein	6.4
SM_b21550*		hypothetical protein	3.5
SM_b21475*		hypothetical protein	4.4
SM_b20708*		methylated-DNA--protein-cysteine methyltransferase, EC:2.1.1.63 (repair of alkylated DNA)	6.0
SMc02586	*helO*	ATP-dependent helicase (DNA replication, transcription, translation, and repair)	-3.5
SMc00397		hypothetical protein	-5.0
SMc03025	*fliI*	Flagellum-specific ATP synthase, EC:3.6.3.14 (Cell motility)	-10.5
SMc01009		hypothetical protein	-10.2
SMc02448	*mutT*	Putative mutator protein 7,8-dihydro-8-oxoguanine-triphosphatase (DNA/RNA repair during replication and transcription)	-6.1
SMa5000		hypothetical protein	-12.3
SMa5015		hypothetical protein	-3.1

Continued on following page

Table 23-Continued

gene ID	Gene name	Production description (functions)	FC *tme*/wt
SMa1101		hypothetical protein	-5.3
SMa1643		hypothetical protein	-6.9
SM_b20257	*cyaM*	adenylate cyclase (conversion of ATP to cAMP)	-9.7
SM_b20375		transcriptional regulator	-4.2
SM_b20494		transcriptional regulator	-3.7
SM_b21027		hypothetical protein	-3.1
SM_b20876		hypothetical protein	-6.1

Genes are listed in order, FC (*tme*/wt) is fold change of gene expression (*S. meliloti* succinate-grown cells of the *tme* mutant vs wild type), and genes also found as significantly regulated in *dme* mutant grown on succinate are labeled by *.Significantly regulated genes: FC $\geq$ 3 and *P*-value (Student's *t* test) $\leq$ 0.05. Minus (-), genes significantly downregulated; wt, *S. meliloti* wild type strains RmP110; *tme*: *S. meliloti tme* mutant RmP2179

Table 24 Differentially regulated genes in a glucose-grown *S. meliloti tme* mutant compared with wild-type strain

gene ID	Gene name	Production description (functions)	FC *tme*/wt
SMc00364	*rplT*	50S ribosomal protein L20	3.1
SMc01159		oxidoreductase	3.1
SMc00796		hypothetical protein	3.2
SMc01316	*rpoC*	DNA-directed RNA polymerase subunit beta, EC:2.7.7.6 (Transcription)	3.6
SMc01186		hypothetical protein	3.6
SMc04220#		transcriptional regulator	10.4
SMc01509#		hypothetical protein	5.7
SMc00682#	*hipO1*	hippurate hydrolase, EC:3.5.1.32 (Phe metabolism)	3.9
SMc04028#	*gltB*	glutamate synthase, EC:1.4.1.13 (Ala, Asp and Glu metabolism)	3.8
SMc03773		hypothetical protein	3.2
SMc04385		Putative aldehyde dehydrogenase transmembrane protein (cofactor: NAD^+/$NADP^+$)	3.4
SMa0044		hypothetical protein	3.2
SMa0431		hypothetical protein	4.4
SMa1053		hypothetical protein	3.1
SMa1093#		hypothetical protein	3.9
SMa1427#		periplasmic solute-binding protein (putative simple sugar ABC transport system)	5.3
SMa1978		hydrolase	6.0
SMa2115	*gst13*	glutathione S-transferase, EC:2.5.1.18	3.1
SM_b20227#	*ndiA-1*	nutrient deprivation-induced protein	3.5
SM_b20251		hypothetical protein	6.2

Continued on following page

Table 24-Continued

gene ID	Gene name	Production description (functions)	FC *tme*/wt
SM_b20263		periplasmic hydroxyproline-binding protein (polar amino acid ABC transport system)	3.4
SM_b20331		hypothetical protein	6.4
SM_b20473		hypothetical protein	3.4
SM_b21032		hypothetical protein	3.8
SM_b21441#		Inosine-5′-monophosphate dehydrogenase, EC:1.1.1.205 (synthesis of GTP from IMP)	3.2
SM_b21486		Putative permease	3.3
SM_b20752		Putative enoyl-CoA hydratase, 4.2.1.17 (Fatty acid metabolism)	3.2
SMc01707		hypothetical protein	-4.3
SMc02372#		Putative MFS permease	-3.4
SMc00613	*acvB*	hypothetical protein	-6.8
SMc02817		hypothetical protein	-4.0
SMc01570		transcriptional regulator	-6.07
SMc02028#		permease protein (peptide/nickel ABC transport system)	-3.1
SMc02416		Putative guanine deaminase	-3.5
SMc03199		Putative molybdenum transport associated protein	-3.7
SMa1339		permease protein (putative multiple sugar ABC transport system)	-4.3
SMa1536	*nuoM2*	NADH:quinone oxidoreductase subunit M 2 (Oxidative phosphorylation)	-4.5
SMa2095		hypothetical protein	-3.3
SMa2347		hypothetical protein	-5.2
SM_b20319		hypothetical protein	-4.4
SM_b20403		Putative oxidoreductase subunit	-3.5

Continued on following page

Table 24-Continued

gene ID	Gene name	Production description (functions)	FC *tme*/wt
SM_b20518		hypothetical protein	-4.6
SM_b21044		Putative ATP-dependent DNA ligase (DNA repair)	-3.8
SM_b21368		cytochrome c oxidase subunit II (Oxidative phosphorylation)	-3.9
SM_b20916		hypothetical protein	-4.4
SM_b20673		ATP-binding protein (simple sugar ABC transport system)	-3.6

Genes are listed in order, FC (*tme*/wt) is fold change of gene expression (*S. meliloti* glucose-grown cells of the *tme* mutant vs wild type, and genes also found as significantly regulated in *dme* mutant grown on glucose are labeled by #. Significantly regulated genes: FC ≥ 3 and *P*-value (Student's *t* test) ≤ 0.05. Minus (-), genes significantly downregulated; wt, *S. meliloti* wild type strains RmP110; *tme*: *S. meliloti tme* mutant RmP2179

Chapter 7 General Conclusion

Symbiotic nitrogen fixation requires a high energy input. To provide energy and reductant for nitrogen fixation, C_4-dicarboxylic acids such as malate and succinate are metabolized via the tricarboxylic acid (TCA) cycle (Poole and Allaway 2000) (Figure 6). The maintenance of metabolic flux through the TCA cycle during C_4-dicarboxylic acid oxidation requires a pathway for the synthesis of acetyl-CoA (Figure 6). The Fix^- phenotype of *S. meliloti dme* mutant on alfalfa indicated that the activity of NAD^+-malic enzyme (DME) is essential for acetyl-CoA generation (Driscoll and Finan 1993). In contrast, *dme* mutants of *B. japonicum*, *R. leguminosarum*, and *Mesorhizobium loti* were shown to form Fix^+ nodules on soybean, pea, and *Lotus*, respectively (Dao *et al*. 2008;Mulley *et al*. 2010), which suggested that the formation of acetyl-CoA could occur either via DME or a pathway catalyzed by phosphoenolpyruvate carboxykinase (PCK). To gain further insight into the role of malic enzymes in nodules, we utilized the broad-host range *Sinorhizobium* strain NGR234 and isolated *dme* and *dme pckA* double mutants of this strain. We found that: 1) NGR234 *dme* mutants formed Fix^+ nodules with nitrogen fixation efficiencies that varied on different host plants (from 27 to 83% of the wild-type level); 2) Substantial PCK enzyme activity was present in NGR234 bacteroids isolated from the different host plants (50 to 180 nmol/minute/mg); and 3) Single *pckA* and single *dme* mutants of NGR234 form Fix^+ nodules with reduced N_2-fixation efficiencies on various host plant, but *dme pckA* double mutants were completely devoid of symbioticN_2-

fixing activity. These NGR234 data, together with other reports, demonstrated that the nitrogen fixation phenotype of *dme* mutants is host plant dependent and also suggested that the completely Fix^- phenotype of *S. meliloti dme* mutants is unusual and perhaps unique to the *S. meliloti*-alfalfa symbiosis.

Other studies suggested that malic enzyme mutants of *A. caulinodans* ORS571 formed Fix^- nodules (Suzuki *et al*. 2007, Tsukada *et al*. 2009), however this report was incomplete as the malic enzymes of *A. caulinodans* ORS571 had not been characterized. Accordingly we sought to examine the malic enzyme-related activities of the proteins encoded by *azc3656* and *azc0119*. These genes were cloned and purified as N-terminal His-tagged proteins. The AZC3656 protein was shown to be an NAD^+-malic enzyme and its activity was allosterically inhibited by acetyl-CoA and stimulated by fumarate and succinate. These characteristics indicated that the AZC3656 NAD^+-malic enzyme plays an important role in regulating the levels of TCA cycle intermediates, which is essential for the maintenance of the metabolic flux through the TCA cycle during C_4-dicarboxylic acid oxidation. Thus, the Fix^- phenotype of *A. caulinodans azc3656* insertion mutants on *Sesbania rostrata* seems to be identical to the Fix^- phenotype of *S. meliloti dme* mutants. Accordingly, we concluded that NAD^+-malic enzyme is essential for symbiotic nitrogen fixation in *A. caulinodans* and *S. meliloti,* but this activity can be bypassed via another pathway(s) in other rhizobia.

S. meliloti contains two distinct malic enzymes: DME and TME. Both proteins share similar apparent K_ms for substrate and cofactors, but differ in their responses to TCA cycle intermediates with allosteric regulation of DME activity (Voegele *et al*. 1999).

Previous reports showed that DME is essential for symbiotic nitrogen fixation and when exogenously expressed, TME failed to even partially function in place of DME for symbiotic N_2-fixation (Driscoll and Finan 1996; Driscoll and Finan 1997; Mitsch *et al*. 2007). One possible explanation for this failure is that the ratio of NADPH/$NADP^+$ in *S. meliloti* bacteroids might be high enough to prevent TME from functioning in the conversion of malate to pyruvate in nodules. However, we have not found any report where the ratios of NADPH/$NADP^+$ in *S. meliloti* bacteroids have been measured. To lower the NADPH/$NADP^+$ ratio, we overexpressed a soluble pyridine nucleotide transhydrogenase (STH) in *S. meliloti* bacteroids. However, the results reported in Chapter 5 indicated that STH activity failed to lower the ratio of NADPH/$NADP^+$ in *S. meliloti*. On the basis of a recent report regarding modification of the cofactor specificities of the human malic enzymes, we conducted a multiple sequence alignment of 15 malic enzyme proteins (8 related strains belonging to proteobacteria). Within the cofactor binding region, six amino acid residues were found to have the distribution tightly related with the cofactor specificity of malic enzymes, which suggested a possibility for us to alter the cofactor specificity of TME from $NADP^+$ to NAD^+ in further studies. It may lead us to know the reason why TME is prevented from functioning in nodules.

As previously reported, the differences in the biochemical characteristics of malic enzymes (Voegele *et al*. 1999) and symbiotic phenotype of *S. meliloti* malic enzyme mutants (Driscoll and Finan 1993;Driscoll and Finan 1996) suggested that DME and TME proteins might play different roles in central carbon metabolism of *S. meliloti*.

Investigation of the physiological functions of both malic enzymes might lead us to understand the reason why DME, but not TME is required for N_2- fixation. To investigate the physiological functions of DME and TME, we sought to identify the changes in gene expression that result from *dme* and *tme* mutants growing with succinate or glucose (chapter 6). The most striking differences in the transcriptome profiles were observed in succinate grown cells of the *dme* mutant. Of the 182 genes that are ≥ 3-fold upregulated, 80 genes (~45%) were involved in transport and metabolism of amino acids and carbohydrates. The functions of the upregulated genes, together with previous metabolite data reported by Smallbone, L.A (2006, M.Sc. thesis), suggest that the *dme* mutation lead to a disturbance of the central carbon metabolism during oxidation of succinate. Together with the biochemical characteristics of the malic enzymes, we assume that DME plays an important role in regulating the levels of TCA cycle intermediates, which is required for the maintenance of metabolic flux through the TCA cycle. On the other side, the changes of gene expression observed in *S. meliloti tme* mutants were too small to reveal a linkage between the physiological functions of TME protein and the central carbon metabolism in *S. meliloti* free-living cells. In view of the limited changes observed in transcriptome profiles and the large numbers of highly regulated genes with unknown functions, the LC-MS based metabolite analysis is a highly sensitive and discriminatory approach that may allow us to assess the differences caused by the disruption of *dme* or *tme* in *S. meliloti.*

REFERENCES

Agledal,L., Niere,M. and Ziegler,M. (2010) The phosphate makes a difference: cellular functions of NADP. *Redox. Rep.* **15**, 2-10.

Amadou,C., Pascal,G., Mangenot,S., Glew,M., Bontemps,C., Capela,D., Carrere,S., Cruveiller,S., Dossat,C., Lajus,A., Marchetti,M., Poinsot,V., Rouy,Z., Servin,B., Saad,M., Schenowitz,C., Barbe,V., Batut,J., Medigue,C. and Masson-Boivin,C. (2008) Genome sequence of the beta-rhizobium Cupriavidus taiwanensis and comparative genomics of rhizobia. *Genome Res.* **18**, 1472-1483.

Anthamatten,D., Scherb,B. and Hennecke,H. (1992) Characterization of a fixLJ-regulated Bradyrhizobium japonicum gene sharing similarity with the Escherichia coli fnr and Rhizobium meliloti fixK genes. *J. Bacteriol.* **174**, 2111-2120.

Arkblad,E.L., Betsholtz,C. and Rydstrom,J. (1996) The cDNA sequence of proton-pumping nicotinamide nucleotide transhydrogenase from man and mouse. *Biochim. Biophys. Acta* **1273**, 203-205.

Arwas,R., Mckay,I.A., Rowney,F.R.P., Dilworth,M.J. and Glenn,A.R. (1985) Properties of Organic-Acid Utilization Mutants of Rhizobium-Leguminosarum Strain-300. *Journal of General Microbiology* **131**, 2059-2066.

Bardin,S.D., Voegele,R.T. and Finan,T.M. (1998) Phosphate assimilation in Rhizobium (Sinorhizobium) meliloti: identification of a pit-like gene. *J. Bacteriol.* **180**, 4219-4226.

Barnett,M.J., Fisher,R.F., Jones,T., Komp,C., Abola,A.P., Barloy-Hubler,F., Bowser,L., Capela,D., Galibert,F., Gouzy,J., Gurjal,M., Hong,A., Huizar,L., Hyman,R.W., Kahn,D., Kahn,M.L., Kalman,S., Keating,D.H., Palm,C., Peck,M.C., Surzycki,R., Wells,D.H., Yeh,K.C., Davis,R.W., Federspiel,N.A. and Long,S.R. (2001) Nucleotide sequence and predicted functions of the entire Sinorhizobium meliloti pSymA megaplasmid. *Proc. Natl. Acad. Sci. U. S. A* **98**, 9883-9888.

Barnett,M.J., Toman,C.J., Fisher,R.F. and Long,S.R. (2004) A dual-genome Symbiosis Chip for coordinate study of signal exchange and development in a prokaryote-host interaction. *Proc. Natl. Acad. Sci. U. S. A* **101**, 16636-16641.

Batista,S., Catalan,A.I., Hernandez-Lucas,I., Martinez-Romero,E., Aguilar,O.M. and Martinez-Drets,G. (2001) Identification of a system that allows a Rhizobium tropici dctA mutant to grow on succinate, but not on other C4-dicarboxylates. *Can. J. Microbiol.* **47**, 509-518.

Batut,J., Andersson,S.G. and O'Callaghan,D. (2004) The evolution of chronic infection strategies in the alpha-proteobacteria. *Nat. Rev. Microbiol.* **2**, 933-945.

Batut,J. and Boistard,P. (1994) Oxygen control in Rhizobium. *Antonie Van Leeuwenhoek* **66**, 129-150.

Bauer,E., Kaspar,T., Fischer,H.M. and Hennecke,H. (1998) Expression of the fixR-nifA operon in Bradyrhizobium japonicum depends on a new response regulator, RegR. *J. Bacteriol.* **180**, 3853-3863.

Becker,A., Berges,H., Krol,E., Bruand,C., Ruberg,S., Capela,D., Lauber,E., Meilhoc,E., Ampe,F., de Bruijn,F.J., Fourment,J., Francez-Charlot,A., Kahn,D., Kuster,H., Liebe,C., Puhler,A., Weidner,S. and Batut,J. (2004) Global changes in gene expression in Sinorhizobium meliloti 1021 under microoxic and symbiotic conditions. *Mol. Plant Microbe Interact.* **17**, 292-303.

Benson,D.R. (1988) The genus Frankia: actinomycete symbionts of plants. *Microbiol. Sci.* **5**, 9-12.

Benson,D.R. and Silvester,W.B. (1993) Biology of Frankia strains, actinomycete symbionts of actinorhizal plants. *Microbiol. Rev.* **57**, 293-319.

Bentley,S.D. and Parkhill,J. (2004) Comparative genomic structure of prokaryotes. *Annu. Rev. Genet.* **38**, 771-792.

Bhandari,B. and Nicholas,D.J. (1985) Proton motive force in washed cells of Rhizobium japonicum and bacteroids from Glycine max. *J. Bacteriol.* **164**, 1383-1385.

Blasing,O.E., Westhoff,P. and Svensson,P. (2000) Evolution of C4 phosphoenolpyruvate carboxylase in Flaveria, a conserved serine residue in the carboxyl-terminal part of the enzyme is a major determinant for C4-specific characteristics. *J. Biol. Chem.* **275**, 27917-27923.

Blondelet-Rouault,M.H., Weiser,J., Lebrihi,A., Branny,P. and Pernodet,J.L. (1997) Antibiotic resistance gene cassettes derived from the omega interposon for use in E. coli and Streptomyces. *Gene* **190**, 315-317.

Bonaldi,K., Gargani,D., Prin,Y., Fardoux,J., Gully,D., Nouwen,N., Goormachtig,S. and Giraud,E. (2011) Nodulation of Aeschynomene afraspera and A. indica by photosynthetic Bradyrhizobium Sp. strain ORS285: the nod-dependent versus the nod-independent symbiotic interaction. *Mol. Plant Microbe Interact.* **24**, 1359-1371.

Boonstra,B., French,C.E., Wainwright,I. and Bruce,N.C. (1999) The udhA gene of Escherichia coli encodes a soluble pyridine nucleotide transhydrogenase. *J. Bacteriol.* **181**, 1030-1034.

Boonstra,B., Rathbone,D.A., French,C.E., Walker,E.H. and Bruce,N.C. (2000) Cofactor regeneration by a soluble pyridine nucleotide transhydrogenase for biological production of hydromorphone. *Appl. Environ. Microbiol.* **66**, 5161-5166.

Boussau,B., Karlberg,E.O., Frank,A.C., Legault,B.A. and Andersson,S.G. (2004) Computational inference of scenarios for alpha-proteobacterial genome evolution. *Proc. Natl. Acad. Sci. U. S. A* **101**, 9722-9727.

Bradford,M.M. (1976) Rapid and Sensitive Method for Quantitation of Microgram Quantities of Protein Utilizing Principle of Protein-Dye Binding. *Analytical Biochemistry* **72**, 248-254.

Brigle,K.E., Weiss,M.C., Newton,W.E. and Dean,D.R. (1987) Products of the iron-molybdenum cofactor-specific biosynthetic genes, nifE and nifN, are structurally homologous to the products of the nitrogenase molybdenum-iron protein genes, nifD and nifK. *J. Bacteriol.* **169**, 1547-1553.

Caetano-Anolles,G., Wrobel-Boerner,E. and Bauer,W.D. (1992) Growth and Movement of Spot Inoculated Rhizobium meliloti on the Root Surface of Alfalfa. *Plant Physiol* **98**, 1181-1189.

Capela,D., Carrere,S. and Batut,J. (2005) Transcriptome-based identification of the Sinorhizobium meliloti NodD1 regulon. *Appl. Environ. Microbiol.* **71**, 4910-4913.

Capela,D., Filipe,C., Bobik,C., Batut,J. and Bruand,C. (2006) Sinorhizobium meliloti differentiation during symbiosis with alfalfa: a transcriptomic dissection. *Mol. Plant Microbe Interact.* **19**, 363-372.

Capoen,W., Oldroyd,G., Goormachtig,S. and Holsters,M. (2010) Sesbania rostrata: a case study of natural variation in legume nodulation. *New Phytol.* **186**, 340-345.

Cermola,M., Fedorova,E., Tate,R., Riccio,A., Favre,R. and Patriarca,E.J. (2000) Nodule invasion and symbiosome differentiation during Rhizobium etli-Phaseolus vulgaris symbiosis. *Mol. Plant Microbe Interact.* **13**, 733-741.

Chan,J.M., Wu,W., Dean,D.R. and Seefeldt,L.C. (2000) Construction and characterization of a heterodimeric iron protein: defining roles for adenosine triphosphate in nitrogenase catalysis. *Biochemistry* **39**, 7221-7228.

Chan,M.K., Kim,J. and Rees,D.C. (1993) The nitrogenase FeMo-cofactor and P-cluster pair: 2.2 A resolution structures. *Science* **260**, 792-794.

Chang,A.C. and Cohen,S.N. (1978) Construction and characterization of amplifiable multicopy DNA cloning vehicles derived from the P15A cryptic miniplasmid. *J. Bacteriol.* **134**, 1141-1156.

Chen,W.M., Laevens,S., Lee,T.M., Coenye,T., De,V.P., Mergeay,M. and Vandamme,P. (2001) Ralstonia taiwanensis sp. nov., isolated from root nodules of Mimosa species and sputum of a cystic fibrosis patient. *Int. J. Syst. Evol. Microbiol.* **51**, 1729-1735.

Clawson,M.L. and Benson,D.R. (1999) Natural diversity of Frankia strains in actinorhizal root nodules from promiscuous hosts in the family Myricaceae. *Appl. Environ. Microbiol.* **65**, 4521-4527.

Cohen,P.T. and Kaplan,N.O. (1970a) Kinetic characteristics of the pyridine nucleotide transhydrogenase from Pseudomonas aeruginosa. *J. Biol. Chem.* **245**, 4666-4672.

Cohen,P.T. and Kaplan,N.O. (1970b) Purification and properties of the pyridine nucleotide transhydrogenase from Pseudomonas aeruginosa. *J. Biol. Chem.* **245**, 2825-2836.

Cooper,J.E. (2007) Early interactions between legumes and rhizobia: disclosing complexity in a molecular dialogue. *J. Appl. Microbiol.* **103**, 1355-1365.

Copeland,L., Quinnell,R.G. and Day,D.A. (1989a) Malic Enzyme-Activity in Bacterioids from Soybean Nodules. *Journal of General Microbiology* **135**, 2005-2011.

Copeland,L., Vella,J. and Hong,Z.Q. (1989b) Enzymes of Carbohydrate-Metabolism in Soybean Nodules. *Phytochemistry* **28**, 57-61.

Corbin,D., Ditta,G. and Helinski,D.R. (1982) Clustering of nitrogen fixation (nif) genes in Rhizobium meliloti. *J. Bacteriol.* **149**, 221-228.

Cowie,A., Cheng,J., Sibley,C.D., Fong,Y., Zaheer,R., Patten,C.L., Morton,R.M., Golding,G.B. and Finan,T.M. (2006) An integrated approach to functional genomics: construction of a novel reporter gene fusion library for Sinorhizobium meliloti. *Appl. Environ. Microbiol.* **72**, 7156-7167.

D'hooghe,I., Michiels,J., Vlassak,K., Verreth,C., Waelkens,F. and Vanderleyden,J. (1995) Structural and functional analysis of the fixLJ genes of Rhizobium leguminosarum biovar phaseoli CNPAF512. *Mol. Gen. Genet.* **249**, 117-126.

Danhorn,T. and Fuqua,C. (2007) Biofilm formation by plant-associated bacteria. *Annu. Rev. Microbiol.* **61**, 401-422.

Danino,V.E., Wilkinson,A., Edwards,A. and Downie,J.A. (2003) Recipient-induced transfer of the symbiotic plasmid pRL1JI in Rhizobium leguminosarum bv. viciae is regulated by a quorum-sensing relay. *Mol. Microbiol.* **50**, 511-525.

Dao,T.V., Nomura,M., Hamaguchi,R., Kato,K., Itakura,M., Minamisawa,K., Sinsuwongwat,S., Le,H.T., Kaneko,T., Tabata,S. and Tajima,S. (2008) NAD-Malic Enzyme Affects Nitrogen Fixing Activity of Bradyrhizobium japonicum USDA 110 Bacteroids in Soybean Nodules. *Microbes. Environ.* **23**, 215-220.

Datsenko,K.A. and Wanner,B.L. (2000) One-step inactivation of chromosomal genes in Escherichia coli K-12 using PCR products. *Proc. Natl. Acad. Sci. U. S. A* **97**, 6640-6645.

David,M., Daveran,M.L., Batut,J., Dedieu,A., Domergue,O., Ghai,J., Hertig,C., Boistard,P. and Kahn,D. (1988) Cascade regulation of nif gene expression in Rhizobium meliloti. *Cell* **54**, 671-683.

Day,D.A. and Copeland,L. (1991) Carbon Metabolism and Compartmentation in Nitrogen-Fixing Legume Nodules. *Plant Physiology and Biochemistry* **29**, 185-201.

de,L.P., Willems,A., Nick,G., Moreira,F., Molouba,F., Hoste,B., Torck,U., Neyra,M., Collins,M.D., Lindstrom,K., Dreyfus,B. and Gillis,M. (1998) Characterization of tropical tree rhizobia and description of Mesorhizobium plurifarium sp. nov. *Int. J. Syst. Bacteriol.* **48 Pt 2**, 369-382.

Dixon,R. and Kahn,D. (2004) Genetic regulation of biological nitrogen fixation. *Nat. Rev. Microbiol.* **2**, 621-631.

Dowling,D.N. and Broughton,W.J. (1986) Competition for nodulation of legumes. *Annu. Rev. Microbiol.* **40**, 131-157.

Driscoll,B.T. and Finan,T.M. (1993) NAD(+)-dependent malic enzyme of Rhizobium meliloti is required for symbiotic nitrogen fixation. *Mol. Microbiol.* **7**, 865-873.

Driscoll,B.T. and Finan,T.M. (1996) $NADP^+$ -dependent malic enzyme of Rhizobium meliloti. *J. Bacteriol.* **178**, 2224-2231.

Driscoll,B.T. and Finan,T.M. (1997) Properties of NAD(+)- and NADP(+)-dependent malic enzymes of Rhizobium (Sinorhizobium) meliloti and differential expression of their genes in nitrogen-fixing bacteroids. *Microbiology* **143 (Pt 2)**, 489-498.

Dupuy,N., Willems,A., Pot,B., Dewettinck,D., Vandenbruaene,I., Maestrojuan,G., Dreyfus,B., Kersters,K., Collins,M.D. and Gillis,M. (1994) Phenotypic and genotypic characterization of bradyrhizobia nodulating the leguminous tree Acacia albida. *Int. J. Syst. Bacteriol.* **44**, 461-473.

Earl,C.D., Ronson,C.W. and Ausubel,F.M. (1987) Genetic and structural analysis of the Rhizobium meliloti fixA, fixB, fixC, and fixX genes. *J. Bacteriol.* **169**, 1127-1136.

Einsle,O., Tezcan,F.A., Andrade,S.L., Schmid,B., Yoshida,M., Howard,J.B. and Rees,D.C. (2002) Nitrogenase MoFe-protein at 1.16 A resolution: a central ligand in the FeMo-cofactor. *Science* **297**, 1696-1700.

el-Din,A.K. (1992) A succinate transport mutant of Bradyrhizobium japonicum forms ineffective nodules on soybeans. *Can. J. Microbiol.* **38**, 230-234.

Elliott,G.N., Chen,W.M., Chou,J.H., Wang,H.C., Sheu,S.Y., Perin,L., Reis,V.M., Moulin,L., Simon,M.F., Bontemps,C., Sutherland,J.M., Bessi,R., de Faria,S.M., Trinick,M.J., Prescott,A.R., Sprent,J.I. and James,E.K. (2007) Burkholderia phymatum is a highly effective nitrogen-fixing symbiont of Mimosa spp. and fixes nitrogen ex planta. *New Phytol.* **173**, 168-180.

Emmerich,R., Hennecke,H. and Fischer,H.M. (2000) Evidence for a functional similarity between the two-component regulatory systems RegSR, ActSR, and RegBA (PrrBA) in alpha-Proteobacteria. *Arch. Microbiol.* **174**, 307-313.

Endre,G., Kereszt,A., Kevei,Z., Mihacea,S., Kalo,P. and Kiss,G.B. (2002) A receptor kinase gene regulating symbiotic nodule development. *Nature* **417**, 962-966.

Englard,S. and Siegal,L. 1969 Mitochondrial L-malate dehydrogenase of beef heart. Mathods enzymol. 13: 99-100.

Ferguson,B.J., Indrasumunar,A., Hayashi,S., Lin,M.H., Lin,Y.H., Reid,D.E. and Gresshoff,P.M. (2010) Molecular analysis of legume nodule development and autoregulation. *J. Integr. Plant Biol.* **52**, 61-76.

Finan,T.M. (2002) Evolving insights: symbiosis islands and horizontal gene transfer. *J. Bacteriol.* **184**, 2855-2856.

Finan,T.M., Hartweig,E., LeMieux,K., Bergman,K., Walker,G.C. and Signer,E.R. (1984) General transduction in Rhizobium meliloti. *J. Bacteriol.* **159**, 120-124.

Finan,T.M., Mcwhinnie,E., Driscoll,B. and Watson,R.J. (1991) Complex Symbiotic Phenotypes Result from Gluconeogenic Mutations in Rhizobium-Meliloti *Molecular Plant-Microbe Interactions* **4**, 386-392.

Finan,T.M., Oresnik,I. and Bottacin,A. (1988) Mutants of Rhizobium meliloti defective in succinate metabolism. *J. Bacteriol.* **170**, 3396-3403.

Finan,T.M., Wood,J.M. and Jordan,D.C. (1981) Succinate transport in Rhizobium leguminosarum. *J. Bacteriol.* **148**, 193-202.

Finan,T.M., Wood,J.M. and Jordan,D.C. (1983) Symbiotic properties of C4-dicarboxylic acid transport mutants of Rhizobium leguminosarum. *J. Bacteriol.* **154**, 1403-1413.

Fischer,H.M. (1994) Genetic regulation of nitrogen fixation in rhizobia. *Microbiol. Rev.* **58**, 352-386.

Fitzmaurice,A.M. and Ogara,F. (1991) Glutamate Catabolism in Rhizobium-Meliloti. *Archives of Microbiology* **155**, 422-427.

Fleischmann,R.D., Adams,M.D., White,O., Clayton,R.A., Kirkness,E.F., Kerlavage,A.R., Bult,C.J., Tomb,J.F., Dougherty,B.A., Merrick,J.M. and . (1995) Whole-genome random sequencing and assembly of Haemophilus influenzae Rd. *Science* **269**, 496-512.

Fraysse,N., Couderc,F. and Poinsot,V. (2003) Surface polysaccharide involvement in establishing the rhizobium-legume symbiosis. *Eur. J. Biochem.* **270**, 1365-1380.

Freiberg,C., Fellay,R., Bairoch,A., Broughton,W.J., Rosenthal,A. and Perret,X. (1997) Molecular basis of symbiosis between Rhizobium and legumes. *Nature* **387**, 394-401.

Freiberg,C., Perret,X., Broughton,W.J. and Rosenthal,A. (1996) Sequencing the 500-kb GC-rich symbiotic replicon of Rhizobium sp. NGR234 using dye terminators and a thermostable "sequenase": a beginning. *Genome Res.* **6**, 590-600.

French,C.E., Boonstra,B., Bufton,K.A. and Bruce,N.C. (1997) Cloning, sequence, and properties of the soluble pyridine nucleotide transhydrogenase of Pseudomonas fluorescens. *J. Bacteriol.* **179**, 2761-2765.

Friedman,T.E. and F.O'Gara. (1943) Pyruvic acid: II the determination of keto acids in the blood and urine. J. Bio. Chem. 147: 421

Fujishige,N.A., Kapadia,N.N., De Hoff,P.L. and Hirsch,A.M. (2006) Investigations of Rhizobium biofilm formation. *FEMS Microbiol. Ecol.* **56**, 195-206.

Gage,D.J. (2004) Infection and invasion of roots by symbiotic, nitrogen-fixing rhizobia during nodulation of temperate legumes. *Microbiol. Mol. Biol. Rev.* **68**, 280-300.

Galibert,F., Finan,T.M., Long,S.R., Puhler,A., Abola,P., Ampe,F., Barloy-Hubler,F., Barnett,M.J., Becker,A., Boistard,P., Bothe,G., Boutry,M., Bowser,L., Buhrmester,J., Cadieu,E., Capela,D., Chain,P., Cowie,A., Davis,R.W., Dreano,S., Federspiel,N.A., Fisher,R.F., Gloux,S., Godrie,T., Goffeau,A., Golding,B., Gouzy,J., Gurjal,M., Hernandez-Lucas,I., Hong,A., Huizar,L., Hyman,R.W., Jones,T., Kahn,D., Kahn,M.L., Kalman,S., Keating,D.H., Kiss,E., Komp,C., Lelaure,V., Masuy,D., Palm,C., Peck,M.C., Pohl,T.M., Portetelle,D., Purnelle,B., Ramsperger,U., Surzycki,R., Thebault,P., Vandenbol,M., Vorholter,F.J., Weidner,S., Wells,D.H., Wong,K., Yeh,K.C. and Batut,J. (2001) The composite genome of the legume symbiont Sinorhizobium meliloti. *Science* **293**, 668-672.

Georgiadis,M.M., Komiya,H., Chakrabarti,P., Woo,D., Kornuc,J.J. and Rees,D.C. (1992) Crystallographic structure of the nitrogenase iron protein from Azotobacter vinelandii. *Science* **257**, 1653-1659.

Gibson,K.E., Kobayashi,H. and Walker,G.C. (2008) Molecular determinants of a symbiotic chronic infection. *Annu. Rev. Genet.* **42**, 413-441.

Giraud,E. and Fleischman,D. (2004) Nitrogen-fixing symbiosis between photosynthetic bacteria and legumes. *Photosynth. Res.* **82**, 115-130.

Giraud,E., Moulin,L., Vallenet,D., Barbe,V., Cytryn,E., Avarre,J.C., Jaubert,M., Simon,D., Cartieaux,F., Prin,Y., Bena,G., Hannibal,L., Fardoux,J., Kojadinovic,M., Vuillet,L., Lajus,A., Cruveiller,S., Rouy,Z., Mangenot,S., Segurens,B., Dossat,C., Franck,W.L., Chang,W.S., Saunders,E., Bruce,D., Richardson,P., Normand,P., Dreyfus,B., Pignol,D., Stacey,G., Emerich,D., Vermeglio,A., Medigue,C. and Sadowsky,M. (2007) Legumes symbioses: absence of Nod genes in photosynthetic bradyrhizobia. *Science* **316**, 1307-1312.

Glazebrook,J., Ichige,A. and Walker,G.C. (1993) A Rhizobium meliloti homolog of the Escherichia coli peptide-antibiotic transport protein SbmA is essential for bacteroid development. *Genes Dev.* **7**, 1485-1497.

Gonzalez,V., Bustos,P., Ramirez-Romero,M.A., Medrano-Soto,A., Salgado,H., Hernandez-Gonzalez,I., Hernandez-Celis,J.C., Quintero,V., Moreno-Hagelsieb,G., Girard,L., Rodriguez,O., Flores,M., Cevallos,M.A., Collado-Vides,J., Romero,D. and Davila,G. (2003) The mosaic structure of the symbiotic plasmid of Rhizobium etli CFN42 and its relation to other symbiotic genome compartments. *Genome Biol.* **4**, R36.

Gonzalez,V., Santamaria,R.I., Bustos,P., Hernandez-Gonzalez,I., Medrano-Soto,A., Moreno-Hagelsieb,G., Janga,S.C., Ramirez,M.A., Jimenez-Jacinto,V., Collado-Vides,J.

and Davila,G. (2006) The partitioned Rhizobium etli genome: genetic and metabolic redundancy in seven interacting replicons. *Proc. Natl. Acad. Sci. U. S. A* **103**, 3834-3839.

Goormachtig,S., Mergaert,P., Van,M.M. and Holsters,M. (1998) The symbiotic interaction between Azorhizobium caulinodans and Sesbania rostrata molecular cross-talk in a beneficial plant-bacterium interaction. *Subcell. Biochem.* **29**, 117-164.

Gordon,A.J., Minchin,F.R., James,C.L. and Komina,O. (1999) Sucrose synthase in legume nodules is essential for nitrogen fixation. *Plant Physiology* **120**, 867-877.

Gosink,M.M., Franklin,N.M. and Roberts,G.P. (1990) The product of the Klebsiella pneumoniae nifX gene is a negative regulator of the nitrogen fixation (nif) regulon. *J. Bacteriol.* **172**, 1441-1447.

Gottfert,M., Rothlisberger,S., Kundig,C., Beck,C., Marty,R. and Hennecke,H. (2001) Potential symbiosis-specific genes uncovered by sequencing a 410-kilobase DNA region of the Bradyrhizobium japonicum chromosome. *J. Bacteriol.* **183**, 1405-1412.

Green,L.S. and Emerich,D.W. (1997) The Formation of Nitrogen-Fixing Bacteroids Is Delayed but Not Abolished in Soybean Infected by an [alpha]-Ketoglutarate Dehydrogenase-Deficient Mutant of Bradyrhizobium japonicum. *Plant Physiol* **114**, 1359-1368.

Guan,C., Pawlowski,K. and Bisseling,T. (1998) Interaction between Frankia and actinorhizal plants. *Subcell. Biochem.* **29**, 165-189.

Gulash,M., Ames,P., Larosiliere,R.C. and Bergman,K. (1984) Rhizobia are attracted to localized sites on legume roots. *Appl. Environ. Microbiol.* **48**, 149-152.

Guo,H., Sun,S., Finan,T.M. and Xu,J. (2005) Novel DNA sequences from natural strains of the nitrogen-fixing symbiotic bacterium Sinorhizobium meliloti. *Appl. Environ. Microbiol.* **71**, 7130-7138.

Hageman,R.V. and Burris,R.H. (1978) Nitrogenase and nitrogenase reductase associate and dissociate with each catalytic cycle. *Proc. Natl. Acad. Sci. U. S. A* **75**, 2699-2702.

Halbleib,C.M. and Ludden,P.W. (2000) Regulation of biological nitrogen fixation. *J. Nutr.* **130**, 1081-1084.

Harborne,J.B. and Williams,C.A. (2000) Advances in flavonoid research since 1992. *Phytochemistry* **55**, 481-504.

Harborne,J.B. and Williams,C.A. (2001) Anthocyanins and other flavonoids. *Nat. Prod. Rep.* **18**, 310-333.

Hartwig,U.A., Maxwell,C.A., Joseph,C.M. and Phillips,D.A. (1990) Effects of alfalfa nod gene-inducing flavonoids on nodABC transcription in Rhizobium meliloti strains containing different nodD genes. *J. Bacteriol.* **172**, 2769-2773.

He,X., Chang,W., Pierce,D.L., Seib,L.O., Wagner,J. and Fuqua,C. (2003) Quorum sensing in Rhizobium sp. strain NGR234 regulates conjugal transfer (tra) gene expression and influences growth rate. *J. Bacteriol.* **185**, 809-822.

Hennecke,H. (1990) Nitrogen fixation genes involved in the Bradyrhizobium japonicum-soybean symbiosis. *FEBS Lett.* **268**, 422-426.

Hill,S. (1988) How is nitrogenase regulated by oxygen? *FEMS Microbiol. Rev.* **4**, 111-129.

Hirsch,A.M., Lum,M.R. and Downie,J.A. (2001) What makes the rhizobia-legume symbiosis so special? *Plant Physiol* **127**, 1484-1492.

Hsieh,J.Y. and Hung,H.C. (2009) Engineering of the cofactor specificities and isoform-specific inhibition of malic enzyme. *J. Biol. Chem.* **284**, 4536-4544.

Ichige,A. and Walker,G.C. (1997) Genetic analysis of the Rhizobium meliloti bacA gene: functional interchangeability with the Escherichia coli sbmA gene and phenotypes of mutants. *J. Bacteriol.* **179**, 209-216.

Jefferson,R.A., Burgess,S.M. and Hirsh,D. (1986) beta-Glucuronidase from Escherichia coli as a gene-fusion marker. *Proc. Natl. Acad. Sci. U. S. A* **83**, 8447-8451.

Jones,J.D. and Gutterson,N. (1987) An efficient mobilizable cosmid vector, pRK7813, and its use in a rapid method for marker exchange in Pseudomonas fluorescens strain HV37a. *Gene* **61**, 299-306.

Jording,D. and Puhler,A. (1993) The membrane topology of the Rhizobium meliloti C4-dicarboxylate permease (DctA) as derived from protein fusions with Escherichia coli K12 alkaline phosphatase (PhoA) and beta-galactosidase (LacZ). *Mol. Gen. Genet.* **241**, 106-114.

Jourand,P., Giraud,E., Bena,G., Sy,A., Willems,A., Gillis,M., Dreyfus,B. and de,L.P. (2004) Methylobacterium nodulans sp. nov., for a group of aerobic, facultatively methylotrophic, legume root-nodule-forming and nitrogen-fixing bacteria. *Int. J. Syst. Evol. Microbiol.* **54**, 2269-2273.

Jourand,P., Renier,A., Rapior,S., Miana de,F.S., Prin,Y., Galiana,A., Giraud,E. and Dreyfus,B. (2005) Role of methylotrophy during symbiosis between Methylobacterium nodulans and Crotalaria podocarpa. *Mol. Plant Microbe Interact.* **18**, 1061-1068.

Kaminski,P.A. and Elmerich,C. (1991) Involvement of fixLJ in the regulation of nitrogen fixation in Azorhizobium caulinodans. *Mol. Microbiol.* **5**, 665-673.

Kaneko,T., Nakamura,Y., Sato,S., Asamizu,E., Kato,T., Sasamoto,S., Watanabe,A., Idesawa,K., Ishikawa,A., Kawashima,K., Kimura,T., Kishida,Y., Kiyokawa,C., Kohara,M., Matsumoto,M., Matsuno,A., Mochizuki,Y., Nakayama,S., Nakazaki,N., Shimpo,S., Sugimoto,M., Takeuchi,C., Yamada,M. and Tabata,S. (2000) Complete genome structure of the nitrogen-fixing symbiotic bacterium Mesorhizobium loti. *DNA Res.* **7**, 331-338.

Kaneko,T., Nakamura,Y., Sato,S., Minamisawa,K., Uchiumi,T., Sasamoto,S., Watanabe,A., Idesawa,K., Iriguchi,M., Kawashima,K., Kohara,M., Matsumoto,M., Shimpo,S., Tsuruoka,H., Wada,T., Yamada,M. and Tabata,S. (2002) Complete genomic sequence of nitrogen-fixing symbiotic bacterium Bradyrhizobium japonicum USDA110. *DNA Res.* **9**, 189-197.

Kaparullina,E.N., Bykova,T.V., Fedorov,D.N., Doronina,N.V. and Trotsenko,I. (2011) [Methanol metabolism in the rhizosphere phytosymbiotic organism Methylobacterium nodulans]. *Mikrobiologiia* **80**, 847-849.

Kape,R., Parniske,M. and Werner,D. (1991) Chemotaxis and nod Gene Activity of Bradyrhizobium japonicum in Response to Hydroxycinnamic Acids and Isoflavonoids. *Appl. Environ. Microbiol.* **57**, 316-319.

Karr,D.B., Waters,J.K., Suzuki,F. and Emerich,D.W. (1984) Enzymes of the Poly-beta-Hydroxybutyrate and Citric Acid Cycles of Rhizobium japonicum Bacteroids. *Plant Physiol* **75**, 1158-1162.

Karunakaran,R., Ramachandran,V.K., Seaman,J.C., East,A.K., Mouhsine,B., Mauchline,T.H., Prell,J., Skeffington,A. and Poole,P.S. (2009) Transcriptomic analysis of Rhizobium leguminosarum biovar viciae in symbiosis with host plants Pisum sativum and Vicia cracca. *J. Bacteriol.* **191**, 4002-4014.

Keyser,H.H., van,B.P. and Weber,D.F. (1982) A Comparative Study of the Physiology of Symbioses Formed by Rhizobium japonicum with Glycine max, Vigna unguiculata, and Macroptilium atropurpurem. *Plant Physiol* **70**, 1626-1630.

Kim,J. and Rees,D.C. (1992) Structural models for the metal centers in the nitrogenase molybdenum-iron protein. *Science* **257**, 1677-1682.

Kim,S. and Burgess,B.K. (1996) Evidence for the direct interaction of the nifW gene product with the MoFe protein. *J. Biol. Chem.* **271**, 9764-9770.

Kim,S.A. and Copeland,L. (1996) Enzymes of Poly-(beta)-Hydroxybutyrate Metabolism in Soybean and Chickpea Bacteroids. *Appl. Environ. Microbiol.* **62**, 4186-4190.

Kouchi,H., Fukai,K., Katagiri,H., Minamisawa,K. and Tajima,S. (1988) Isolation and Enzymological Characterization of Infected and Uninfected Cell Protoplasts from Root-Nodules of Glycine-Max. *Physiologia Plantarum* **73**, 327-334.

Kouchi,H. and Nakaji,K. (1985) Utilization and Metabolism of Photoassimilated C-13 in Soybean Roots and Nodules. *Soil Science and Plant Nutrition* **31**, 323-334.

Kumar,S., Bourdes,A. and Poole,P. (2005) De novo alanine synthesis by bacteroids of Mesorhizobium loti is not required for nitrogen transfer in the determinate nodules of Lotus corniculatus. *J. Bacteriol.* **187**, 5493-5495.

Kundig,C., Hennecke,H. and Gottfert,M. (1993) Correlated physical and genetic map of the Bradyrhizobium japonicum 110 genome. *J. Bacteriol.* **175**, 613-622.

Kuzma,M.M., Hunt,S. and Layzell,D.B. (1993) Role of Oxygen in the Limitation and Inhibition of Nitrogenase Activity and Respiration Rate in Individual Soybean Nodules. *Plant Physiol* **101**, 161-169.

Lafay,B., Bullier,E. and Burdon,J.J. (2006) Bradyrhizobia isolated from root nodules of Parasponia (Ulmaceae) do not constitute a separate coherent lineage. *Int. J. Syst. Evol. Microbiol.* **56**, 1013-1018.

Laguerre,G., Allard,M.R., Revoy,F. and Amarger,N. (1994) Rapid Identification of Rhizobia by Restriction Fragment Length Polymorphism Analysis of PCR-Amplified 16S rRNA Genes. *Appl. Environ. Microbiol.* **60**, 56-63.

Lee,K.B., De,B.P., Aono,T., Liu,C.T., Suzuki,S., Suzuki,T., Kaneko,T., Yamada,M., Tabata,S., Kupfer,D.M., Najar,F.Z., Wiley,G.B., Roe,B., Binnewies,T.T., Ussery,D.W., D'Haeze,W., Herder,J.D., Gevers,D., Vereecke,D., Holsters,M. and Oyaizu,H. (2008) The genome of the versatile nitrogen fixer Azorhizobium caulinodans ORS571. *BMC. Genomics* **9**, 271.

Lerouge,P., Roche,P., Faucher,C., Maillet,F., Truchet,G., Prome,J.C. and Denarie,J. (1990) Symbiotic host-specificity of Rhizobium meliloti is determined by a sulphated and acylated glucosamine oligosaccharide signal. *Nature* **344**, 781-784.

Leung,K., Wanjage,F.N. and Bottomley,P.J. (1994) Symbiotic Characteristics of Rhizobium leguminosarum bv. trifolii Isolates Which Represent Major and Minor Nodule-Occupying Chromosomal Types of Field-Grown Subclover (Trifolium subterraneum L.). *Appl. Environ. Microbiol.* **60**, 427-433.

Levy,J., Bres,C., Geurts,R., Chalhoub,B., Kulikova,O., Duc,G., Journet,E.P., Ane,J.M., Lauber,E., Bisseling,T., Denarie,J., Rosenberg,C. and Debelle,F. (2004) A putative Ca2+ and calmodulin-dependent protein kinase required for bacterial and fungal symbioses. *Science* **303**, 1361-1364.

Limpens,E. and Bisseling,T. (2003) Signaling in symbiosis. *Curr. Opin. Plant Biol.* **6**, 343-350.

Lin,D.X., Wang,E.T., Tang,H., Han,T.X., He,Y.R., Guan,S.H. and Chen,W.X. (2008) Shinella kummerowiae sp. nov., a symbiotic bacterium isolated from root nodules of the herbal legume Kummerowia stipulacea. *Int. J. Syst. Evol. Microbiol.* **58**, 1409-1413.

Lodwig,E. and Poole,P. (2003) Metabolism of Rhizobium bacteroids. *Critical Reviews in Plant Sciences* **22**, 37-78.

Lodwig,E.M., Hosie,A.H., Bourdes,A., Findlay,K., Allaway,D., Karunakaran,R., Downie,J.A. and Poole,P.S. (2003) Amino-acid cycling drives nitrogen fixation in the legume-Rhizobium symbiosis. *Nature* **422**, 722-726.

Loeber,G., Dworkin,M.B., Infante,A. and Ahorn,H. (1994a) Characterization of cytosolic malic enzyme in human tumor cells. *FEBS Lett.* **344**, 181-186.

Loeber,G., Infante,A.A., Maurer-Fogy,I., Krystek,E. and Dworkin,M.B. (1991) Human NAD(+)-dependent mitochondrial malic enzyme. cDNA cloning, primary structure, and expression in Escherichia coli. *J. Biol. Chem.* **266**, 3016-3021.

Loeber,G., Maurer-Fogy,I. and Schwendenwein,R. (1994b) Purification, cDNA cloning and heterologous expression of the human mitochondrial NADP(+)-dependent malic enzyme. *Biochem. J.* **304 (Pt 3)**, 687-692.

Lohar,D.P., Sharopova,N., Endre,G., Penuela,S., Samac,D., Town,C., Silverstein,K.A. and VandenBosch,K.A. (2006) Transcript analysis of early nodulation events in Medicago truncatula. *Plant Physiol* **140**, 221-234.

Lois,A.F., Weinstein,M., Ditta,G.S. and Helinski,D.R. (1993) Autophosphorylation and phosphatase activities of the oxygen-sensing protein FixL of Rhizobium meliloti are coordinately regulated by oxygen. *J. Biol. Chem.* **268**, 4370-4375.

Long,S.R. (1989) Rhizobium-legume nodulation: life together in the underground. *Cell* **56**, 203-214.

Long,S.R. (1996) Rhizobium symbiosis: nod factors in perspective. *Plant Cell* **8**, 1885-1898.

MacLean,A.M., Finan,T.M. and Sadowsky,M.J. (2007) Genomes of the symbiotic nitrogen-fixing bacteria of legumes. *Plant Physiol* **144**, 615-622.

Madsen,E.B., Madsen,L.H., Radutoiu,S., Olbryt,M., Rakwalska,M., Szczyglowski,K., Sato,S., Kaneko,T., Tabata,S., Sandal,N. and Stougaard,J. (2003) A receptor kinase gene of the LysM type is involved in legume perception of rhizobial signals. *Nature* **425**, 637-640.

Mandon,K., Kaminski,P.A. and Elmerich,C. (1994) Functional analysis of the fixNOQP region of Azorhizobium caulinodans. *J. Bacteriol.* **176**, 2560-2568.

Marchler-Bauer,A., Lu,S., Anderson,J.B., Chitsaz,F., Derbyshire,M.K., DeWeese-Scott,C., Fong,J.H., Geer,L.Y., Geer,R.C., Gonzales,N.R., Gwadz,M., Hurwitz,D.I., Jackson,J.D., Ke,Z., Lanczycki,C.J., Lu,F., Marchler,G.H., Mullokandov,M., Omelchenko,M.V., Robertson,C.L., Song,J.S., Thanki,N., Yamashita,R.A., Zhang,D., Zhang,N., Zheng,C. and Bryant,S.H. (2011) CDD: a Conserved Domain Database for the functional annotation of proteins. *Nucleic Acids Res.* **39**, D225-D229.

Maria de Souza,M.F., Cruz,L., Miana de,F.S., Marsh,T., Martinez-Romero,E., de Oliveira,P.F., Maria,P.R. and Peter,W.Y. (2006) Azorhizobium doebereinerae sp. Nov. Microsymbiont of Sesbania virgata (Caz.) Pers. *Syst. Appl. Microbiol.* **29**, 197-206.

Marie,C., Barny,M.A. and Downie,J.A. (1992) Rhizobium leguminosarum has two glucosamine synthases, GlmS and NodM, required for nodulation and development of nitrogen-fixing nodules. *Mol. Microbiol.* **6**, 843-851.

Martinez-Romero,E., Segovia,L., Mercante,F.M., Franco,A.A., Graham,P. and Pardo,M.A. (1991) Rhizobium tropici, a novel species nodulating Phaseolus vulgaris L. beans and Leucaena sp. trees. *Int. J. Syst. Bacteriol.* **41**, 417-426.

Masson-Boivin,C., Giraud,E., Perret,X. and Batut,J. (2009) Establishing nitrogen-fixing symbiosis with legumes: how many rhizobium recipes? *Trends Microbiol.* **17**, 458-466.

McAllister,C.F. and Lepo,J.E. (1983) Succinate transport by free-living forms of Rhizobium japonicum. *J. Bacteriol.* **153**, 1155-1162.

Mckay,I.A., Dilworth,M.J. and Glenn,A.R. (1988) C-4-Dicarboxylate Metabolism in Free-Living and Bacteroid Forms of Rhizobium-Leguminosarum Mnf3841. *Journal of General Microbiology* **134**, 1433-1440.

Mckay,I.A., Dilworth,M.J. and Glenn,A.R. (1989) Carbon Catabolism in Continuous Cultures and Bacteroids of Rhizobium-Leguminosarum Mnf-3841. *Archives of Microbiology* **152**, 606-610.

Mckay,I.A., Glenn,A.R. and Dilworth,M.J. (1985) Gluconeogenesis in Rhizobium-Leguminosarum Mnf3841. *Journal of General Microbiology* **131**, 2067-2073.

Meade,H.M., Long,S.R., Ruvkun,G.B., Brown,S.E., and Ausubel,F.M. (1982) Physical and genetic characterization of symbiotic and auxotrophic mutants of Rhizobium meliloti induced by transposon Tn5 mutagenesis. J.Bacteriol. 149, 114-122.

Mesa,S., Hauser,F., Friberg,M., Malaguti,E., Fischer,H.M. and Hennecke,H. (2008) Comprehensive assessment of the regulons controlled by the FixLJ-FixK2-FixK1 cascade in Bradyrhizobium japonicum. *J. Bacteriol.* **190**, 6568-6579.

Mitra,R.M., Gleason,C.A., Edwards,A., Hadfield,J., Downie,J.A., Oldroyd,G.E. and Long,S.R. (2004) A Ca2+/calmodulin-dependent protein kinase required for symbiotic nodule development: Gene identification by transcript-based cloning. *Proc. Natl. Acad. Sci. U. S. A* **101**, 4701-4705.

Mitsch,M.J., Cowie,A. and Finan,T.M. (2007) Malic enzyme cofactor and domain requirements for symbiotic N2 fixation by Sinorhizobium meliloti. *J. Bacteriol.* **189**, 160-168.

Mitsch,M.J., Voegele,R.T., Cowie,A., Osteras,M. and Finan,T.M. (1998) Chimeric structure of the NAD(P)+- and NADP+-dependent malic enzymes of Rhizobium (Sinorhizobium) meliloti. *J. Biol. Chem.* **273**, 9330-9336.

Monson,E.K., Weinstein,M., Ditta,G.S. and Helinski,D.R. (1992) The FixL protein of Rhizobium meliloti can be separated into a heme-binding oxygen-sensing domain and a functional C-terminal kinase domain. *Proc. Natl. Acad. Sci. U. S. A* **89**, 4280-4284.

Moulin,L., Munive,A., Dreyfus,B. and Boivin-Masson,C. (2001) Nodulation of legumes by members of the beta-subclass of Proteobacteria. *Nature* **411**, 948-950.

Mulley,G., Lopez-Gomez,M., Zhang,Y., Terpolilli,J., Prell,J., Finan,T. and Poole,P. (2010) Pyruvate is synthesized by two pathways in pea bacteroids with different efficiencies for nitrogen fixation. *J. Bacteriol.* **192**, 4944-4953.

Murai,T., Tokushige,M., Nagai,J. and Katsuki,H. (1971a) Physiological functions of NAD- and NADP-linked malic enzymes in Escherichia coli. *Biochem. Biophys. Res. Commun.* **43**, 875-881.

Murai,T., Tokushige,M., Nagai,J. and Katsuki,H. (1971b) Physiological functions of NAD- and NADP-linked malic enzymes in Escherichia coli. *Biochem. Biophys. Res. Commun.* **43**, 875-881.

Nakamura,M., Bhatnagar,A. and Sadoshima,J. (2012) Overview of pyridine nucleotides review series. *Circ. Res.* **111**, 604-610.

Nap,J.P. and Bisseling,T. (1990) Developmental biology of a plant-prokaryote symbiosis: the legume root nodule. *Science* **250**, 948-954.

Nellen-Anthamatten,D., Rossi,P., Preisig,O., Kullik,I., Babst,M., Fischer,H.M. and Hennecke,H. (1998) Bradyrhizobium japonicum FixK2, a crucial distributor in the FixLJ-dependent regulatory cascade for control of genes inducible by low oxygen levels. *J. Bacteriol.* **180**, 5251-5255.

Ngom,A., Nakagawa,Y., Sawada,H., Tsukahara,J., Wakabayashi,S., Uchiumi,T., Nuntagij,A., Kotepong,S., Suzuki,A., Higashi,S. and Abe,M. (2004) A novel symbiotic nitrogen-fixing member of the Ochrobactrum clade isolated from root nodules of Acacia mangium. *J. Gen. Appl. Microbiol.* **50**, 17-27.

Nissen,T.L., Anderlund,M., Nielsen,J., Villadsen,J. and Kielland-Brandt,M.C. (2001) Expression of a cytoplasmic transhydrogenase in Saccharomyces cerevisiae results in formation of 2-oxoglutarate due to depletion of the NADPH pool. *Yeast* **18**, 19-32.

Oke,V. and Long,S.R. (1999a) Bacterial genes induced within the nodule during the Rhizobium-legume symbiosis. *Mol. Microbiol.* **32**, 837-849.

Oke,V. and Long,S.R. (1999b) Bacteroid formation in the Rhizobium-legume symbiosis. *Curr. Opin. Microbiol.* **2**, 641-646.

Oldroyd,G.E. and Downie,J.A. (2008) Coordinating nodule morphogenesis with rhizobial infection in legumes. *Annu. Rev. Plant Biol.* **59**, 519-546.

Osteras,M., Finan,T.M. and Stanley,J. (1991) Site-directed mutagenesis and DNA sequence of pckA of Rhizobium NGR234, encoding phosphoenolpyruvate carboxykinase: gluconeogenesis and host-dependent symbiotic phenotype. *Mol. Gen. Genet.* **230**, 257-269.

Ott,T., van Dongen,J.T., Gunther,C., Krusell,L., Desbrosses,G., Vigeolas,H., Bock,V., Czechowski,T., Geigenberger,P. and Udvardi,M.K. (2005) Symbiotic leghemoglobins are crucial for nitrogen fixation in legume root nodules but not for general plant growth and development. *Curr. Biol.* **15**, 531-535.

Ouyang,L.J., Whelan,J., Weaver,C.D., Roberts,D.M. and Day,D.A. (1991) Protein phosphorylation stimulates the rate of malate uptake across the peribacteroid membrane of soybean nodules. *FEBS Lett.* **293**, 188-190.

Parniske,M. and Downie,J.A. (2003) Plant biology: locks, keys and symbioses. *Nature* **425**, 569-570.

Patriarca,E.J., Tate,R. and Iaccarino,M. (2002) Key role of bacterial NH(4)(+) metabolism in Rhizobium-plant symbiosis. *Microbiol. Mol. Biol. Rev.* **66**, 203-222.

Perez-Mendoza,D., Dominguez-Ferreras,A., Munoz,S., Soto,M.J., Olivares,J., Brom,S., Girard,L., Herrera-Cervera,J.A. and Sanjuan,J. (2004) Identification of functional mob regions in Rhizobium etli: evidence for self-transmissibility of the symbiotic plasmid pRetCFN42d. *J. Bacteriol.* **186**, 5753-5761.

Perret,X., Staehelin,C. and Broughton,W.J. (2000) Molecular basis of symbiotic promiscuity. *Microbiol. Mol. Biol. Rev.* **64**, 180-201.

Phillips,D.A. (1980) Efficiency of Symbiotic Nitrogen-Fixation in Legumes. *Annual Review of Plant Physiology and Plant Molecular Biology* **31**, 29-49.

Pollak,N., Dolle,C. and Ziegler,M. (2007) The power to reduce: pyridine nucleotides--small molecules with a multitude of functions. *Biochem. J.* **402**, 205-218.

Poole,P. and Allaway,D. (2000) Carbon and nitrogen metabolism in Rhizobium. *Adv. Microb. Physiol* **43**, 117-163.

Preisig,O., Anthamatten,D. and Hennecke,H. (1993) Genes for a microaerobically induced oxidase complex in Bradyrhizobium japonicum are essential for a nitrogen-fixing endosymbiosis. *Proc. Natl. Acad. Sci. U. S. A* **90**, 3309-3313.

Preisig,O., Zufferey,R., Thony-Meyer,L., Appleby,C.A. and Hennecke,H. (1996) A high-affinity cbb3-type cytochrome oxidase terminates the symbiosis-specific respiratory chain of Bradyrhizobium japonicum. *J. Bacteriol.* **178**, 1532-1538.

Prell,J., Boesten,B., Poole,P. and Priefer,U.B. (2002) The Rhizobium leguminosarum bv. viciae VF39 gamma-aminobutyrate (GABA) aminotransferase gene (gabT) is induced by GABA and highly expressed in bacteroids. *Microbiology* **148**, 615-623.

Prell,J. and Poole,P. (2006) Metabolic changes of rhizobia in legume nodules. *Trends in Microbiology* **14**, 161-168.

Prentki,P. and Krisch,H.M. (1984) In vitro insertional mutagenesis with a selectable DNA fragment. *Gene* **29**, 303-313.

Pueppke,S.G. and Broughton,W.J. (1999) Rhizobium sp. strain NGR234 and R-fredii USDA257 share exceptionally broad, nested host ranges. *Molecular Plant-Microbe Interactions* **12**, 293-318.

Quandt,J. and Hynes,M.F. (1993) Versatile suicide vectors which allow direct selection for gene replacement in gram-negative bacteria. *Gene* **127**, 15-21.

Radutoiu,S., Madsen,L.H., Madsen,E.B., Felle,H.H., Umehara,Y., Gronlund,M., Sato,S., Nakamura,Y., Tabata,S., Sandal,N. and Stougaard,J. (2003) Plant recognition of symbiotic bacteria requires two LysM receptor-like kinases. *Nature* **425**, 585-592.

Rees,D.C. and Howard,J.B. (2000) Nitrogenase: standing at the crossroads. *Curr. Opin. Chem. Biol.* **4**, 559-566.

Reeve,W., Chain,P., O'Hara,G., Ardley,J., Nandesena,K., Brau,L., Tiwari,R., Malfatti,S., Kiss,H., Lapidus,A., Copeland,A., Nolan,M., Land,M., Hauser,L., Chang,Y.J., Ivanova,N., Mavromatis,K., Markowitz,V., Kyrpides,N., Gollagher,M., Yates,R., Dilworth,M. and Howieson,J. (2010a) Complete genome sequence of the Medicago microsymbiont Ensifer (Sinorhizobium) medicae strain WSM419. *Stand. Genomic. Sci.* **2**, 77-86.

Reeve,W., O'Hara,G., Chain,P., Ardley,J., Brau,L., Nandesena,K., Tiwari,R., Copeland,A., Nolan,M., Han,C., Brettin,T., Land,M., Ovchinikova,G., Ivanova,N., Mavromatis,K., Markowitz,V., Kyrpides,N., Melino,V., Denton,M., Yates,R. and Howieson,J. (2010b) Complete genome sequence of Rhizobium leguminosarum bv. trifolii strain WSM1325, an effective microsymbiont of annual Mediterranean clovers. *Stand. Genomic. Sci.* **2**, 347-356.

Renalier,M.H., Batut,J., Ghai,J., Terzaghi,B., Gherardi,M., David,M., Garnerone,A.M., Vasse,J., Truchet,G., Huguet,T. and . (1987) A new symbiotic cluster on the pSym megaplasmid of Rhizobium meliloti 2011 carries a functional fix gene repeat and a nod locus. *J. Bacteriol.* **169**, 2231-2238.

Rivas,R., Velazquez,E., Willems,A., Vizcaino,N., Subba-Rao,N.S., Mateos,P.F., Gillis,M., Dazzo,F.B. and Martinez-Molina,E. (2002) A new species of Devosia that forms a unique nitrogen-fixing root-nodule symbiosis with the aquatic legume Neptunia natans (L.f.) druce. *Appl. Environ. Microbiol.* **68**, 5217-5222.

Rivas,R., Willems,A., Subba-Rao,N.S., Mateos,P.F., Dazzo,F.B., Kroppenstedt,R.M., Martinez-Molina,E., Gillis,M. and Velazquez,E. (2003) Description of Devosia neptuniae sp. nov. that nodulates and fixes nitrogen in symbiosis with Neptunia natans, an aquatic legume from India. *Syst. Appl. Microbiol.* **26**, 47-53.

Roberts,G.P. and Brill,W.J. (1981) Genetics and regulation of nitrogen fixation. *Annu. Rev. Microbiol.* **35**, 207-235.

Robertson,J.G., Lyttleton,P., Bullivant,S. and Grayston,G.F. (1978) Membranes in lupin root nodules. I. The role of Golgi bodies in the biogenesis of infection threads and peribacteroid membranes. *J. Cell Sci.* **30**, 129-149.

Roche,P., Maillet,F., Plazanet,C., Debelle,F., Ferro,M., Truchet,G., Prome,J.C. and Denarie,J. (1996) The common nodABC genes of Rhizobium meliloti are host-range determinants. *Proc. Natl. Acad. Sci. U. S. A* **93**, 15305-15310.

Romanov,V.I., Hernandez-Lucas,I. and Martinez-Romero,E. (1994) Carbon Metabolism Enzymes of Rhizobium tropici Cultures and Bacteroids. *Appl. Environ. Microbiol.* **60**, 2339-2342.

Rome,S., Fernandez,M.P., Brunel,B., Normand,P. and Cleyet-Marel,J.C. (1996) Sinorhizobium medicae sp. nov., isolated from annual Medicago spp. *Int. J. Syst. Bacteriol.* **46**, 972-980.

Ronson,C.W., Astwood,P.M., Nixon,B.T. and Ausubel,F.M. (1987) Deduced products of C4-dicarboxylate transport regulatory genes of Rhizobium leguminosarum are homologous to nitrogen regulatory gene products. *Nucleic Acids Res.* **15**, 7921-7934.

Ronson,C.W., Lyttleton,P. and Robertson,J.G. (1981) C4-Dicarboxylate Transport Mutants of Rhizobium-Trifolii Form Ineffective Nodules on Trifolium-Repens. *Proceedings of the National Academy of Sciences of the United States of America-Biological Sciences* **78**, 4284-4288.

Rosendahl,L., Vance,C.P. and Pedersen,W.B. (1990) Products of Dark Co2 Fixation in Pea Root-Nodules Support Bacteroid Metabolism. *Plant Physiology* **93**, 12-19.

Ruvkun,G.B., Sundaresan,V. and Ausubel,F.M. (1982) Directed transposon Tn5 mutagenesis and complementation analysis of Rhizobium meliloti symbiotic nitrogen fixation genes. *Cell* **29**, 551-559.

Rydstrom,J. (2006) Mitochondrial NADPH, transhydrogenase and disease. *Biochim. Biophys. Acta* **1757**, 721-726.

Sanchez,A.M., Andrews,J., Hussein,I., Bennett,G.N. and San,K.Y. (2006) Effect of overexpression of a soluble pyridine nucleotide transhydrogenase (UdhA) on the production of poly(3-hydroxybutyrate) in Escherichia coli. *Biotechnology Progress* **22**, 420-425.

Sanwal,B.D. (1970) Regulatory characteristics of the diphosphopyridine nucleotide-specific malic enzyme of Escherichia coli. *J. Biol. Chem.* **245**, 1212-1216.

Sanwal,B.D. and Smando,R. (1969a) Malic enzyme of Escherichia coli. Diversity of the effectors controlling enzyme activity. *J. Biol. Chem.* **244**, 1817-1823.

Sanwal,B.D. and Smando,R. (1969b) Malic enzyme of Escherichia coli. Possible mechanism for allosteric effects. *J. Biol. Chem.* **244**, 1824-1830.

Sanwal,B.D., Wright,J.A. and Smando,R. (1968) Allosteric control of the activity of malic enzyme in Escherichia coli. *Biochem. Biophys. Res. Commun.* **31**, 623-627.

Sauer,L.A., Dauchy,R.T., Nagel,W.O. and Morris,H.P. (1980) Mitochondrial malic enzymes. Mitochondrial NAD(P)+-dependent malic enzyme activity and malate-dependent pyruvate formation are progression-linked in Morris hepatomas. *J. Biol. Chem.* **255**, 3844-3848.

Schluter,A., Patschkowski,T., Quandt,J., Selinger,L.B., Weidner,S., Kramer,M., Zhou,L., Hynes,M.F. and Priefer,U.B. (1997) Functional and regulatory analysis of the two copies of the fixNOQP operon of Rhizobium leguminosarum strain VF39. *Mol. Plant Microbe Interact.* **10**, 605-616.

Schmeisser,C., Liesegang,H., Krysciak,D., Bakkou,N., Le,Q.A., Wollherr,A., Heinemeyer,I., Morgenstern,B., Pommerening-Roser,A., Flores,M., Palacios,R., Brenner,S., Gottschalk,G., Schmitz,R.A., Broughton,W.J., Perret,X., Strittmatter,A.W. and Streit,W.R. (2009) Rhizobium sp. strain NGR234 possesses a remarkable number of secretion systems. *Appl. Environ. Microbiol.* **75**, 4035-4045.

Scrutton,M.C. 1971. Pyridine-nucleotide-linked decarboxylases. Methods in Microbiol. 6A: 526-529.

Sebbane,N., Sahnoune,M., Zakhia,F., Willems,A., Benallaoua,S. and de,L.P. (2006) Phenotypical and genotypical characteristics of root-nodulating bacteria isolated from annual Medicago spp. in Soummam Valley (Algeria). *Lett. Appl. Microbiol.* **42**, 235-241.

Seefeldt,L.C., Dance,I.G. and Dean,D.R. (2004) Substrate interactions with nitrogenase: Fe versus Mo. *Biochemistry* **43**, 1401-1409.

Sepulveda,E., Perez-Mendoza,D., Ramirez-Romero,M.A., Soto,M.J., Lopez-Lara,I.M., Geiger,O., Sanjuan,J., Brom,S. and Romero,D. (2008) Transcriptional interference and repression modulate the conjugative ability of the symbiotic plasmid of Rhizobium etli. *J. Bacteriol.* **190**, 4189-4197.

Singh,A., Agarwala,R., Kashyap,L.R. and Kumar,S. (1988) Behaviour of expression of nif HDK and fix ABCX promoters of Rhizobium meliloti in R. leguminosarum. *Indian J. Biochem. Biophys.* **25**, 389-391.

Smit,P., Raedts,J., Portyanko,V., Debelle,F., Gough,C., Bisseling,T. and Geurts,R. (2005) NSP1 of the GRAS protein family is essential for rhizobial Nod factor-induced transcription. *Science* **308**, 1789-1791.

Spaink,H.P. (2000) Root nodulation and infection factors produced by rhizobial bacteria. *Annu. Rev. Microbiol.* **54**, 257-288.

Stanley,J., Dowling,D.N. and Broughton,W.J. (1988) Cloning of Hema from Rhizobium Sp Ngr234 and Symbiotic Phenotype of A Gene-Directed Mutant in Diverse Legume Genera. *Molecular & General Genetics* **215**, 32-37.

Steinmetz,M., Le,C.D., Aymerich,S., Gonzy-Treboul,G. and Gay,P. (1985) The DNA sequence of the gene for the secreted Bacillus subtilis enzyme levansucrase and its genetic control sites. *Mol. Gen. Genet.* **200**, 220-228.

Stiens,M., Schneiker,S., Keller,M., Kuhn,S., Puhler,A. and Schluter,A. (2006) Sequence analysis of the 144-kilobase accessory plasmid pSmeSM11a, isolated from a dominant Sinorhizobium meliloti strain identified during a long-term field release experiment. *Appl. Environ. Microbiol.* **72**, 3662-3672.

Stocchi,V., Cucchiarini,L., Magnani,M., Chiarantini,L., Palma,P. and Crescentini,G. (1985) Simultaneous Extraction and Reverse-Phase High-Performance Liquid-Chromatographic Determination of Adenine and Pyridine-Nucleotides in Human Red Blood-Cells. *Analytical Biochemistry* **146**, 118-124.

Stovall,I. and Cole,M. (1978) Organic Acid Metabolism by Isolated Rhizobium japonicum Bacteroids. *Plant Physiol* **61**, 787-790.

Stracke,S., Kistner,C., Yoshida,S., Mulder,L., Sato,S., Kaneko,T., Tabata,S., Sandal,N., Stougaard,J., Szczyglowski,K. and Parniske,M. (2002) A plant receptor-like kinase required for both bacterial and fungal symbiosis. *Nature* **417**, 959-962.

Sullivan,J.T. and Ronson,C.W. (1998) Evolution of rhizobia by acquisition of a 500-kb symbiosis island that integrates into a phe-tRNA gene. *Proc. Natl. Acad. Sci. U. S. A* **95**, 5145-5149.

Sullivan,J.T., Trzebiatowski,J.R., Cruickshank,R.W., Gouzy,J., Brown,S.D., Elliot,R.M., Fleetwood,D.J., McCallum,N.G., Rossbach,U., Stuart,G.S., Weaver,J.E., Webby,R.J., de Bruijn,F.J. and Ronson,C.W. (2002) Comparative sequence analysis of the symbiosis island of Mesorhizobium loti strain R7A. *J. Bacteriol.* **184**, 3086-3095.

Suominen,L., Roos,C., Lortet,G., Paulin,L. and Lindstrom,K. (2001) Identification and structure of the Rhizobium galegae common nodulation genes: evidence for horizontal gene transfer. *Mol. Biol. Evol.* **18**, 907-916.

Suzuki,S., Aono,T., Lee,K.B., Suzuki,T., Liu,C.T., Miwa,H., Wakao,S., Iki,T. and Oyaizu,H. (2007) Rhizobial factors required for stem nodule maturation and maintenance in Sesbania rostrata-Azorhizobium caulinodans ORS571 symbiosis. *Appl. Environ. Microbiol.* **73**, 6650-6659.

Sy,A., Giraud,E., Samba,R., de,L.P., Gillis,M. and Dreyfus,B. (2001) [Nodulation of certain legumes of the genus Crotalaria by the new species Methylobacterium]. *Can. J. Microbiol.* **47**, 503-508.

Szeto,W.W., Zimmerman,J.L., Sundaresan,V. and Ausubel,F.M. (1984) A Rhizobium meliloti symbiotic regulatory gene. *Cell* **36**, 1035-1043.

Tighe,S.W., de,L.P., Dipietro,K., Lindstrom,K., Nick,G. and Jarvis,B.D. (2000) Analysis of cellular fatty acids and phenotypic relationships of Agrobacterium, Bradyrhizobium, Mesorhizobium, Rhizobium and Sinorhizobium species using the Sherlock Microbial Identification System. *Int. J. Syst. Evol. Microbiol.* **50 Pt 2**, 787-801.

Timm,A. and Steinbuchel,A. (1992) Cloning and molecular analysis of the poly(3-hydroxyalkanoic acid) gene locus of Pseudomonas aeruginosa PAO1. *Eur. J. Biochem.* **209**, 15-30.

Tirichine,L., Sandal,N., Madsen,L.H., Radutoiu,S., Albrektsen,A.S., Sato,S., Asamizu,E., Tabata,S. and Stougaard,J. (2007) A gain-of-function mutation in a cytokinin receptor triggers spontaneous root nodule organogenesis. *Science* **315**, 104-107.

Trinick,M.J. and Hadobas,P.A. (1989) Competition by Bradyrhizobium Strains for Nodulation of the Nonlegume Parasponia andersonii. *Appl. Environ. Microbiol.* **55**, 1242-1248.

Trujillo,M.E., Willems,A., Abril,A., Planchuelo,A.M., Rivas,R., Ludena,D., Mateos,P.F., Martinez-Molina,E. and Velazquez,E. (2005) Nodulation of Lupinus albus by strains of Ochrobactrum lupini sp. nov. *Appl. Environ. Microbiol.* **71**, 1318-1327.

Tsien,R.Y. (1998) The green fluorescent protein. *Annu. Rev. Biochem.* **67**, 509-544.

Tsukada,S., Aono,T., Akiba,N., Lee,K.B., Liu,C.T., Toyazaki,H. and Oyaizu,H. (2009) Comparative genome-wide transcriptional profiling of Azorhizobium caulinodans ORS571 grown under free-living and symbiotic conditions. *Appl. Environ. Microbiol.* **75**, 5037-5046.

Tun-Garrido,C., Bustos,P., Gonzalez,V. and Brom,S. (2003) Conjugative transfer of p42a from rhizobium etli CFN42, which is required for mobilization of the symbiotic plasmid, is regulated by quorum sensing. *J. Bacteriol.* **185**, 1681-1692.

Udvardi,M.K. and Day,D.A. (1989) Electrogenic ATPase Activity on the Peribacteroid Membrane of Soybean (Glycine max L.) Root Nodules. *Plant Physiol* **90**, 982-987.

Udvardi,M.K. and Day,D.A. (1997) Metabolite transport across symbiotic membranes of legume nodules. *Annual Review of Plant Physiology and Plant Molecular Biology* **48**, 493-523.

Vallari,D.S., Jackowski,S. and Rock,C.O. (1987) Regulation of pantothenate kinase by coenzyme A and its thioesters. *J. Biol. Chem.* **262**, 2468-2471.

Valverde,A., Velazquez,E., Fernandez-Santos,F., Vizcaino,N., Rivas,R., Mateos,P.F., Martinez-Molina,E., Igual,J.M. and Willems,A. (2005) Phyllobacterium trifolii sp. nov., nodulating Trifolium and Lupinus in Spanish soils. *Int. J. Syst. Evol. Microbiol.* **55**, 1985-1989.

Van Brussel,A.A., Zaat,S.A., Cremers,H.C., Wijffelman,C.A., Pees,E., Tak,T. and Lugtenberg,B.J. (1986) Role of plant root exudate and Sym plasmid-localized nodulation genes in the synthesis by Rhizobium leguminosarum of Tsr factor, which causes thick and short roots on common vetch. *J. Bacteriol.* **165**, 517-522.

van Slooten,J.C., Bhuvanasvari,T.V., Bardin,S. and Stanley,J. (1992) Two C4-dicarboxylate transport systems in Rhizobium sp. NGR234: rhizobial dicarboxylate transport is essential for nitrogen fixation in tropical legume symbioses. *Mol. Plant Microbe Interact.* **5**, 179-186.

van,R.P. and Vanderleyden,J. (1995) The Rhizobium-plant symbiosis. *Microbiol. Rev.* **59**, 124-142.

Vandamme,P. and Coenye,T. (2004) Taxonomy of the genus Cupriavidus: a tale of lost and found. *Int. J. Syst. Evol. Microbiol.* **54**, 2285-2289.

Vandamme,P., Goris,J., Chen,W.M., De,V.P. and Willems,A. (2002) Burkholderia tuberum sp. nov. and Burkholderia phymatum sp. nov., nodulate the roots of tropical legumes. *Syst. Appl. Microbiol.* **25**, 507-512.

Vandamme,P., Pot,B., Gillis,M., De,V.P., Kersters,K. and Swings,J. (1996) Polyphasic taxonomy, a consensus approach to bacterial systematics. *Microbiol. Rev.* **60**, 407-438.

Vasse,J., de,B.F., Camut,S. and Truchet,G. (1990) Correlation between ultrastructural differentiation of bacteroids and nitrogen fixation in alfalfa nodules. *J. Bacteriol.* **172**, 4295-4306.

Vinardell,J.M., Fedorova,E., Cebolla,A., Kevei,Z., Horvath,G., Kelemen,Z., Tarayre,S., Roudier,F., Mergaert,P., Kondorosi,A. and Kondorosi,E. (2003) Endoreduplication

mediated by the anaphase-promoting complex activator CCS52A is required for symbiotic cell differentiation in Medicago truncatula nodules. *Plant Cell* **15**, 2093-2105.

Viprey,V., Rosenthal,A., Broughton,W.J. and Perret,X. (2000) Genetic snapshots of the Rhizobium species NGR234 genome. *Genome Biol.* **1**, RESEARCH0014.

Virts,E.L., Stanfield,S.W., Helinski,D.R. and Ditta,G.S. (1988) Common regulatory elements control symbiotic and microaerobic induction of nifA in Rhizobium meliloti. *Proc. Natl. Acad. Sci. U. S. A* **85**, 3062-3065.

Voegele,R.T., Mitsch,M.J. and Finan,T.M. (1999) Characterization of two members of a novel malic enzyme class. *Biochim. Biophys. Acta* **1432**, 275-285.

Voordouw,G., van,d., V, Scholten,J.W. and Veeger,C. (1980) Pyridine nucleotide transhydrogenase from Azotobacter vinelandii. Differences in properties between the purified and the cell-free extract enzyme. *Eur. J. Biochem.* **107**, 337-344.

Voordouw,G., van,d., V and Themmen,A.P. (1983) Why are two different types of pyridine nucleotide transhydrogenase found in living organisms? *Eur. J. Biochem.* **131**, 527-533.

Voordouw,G., Veeger,C., Van Breemen,J.F. and Van Bruggen,E.F. (1979) Structure of pyridine nucleotide transhydrogenase from Azotobacter vinelandii. *Eur. J. Biochem.* **98**, 447-454.

Wasson,A.P., Pellerone,F.I. and Mathesius,U. (2006) Silencing the flavonoid pathway in Medicago truncatula inhibits root nodule formation and prevents auxin transport regulation by rhizobia. *Plant Cell* **18**, 1617-1629.

Watson,R.J. (1990) Analysis of the C-4-Dicarboxylate Transport Genes of Rhizobium-Meliloti - Nucleotide-Sequence and Deduced Products of Dcta, Dctb, and Dctd. *Molecular Plant-Microbe Interactions* **3**, 174-181.

Watson,R.J., Chan,Y.K., Wheatcroft,R., Yang,A.F. and Han,S.H. (1988) Rhizobium-Meliloti Genes Required for C-4-Dicarboxylate Transport and Symbiotic Nitrogen-Fixation Are Located on A Megaplasmid. *Journal of Bacteriology* **170**, 927-934.

Weaver,C.D., Crombie,B., Stacey,G. and Roberts,D.M. (1991) Calcium-dependent phosphorylation of symbiosome membrane proteins from nitrogen-fixing soybean nodules : evidence for phosphorylation of nodulin-26. *Plant Physiol* **95**, 222-227.

Weaver,C.D., Shomer,N.H., Louis,C.F. and Roberts,D.M. (1994) Nodulin 26, a nodule-specific symbiosome membrane protein from soybean, is an ion channel. *J. Biol. Chem.* **269**, 17858-17862.

Wedding,R.T. (1989) Malic Enzymes of Higher-Plants - Characteristics, Regulation, and Physiological-Function. *Plant Physiology* **90**, 367-371.

Weinstein,M., Lois,A.F., Ditta,G.S. and Helinski,D.R. (1993) Mutants of the two-component regulatory protein FixJ of Rhizobium meliloti that have increased activity at the nifA promoter. *Gene* **134**, 145-152.

Widmer,F. and Kaplan,N.O. (1977) Pseudomonas aeruginosa transhydrogenase: affinity of substrates for the regulatory site and possible hysteretic behavior. *Biochem. Biophys. Res. Commun.* **76**, 1287-1292.

Wilkinson,A., Danino,V., Wisniewski-Dye,F., Lithgow,J.K. and Downie,J.A. (2002) N-acyl-homoserine lactone inhibition of rhizobial growth is mediated by two quorum-sensing genes that regulate plasmid transfer. *J. Bacteriol.* **184**, 4510-4519.

Willems,A. and Collins,M.D. (1993) Phylogenetic analysis of rhizobia and agrobacteria based on 16S rRNA gene sequences. *Int. J. Syst. Bacteriol.* **43**, 305-313.

Williams,A., Wilkinson,A., Krehenbrink,M., Russo,D.M., Zorreguieta,A. and Downie,J.A. (2008) Glucomannan-mediated attachment of Rhizobium leguminosarum to pea root hairs is required for competitive nodule infection. *J. Bacteriol.* **190**, 4706-4715.

Yamaguchi,M., Tokushige,M. and Katsuki,H. (1973) Studies on regulatory functions of malic enzymes. II. Purification and molecular properties of nicotinamide adenine dinucleotide-linked malic enzyme from Eschericha coli. *J. Biochem.* **73**, 169-180.

Yanagi,M. and Yamasato,K. (1993) Phylogenetic analysis of the family Rhizobiaceae and related bacteria by sequencing of 16S rRNA gene using PCR and DNA sequencer. *FEMS Microbiol. Lett.* **107**, 115-120.

Yao,Z.Y., Kan,F.L., Wang,E.T., Wei,G.H. and Chen,W.X. (2002) Characterization of rhizobia that nodulate legume species of the genus Lespedeza and description of Bradyrhizobium yuanmingense sp. nov. *Int. J. Syst. Evol. Microbiol.* **52**, 2219-2230.

Yarosh,O.K., Charles,T.C. and Finan,T.M. (1989) Analysis of C4-dicarboxylate transport genes in Rhizobium meliloti. *Mol. Microbiol.* **3**, 813-823.

Young,J.P., Crossman,L.C., Johnston,A.W., Thomson,N.R., Ghazoui,Z.F., Hull,K.H., Wexler,M., Curson,A.R., Todd,J.D., Poole,P.S., Mauchline,T.H., East,A.K., Quail,M.A., Churcher,C., Arrowsmith,C., Cherevach,I., Chillingworth,T., Clarke,K., Cronin,A., Davis,P., Fraser,A., Hance,Z., Hauser,H., Jagels,K., Moule,S., Mungall,K., Norbertczak,H., Rabbinowitsch,E., Sanders,M., Simmonds,M., Whitehead,S. and Parkhill,J. (2006) The genome of Rhizobium leguminosarum has recognizable core and accessory components. *Genome Biol.* **7**, R34.

Yuan,Z.C., Zaheer,R. and Finan,T.M. (2005) Phosphate limitation induces catalase expression in Sinorhizobium meliloti, Pseudomonas aeruginosa and Agrobacterium tumefaciens. *Mol. Microbiol.* **58**, 877-894.

Yuan,Z.C., Zaheer,R. and Finan,T.M. (2006) Regulation and properties of PstSCAB, a high-affinity, high-velocity phosphate transport system of Sinorhizobium meliloti. *J. Bacteriol.* **188**, 1089-1102.

Yurgel,S., Mortimer,M.W., Rogers,K.N. and Kahn,M.L. (2000) New substrates for the dicarboxylate transport system of Sinorhizobium meliloti. *Journal of Bacteriology* **182**, 4216-4221.

Yurgel,S.N. and Kahn,M.L. (2004) Dicarboxylate transport by rhizobia. *Fems Microbiology Reviews* **28**, 489-501.

Zahran,H.H., Abdel-Fattah,M., Ahmad,M.S. and Zaky,A.Y. (2003) Polyphasic taxonomy of symbiotic rhizobia from wild leguminous plants growing in Egypt. *Folia Microbiol. (Praha)* **48**, 510-520.

Zakhia,F. and de,L.P. (2006) [Modern bacterial taxonomy: techniques review--application to bacteria that nodulate leguminous plants (BNL)]. *Can. J. Microbiol.* **52**, 169-181.

Zhang,Y., Aono,T., Poole,P. and Finan,T.M. (2012) NAD(P)+-malic enzyme mutants of Sinorhizobium sp. strain NGR234, but not Azorhizobium caulinodans ORS571, maintain symbiotic N2 fixation capabilities. *Appl. Environ. Microbiol.* **78**, 2803-2812.